

Titre: Novel Conductive Polymer Blends
Title:

Auteur: Sepehr Ravati
Author:

Date: 2010

Type: Mémoire ou thèse / Dissertation or Thesis

Référence: Ravati, S. (2010). Novel Conductive Polymer Blends [Thèse de doctorat, École
Citation: Polytechnique de Montréal]. PolyPublie. <https://publications.polymtl.ca/286/>

 **Document en libre accès dans PolyPublie**
Open Access document in PolyPublie

URL de PolyPublie: <https://publications.polymtl.ca/286/>
PolyPublie URL:

**Directeurs de
recherche:** Basil D. Favis
Advisors:

Programme: Génie chimique
Program:

UNIVERSITÉ DE MONTRÉAL

NOVEL CONDUCTIVE POLYMER BLENDS

SEPEHR RAVATI

DÉPARTEMENT DE GÉNIE CHIMIQUE
ÉCOLE POLYTECHNIQUE DE MONTRÉAL

THÈSE PRÉSENTÉE EN VUE DE L'OBTENTION
DU DIPLÔME DE PHILOSOPHIAE DOCTOR (Ph.D.)
(GÉNIE CHIMIQUE)

AVRIL 2010

© Sepehr Ravati, 2010.

UNIVERSITÉ DE MONTRÉAL

ÉCOLE POLYTECHNIQUE DE MONTRÉAL

Cette thèse intitulée:

NOVEL CONDUCTIVE POLYMER BLENDS

présentée par : RAVATI Sepehr

en vue de l'obtention du diplôme de : Philosophiae Doctor

a été dûment acceptée par le jury d'examen constitué de :

M. FRADETTE Louis, Ph.D., président

M. FAVIS Basil, Ph.D., membre et directeur de recherche

Mme HEUZEY Marie-Claude, Ph.D., membre

M. SUNDARARAJ Uttandaraman (U.T.), Ph.D., membre

DEDICATED

To my parents

ACKNOWLEDGEMENTS

I would like to express my gratitude to my advisor Professor Basil D. Favis for all our insightful conversations. His thoughtful advice and enthusiasm for science have always inspired me. All what I learned from him, not only academically but in ways to do research, is priceless.

There are many other people I need to thank who contributed to the success of this dissertation in different ways. Among them, special thanks to François Normandin from IMI for his direct help on assembling a particular setup to measure conductivity throughout the sample for my project. Thanks to Carol and Jacques for technical help in providing the particular equipments for both the layer-by-layer and blending process parts. Thanks also to Mélina for her assistance and discussions on the rheological part. I would also like to thank Patricia Moraille for her assistance in AFM, Éric Duchesne for introducing SEM to me and Jean-Philippe Masse for helping me with FIB equipment and for helpful discussions.

My sincere thanks to my friends Sina Mortazy, Reza Shirazi, Nick Virgilio, Pierre Sarazin, and Mehdi Maziane for their assistance and useful discussions in this thesis.

This thesis and all of my past academic success is due in large part to the support of my brothers: Shahrooz, Babak, and Sasan, without whom I could not have this glorious moment in my life. My deepest gratitude goes to my parents for their unconditional love and support. They taught me the right way to live and no rewards without hard working by their own life.

RÉSUMÉ

Cette thèse présente, pour la première fois, une étude complète des morphologies de contact interfacial (engloutissement complet) pour des mélanges ternaires, quaternaires et quinaires de polyaniline (PANI) avec quatre polymères commercialement disponibles : le polyéthylène à haute densité (HDPE), le polystyrène (PS), le poly(méthyl méthacrylate) (PMMA) et le polyfluorure de vinylidène (PVDF). La morphologie d'engloutissement complet est une structure dictée par la tension interfaciale et est thermodynamiquement prévisible selon la théorie d'étalement de Harkins. Ce type de microstructure est formé dans un mélange polymère ternaire quand un des coefficients d'étalement, tel que calculé par les tensions interfaciales des paires de polymères dans le système, a une valeur positive. L'extension aux systèmes quaternaires et quinaires de définitions thermodynamiques similaires mène à la prédiction et à la formation de mélanges à plusieurs composants ordonnés hiérarchiquement. Le contrôle de la composition des composants de tels systèmes ordonnés hiérarchiquement, dans le cas des mélanges binaires, ternaires, quaternaires et quinaires, permet de produire des structures à percolation multiple, dans lesquelles toutes les phases sont pleinement interconnectées et interpénétrées. Cette approche est utilisée pour atteindre l'objectif de ce travail de recherche qui est d'échafauder un ensemble de techniques pour réduire le seuil de percolation des composants dans les mélanges. Le seuil de percolation des phases est défini comme étant la formation de connectivité sur une longue distance dans un système aléatoire. Les restrictions géométriques des phases dans des systèmes auto-assemblés, par exemple dans des structures dictées par la tension interfaciale telles les morphologies à percolation multiple, peuvent réduire le seuil de percolation des phases de manière significative. Une autre partie de ce travail visait la préparation de substrats poreux à très petite surface provenant de mélanges polymères à percolation multiple, suivie par la déposition de PANI, un polymère conducteur, sur la surface interne poreuse par une technique couche par couche.

Des mélanges polymères constitués de plusieurs composants, dont le HDPE, le PS, le PMMA, le PVDF et le PANI, et, dans certains cas, le PP, le PEMA, et le PS-co-PMMA, ont été préparés dans un mélangeur interne. Des échantillons en forme de disque ont été préparés dans une presse

chaude par moulage par compression dans le but d'en mesurer la conductivité. Certains échantillons ont été de nouveau moulés par compression pour effectuer des tests de recuit statique, dans le but d'augmenter la taille des pores. L'extraction par solvant a été utilisée pour extraire divers composants et générer de la porosité dans le substrat. L'extraction par solvant permet aussi de déterminer le pourcentage de continuité des différents composants du mélange. Deux techniques qualitatives de caractérisation sont utilisées dans le but de mieux comprendre la morphologie des mélanges polymères. La microscopie électronique par balayage (MEB) et la microscopie par force atomique (MFA) accompagnée d'irradiation par faisceau ionique focalisé (FIF) fournissent de l'information sur la morphologie des échantillons et sur l'épaisseur de la structure multicouche construite. Après une préparation par microtomie cryogénique et une déposition d'or-palladium, l'échantillon est gravé par FIF, révélant un contraste topographique entre les phases. Une telle topographie permet de distinguer les phases et cette distinction est quantifiée par MFA. Des mesures de conductivité ont été effectuées avec un électromètre à travers l'épaisseur verticale des substrats.

Dans la première partie de cette étude, un dispositif conducteur solide à trois dimensions, avec un faible seuil de percolation, est fabriqué en contrôlant les effets d'encapsulation multiple dans un mélange polymère à cinq composants. Cette approche de structure à percolation multiple est contrôlée thermodynamiquement selon la théorie d'étalement de Harkins, qui prévoit l'étalement de toutes les phases, y compris la phase de polymère conducteur, à travers le mélange, un mélange quinaire de PANI et de quatre autres composants (PE, PS, PMMA et PVDF) sélectionnés pour présenter une structure à percolation multiple avec un seuil de percolation de moins de 5 %. Afin de localiser le PANI au coeur de cette structure à percolation quadruple, toutes les tensions interfaciales doivent satisfaire l'équation de Harkins et les phases doivent avoir un comportement d'engloutissement complet avec la hiérarchie désirée (HDPE|PS|PMMA|PVDF|PANI). Dans la première partie du travail, la morphologie et les diagrammes de continuité détaillés des mélanges binaires, ternaires, quaternaires et quinaires de PE, PS, PMMA, PVDF et PANI, sont étudiés systématiquement afin de déterminer les plages de concentration qui permettront la formation de cette structure morphologique innovatrice, l'encapsulation multiple. Il est démontré qu'à travers le contrôle de la composition des couches intérieures et extérieures des structures en oignon des phases dispersées, la morphologie peut

devenir une structure hiérarchique auto-assemblée à percolation multiple. Cette approche aide à contrôler la morphologie des phases continues, menant à une restriction géométrique pour les phases et réduisant abruptement le seuil de percolation des phases, alors que la conductivité du mélange quinaire peut être augmentée de 10^{-15} S cm⁻¹ (PE pur) à 10^{-5} S cm⁻¹ à 5 % de PANI et jusqu'à 10^{-3} S cm⁻¹ à 10 % de PANI. Il s'agit des plus hautes valeurs de conductivité jamais rapportées à ces concentrations de PANI dans des mélanges préparés à l'état fondu.

Dans la deuxième partie de l'étude, les efforts ont été dirigés vers la création de très grands substrats poreux dans le but de mieux comprendre la nature des morphologies à percolation multiple. Ces substrats étaient destinés à servir de substrat tridimensionnel dans la technique de dépôt couche par couche. Des mélanges polymères à percolation double et triple ont été préparés à l'état fondu : HDPE/PS/PVDF, HDPE/PMMA/PVDF, et HDPE/PS/PMMA/PVDF. Il est démontré que le recuit statique d'un échantillon à percolation multiple est un procédé rapide qui mène à de très grandes tailles de pores. Puisque les structures à percolation multiple sont constituées de phases continues assemblées dans un ordre précis, l'extraction d'une ou de plusieurs phases permet la formation d'ultra-pores, à cause des restrictions géométriques. Un recuit des échantillons suivi d'une extraction par solvant permet la création de substrats poreux de HDPE entièrement interconnectés, avec une surface très faible. Suite à la préparation d'un substrat idéal pour l'addition subséquente de polyaniline, des couches alternées de PSS et de PANI sont déposées sur sa surface intérieure. Cette approche permet de réduire le seuil de percolation à aussi peu que 0,19 % de PANI. De plus, selon la quantité de PANI déposée, la conductivité du substrat poreux peut être contrôlée entre 10^{-15} S cm⁻¹ et 10^{-3} S cm⁻¹. Le dépôt de polyélectrolytes sur un substrat polymère poreux tridimensionnel a été étudié en détail et le profil de dépôt massique montre un comportement oscillatoire suivant un motif en zig-zag. Les expériences révèlent qu'un dépôt plus uniforme et des couches plus épaisses de PSS/PANI sont produits en présence de sel dans la solution polyanionique. L'application d'une charge sur le substrat peut constituer un autre paramètre de contrôle : une charge plus importante mène à des valeurs de conductivité plus élevées (jusqu'à 10^{-3} S cm⁻¹). Dans la deuxième partie du travail, l'emphase a été mise sur des substrats à très faible surface afin de déterminer le plus faible seuil de percolation possible pour le polyaniline, mais des substrats à grande surface peuvent aussi être préparés en utilisant cette approche.

Dans la dernière partie de cette étude, des mélanges polymères ternaires montrent un comportement de mouillage complet. Conceptuellement, il s'agit de l'état où un des composants aura toujours tendance à séparer les deux autres complètement, et du point de vue thermodynamique, deux des trois coefficients d'étalement binaires sont négatifs et l'autre est positif, selon la théorie d'étalement de Harkins. Ce travail couvre l'étendue totale des états morphologiques possibles pour un tel système préparé à l'état fondu, sur tout le diagramme de composition ternaire. Un mélange polymère ternaire composé de HDPE, de PS et de PMMA est choisi comme système modèle montrant un mouillage complet, alors que le coefficient d'étalement positif $\lambda_{PS/PMMA} = 2,6$ mN/m indique que le PS sépare les phases de HDPE et de PMMA. Quatre sous-catégories de morphologie peuvent être identifiées : a) matrice/phase dispersée coeur-coquille; b) tricontinuité; c) bicontinuité/phase dispersée; d) matrice/deux phases dispersées distinctes. La microscopie électronique, de même qu'une technique basée sur l'irradiation par faisceau ionique focalisé combinée à la microscopie par force atomique, est utilisée afin d'illustrer clairement et d'identifier les différentes phases. L'extraction par solvant et la gravimétrie sont utilisées pour mesurer le degré de continuité des systèmes afin d'identifier efficacement les régions de haute continuité. Les diagrammes de composition triangulaires sont utilisés pour distinguer ces différentes régions morphologiques et les résultats sont interprétés à la lumière des tensions interfaciales des différentes paires et de leurs coefficients d'étalement subséquents. L'effet de la masse moléculaire et du ratio de viscosité sur la taille des phases des différentes structures est également considéré. Il est démontré que typiquement, un plus haut ratio de viscosité, de même qu'une plus haute tension interfaciale, mène à une plus grande taille de phases.

ABSTRACT

This thesis presents, for the first time, a comprehensive survey on the subject of self-assembled, multi-encapsulated structures for ternary, quaternary, and quinary polymer blends demonstrating complete wetting. The work targets the development of novel conductive devices possessing low percolation threshold concentrations of conductive polymer. The blends studied are comprised of conductive polyaniline and four commercial polymers: HDPE, PS, PMMA, and PVDF. A complete wetting morphology is an interfacial tension driven structure which can be thermodynamically predicted by the Harkins spreading theory. This type of microstructure in a ternary polymer blend is formed when one of the spreading coefficients, as calculated from the interfacial tensions of polymer pairs in the system, has a positive value. Conceptually, for a ternary blend, complete wetting is the state where one of the components will always tend to completely separate the other two. The development of similar thermodynamic definitions to quaternary and quinary systems results in the prediction and construction of hierarchically ordered multi-encapsulated, multi-component blends. Controlling the compositions of components in such hierarchically ordered systems in ternary, quaternary, and quinary blends allows for the preparation of multi-percolated structures in which all phases are fully interconnected and interpenetrated. This approach is employed to attain the goal of this research which is to build a foundation of methods to reduce the percolation threshold of components in multi-component blends. The percolation threshold of phases is defined as the formation of long-range connectivity in random systems. The geometrical restriction of phases in self-assembled systems, for example in interfacial tension driven structures such as a multi-percolated morphologies, can significantly reduce the percolation threshold of phases. Another part of the work has focused on the preparation of ultra-low surface area porous substrates derived from multi-percolated polymer blends, followed by the deposition of polyaniline conductive polymer (PANI) on the internal porous surface using a layer-by-layer technique.

Polymer blends comprising various components including HDPE, PS, PMMA, PVDF, and PANI, and in some cases PP, PEMA, and PS-co-PMMA are prepared in an internal mixer. Disc-shaped samples for conductivity testing are compression molded in a hot press. Some of the samples, after melt processing, are compression molded in a hot press to perform quiescent

annealing to increase the phase sizes. Solvent extraction was used to extract various components and generate porosity in the substrate. Selective solvent extraction also allows for the determination of the percent continuity of the different components in the blend system. The characterization, aimed at gaining insight on the morphology of polymer blends, is carried out via two techniques. Scanning electron microscopy (SEM) and focused ion beam (FIB)-atomic force microscopy (AFM) provide information about the morphology of the samples and the thickness of the constructed multilayer. After cryogenically microtoming the sample and coating it with a gold-palladium layer, the sample is etched by using FIB, demonstrating a topographic contrast between phases. Such topography allows the phases to be distinguished and this is quantified by AFM. Conductivity measurements were performed through the vertical thickness of the substrates with an electrometer.

In the first part of this study, a solid, 3D, low percolation threshold conductive device prepared through the control of multiple encapsulation effects in a five-component polymer blend system through melt processing is fabricated. This multi-percolated structure approach is thermodynamically controlled and is described by the Harkins spreading theory, demonstrating spreading of all phases, including the conductive polymer phase, throughout the blend. A quinary blend of PANI and four other components: polyethylene (PE), polystyrene (PS), poly(methyl methacrylate) PMMA, and poly(vinylidene fluoride) (PVDF) are precisely selected to show multi-percolated structure with a percolation threshold less than 5%. In order to locate PANI at the core of this quadruple-percolated structure, all the interfacial tensions between phases must satisfy the Harkins equation and show various complete wetting morphologies with the desirable hierarchical ordering of the phases (HDPE|PS|PMMA|PVDF|PANI). The detailed morphology and continuity diagrams of binary, ternary, quaternary, and finally, quinary systems for PE, PS, PMMA, PVDF, and PANI, are progressively studied in order to systematically demonstrate the concentration regimes resulting in the formation of these novel multiple-encapsulated morphological structures. It is shown that through the control of the composition of the inner and outer layers in the onion-type dispersed phase structures, the morphology can be transformed to a hierarchical self-assembled, multi-percolated structure. This approach helps control the morphology of continuous phases, leading to a geometrical restriction for the phases and sharply reduces the percolation threshold of phases. In this fashion, the conductivity of the quinary blend

system can be increased from 10^{-15} S cm⁻¹ (pure PE) to 10^{-5} S cm⁻¹ at 5% PANI and up to 10^{-3} S cm⁻¹ for 10% PANI. These are the highest conductivity values ever reported for these PANI concentrations in melt processed systems.

In the second part of the study, a novel 3D porous polymeric conducting device is derived from multi-percolated polymer blend systems. The work has focused on the preparation of ultra-low surface area porous substrates followed by the deposition of polyaniline conductive polymer (PANI) on the internal porous surface using a layer-by-layer self-assembly technique. The approach reported here allows for the percolation threshold concentration of polyaniline conductive polymer (PANI) to be reduced to values as low as 0.19%. Furthermore, depending on the amount of PANI deposited, the conductivity of the porous substrate can be controlled from 10^{-15} S cm⁻¹ to 10^{-3} S cm⁻¹. Ternary and quaternary multi-percolated systems comprised of high-density polyethylene(HDPE), polystyrene(PS), poly(methyl methacrylate)(PMMA) and poly(vinylidene fluoride)(PVDF) are prepared by melt mixing and subsequently annealed in order to obtain large interconnected phases. Selective extraction of PS, PMMA and PVDF result in a fully interconnected porous HDPE substrate of ultra low surface area and highly uniform sized channels. This provides an ideal substrate for subsequent polyaniline(PANI) addition. Using a layer-by-layer(LbL) approach, alternating poly(styrene sulfonate)(PSS)/PANI layers are deposited on the internal surface of the 3-dimensional porous polymer substrate. The PANI and sodium poly(styrene sulfonate)(NaPSS) both adopt an inter-diffused network conformation on the surface. The sequential deposition of PSS and PANI has been studied in detail and the mass deposition profile demonstrates oscillatory behavior following a zigzag-type pattern. The presence of salt in the deposition solution results in a more uniform deposition and more thickly deposited PSS/PANI layers. The conductivity of these samples was measured and the conductivity can be controlled from 10^{-15} S cm⁻¹ to 10^{-5} S cm⁻¹ depending on the number of deposited layers. Applying a load to the substrate can be used as an additional control parameter. Higher loads result in higher conductivity values with values as high as 10^{-3} S cm⁻¹ obtained. The work described above has focused on very low surface area porous substrates in order to determine the lowest possible percolation threshold values of polyaniline, but high surface area substrates can also be readily prepared using this approach.

The final part of the work focuses on the complex morphological structures which can be generated from a ternary polymer blend demonstrating complete wetting behavior. This work examines the complete range of possible morphological states for such a system over the entire ternary composition diagram as prepared by melt mixing. A ternary polymer blend comprised of HDPE, PS, and PMMA is selected as a model system demonstrating complete wetting. The positive spreading coefficient of $\lambda_{PS/PMMA}=2.6$ mN/m indicates that PS separates the HDPE and PMMA phases. Four thermodynamically stable sub-categories of morphologies can be identified: a) matrix/core-shell dispersed phase; b) tri-continuous; c) bi-continuous/dispersed phase; and d) matrix/two separate dispersed phases. Electron microscopy as well as focused ion beam irradiation and atomic force microscopy are used to clearly illustrate and identify the various phases. Solvent extraction/gravimetry is used to examine the extent of continuity of the systems so as to effectively identify regions of high continuity. Triangular compositional diagrams are used to distinguish these various morphological regions and the results are interpreted in light of the interfacial tension of the various binary combinations and their subsequent spreading coefficients. The effect of the molecular weight and viscosity ratio on the phase size of the various structures is also considered. It is shown that the viscosity of the phases can influence the interfacial area between phases, but does not affect the morphological state classification.

CONDENSÉ EN FRANÇAIS

Dans ce travail, nous avons étudié la morphologie de mélanges à plusieurs composants préparés à l'état fondu, suivi de gravure par solvant, afin de générer de nouveaux dispositifs conducteurs avec un seuil de percolation extrêmement faible. Cette thèse mesure et élabore sur l'évolution de la continuité dans les morphologies co-continues à percolation double, triple et quadruple, dans le but de trouver le moyen de réduire considérablement le seuil de percolation de toutes les phases dans le mélange.

L'utilisation de structures continues dans les mélanges polymères constitue une manière élégante de réduire la continuité et/ou le seuil de percolation électrique d'un polymère conducteur. À cette fin, le polyaniline (PANI) et quatre autres polymères, disponibles commercialement, avec les tensions de surface, les polarités et les tensions interfaciales désirées, sont sélectionnés. Les tensions interfaciales entre les différents composants se situent dans une plage variant entre 1 mN/m, pour le PVDF/PMMA, et 26,9 mN/m, pour le PANI/HDPE. La caractérisation morphologique des échantillons est effectuée en utilisant la microscopie électronique à balayage (MEB) et le faisceau ionique focalisé (FIF) couplé à la microscopie par force atomique (MFA). Les mélanges polymères sont préparés à l'état fondu dans un mélangeur interne, à 50 tr/min pendant 8 minutes à 200°C. L'extraction sélective des phases par solvant est utilisée, soit pour aider à mieux distinguer les phases afin de recueillir de l'information qualitative, soit pour produire des échantillons poreux. La combinaison du traitement par FIF et de la MFA permet de distinguer clairement les phases à partir du contraste topographique résultant de la différence des taux de gravure des matériaux par FIF. Afin d'étudier l'effet du ratio de viscosité dans les mélanges ternaires, deux polyméthacrylates de méthyle (PMMA) sont choisis pour leurs masses moléculaires différentes. Des matériaux poreux entièrement interconnectés sont utilisés comme substrats pour la déposition alternée de PSS et de PANI.

Dans la première étape, trois composants, soit le polyéthylène à haute densité (HDPE), le polystyrène (PS) et le PMMA sont soigneusement sélectionnés pour satisfaire les conditions thermodynamiques. Le coefficient d'étalement positif $\lambda_{PS/PMMA} = 2,6$ mN/m, basé sur les trois tensions interfaciales des paires de polymères (HDPE/PS ($\gamma_{PS/HDPE} = 4,7$ mN/m), PS/PMMA ($\gamma_{PS/PMMA} = 1,1$ mN/m), et HDPE/PMMA ($\gamma_{HDPE/PMMA} = 8,4$ mN/m)), prévoit que la phase de PS

se localisera à l'interface des phases de HDPE et de PMMA dans une morphologie d'engloutissement complet. Les résultats expérimentaux confirment la prédiction de la morphologie par la théorie d'étalement, l'identification des phases étant clairement établie par la topographie induite par la gravure par FIF et subséquentement quantifiée par l'analyse par MFA en mode topographique. Un article publié, présentant pour la première fois une structure à percolation double avec une couche de PS en forme de microgaine située à l'interface entre le HDPE et le PMMA, est inclus en annexe. Il est démontré que par une combinaison de la théorie classique de l'étalement et du contrôle de la concentration des phases, une couche uniforme de PS est assemblée entre les phases avec un seuil de percolation extrêmement faible de 3 % de PS.

L'ajout d'une quatrième phase (polyfluorure de vinylidène, PVDF) au mélange ternaire avec un engloutissement complet de HDPE/PS/PMMA, en autant que toutes les équations thermodynamiques d'étalement soient satisfaites, mène à un ordre hiérarchique des phases, HDPE|PS|PMMA|PVDF. Dans cette morphologie particulière, les phases de HDPE et de PVDF deviennent les phases extérieures, alors que le PS et le PMMA se situent dans le milieu; le PS est adjacent au HDPE, et le PMMA, adjacent au PVDF. Il est démontré que l'ordre des phases dans tous les mélanges ternaires, HDPE|PS|PMMA, HDPE|PS|PVDF, HDPE|PMMA|PVDF, et PS|PMMA|PVDF, est correctement prédit par l'équation de Harkins et est en accord avec l'ordre des phases dans le mélange quaternaire HDPE|PS|PMMA|PVDF. La valeur positive du coefficient d'étalement $\lambda_{PS/PVDF} = 3,8 \text{ mN/m}$ dans le système ternaire HDPE/PS/PVDF indique également que la phase de PS se situe entre le HDPE et le PVDF, ce qui est en accord avec l'ordre du PS dans le mélange quaternaire. La théorie d'étalement de Harkins prédit que l'ajout de PANI au mélange quaternaire HDPE|PS|PMMA|PVDF mènera à une structure ordonnée hiérarchiquement HDPE|PS|PMMA|PVDF|PANI. Les coefficients d'étalement positifs des différents mélanges ternaires montrent que tous les mélanges quaternaires, de même que le mélange quinaire, de ces cinq polymères, devraient être ordonnés selon cette hiérarchie. Les résultats expérimentaux sont en excellent accord avec ces prédictions.

Suite à la détermination théorique de l'ordre de toutes les phases, le contrôle de la composition des phases permet de générer des morphologies innovatrices, telles la morphologie en « oignon » et les structures à percolation multiple. Les micrographies obtenues par MEB confirment la structure en oignon d'un mélange quaternaire HDPE/PS/PMMA/PVDF, avec une matrice de HDPE et des gouttelettes de PVDF encapsulées par une première coquille de PMMA et une

deuxième coquille de PS. Les phases les plus importantes du mélange HDPE/PS/PMMA/PVDF sont les première (HDPE) et dernière (PVDF) phases. La variation de la concentration de ces deux phases, en maintenant les deux autres constantes, dicte l'évolution de la morphologie d'une structure en oignon vers une structure à percolation multiple. Dans une structure à percolation multiple, toutes les phases sont entièrement interconnectées et interpénétrées. Une région de percolation multiple est une région de concentration dans laquelle toutes les phases dans le mélange quaternaire HDPE/PS/PMMA/PVDF sont interconnectées, comme dans la région à deux phases du diagramme de co-continuité d'un mélange binaire. Cette région est déterminée par plusieurs paramètres, dont les ratios de viscosité et les tensions interfaciales entre les paires de polymères. Afin de cerner quantitativement et précisément la région de percolation multiple, l'extraction par solvant, suivie de mesures gravimétriques, a été utilisée pour obtenir le pourcentage de continuité de chaque phase. La continuité maximale pour toutes les phases des mélanges quaternaires a été obtenue à des compositions de 30/15/15/40 et 40/15/15/30 HDPE/PS/PMMA/PVDF. L'ajout de PANI à des mélanges quaternaires fortement continus situés dans cette plage de composition mène à une morphologie à percolation quadruple avec les phases ordonnées selon la hiérarchie HDPE/PS/PMMA/PVDF/PANI. Comme le PANI se situe à la phase intérieure, il est porté à s'étaler entre les autres phases percolées, même à de faibles concentrations. En conséquence, dans cette étude, pour la première fois, le seuil de percolation de la phase intérieure (PANI) a été dramatiquement réduite à moins de 5 %. Le PANI utilisé dans ce travail peut être mis en oeuvre à l'état fondu et contient 25 % massique de PANI pur et 75 % massique de composé de zinc. Ceci indique que le volume réel de PANI pur présent dans le mélange est inférieur à 5 % volumétrique. La morphologie du réseau de PANI est montrée après l'extraction de toutes les phases, sauf le PANI, par le diméthylformamide, suivie d'un procédé de lyophilisation, à partir d'un mélange 25/25/25/25 PS/PMMA/PVDF/PANI.

Dans une autre partie de ce premier article, l'effet de l'ajout de PS-co-PMMA au mélange quinaire HDPE/PS/PMMA/PVDF/PANI à percolation quadruple est étudié. L'ajout d'un agent compatibilisant pour deux phases adjacentes (ici, PS et PMMA) montre une réduction de la taille des phases de PS et de PMMA dans le mélange. Puisque toutes les phases sont assemblées dans un ordre hiérarchique, la réduction de la taille des phases de deux couches induit une réduction de la taille des autres couches assemblées. L'ajout de 10% de PS-co-PMMA au mélange 30/30/30/10 PS/PMMA/PVDF/PANI, un système à encapsulation multiple, cause une réduction

de toutes les tailles de phase dans le système encapsulé. Les micrographies des échantillons contenant du copolymère montrent un réseau de PANI plus fin et plus uniforme, avec des branches homogènes distribuées à travers l'échantillon.

Ce travail évalue l'effet du nombre de phases dans une structure à percolation multiple. Des mélanges ternaires, quaternaires, quinaires et à six composants, contenant 5 % de PANI, sont préparés. Les résultats indiquent que l'augmentation du nombre de composants réduit le seuil de percolation de toutes les phases, incluant le PANI, à cause des restrictions géométriques des phases. La valeur très faible de conductivité, près de 10^{-12} S cm⁻¹, indique qu'aucun chemin conducteur ne se forme dans le mélange ternaire PS/PMMA/PANI, puisque le 5 % de PANI est présent sous forme de gouttelettes distribuées comme phase dispersée. Pour obtenir une phase de PANI étalée, au moins quatre composants, dans une structure à percolation multiple, sont requis. La conductivité augmente abruptement de presque six ordres de grandeurs avec l'ajout d'un quatrième composant au système. L'ajout subséquent de phases n'augmente que légèrement la conductivité, et la continuité du PANI, puisque quatre composants suffisent pour étaler la phase de PANI à travers le mélange.

Dans le deuxième article, à travers le développement d'une morphologie à percolation multiple accompagné d'une approche couche par couche (CPC), un nouveau dispositif conducteur polymère poreux (DCPP) tridimensionnel est créé. Cette technique permet l'abaissement du seuil de percolation du PANI conducteur à une valeur aussi faible que 0,19 %. Un substrat de HDPE, poreux et entièrement interconnecté, avec une surface extrêmement faible, est préparé par la création de systèmes à percolation double et triple, suivie d'un recuit et d'une extraction sélective des phases par solvant. Tel que mentionné plus haut, le HDPE, le PS, le PMMA et le PVDF produisent une structure à percolation multiple avec des phases ordonnées hiérarchiquement, puisque les tensions interfaciales des différentes paires satisfont les conditions positives des équations de Harkins. Des mélanges ternaires de 33% HDPE/33% PS/33% PVDF, et 33% HDPE/33% PMMA/33% PVDF, et des mélanges quaternaires de 40% HDPE/30% PS/10% PMMA/20% PVDF et 40% HDPE/10% PS/40% PMMA/10% PVDF ont été préparés. Après un recuit statique de 15 minutes dans une presse chaude à une pression de contact très faible, une augmentation substantielle dans la taille moyenne des phases est observée. Il est démontré que la coalescence se produit beaucoup plus rapidement dans les systèmes à percolation multiple que dans les mélanges binaires. L'extraction sélective par solvant dans les

structures à percolation multiple mène à la préparation de substrats avec un volume de vide plus élevé. Ainsi, un substrat de HDPE poreux entièrement interconnecté à faible surface est préparé à partir de morphologies à percolation double et triple. Les très grands pores des substrats de HDPE favorisent aussi la pénétration de la solution PANI/PSS vers la zone poreuse interconnectée. Jusqu'à 38 couches de PSS et de PANI ont été déposées sur la surface interne du substrat polymère poreux tridimensionnel, en une conformation en réseau interdiffusé. L'information sur la microstructure recueillie par MEB et par MFA dépeint une structure multicouche de polyélectrolyte relativement épaisse, jusqu'à 5,5 μm pour 38 couches de PSS et de PANI sur la surface du substrat poreux de HDPE, dont la fraction de vide est de 66 %. Cette épaisseur est attribuable à la diffusion du polyélectrolyte vers l'intérieur et vers l'extérieur dans la structure multicouche au cours du procédé CPC. Le profil de dépôt massique du PANI/PSS en fonction du nombre de couches montre une croissance non linéaire inhabituelle avec un comportement oscillatoire. Ceci implique qu'après le trempage du substrat dans la solution de PSS, la masse déposée augmente, et elle diminue ensuite après trempage dans la solution de PANI, à cause de l'enlèvement partiel d'une couche précédemment adsorbée. Dans cet article, le dépôt oscillatoire indique que les électrolytes PANI et PSS diffusent dans les couches déposées auparavant. Les chaînes entrent en contact avec des chaînes semblables, et conséquemment, un réseau interdiffusé de PANI et de PSS est généré. Puisqu'un sel est généralement ajouté dans les procédés de dépôt CPC, l'effet de l'ajout de NaCl à 1 M à l'anion PSS dans la construction de la structure multicouche est étudié. D'abord, le sel rend la structure multicouche plus uniforme. Ensuite, le comportement oscillatoire est mis en évidence par un changement dans la surcompensation des couches. Finalement, il est montré que des structures multicouches plus épaisses sont construites en présence de sel dans le polyanion; cependant, la valeur de conductivité est indépendante de la présence ou de l'absence de sel.

On en conclut que la surcompensation des charges à la surface de la structure multicouche est le résultat de deux choses : l'ajout de sel à la solution, et la faiblesse du polycation (le PANI). De plus, le déplacement de petits contre-ions et de segments de polymère chargés mène à des polymères très gonflés, puisque des molécules d'eau liées aux ions y seront introduites.

Les mesures de conductivité démontrent que le seuil de percolation du PANI dans les dispositifs poreux est atteint à un maximum de huit couches. Cette valeur correspond à 0,19 % massique de PANI pour un substrat poreux fabriqué à partir d'un mélange de 33% HDPE/ 33% PS / 33%

PVDF, et à 0,28 % pour un substrat poreux fabriqué à partir d'un mélange de 33% HDPE/ 33% PMMA / 33% PVDF. Il est montré que la conductivité de l'échantillon augmente avec l'augmentation du nombre de couches de PSS/PANI déposées, jusqu'à un plateau de saturation, qui est atteint après 32 couches déposées. Dans les matériaux poreux, la géométrie des pores (incluant la taille et la distribution des pores) joue un rôle majeur dans la conductivité du matériau, de même que la perfection du contact du matériau conducteur et la nature du matériau qui remplit les pores. La compression des échantillons poreux peut être utilisée comme un autre paramètre de contrôle, dans le but d'atteindre une large gamme de conductivités dans ces dispositifs conducteurs poreux. L'application d'une compression sur les échantillons conducteurs hautement poreux pousse et oblige les tiges et les murs du substrat à se déplacer vers l'intérieur. Pour un substrat à 67 % de porosité, la conductivité augmente de $10^{-8} \text{ S cm}^{-1}$ à 0.002 S cm^{-1} après le dépôt, mais pour un substrat à 60 % de vide, aucune déformation n'est observée.

Dans le dernier article, des mélanges ternaires à compositions variées de HDPE/PS/PMMA représentent un cas de mouillage complet, avec la formation d'une couche thermodynamiquement stable de PS entre les couches de HDPE et de PMMA. Quatre sous-catégories de morphologie thermodynamiquement stables existent pour le mélange HDPE/PS/PMMA, selon la composition des phases : a) matrice/phase dispersée coeur-coquille (60/10/30 HDPE/PS/PMMA); b) morphologie tri-continue (40/25/25); c) morphologie bi-continue/phase dispersée (50/25/25); d) matrice/deux phases dispersées distinctes (20/60/20). L'extraction par solvant, suivie de mesures gravimétriques, est utilisée pour étudier le degré de continuité des composants. La morphologie matrice/coeur-coquille dans un mélange ternaire A/B/C est constituée de gouttelettes de phase A encapsulée dans la phase B, le tout dans la matrice C. Dans ce cas, l'augmentation de la concentration du coeur induit la coalescence des phases de coeur, ce qui mène à la formation d'une morphologie tri-continue. Les structures tri-continues peuvent être classées en deux catégories : type I et type II. Dans le premier cas, la concentration de la phase centrale (PS) est assez faible pour qu'elle puisse se situer à l'interface, mis à part quelques gouttelettes dans la phase extérieure (PMMA). Dans le cas du type II, avec l'augmentation de la concentration de PS, davantage de gouttelettes de PS se situent dans le PMMA, puisque l'interface HDPE/PS/PMMA est déjà saturée de PS. Au fur et à mesure que la concentration de PS augmente, ces gouttelettes coalescent en des structures allongées, jusqu'à ce que le PS forme aussi, au sein du PMMA, une phase pleinement continue et interconnectée. Un

autre sous-type de morphologie dans le cas du mouillage complet de HDPE/PS/PMMA est celui d'une matrice avec deux phases dispersées distinctes. La morphologie bi-continue/phase dispersée est constituée d'une structure co-continue pour deux phases, avec la troisième se présentant sous forme de phase dispersée. Ce cas se produit quand la concentration de la phase centrale, qui sépare les deux autres phases, augmente, ce qui donne une structure co-continue pour la phase centrale avec une des deux autres phases. Un diagramme triangulaire de composition et de morphologie, représentant diverses compositions de HDPE/PS/PMMA, est préparé, afin de mieux comprendre la relation entre la composition et les différents états morphologiques pour le mouillage complet, et les changements de phase (interconversion). Ce diagramme montre les régimes de concentration pour : a) les mélanges tri-continus de type I et de type II; b) une morphologie de type matrice/phases dispersées distinctes, avec le PS comme matrice; c) une morphologie matrice bi-continue/phase dispersée, avec soit le HDPE, soit le PMMA sous forme de gouttelettes; d) une morphologie matrice/coeur-coquille, avec soit le PMMA ou le HDPE comme matrice. Ces régions sont déterminées par une combinaison de MEB et de FIF-MFA, et grâce à l'extraction sélective et l'analyse gravimétrique, utilisées comme technique quantitative pour repérer les points d'inversion. Des diagrammes triangulaires de continuité sont présentés pour montrer la continuité des phases de PS et de PMMA. Dans un mélange binaire, le seuil de percolation continue n'est qu'un point. Dans un mélange ternaire, il devient une courbe, à cause du changement simultané des concentrations des deux autres phases du mélange. Ce diagramme se compare aux courbes de co-continuité dans les mélanges binaires, dans lesquelles la région de continuité double et le point d'inversion de phase sont distincts. Deux courbes de composition, ou scénarios, qui recourent de multiples états morphologiques à travers le diagramme triangulaire à trois axes, sont choisis pour étudier l'effet de la concentration des phases intérieure (HDPE) et centrale (PS) sur la morphologie de la phase centrale, et l'effet de la composition de la phase intérieure (HDPE) et extérieure (PMMA) sur la morphologie de la phase centrale (PS). L'observation la plus importante pour le scénario a), où la concentration de PMMA est maintenue constante à 40 %, est qu'à cause des limitations thermodynamiques de l'étalement, le système ne peut jamais former des gouttelettes de PS, même à de très faibles concentrations de PS. Ainsi, même la plus petite quantité de PS dans le scénario a) présente une structure en couches plutôt qu'en gouttelettes. Le scénario b) indique que, au pic du diagramme

de continuité, une couche continue et parfaitement uniforme de 10 % de PS, avec une continuité de 97 %, se localise à l'interface des phases co-continues de HDPE et de PMMA.

Il est démontré que des changements radicaux dans la viscosité de la phase PMMA (L-PMMA et H-PMMA) dans un mélange PS/HDPE/PMMA de composition constante, ne modifie pas les structures morphologiques; le PS sépare toujours le HDPE et le PMMA. La viscosité du PMMA à haute masse moléculaire utilisé ici est presque 200 fois plus élevée que celle du PMMA à faible masse moléculaire, ce qui correspond à une énorme augmentation du ratio de viscosités PS/PMMA, mais ne change aucunement la classification morphologique du mélange. La phase L-PMMA se présente sous forme de nombreuses gouttelettes encapsulées de PS, alors que le H-PMMA se présente sous forme de quelques grosses gouttelettes encapsulées dans des coquilles minces de PS. L'échelle des structures morphologiques a donc été significativement altérée par la viscosité du PMMA, le système essayant de répondre à la réduction dramatique de l'aire interfaciale des gouttelettes de H-PMMA. Il est démontré que la composition, la tension interfaciale, et le ratio de viscosité jouent un rôle important dans la détermination de la taille des phases dans les mélanges polymères ternaires. Le PMMA est beaucoup moins visqueux que le PS, lui-même moins visqueux que le HDPE. Également, la tension interfaciale PS/PMMA est beaucoup plus faible que celles des couples PS/HDPE et PMMA/HDPE. Pour le cas du mélange 50/40/10 HDPE/PS/PMMA, le PMMA est présent en faible concentration (10 %), le ratio de viscosité PMMA/PS est faible, de même que la tension interfaciale PMMA/PS; ainsi, le PMMA est distribué dans la phase de PS. Dans le mélange ternaire 50/25/25 HDPE/PS/PMMA, l'augmentation de la concentration de PMMA induit la coalescence des gouttelettes de PMMA, ce qui mène à la formation de grosses gouttelettes de PMMA, tel que montré par la topographie obtenue par FIF-MFA pour ce mélange.

TABLE OF CONTENTS

DEDICATION.....	III
ACKNOWLEDGEMENTS	IV
RÉSUMÉ	V
ABSTRACT.....	IX
CONDENSÉ EN FRANÇAIS	XIII
TABLE OF CONTENTS	XXI
LIST OF TABLES	XXVIII
LIST OF FIGURES	XXIX
NOMENCLATURE.....	XL
LIST OF ABBREVIATIONS	XLIII
LIST OF APPENDICES	XLVI
CHAPTER 1 - INTRODUCTION AND OBJECTIVES.....	1
1.1 Introduction.....	1
1.2 Objectives	6
1.2.1 Specific objectives:	7
CHAPTER 2 - LITERATURE REVIEW.....	9
2.1 Polymer Blends.....	9
2.1.1 Miscible Polymer Blends.....	9
2.1.2 Immiscible Polymer Blends	12
2.1.2.1 Binary Polymer Blends	15
2.1.2.1.1 Co-continuous Morphology	15
2.1.2.1.2 Interfacial Modification of Binary Blends	20

2.1.2.2	Ternary Polymer Blends	22
2.1.2.2.1	Composite Droplet Morphology	25
2.1.2.2.2	Double-Percolated Systems.....	30
2.1.2.2.3	Effect of Composition on Ternary Blends with Complete Wetting Morphology.....	33
2.1.2.2.4	Interfacially Modified Ternary Polymer Blends	34
2.1.2.3	Quaternary Polymer Blend Systems	35
2.1.3	Porous Polymeric Substrates Prepared by Melt-Blending.....	37
2.1.3.1	Controlling the Pore Size in the Substrate	37
2.1.3.1.1	Coarsening of Binary and Ternary Polymeric Systems	38
2.2	Percolation Theory.....	40
2.2.1	Universality Systems	42
2.3	Conductive Materials	43
2.3.1	Electrically Conductive Polymers and Composites.....	45
2.3.1.1	Conducting Polymer Composite Materials (CPCM)	46
2.3.1.1.1	Parameters Influencing the Percolation Threshold of Conductive Fillers ..	49
2.3.1.1.2	Percolation Threshold of Carbon-Nanotube Polymer Composites.....	54
2.3.1.1.3	Disadvantages of Conductive Fillers, Especially Carbon Black.....	54
2.3.1.2	Intrinsically Conductive Polymers.....	56
2.3.1.2.1	Polyaniline.....	59
2.3.1.2.1.1	Binary PANI/Polymer or Ternary PANI/Polymer/Polymer Blends	59
2.4	Self-assembly Processes in Material Science	66
2.4.1	Layer-by-Layer Self-Assembly Technique.....	66
2.4.1.1	Fabrication of Conductive Multilayers by the LbL Method.....	70

2.4.1.1.1	Charged Polymer Adsorption.....	71
2.4.1.1.2	Polymer Adsorption on the Surface	73
2.4.1.1.3	Adsorption of Polyelectrolytes on the Surface of a Substrate.....	75
2.4.1.1.4	Various Mechanisms of Film Growth.....	78
2.4.1.1.5	Effect of Polyelectrolyte Concentration on Multilayers	79
2.4.1.1.6	Effect of Molecular Weight on Multilayers	80
2.4.1.1.7	Effect of Salt on Multilayers.....	81
2.4.1.1.8	Overcompensation of the Multilayer/Solution Interface.....	83
2.4.1.1.8.1	Overcompensation due to Difussion of Polyelectrolytes inside Multilayers	83
2.4.1.1.8.2	Overcompensation due to the Addition of Salt	85
2.4.1.1.9	LbL Deposition on Curved Surfaces.....	88
2.4.1.1.10	Effect of Roughness on the Multilayer Thickness	88
2.4.1.1.11	Important Views on PANI/PSS LbL Adsorption.....	89
2.4.1.1.12	Characterization Techniques for LbL Deposited Layers	90
CHAPTER 3 - ORGANIZATION OF THE ARTICLES.....		91
CHAPTER 4 - LOW PERCOLATION THRESHOLD CONDUCTIVE DEVICE DERIVED FROM A FIVE-COMPONENT POLYMER BLEND		95
4.1	Abstract.....	95
4.2	Introduction.....	95
4.3	Experimental Methods.....	102
4.3.1	Materials	102
4.3.2	Rheological Analysis	103
4.3.3	Sample Preparation.....	104
4.3.4	Solvent Extraction.....	105

4.3.5	Characterization of Phase Morphology	106
4.3.5.1	Microtoming and Scanning Electron Microscopy (SEM)	106
4.3.5.2	Focused Ion Beam (FIB), Atomic Force Microscopy (AFM)	106
4.3.6	Conductivity Measurements	107
4.4	Results and Discussions.....	107
4.4.1	Reducing the Percolation Threshold of PANI in a Multi-component Polymer Blend	107
4.4.2	Self-Assembled Onion Morphology and the Hierarchical Ordering of Phases	110
4.4.3	Generating Highly Continuous (Multiple-Percolated) Quaternary Polymer Blends	115
4.4.4	Generating Highly Continuous Quinary Polymer Blends	121
4.4.5	The Effect of Diblock Copolymer on the Morphology and Conductivity of Multiple-Percolated Blend Systems.....	125
4.4.6	The Effect of the Number of Components of Multi-Percolated Structures on Conductivity.....	127
4.5	Conclusions.....	131
4.6	Acknowledgements.....	132
CHAPTER 5 - 3D POROUS POLYMERIC MATERIAL WITH LOW PERCOLATION THRESHOLD OF CONDUCTIVE POLYMER PREPARED USING LBL DEPOSITION.....		136
5.1	Abstract.....	136
5.2	Introduction.....	137
5.3	Experimental Methods	141
5.3.1	Materials	141
5.3.2	Rheological Analysis	142
5.3.3	Substrate Preparation	143

5.3.4	Annealing Test.....	144
5.3.5	Solvent Extraction.....	144
5.3.6	Layer-by-Layer Deposition.....	145
5.3.7	Filling the Porous Sample with a Resin.....	145
5.3.8	Characterization and Phase Morphology	145
5.3.8.1	Microtomy and Scanning Electron Microscopy	145
5.3.8.2	Focused Ion Beam and Atomic Force Microscopy.....	146
5.3.8.3	Conductivity Measurements	146
5.4	Results and Discussion	146
5.4.1	Multiple-Percolated Morphology with Large Continuous Domain Phases.....	146
5.4.2	Annealing the Samples in order to Increase Pore Size	152
5.4.3	Continuity and Surface Areas of Substrates	154
5.4.4	Layer-by-Layer Deposition of PSS/PANI	156
5.4.5	Mass Deposition Dynamics of PSS/PANI.....	158
5.4.6	The Effect of Salt on the Mass Deposition Growth of PSS/PANI	162
5.4.7	Conductivity Measurement of the Conductive Porous Polymer Device	165
5.4.8	Conductivity of the Conductive Porous Polymer Device under Loads	167
5.5	Conclusions.....	168
5.6	Acknowledgements.....	169
5.7	References.....	169
CHAPTER 6 - MORPHOLOGICAL STATES FOR A TERNARY POLYMER BLEND DEMONSTRATING COMPLETE WETTING.....		172
6.1	Abstract.....	172
6.2	Introduction.....	173

6.3	Experimental	177
6.3.1	Materials	177
6.3.2	Rheological Analysis	178
6.3.3	Sample Preparation	179
6.3.4	Solvent Extraction.....	179
6.3.5	Characterization of Phase Morphology	180
6.3.5.1	Microtoming and Scanning Electron Microscopy (SEM)	180
6.3.5.2	Focused Ion Beam (FIB) and Atomic Force Microscopy (AFM)	181
6.4	Results and Discussion	181
6.4.1	Matrix/Core-Shell Dispersed Phase Morphology.....	182
6.4.2	Tri-continuous Morphology.....	184
6.4.3	Matrix/ Two Separate Dispersed Phases Morphology.....	185
6.4.4	Bi-Continuous/Dispersed Phase Morphology.....	186
6.4.5	Triangular Composition/Morphology Diagram.....	187
6.4.6	Continuity, Co-continuity, and Tri-continuity of Phases.....	191
6.4.7	Morphology Evolution due to Concentration Ratio of Two Components in Complete Wetting Case	194
6.4.8	Observations on the Effect of Viscosity on the Morphological State.....	199
6.4.9	Factors Influencing Phase Sizes.....	201
6.5	Conclusions.....	203
6.6	Acknowledgement	204
6.7	References.....	204
CHAPTER 7 - GENERAL DISCUSSIONS AND PERSPECTIVE.....		206
CONCLUSION AND RECOMMENDATIONS.....		209

REFERENCES..... 211
APPENDICES..... 234

LIST OF TABLES

Table 2-1. Relationship between concentration of the Polyanion and thickness of the Monolayers in L-b-L deposition technique(Cheung, et al., 1997).....	80
Table 4-1. Material Characteristics.....	103
Table 4-2. Surface Tension, Polar Contribution, Dispersive Contribution, Polarity, and Rate of Surface Tension per Temperature for Homopolymers	109
Table 4-3. Theoretical and Experimental Interfacial Tension for Polymer Pairs.....	109
Table 4-4. Spreading Coefficients in Different Ternary Blends and Predicted Order of Phases in Blends	112
Table 4-5. Number of Components and Compositions of Samples Shown in Figure 4-14.....	128
Table 5-1. Characteristic Properties of Homopolymers	141
Table 5-2. Composition of Polymer Components in Ternary and Quaternary Blends.....	143
Table 5-3. Continuity of the Porous Morphology With and Without annealing (PS, PMMA and PVDF extracted).....	154
Table 5-4. Surface Area Measurements of Porous Polymer Substrates by BET.....	154
Table 5-5. Comparison of Surface Areas Reported in Previous Studies and in the Current Work (last two rows).	156
Table 6-1. Material Characteristics.....	177
Table 6-2. Interfacial Tension of Polymer Pairs from (Reignier & Favis, 2000) and Positive Spreading Coefficient of Ternary Blends	178

LIST OF FIGURES

Figure 1-1. a) Capillary vessels in eye(Malek et al., 2005) b) renal corpuscles tissue (Rahmy, 2001) c)(Rahmy, 2001) Hypertrophied parietal cell d)(Rahmy, 2001) Epithelial lining cells of a proximal convoluted	2
Figure 1-2. Human heart, longitudinal collagen fibers (bar = 50 μ m)(Wang Gusukuma, Prates, & Smith, 2004).....	3
Figure 1-3. a), b), c) Some of the polymer blend samples observed by Veeco lab(http://www.veeco.com/library/resources/Sample_Preparation/index.aspx), d)three-phase contact morphology(Virgilio, Desjardins, L'Esperance, & Favis, 2009), e)two-phase contact morphology(Zhang, Ravati, Virgilio, & Favis, 2007), f) Spherulitic crystallization behavior of polymers(Feng & Kamal, 2005) g) gold nanoparticles and their incorporation into polymer matrices(Meli & Lennox, 2003)	4
Figure 1-4. a), b) A model of the polyurethane foam made of interconnected rods, b) a model of interconnected macroporosity, c)ultra-porous structure with 99% porosity made of PDADMAC/BSA(Roy, Sarazin, & Favis, 2006)	4
Figure 1-5. MIT and Cambridge University scientists developed this tissue scaffold that could help repair knees and other joints. The top section, indicated by the green arrow, stimulates bone growth, while the lower half, marked by the orange arrow, stimulates cartilage growth(http://web.mit.edu/newsoffice/2009/cartilage-0511.html).....	5
Figure 2-1. Electrical conductivity versus PANI content of polymer/PANI binary blends(Zilberman, et al., 2000d).....	20
Figure 2-2. Action of the diblock copolymer to reduce the pore size for 50/50 PLLA/PS blends at copolymer concentrations of (a) 2.5%, (b) 5%, (c) 8%, (d) 12%, (e) 15%, and (f) 20%. Copolymer concentration shown is based on the weight of polystyrene. The white bar indicates 1 micron(Sarazin & Favis, 2003).....	21

Figure 2-3. a), b), c) Ternary blends with partial wetting case, and d), e), f) ternary blends with complete wetting case	23
Figure 2-4. SEM micrographs of the 80 (HDPE) /20 (PS/PMMA) I) a) fracture surface etched with acetic acid for 2 min, 14%PS/86%H-PMMA; b) microtomed surface etched 24 h with cyclohexane, 9%PS/91%H-PMMA; and c) microtomed surface etched 24 h with cyclohexane, 9%PS/91%L-PMMA, II) Evolution of the shell formation process with increasing PS content (vol. % based on the dispersed phase) for the 80(HDPE)/20(PS/L-PMMA)(cryofractured samples after being etched for 10 s with acetic acid).....	26
Figure 2-5. SEM micrograph of 70PA6/15PP/15PS blends: (a) cryofractured and (b) chloroform extracted surfaces.(Harrats, et al., 2005).....	27
Figure 2-6. Dependence of the composite dispersed morphology on PS and PMMA molecular weights. SEM photomicrographs of (a) HDPE/L-PS/L-PMMA; PMMA is extracted by acetic acid and (b) HDPE/H-PS/H-PMMA; PS is extracted by cyclohexane. The white bar denotes 1 μm (Reignier, et al., 2003).	29
Figure 2-7. a, b) FIB-AFM images of HDPE/PS/PMMA ternary blends. The white line in Figure 7b indicates the section analyzed below, and c) Continuity of PS or PMMA as a function of the composition using the solvent dissolution technique(Zhang, et al., 2007)	30
Figure 2-8. Scanning electron micrograph of a) 40PA6/30PP/30PS; formic acid extracted surfaces, and b) 40PA6/(25/5)(PP/PP-MA2)/(25/5)(PS/SMA2); formic acid extracted surfaces (Harrats, et al., 2005).....	31
Figure 2-9. Electrical conductivity versus LLDPE content for CoPA/LLDPE/PANI ternary blends containing 10 and 20 wt% PANI(Zilberman, et al., 2000b).....	32
Figure 2-10. Electrical conductivity versus LLDPE content for (PS/DOP)/LLDPE/PANI blends containing 10 and 20 wt% PANI(Zilberman, et al., 2000b).....	32
Figure 2-11. a) 70%HDPE/15%PS/15%PMMA, b) 15%PMMA/70%PS/15%HDPE(PMMA extracted fracture surface), and c) 70%PMMA/15%PS/15%HDPE (PS extracted fracture surface) (Guo, Packirisamy, et al., 1997)	33

- Figure 2-12. SEM photomicrograph of a) 70%HDPE(A)/20%PP(B)/10%PS(C), b) 70%HDPE(A)/20%PP(B)/10%PS(C) + 0.5% S-E block copolymer, and c) 70%HDPE(A)/20%PP(B)/10%PS(C) + 2% S-E block copolymer(Guo, Packirisamy, et al., 1997)..... 35
- Figure 2-13. SEM photomicrograph of a) 10%PMMA(D)/10%PS(C)/60%PP(A)/20%HDPE(B), b) 10%PMMA(D)/60%PS(A)/20%PP(B)/10%HDPE(C), c) 60%PMMA(A)/20%PS(B)/10%PP(C)/10%HDPE(D), and d) 10%PMMA(D)/10%PS(C)/20%PP(B)/60%HDPE(A)(Guo, Gvozdic, et al., 1997) 36
- Figure 2-14. Coarsening process in co-continuous structure upon annealing.(a) the thin rod merges/flows into thick ones at both sides, the thick rod merges into a much thicker one at the same time; (b) the thin rod becomes thinner during the merging process; (c) the thin rod breaks/splits; and (d) the residual parts retract/shrink to the thick rods.(Yuan, 2005) 39
- Figure 2-15. Experimental pore size growth (points) with the theoretical model (solid lines) for different blends annealed at 200°C. (Yuan, 2005) 40
- Figure 2-16. Detail of a bond percolation on the square lattice in two dimensions with percolation probability $p=51$ (Stauffer & Aharony, 1994b) 41
- Figure 2-17. Logarithmic conductivity ladder locating some metals and conducting polymers(Pratt, 2001)..... 44
- Figure 2-18. Simultaneous measurement of the nanocomposite (MWCNT/epoxy) electrical conductivity as function of the nanotube weight fraction, performed in the liquid state prior to curing at 0.1 s^{-1} and $20 \text{ }^\circ\text{C}$. The rheological percolation threshold is located at 0.1 wt% and the electrical one at 0.04 wt%(Du, et al., 2004). 47
- Figure 2-19. Approaching the percolation threshold in a binary blend 49
- Figure 2-20. Schematic illustrations of conductivity establishment for polymer composites with (a) spherical fillers, (b) high aspect ratio fillers (fiber/wire) and (c)

percolation threshold (V_c) in a resistivity vs. filler loading plot(Wong, 2003-2008)	50
Figure 2-21. Transmission electron micrograph of silver nanowires(Wong, 2003-2008)	51
Figure 2-22: Dependence of PE continuity fraction on the CB content in 5/95 and 10/90	53
Figure 2-23. TEM micrograph of a 50/50 PS/PMMA blend filled with 2 wt% CB.....	54
Figure 2-24. Plot of the total number of publications per polymer system versus the minimum percolation threshold achieved with the respective system(Bauhofer & Kovacs, 2009).	55
Figure 2-25. Resistivity of carbon black/polymer composite as a function of carbon black volume fraction(Rosner, 2000)	55
Figure 2-26. The structure of a number of intrinsically conducting polymers (ICP).	58
Figure 2-27. Transmission electron micrographs of extracted PANI-CSA/PMMA polyblend films containing (a) Vol% = 0.5% , and (b) Vol% = 0.25% PANI-CSA(Yang, et al., 1993a).....	62
Figure 2-28. a) Conductivity vs volume fraction(f) of PANI-CSA at $T=300K$ and $T=10K$, b) conductivity vs ($f-f_c$) where percolation threshold (f_c) is 0.3%. The solid lines through the points correspond to $t=1.99$ at $T=10K$ and $t=1.33$ at $T=300K$ (Yang, et al., 1993a).....	62
Figure 2-29: Conductivity vs. concentration of PANI/polymer prepared via a) dispersion mixing, b) melt-blending(Narkis, et al., 2000a).....	63
Figure 2-30. Electrical conductivity vs. CoPA content for (PS/DOP)/CoPA/PANI-pTSA blends of various PANI-pTSA contents(Narkis, et al., 2000a).....	64
Figure 2-31: Conductivity of PVDF/PANI and pure doped PANI as a function of PANI content(Wt%).....	65
Figure 2-32: Conductivity of PANI/PVDF binary blend based on PANI concentration a) (Malmonge, et al., 2006) and b) (Privalko, et al., 2005).....	65
Figure 2-33. LbL multilayers publications per year	69

Figure 2-34. Schematic view of different polymer types: (a) linear homopolymers that are the main subject of this review, (b) branched polymers, (c) charged polymers or polyelectrolytes (PEs), and (d) a disordered copolymer with no specific order of the different monomers.	71
Figure 2-35. Schematic view of the four scaling ranges in the Gaussian-persistent regime(Netz & Andelman, 2003).....	72
Figure 2-36. Different possibilities of substrates: (a) the prototype, a flat, homogeneous substrate; (b) a corrugated, rough substrate. Note that experimentally, every substrate exhibits a certain degree of roughness on some length scale; (c) a spherical adsorption substrate, such as a colloidal particle. If the colloidal radius is much larger than the polymer size, curvature effects (which means the deviation from the planar geometry) can be neglected; (d) a flat but chemically heterogeneous substrate;	74
Figure 2-37. The ‘tail’, ‘train’ and ‘loop’ sections of the adsorbing chain.....	75
Figure 2-38. Schematic drawing of single-chain adsorption. (a) In the limit of strong coupling, and (b) in the case of weak coupling.....	76
Figure 2-39. Macromolecule with a) small persistence length, b) medium persistence length, and c) large persistence length.....	77
Figure 2-40. Schematic picture of a) the adsorbed polymer layer when the effective persistence length is large, (b) Adsorbed layer for the case when the persistence length is small. In this case the polymer forms a random coil with many loops	77
Figure 2-41. Deposition of layer in LbL process a) in the absence of salt and b) in the presence of salt.....	81
Figure 2-42. Surface charge in LbL process as a function of salt concentration(Schlenoff & Dubas, 2001)	82
Figure 2-43. Penetration of polyelectrolyte chain inward and outward of a multilayer film	84
Figure 2-44. Displacement of polyelectrolyte ions with salt counter-ions	86

- Figure 4-1. Schematic representation of (a) the complete wetting case where phase B spreads between, and fully separates, phases A and C and (b) the partial wetting case all phases are in contact with each other 97
- Figure 4-2. Complex viscosity as a function of frequency at 190°C for the homopolymers. The complex viscosity of PANI is at 180°C. 104
- Figure 4-3. a) FIB-AFM image of the composite-droplet morphology of 30/10/60 HDPE/PS/PMMA showing PS as a layer separating HDPE and PMMA. Scan size is $5\mu\text{m}\times 5\mu\text{m}$. The bar to the right of the FIB/AFM micrograph indicates the colours associated with the topographical height in nm. The white line in the image indicates the section analyzed below, and b) SEM micrograph of a 45/10/45 HDPE/PVDF/PANI blend after extraction of the PVDF phase by DMF. The voids show that PVDF was present as a layer separating HDPE and PANI. 108
- Figure 4-4. Schematic illustration of various encapsulated structures, a) dispersed phase B in matrix A, b) core-shell morphology B/C in matrix A, c) quaternary onion morphology B/C/D in matrix A, and d) quinary onion morphology B/C/D/E in matrix A. 111
- Figure 4-5. SEM micrograph of a) matrix-droplet morphology of 80/20 PMMA/PS, b) PVDF core-PMMA shell morphology in an HDPE matrix for 60/20/20 HDPE/PMMA/PVDF (PMMA extracted), and c) onion morphology in an HDPE matrix for 60/13/13/13 HDPE/PS/PMMA/PVDF (PMMA extracted) 113
- Figure 4-6. SEM micrographs of 50/10/20/10/10 HDPE/PMMA/PS/PVDF/PANI after extraction of (a) all phases except HDPE, (b) PS by cyclohexane (c) PMMA by acetic acid, and (d) PS and PMMA by combining cyclohexane and acetic acid..... 115
- Figure 4-7. SEM micrographs and schematics of HDPE/PS/PMMA/PVDF after extraction of PMMA by acetic acid for a) and b) onion morphology in an HDPE matrix for 60/13/13/13, c) and d) more elongated morphology of 50/17/17/17, and e) triple-percolated morphology of 30/15/15/40 (microtomed surface). The voids show that PMMA is present as a layer separating PS and PVDF. 117

- Figure 4-8. SEM micrographs of various quaternary HDPE/PS/PMMA/PVDF blends after microtoming and extraction of the PMMA phase; (a) 10/15/15/60, (b) 20/15/15/50, (c) 30/15/15/40, (d) 40/15/15/30, (e) 50/15/15/20, (f) 60/15/15/10. .. 118
- Figure 4-9. Continuity level of PS, PMMA, and PS+PMMA obtained by solvent extraction/gravimetry for 6 blends comprised of HDPE/PS/PMMA/PVDF; (a) 10/15/15/60, (b) 20/15/15/50, (c) 30/15/15/40, (d) 40/15/15/30, (e) 50/15/15/20, (f) 60/15/15/10. 120
- Figure 4-10. SEM micrographs of the multi-percolated 30/15/15/30/10 blend comprised of HDPE/PS/PMMA/PVDF/PANI after extraction of (a) all phases except HDPE, (b) PMMA by acetic acid (c) PS by cyclohexane, (d) PS and PMMA by combining cyclohexane and acetic acid, and (e) PANI by chromic acid 122
- Figure 4-11. SEM micrographs of a), b) continuous PANI network of quaternary 25/25/25/25 PS/PMMA/PVDF/PANI blend after extraction of all phases by DMF followed by a freeze drying process, and c, d, e) continuous PANI network derived from a 15/20/15/25/25 PS/PS-co-PMMA/PMMA/PVDF/PANI blend after extraction of all phases by DMF followed by freeze drying process. The thickness of the PANI network walls are shown in Figure 4-11e..... 123
- Figure 4-12. a) Schematic representation of quinary multi-percolated morphology, the yellow phase is PANI, the blue phase is HDPE, and all other phases are located between them, b) schematic of a PANI network obtained after removal of all phases except PANI, and c) a 3D image constructed from 2D SEM images of the interconnected PANI network in the quinary 15/20/15/25/25 PS/PS-co-PMMA/PMMA/PVDF/PANI blend after extraction of all other phases. 124
- Figure 4-13. SEM micrograph of a) 30/30/30/10 PMMA/PS/PVDF/PANI blend after extraction of PS and PMMA, b) 20/20/20/30/10 PS/PS-co-PMMA/PMMA/PVDF/PANI after extraction of PS and PMMA, c) 30/30/30/10 PMMA/PS/PVDF/PANI blend after extraction of PANI by chromic acid, and d) 20/20/20/30/10 PS/PS-co-PMMA/PMMA/PVDF/PANI after extraction of PANI by chromic acid..... 126

- Figure 4-14. Conductivity of multi-percolated blends of ternary, quaternary, quinary, as well as interfacially modified quaternary and quinary systems as a function of the volume fraction of PANI. Note that point O is a co-continuous binary blend of PS and PANI. 129
- Figure 5-1. 3D schematic showing the approach used to prepare the porous polymeric conducting device via LbL deposition. (a) solid multi-percolated structure comprised of HDPE, PS, PMMA and PVDF after melt blending and annealing; (b) porous polymeric conducting device after extraction of PS, PMMA and PVDF, followed by LbL deposition of PSS and PANI. 147
- Figure 5-2. (a) FIB-AFM topographic surface image of 40/20/40 HDPE/PS/PMMA. The topographical height vs distance is shown to the right. The white line in the image indicates the trace line used in the height vs distance analysis. and (b) Scanning electron micrograph of 40/10/50 HDPE/PS/PMMA after extraction of the PS phase by cyclohexane 148
- Figure 5-3. Scanning electron micrographs of binary and ternary samples after extraction of all phases (except polyethylene) by DMF for and (a) 33/33/33 HDPE/PMMA/PVDF, (b) 33/67 HDPE/PVDF, and (c) 50/50 HDPE/PVDF 149
- Figure 5-4. Scanning electron micrographs of quaternary polymer blends for various compositions compounded via melt-blending (a) 50/16/16/16 HDPE/PS/PMMA/PVDF after extraction of PMMA by acetic acid, (b) 50/20/10/20 HDPE/PS/PMMA/PVDF after extraction of PMMA by acetic acid, (b) 50/20/10/20 HDPE/PS/PMMA/PVDF after extraction of PS by cyclohexane, and d) 40/10/40/10 HDPE/PS/PMMA/PVDF after extraction of all phases except HDPE 151
- Figure 5-5. Scanning electron microscope images of the morphologies of the porous structures showing the influence of annealing. The top row is without annealing, the bottom row is after annealing. All components have been extracted except HDPE. a),e) Sample (A); b),f) Sample (B); c),g) Sample (C); and d),h) Sample (D). 153

- Figure 5-6. a),b) Scanning electron micrographs of the morphology of sample (B) after extraction of PMMA, PVDF and deposition of 38 PSS/PANI layers; c),d) SEM and FIB-AFM of sample(B) after extraction of PMMA, PVDF and deposition of 38 PSS/PANI layers. Pores are filled with epoxy resin. 157
- Figure 5-7. Mass increase (%) indicating cumulative deposited mass as a function of number of deposited PSS and PANI layers for solutions containing salt and without salt. a) sample(A); b) sample (B); c) sample(C); and d) sample (D)..... 160
- Figure 5-8. Schematic of exponential growth of PSS/PANI multilayer thickness on the internal surface of the substrate. 162
- Figure 5-9. Mass increase (%) indicating cumulative deposited mass as a function of number of deposited PSS and PANI layers for sample (A). a) solution containing salt, and b) solution without salt. 165
- Figure 5-10. Conductivity as a function of the number of deposited layers for various samples at a 5 lb load. The effect of a 10 lb load is shown for two samples as indicated by the arrows. 165
- Figure 6-1. (a) schematic representation of the evolution of morphology in a binary blend, (b) matrix/dispersed morphology, and (c) co-continuous morphology 173
- Figure 6-2. Schematic representation of (a) complete wetting: the case that one phase locates between two other phases, and (b) partial wetting: the case that all phases are in contact with each other 176
- Figure 6-3. Complex viscosity as a function of frequency at 190°C for homopolymers..... 179
- Figure 6-4. FIB-AFM image of complete wetting morphology for ternary 40/20/40 HDPE/PS/PMMA blend showing the layer of PS at the interface of HDPE and PMMA. Scan size is $25\mu\text{m}\times 25\mu\text{m}$. The bar to the right of the FIB/AFM micrograph indicates the colours associated with the topographical height in nm. The white line in the image indicates the section analyzed. 182
- Figure 6-5. (a) Schematic representation of the matrix/core-shell dispersed phase morphology, (b) SEM micrograph of 60/10/30 HDPE/PS/PMMA blend after extraction of PS by cyclohexane, (c) schematic representation of tri-continuous

morphology (type I), (d) FIB-AFM image of 40/20/40 HDPE/PS/PMMA showing tri-continuous morphology. Scan size is $25\mu\text{m}\times 25\mu\text{m}$. The bar to the right of the FIB/AFM micrograph indicates the colours associated with the topographical height in nm, (e) schematic representation of tri-continuous(type II), (f) SEM micrograph of 30/30/40 HDPE/PS/PMMA after extraction of PS by cyclohexane, (g) schematic representation of matrix/two separate dispersed phases morphology, and (h) SEM micrograph of 10/80/10 HDPE/PS/PMMA microtomed. 184

Figure 6-6. a) Schematic representations of bi-continuous/dispersed phase morphology with small droplets of white phase, b) FIB-AFM image of 50/40/10 HDPE/PS/PMMA showing bi-continuous/dispersed phase morphology with small droplets of PMMA. Scan size is $8\mu\text{m}\times 8\mu\text{m}$, (c) FIB-AFM image of 50/25/25 HDPE/PS/PMMA showing bi-continuous/dispersed phase morphology with droplets of PMMA. Scan size is $4\mu\text{m}\times 4\mu\text{m}$, d) schematic representations of bi-continuous-dispersed phase morphology with small droplets of black phase, e) FIB-AFM image of 10/30/60 HDPE/PS/PMMA showing bi-continuous/dispersed phase morphology with droplets of HDPE. Scan size is $11.7\mu\text{m}\times 11.7\mu\text{m}$, and f) SEM micrograph of 10/30/60 HDPE/PS/PMMA after extraction of PS. Small droplets of HDPE are distributed in PS 187

Figure 6-7: Evolution of the morphology in a ternary A/B/C blend demonstrating complete wetting as a function of the concentration of phases B and C. Phase A concentration is held constant. 188

Figure 6-8. a) Triangular concentration diagram showing the composition of the various ternary HDPE/PS/PMMA blends examined in this study, b) various morphological states for ternary HDPE/PS/PMMA, and c) triangular concentration diagram showing the various regions of in the morphological states for ternary HDPE/PS/PMMA 190

Figure 6-9. Continuity diagrams for ternary HDPE/PS/PMMA blends. a) quantitative continuity level of PMMA (percolation threshold line is shown in black), b) quantitative continuity level of PS (percolation threshold line is shown in black),

- and c) triangular concentration diagram showing the various regions of in the morphological states for ternary HDPE/PS/PMMA after correction with the PS and PMMA continuity data..... 193
- Figure 6-10. Triangular concentration diagram showing two pathways: Continuity Scheme (a), and Continuity Scheme (b). Scheme (a) is shown in Figure 6-11 and represents the case where the concentration of PMMA is kept constant at 40% of total while the concentration ratio of the PS and HDPE phases change. Scheme (b) is shown in Figure 6-12 where the concentration of PS is kept constant at 10% of total while the concentration ratio of PMMA and HDPE phases change. These two pathways were chosen since they pass through a range of different morphological states. 195
- Figure 6-11. PS continuity and the corresponding morphology as a function of HDPE concentration following Scheme (a) from Figure 6-10. The PMMA phase concentration is held constant at 40% volume fraction in all samples. In the schematics, green is the PMMA phase, red is the PS phase and blue is the HDPE phase..... 196
- Figure 6-12. PS continuity and the corresponding morphology as a function of HDPE concentration following Scheme (b) from Figure 6-10. The PS phase concentration is held constant at 10% volume fraction in all samples. In the schematics, green is the PMMA phase, red is the PS phase and blue is the HDPE phase..... 198
- Figure 6-13. SEM micrograph of morphology of (a) 35/40/25 HDPE/PS/L-PMMA after extraction of L-PMMA by acetic acid, (b) 35/40/25 HDPE/PS/L-PMMA after extraction of PS by cyclohexane, (c) 35/40/25 HDPE/PS/H-PMMA(cryofracture), (d) 35/40/25 HDPE/PS/H-PMMA after extraction of PMMA by acetic acid, and (e) 35/40/25 HDPE/PS/H-PMMA after extraction of PS by cyclohexane, 200
- Figure 6-14. FIB-AFM topographic surface image of HDPE/PS/PMMA at various compositions, (a) 50/40/10, (b) 50/25/25, and (c) 10/30/60. The white lines in the images indicate the sections analyzed for each blend..... 202

NOMENCLATURE

A	cross-sectional area
a	order parameter
A_{ij}	interfacial area
F	Helmholtz free energy
f	shape factor of pores
G	conductance of porous material
G	Gibbs free energy
G	storage modulus
G_0	conductance of the pure material
G_{mix}	Gibbs free energy of the mixture
H	enthalpy
H_{mix}	enthalpy of mixing
I	electric current
k	Boltzmann constant
l	length
l	length of the sample
L_{el}	Gaussian segment length
m_i	mass of component (i)
M_i	Number of segments of polymer i
M_w	weight average molecular weight
N	number of molecules

n	number of moles
p	concentration of the conductive material
P	probability
p_c	percolation threshold concentration of conductive material
R	resistance
R_0	initial radius of droplet
R_{el}	Gaussian blob size
S	entropy
S_{mix}	entropy of Mixing
t	dimensionless index for percolation equation
T	absolute temperature
$\tan \delta$	the ratio of storage modulus to loss modulus
V	electric voltage
V_i	volume of component (i)
V_s	volume of segments
W_a	work of adhesion
X^P	polarity

Greek letters

γ_i^d	dispersive contribution to the surface tension of component (i)
γ_{ij}	interfacial tension between phases (i) and (j)
γ_i^p	polar distribution to the surface tension of component (i)

$\dot{\gamma}$	shear stress
$\eta(\dot{\gamma})_i$	viscosity of phase i at specific shear stress
η_0	zero shear viscosity
λ	wavelength of the distortion in Tomotika's equation
λ	viscosity ratio
λ_{ij}	spreading coefficient of phase (i) over phase (j)
ρ_i	density of component (i)
ρ	resistivity
σ	conductivity of the porous material
σ_0	conductivity of the pure material
ϕ_m	maximum packing volume fraction
ϕ_c	percolation threshold
Θ	porosity
ξ	relative linear dimension of the contact in conductive network
φ_i	volume fraction of phase i
χ	Flory-Huggins interaction
Ω	number of configuration of molecules\

LIST OF ABBREVIATIONS

AFM	atomic force microscopy
BET	Brunauer Emmett and Teller nitrogen adsorption technique
CB	carbon black
CLSM	confocal laser scanning microscopy
CoPA	copolyamide
CPC	conductive polymer composite
CPCM	conducting polymer composite material
CSA	camphor-10-sulfonic acid
DBSA	dodecylbenzenesulfonic acid
DMA	dimethylacetamide
DMF	dimethylformamide
DNNDSA	dinonylnaphthalenedisulfonic acid
DOP	dioctyl phthalate
EB	emeraldine base
FIB	focused ion beam
HA	hyaluronan
HDPE	high density polyethylene
H-PMMA	high molecular weight poly(methyl methacrylate)
ICP	intrinsically conducting polymer
LbL	Layer-by-Layer technique
LED	light emitting diode
LLDPE	linear low density polyethylene

L-PMMA	low molecular weight poly(methyl methacrylate)
MWCNT	multi-wall carbon nanotube
OWLS	optical waveguide lightmode spectroscopy
PA	polyacetylene
PA6	polyamide 6
PAA	poly(acrylic acid)
PAH	poly(allylamine hydrochloride)
PANI	polyaniline
PCL	poly(ϵ -caprolactone)
PDADMAC	poly(diallyldimethylammonium chloride)
PDADMAC	polydiallyl dimethyl ammonium chloride
PEM	polyelectrolyte multilayer
PEMA	poly(ethyl methacrylate)
PET	polyethylene terephthalate
PFU	polyfuran
PGA	poly(L-glutamic acid)
PI	polyimide
PLL	poly(L-lysine)
PLLA	poly(L-lactide)
PMMA	poly(methyl methacrylate)
PP	polypropylene
PPP	poly <i>p</i> -phenylene
PPY	polypyrrole
PS	polystyrene

PS-co-PMMA	copolymer of PS and PMMA
PSS	poly(sodium 4-styrenesulfonate)
PT	polythiophene
PU	polyurethane
PVA	polyvinyl alcohol
PVC	polyvinyl chloride
PVDF	Polyvinyl difluoride
QCM	quartz crystal microbalance
SEB	styrene-ethylene-butylene diblock copolymer
SEBS	styrene-ethylene-butylene-styrene triblock copolymer
SEM	scanning electron microscopy
SMA	styrene-maleic anhydride copolymer
SPM	streaming potential measurements
SPR	surface plasmon resonance
TSA	toluenesulfonic acid

LIST OF APPENDICES

A- 1	Ultra-Low Percolation Thresholds in Ternary Co-Continuous Polymer Blends.....	234
A- 2	Estimation of Conductivity of Porous Conductive Devices by Semi-Empirical Models	246
A- 3	Mechanism of Aggregation of Weak Polyelectrolytes	250
A- 4	Relationship between Conductivity and Morphology of Ternary Polymer Blends	252

CHAPTER 1 - INTRODUCTION AND OBJECTIVES

1.1 Introduction

The study of the development of morphology in immiscible polymer blends is a domain of great interest due to the influence of morphology on the physico-mechanical properties of the materials as well as the control of the microstructure. Although obtaining desired properties (Paul & Newman, 1978) by blending two or several components is a key challenge in polymer blends, it is also important because novel complex microstructures for special applications can be prepared. Polymer melt-blending is even more interesting, since by controlling the determining parameters in the liquid-state, desirable structures with different geometries can be obtained. Therefore, providing the required thermodynamic and kinetic conditions for a multi-component blend processed via melt-blending results in the preparation of the desired self-assembly (the notion that physical or chemical driving forces produce the necessary material microstructure without the need for any external intervention) materials. For example, a binary blend of 40/60 polymer A/polymer B can show both matrix-dispersed morphology and co-continuous structure depending on the mentioned properties. This implies that these systems, due to governing properties, self-assemble to matrix-dispersed morphology or co-continuous morphology. Ternary polymer blends in the polymer blend world is a critical case. It has been shown that due to thermodynamic properties, three polymers can either be in contact with one another and make three-phase contact, or one polymer can separate the second and third ones. These two cases are seen in all the systems where liquids are in contact with each other. The most important ones are detected in cell structures. Some of the examples are represented in Figure 1-1. More complicated cases can be found in cell structures as phases hierarchically assembled in order (Figure 1-2).

A key challenge in polymer blends is how to provide the system requirements to obtain desired morphologies. The structures shown in Figure 1-1 are very close to the thermodynamically controlled self-assembled structures made by polymer blends. In this case, the goal is designing novel materials and finally replacing them with real materials or applying them in high-technology applications. Some of the important structures produced are introduced in Figure 1-3.

Particular morphologies can be developed by employing block copolymers as compatibilizers in polymer blends and as templates for ordered structures.

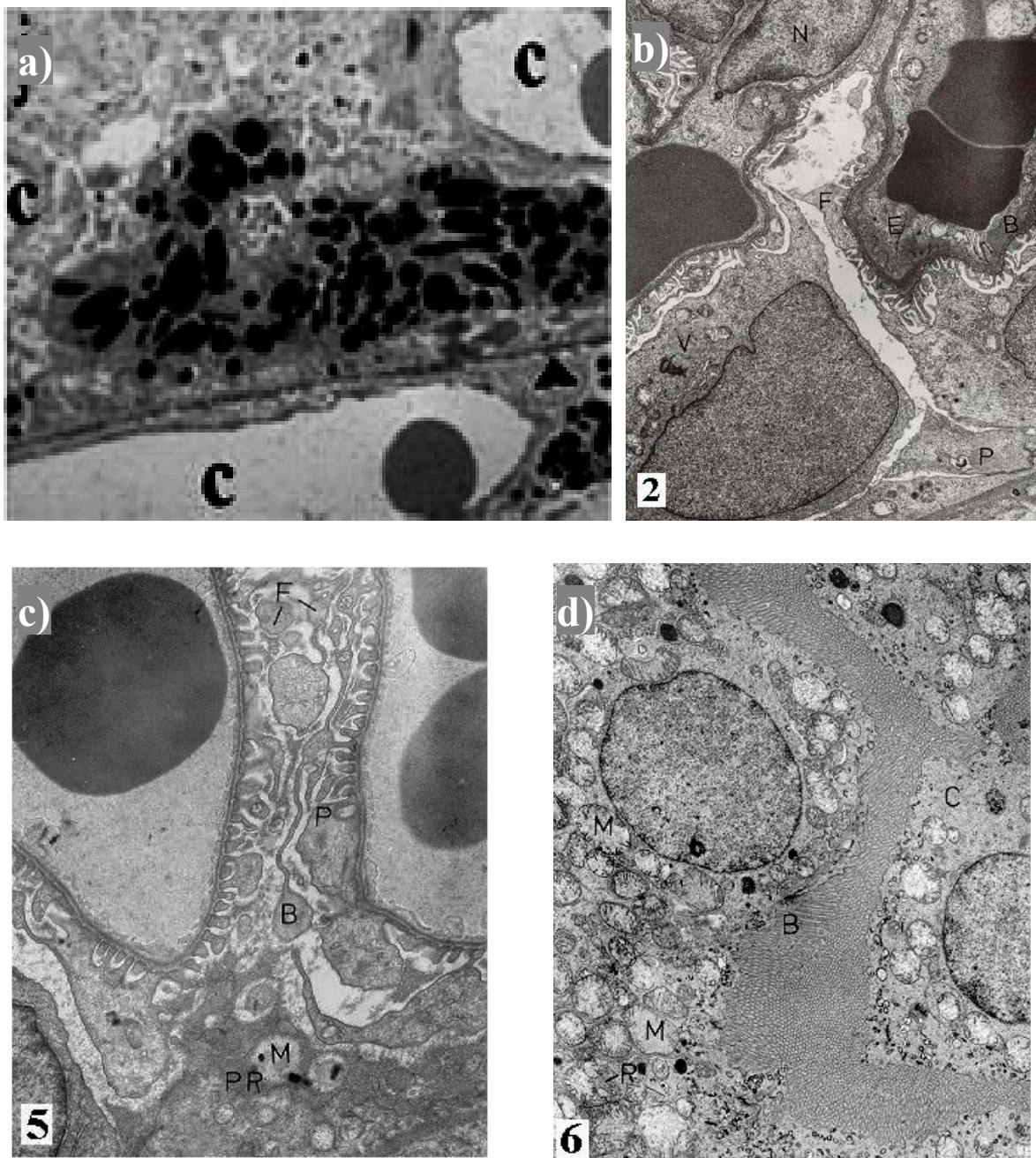


Figure 1-1. a) Capillary vessels in eye(Malek et al., 2005) b) renal corpuscles tissue (Rahmy, 2001) c)(Rahmy, 2001) Hypertrophied parietal cell d)(Rahmy, 2001) Epithelial lining cells of a proximal convoluted

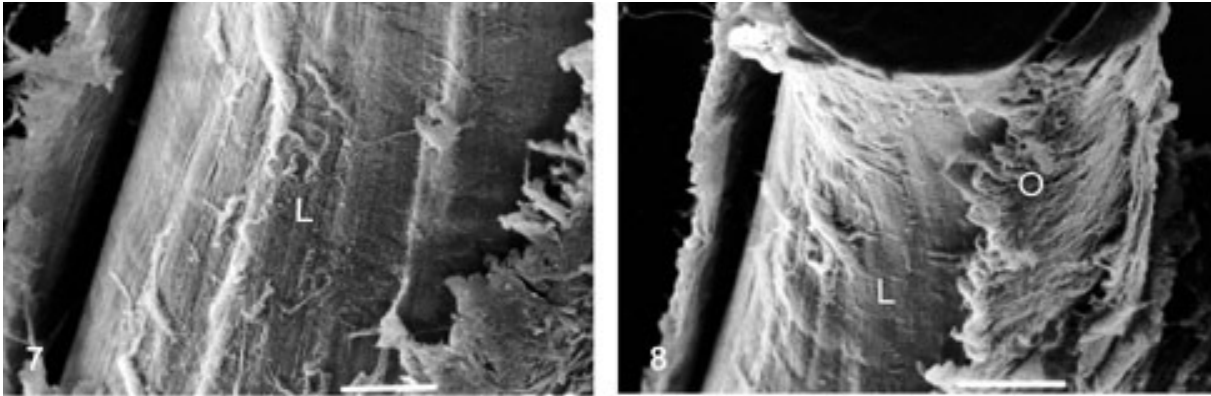
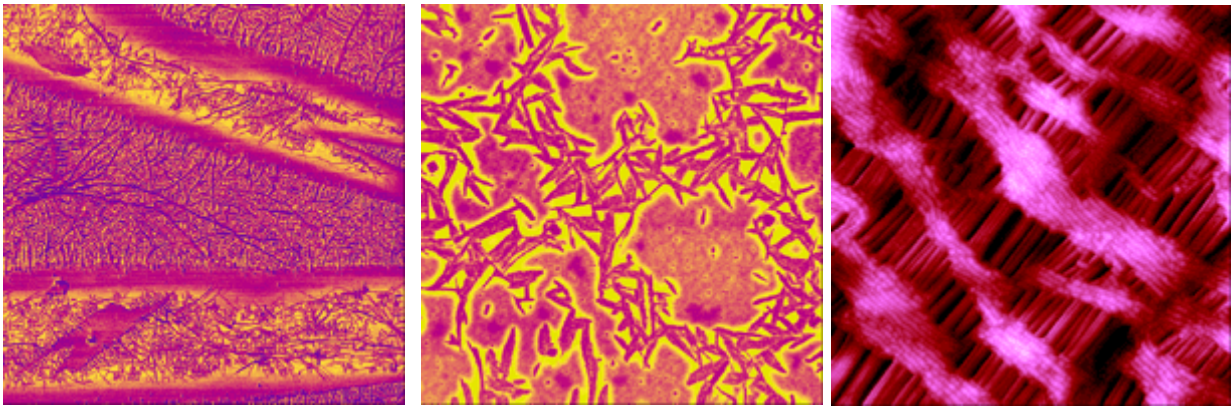
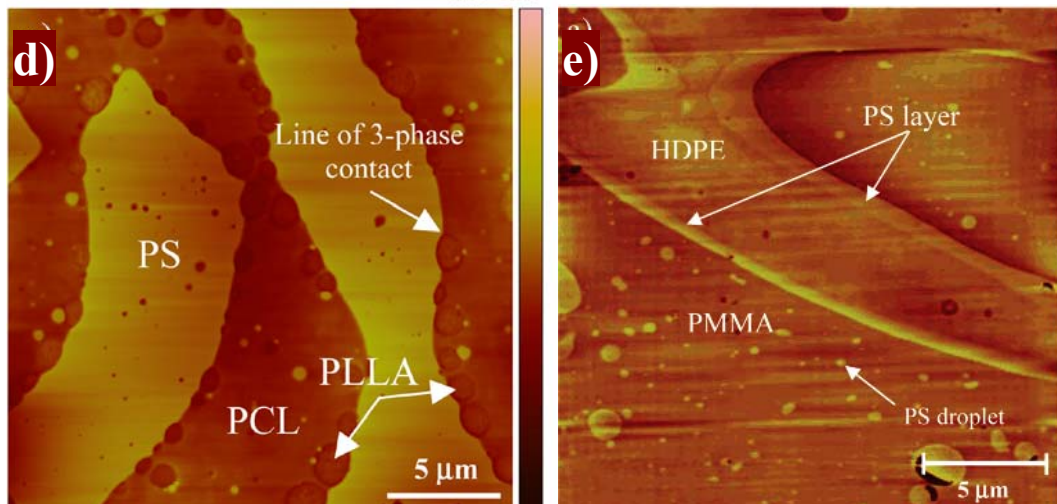


Figure 1-2. Human heart, longitudinal collagen fibers (bar = 50 μm)(Gusukuma, Prates, & Smith, 2004)



125 nm



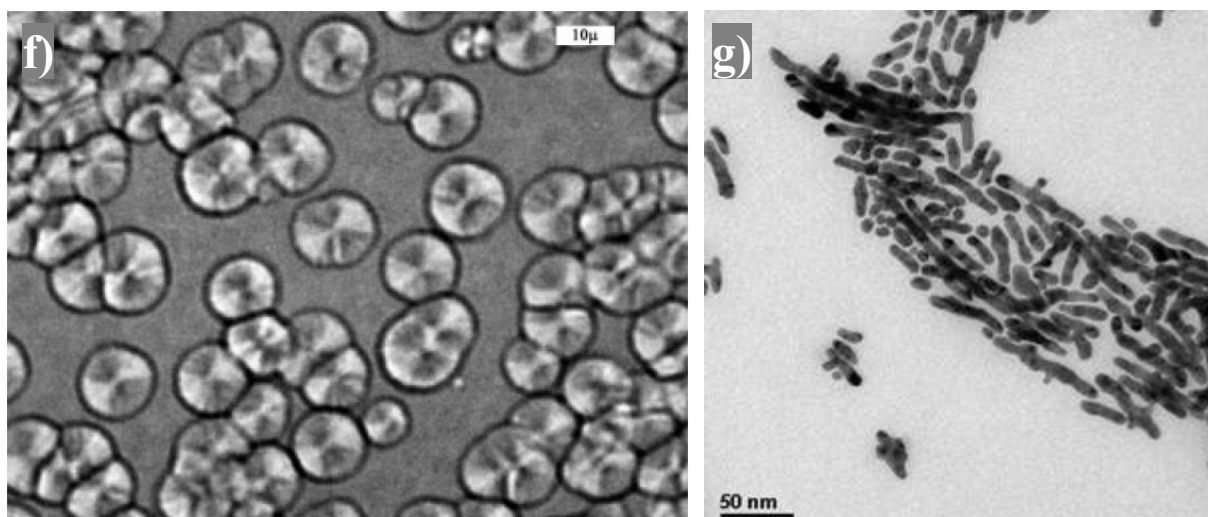


Figure 1-3. a), b), c) Some of the polymer blend samples observed by Veeco lab(http://www.veeco.com/library/resources/Sample_Preparation/index.aspx), d) three-phase contact morphology (Virgilio, Desjardins, L'Esperance, & Favis, 2009), e) two-phase contact morphology (Zhang, Ravati, Virgilio, & Favis, 2007), f) Spherulitic crystallization behavior of polymers (Feng & Kamal, 2005) g) gold nanoparticles and their incorporation into polymer matrices (Meli & Lennox, 2003)

In more recent works, novel complex microstructures for special applications are prepared by a combination of melt-blending and other techniques. For example, porous templates can be made by polymer melt-blending followed by selective extraction of one or several phases (Figure 1-4).

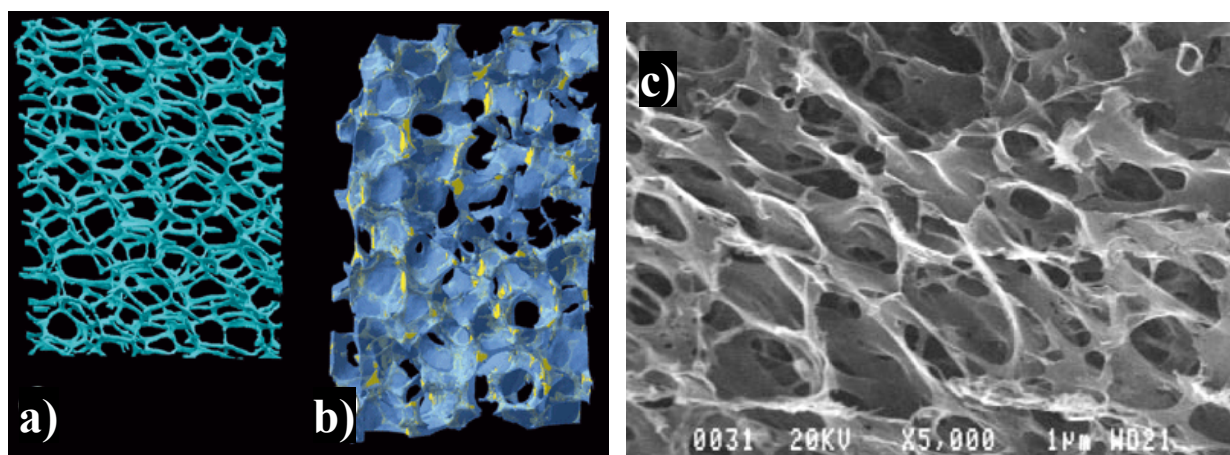


Figure 1-4. a), b) A model of the polyurethane foam made of interconnected rods, b) a model of interconnected macroporosity, c) ultra-porous structure with 99% porosity made of PDADMAC/BSA (Roy, Sarazin, & Favis, 2006)

One of the applications for porous biomaterial polymer blends is bone substitutions. The proposed polymeric scaffolds are able to stimulate the bone regeneration process and to induce the mineralization of the surrounding tissue. Scaffolds with high mechanical properties and high porosity can be prepared in order to produce scaffolds for load bearing applications (Figure 1-5).

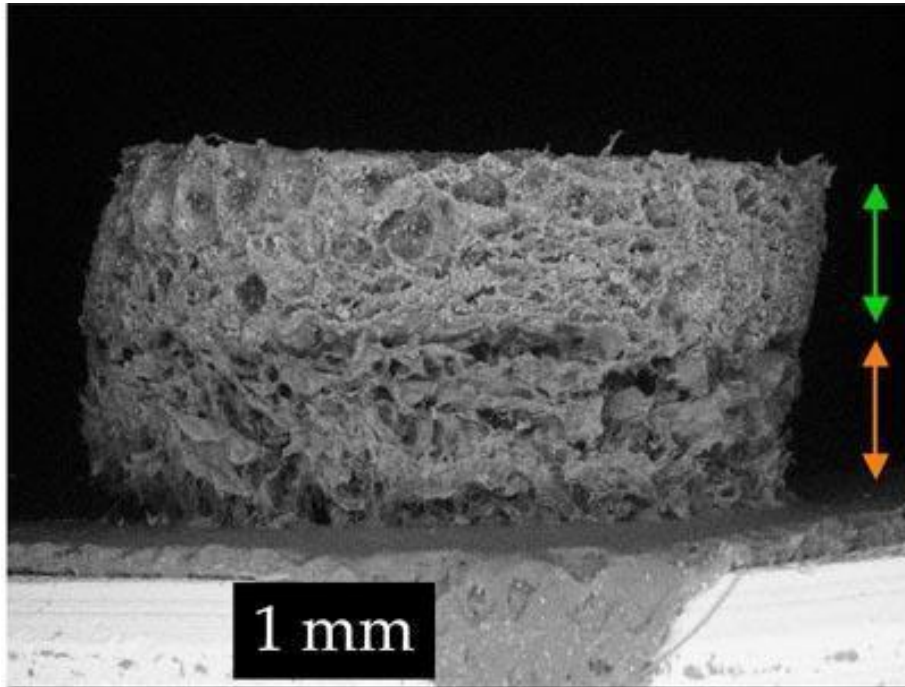


Figure 1-5. MIT and Cambridge University scientists developed this tissue scaffold that could help repair knees and other joints. The top section, indicated by the green arrow, stimulates bone growth, while the lower half, marked by the orange arrow, stimulates cartilage growth(<http://web.mit.edu/newsoffice/2009/cartilage-0511.html>)

As well, hierarchical systems exhibiting a multi-level distribution of porosity can be widely employed in tissue engineering applications. Polymeric scaffolds characterized by macro-pores (100-500 μm) and micro-pores (10-50 μm) are useful as carriers for mesoporous (2-10 nm) silica spheres (e.g. MCM-41), with the objective of loading them with drug molecules (ibuprofen). These three pore sizes are very important in drug delivery systems. Whereas macro-pores can be used for cell colonization and blood vessel access, micro-pores are necessary for the diffusion of nutrients/fluids inside a graft, and meso-pores are exploited for drug uptake and release.

The scaffold could offer a potential new treatment for sports injuries and other cartilage damage. Three dimensional (3D) modelling and analysis of the reconstruction of the specimens is required to facilitate the study of the porous subjects and also to control and produce the desirable structures.

1.2 Objectives

Devices made from semiconductor materials such as radios and computers are the foundation of modern electronics. Semiconductor devices include the various types of transistors, solar cells, and many kinds of diodes, which work with different conductivity values in a range from 10^{-8} to 10^{-2} S Cm⁻¹. Controlling the conductivity and resistivity of materials for various applications is a challenging problem.

Polyaniline (PANI) is popular for its ease of preparation, good level of electrical conductivity, and environmental stability. Green protonated emeraldine has a conductivity on a semiconductor level in the order of 10^0 S cm⁻¹. Although the conducting form of PANI has a good chemical stability combined with relatively high levels of electrical conductivity, PANI suffers from the common disadvantage of conducting polymers, which is poor processibility. For this reason, PANI is used as a filler in the preparation of conducting composites, and for the surface modification of microparticles, powders, fibers, textiles, membranes, and porous substrates, endowing them with new electrical, chemical, and surface properties. A proposed way to cope with the poor processibility of conducting polymers is the preparation of PANI colloids, but this technique is limited to special applications. Melt-processing of PANI was suggested by several groups (Haba, Segal, Narkis, Titelman, & Siegmann, 2000; Narkis et al., 2000a; Segal, Haba, Narkis, & Siegmann, 2001; Shacklette, Han, & Luly, 1993) to combine the desired properties of conventional polymers and PANI. They were not successful in controlling the morphology of the blend, and consequently were unable to reach a percolation threshold lower than 15%. Also, in those cases the percolation threshold area is narrow and a resistive blend is quickly converted to a conductive blend. Therefore, the conductivity value of the material is not controllable in the range of semi-conductivity.

On the other hand, a novel tri-continuous structure derived from HDPE/PS/PMMA double-percolated morphology was reported, with a percolation threshold of PS as low as 3%(Zhang, et al., 2007). Though this model is not usable for PANI due to its high surface tension and polarity, a similar way is sought to spread the PANI phase throughout the blend.

Since the conductivity of the blend depends on the volume fraction of the conductive phase and its morphology, the conductivity value of a sample can be controlled by manipulating the structure of PANI and its possible pathways in the blend. As discussed, it is very important to obtain a material with the exact desired conductivity value for special applications. Also, it is important to prepare samples in 3D bulk and porous structures. Most of the other preparation techniques produce 2D samples.

The main objective of this work is developing novel and complex morphologies for the preparation of highly controllable 3D conductive materials. The study will also analyse the relationship between control of the multi-component blend morphology and reduction of the percolation threshold of the conductive phase.

1.2.1 Specific objectives:

- Understand and develop the morphology of ternary, quaternary, and quinary polymer blends with complete wetting structure;
- Study the development of multi-percolated (double, triple,...) morphologies to obtain the lowest possible continuity and conductivity percolation threshold in ternary, quaternary, and quinary polymer blends;
- Evaluate the potential of both melt-blending/solvent extraction/LbL and multi-processing techniques to reduce the conductivity percolation threshold of a conductive polymer with high surface tension and polarity;
- Study the effect of interfacial modifier on the continuity and conductivity of multi-percolated morphology in quaternary blends;

- Evaluate the thermodynamic and composition parameters on continuity diagrams of binary, ternary, quaternary and quinary systems in multi-component blends with multiple-encapsulated morphological structures;
- Develop a method based on the Harkins equations set to predict the complex morphologies in multi-component blends;
- Understand the mechanism and effect of parameters on the self-assembly LbL technique and the formation of deposited multilayers for a weak polycation and a strong polyanion.

CHAPTER 2 - LITERATURE REVIEW

2.1 Polymer Blends

One of the most important ways to make novel, high performance polymer materials over the last 40 years has been polymer blending, which has found applications in many different scientific fields. By using this method, many properties such as electrical, mechanical, physical and other properties can be combined in a material and adjusted to the needs of particular end-use applications (Hara & Sauer, 1998), although blends are also used for manufacturing polymeric materials at lower cost or with improved processing behaviour. Polymers are macromolecules with high molecular weight and particular structures; thus, most of them do not have favorable interactions with each other.

There are two different groups of polymer blends: miscible and immiscible polymer blends. The former are homogeneous and stable with intermediate properties. The latter group represents the majority of polymers, with morphology-dependent properties. When polymers are mixed, a phase-separated mixture is formed.

2.1.1 Miscible Polymer Blends

Development of thermodynamics of binary mixtures of low molecular weight liquids followed by study of miscibility of a binary polymer blend started in the 19th century. For over 50 years, the cornerstone of polymer solution thermodynamics has been the Flory-Huggins model. Theoretical equations of state for polymer liquids were explained in the mid-1960's by Flory and co-workers (Flory, 1965; Flory, Orwoll, & Vrij, 1964).

Thermodynamics determine the equilibrium states that can be achieved for any given set of conditions when two polymers A and B are mixed together. Gibbs (Gibbs, 1876) formulated the stability of multiphase systems in terms of the quantity G defined as follows:

Equation 2-1.
$$G = H - TS$$

where H is enthalpy, T is absolute temperature, and S is entropy. The necessary condition for two substances A and B to be miscible is that the Gibbs free energy of the mixture must be lower than the sum of the Gibbs free energies of the separate constituents, or in other words, $\Delta G_{mix} < 0$. Therefore, the necessary condition can be extended to:

Equation 2-2.
$$\Delta G_{mix} = \Delta H_{mix} - T\Delta S_{mix} < 0$$

where ΔH_{mix} is the enthalpy of mixing and ΔS_{mix} is the entropy of mixing. Enthalpy and entropy of mixing have been modeled extensively. The combinatorial entropy is the most important factor leading to miscibility in low molecular weight materials. For higher molecular weight components, the $T\Delta S_{mix}$ term is small and the enthalpy of mixing can dominate the miscibility. However, the Equation 2-2 is not a sufficient requirement, as the following expression must also be satisfied:

Equation 2-3.
$$\left(\frac{\partial^2 \Delta G_m}{\partial \phi_i^2} \right)_{T,P} > 0$$

Negative value of this equation can yield a region of the phase diagram where the mixture separates into a phase rich in component A and another phase rich in component B (Denbigh, 1971). The entropy of mixing for dissimilar components can be determined (Clausius, 1864) with the Boltzmann relationship as:

Equation 2-4.
$$\Delta S_m = k \ln \Omega$$

k is the Boltzmann constant and Ω represents the number of configurations or the summation of combinations of arranging N_1 and N_2 molecules into a regular lattice of N cells:

Equation 2-5.
$$\Omega = \frac{(N_1 + N_2)!}{N_1! N_2!}$$

Based on Sterling's approximation:

Equation 2-6.
$$\ln N! = N \ln N - N$$

Installation of Equations 2-5 and 2-6 in the Equation 2-4 yields:

Equation 2-7.
$$\Delta S_m = -k(N_1 \ln x_1 + N_2 \ln x_2)$$

where $x_1 = \frac{N_1}{N}$ and $x_2 = \frac{N_2}{N}$. For mixing of polymer components, calculation of entropy of mixing can be developed to (Flory, 1942, 1944; Huggins, 1942):

Equation 2-8.
$$\Delta S_m = -kV \left(\frac{\phi_1}{V_1} \ln x_1 + \frac{\phi_2}{V_2} \ln x_2 \right)$$

where V is volume of each polymer molecule and ϕ_i represents the volume fraction of phases.

The enthalpy of mixing was expressed by Flory (Flory, 1953) as:

Equation
$$\Delta H_m = \phi_2 k T N_1 \chi_{12}$$

where χ_{12} is the Flory-Huggins interaction parameter and characterizes the interaction energy per solution molecule divided by kT. Consequently, the free energy of solution for low molecular weight molecules was expressed by Meyer-Flory-Huggins as:

Equation 2-9.
$$\Delta G_m = kT(N_1 \ln \phi_1 + N_2 \ln \phi_2 + \chi N_1 \phi_2)$$

McMaster found that volume changes during the mixing of polymers should be considered in the represented formulation (McMaster, 2002).

Scott extended the calculation of free energy to polymer blends by the following relationship:

Equation 2-10.
$$\Delta G_m = kT \left(\frac{V}{V_s} \right) \left(\frac{\phi_1}{M_1} \ln \phi_1 + \frac{\phi_2}{M_2} \ln \phi_2 + \chi \phi_1 \phi_2 \right)$$

where the number of segments of the two polymers are represented by M_1 and M_2 , and V_s is the volume of the segments(Scott, 1949).

2.1.2 Immiscible Polymer Blends

Most polymer blends are immiscible, showing phase-separated mixture. Morphology of multiphase polymer blend materials can be controlled by controlling the interfacial chemistry and the microstructure. Three parameters determine the properties of these multiphase materials: properties of the component polymers, interaction and adhesion between phases and morphology(Utracki, 1998). The properties of multiphase materials are strongly dependent on their phase morphology. Controlling parameters on morphology of polymer blends include composition of phases, kinematic or rheological properties (elasticity and viscosity), processing conditions (shear stress, processing temperature,...), and the most important one which is a thermodynamic parameter: the interfacial tension of the pair of phases(Favis, 2000; Steinmann, Gronski, & Friedrich, 2001). Thermodynamics of interfaces defines the interfacial tension between two phases as the area derivative of the surface free energy per unit area of an interface.

Equation 2-11.
$$\gamma_{ij} = \left(\frac{\partial G}{\partial A_{ij}} \right)_{T,P,n} \quad \text{and}$$

Equation 2-12.
$$\gamma_{ij} = \left(\frac{\partial F}{\partial A_{ij}} \right)_{T,V,n}$$

where G is the Gibbs free energy, F is the Helmholtz free energy of the whole system, and A_{ij} is the interfacial area between phases i and j .

There are different ways to measure interfacial tension of two polymers, including theoretical methods such as Antonoff's rule(Antonoff, 1942; Antonoff, 1907), the Good and Girifalco equation(Girifalco & Good, 1957; Good & Girifalco, 1964), and harmonic mean equation, and experimental methods such as the breaking thread, pendant drop, and sessile drop methods.

Antonoff's rule (Equation 2-13) is valid only when phase 1 and phase 2 have a zero contact angle and two phases are in equilibrium vapor adsorption (Donahue & Bartell, 1952).

$$\text{Equation 2-13.} \quad \gamma_{12} = \gamma_2 - \gamma_1 \quad \gamma_2 \geq \gamma_1$$

Since polymers have negligible vapor pressure, equilibrium vapor adsorption can not occur within the experiment time. Therefore, this relation is invalid for polymers.

Good and Girifalco (Girifalco & Good, 1957; Good & Girifalco, 1964) introduced an interaction parameter (ϕ) based on work of adhesion as follows:

$$\text{Equation 2-14} \quad \gamma_{12} = \gamma_2 + \gamma_1 - W_a$$

$$\text{Equation 2-15} \quad \gamma_{12} = \gamma_2 + \gamma_1 - 2\phi(\gamma_1\gamma_2)^{0.5}$$

The calculated ϕ values for small-molecule organic liquids give reasonable predictions of the interfacial tensions (Good & Girifalco, 1964).

The harmonic mean equation (Equation 2-16) is a result of the fractional polarity theory in which various molecular forces are linearly additive (Wu, 1982). It is valid for low energy materials (Wu, 1971) and represents the combination of the polar component and the dispersion component of the work of adhesion as,

$$\text{Equation 2-16} \quad \gamma_{12} = \gamma_2 + \gamma_1 - 4 \frac{\gamma_1^d \gamma_2^d}{\gamma_1^d + \gamma_2^d} - 4 \frac{\gamma_1^p \gamma_2^p}{\gamma_1^p + \gamma_2^p}$$

Interfacial tension between a low-energy material and a high-energy material is obtained by the geometric mean equation (Wu, 1971) as follows:

$$\text{Equation 2-17} \quad \gamma_{12} = \gamma_2 + \gamma_1 - 2(\gamma_1^d \gamma_2^d)^{0.5} - 2(\gamma_1^p \gamma_2^p)^{0.5}$$

Due to high molecular weight and viscosity of polymers, several interfacial tension measurement methods have been suggested. Generally, calculations of interfacial tensions in these methods are

carried out by comparing minimization of interfacial area and a driving force (gravitational, centrifugal, shearing force, etc).

Bashforth and Adams(Bashforth & Adams, 1883) related the surface tension to the difference of density between two liquids and the geometrical profile of a drop. The pendant drop method determines the profile of a drop of one denser liquid suspended in a less dense liquid at mechanical equilibrium.

A similar method to pendant drop method is the sessile drop method. In this technique, interfacial tension is calculated for a liquid surrounded by another liquid with smaller density on a flat surface based on the balance between gravity and surface forces. It implies that from the shape of the drop at mechanical equilibrium, interfacial tension can be calculated.

The breaking thread technique is a well-known method in which interfacial tension is calculated based on the evolution of the shape of a thread imbedded in a second phase. Small distortions with certain wavelengths are generated at the interface of the phases due to Brownian motion. These small distortions are expanded based on the interfacial tension and the viscosity of the polymers. Two theories relate the evolution of the thread to interfacial tension: the theory of Tomotika(Tomotika, 1935b) and the theory of Tjahjadi(Tjahjadi, Ottino, & Stone, 1994).

Different morphologies can be obtained for melt processing of immiscible polymer blends. Simple morphologies such as matrix/dispersed particles structures, matrix-fiber structures, lamellar structures and complex morphologies such as co-continuous structures, composite droplet structures, and multiple percolated structures can be generated(Favis, 2000; Potschke & Paul, 2003). These kinds of morphologies can easily be transformed by changing effective parameters such as applied shear, elongation stress, interfacial tension between phases, and coalescence and breakup of the phases during processing. For instance, the dispersed phase can be distorted into long fibrils by applying further shear stress. Breakup mechanism can occur due to lowering interfacial tension between components dispersing fibrils into droplets. Broken droplets can be coalesced and form fibrils or larger droplets by coalescence mechanisms. All other mentioned parameters affect the size and shape of droplets, fibrils, or continuous structure of phases. The combination of these processes can potentially provide us many kinds of phase morphologies suitable for various applications.

2.1.2.1 Binary Polymer Blends

2.1.2.1.1 Co-continuous Morphology

There is currently an increasing interest in techniques used to control interfacial properties of polymeric materials. Through controlling morphology of polymer blends, novel materials for different applications can be designed. For immiscible polymer binary blends, two types of morphologies, namely matrix/dispersed structure and co-continuous morphologies, have been realized. At low concentration of one phase, dispersed droplets of that phase in the other component is observed. By increasing the concentration of the minor phase, phase inversion occurs and a dual phase region is reached in which various levels of co-continuous structure co-exist. At concentrations near the phase inversion region, blends with two fully interconnected and interpenetrating structures in three dimensions are observed. In other words, a binary blend is formed of two polymers in which the surface of each phase is an exact topological replica of the other (antitropic). Generally, in polymer blends, the matrix dominates the properties of blend; thus, in binary co-continuous blends both polymers have approximately equal contributions to the blend properties. Moreover, their interpenetrating assembly can lead to synergistic improvement of specific conductivity, permeability, and mechanical properties. A process in which two phases switch their functions is defined as phase inversion. In a certain concentration range around the phase inversion concentration, which is defined as the co-continuity interval, co-continuous morphologies are formed. The phase inversion concentration is regarded as the center of this area and its correct determination is of great importance in which the former dispersed phase becomes the matrix and vice-versa. Consequently, the position and width of the phase inversion concentration are influenced by many rheophysical material parameters of the blend's constituents, such as interfacial tension. Willemse et al. (Willemse, Posthuma de Boer, van Dam, & Gotsis, 1999) showed that for different blends with various matrix viscosities and viscosity ratios, the composition range within which fully co-continuous polymer blend structures form is influenced by interfacial tension. It was found (He, Bu, & Zeng, 1997) that phase co-continuity occurs in a wide composition range at a short mixing time, but with

increasing mixing time, this interval gets narrow and finally shrinks to one point. Veenstra et al.(Veenstra, Norder, van Dam, & Posthuma de Boer, 1999) observed a direct correlation between the width of the co-continuity interval under shear flow and the capillary number. The above mentioned factors influence the width of the co-phase area, whereas several factors affect the position of the phase inversion. The most important one is phase viscosities and their ratio. Investigations have shown that for a binary blend consisting of components of equal viscosity, phase inversion occurs around a volume fraction of 0.5(Miles & Zurek, 1988b). Several works(Jordhamo, Manson, & Sperling, 1986; Mekhilef & Verhoogt, 1996) showed that when component viscosities differ significantly, the phase inversion point is shifted towards compositions richer in the high viscosity component. Several authors have proposed semi-empirical equations based on rheological properties, particularly viscosity, in order to predict co-continuity point. Paul and Barlow(Paul & Barlow, 1980b), according to the observations made by Avgeropolous(Avgeropoulos, Weissert, Biddison, & Boehm, 1976) and the work developed by Jordhamo et al.(Jordhamo, et al., 1986), suggested a model for blends prepared at low shear rates as follows:

Equation 2-18.

$$\frac{\phi_{11}}{\phi_{12}} = \frac{\eta_{01}}{\eta_{02}}$$

where ϕ_i and η are volume fraction and zero shear viscosity of each phase, respectively, at the phase inversion point. Miles et al.(Miles & Zurek, 1988a) argued that the point of phase inversion should be more precisely related to the effective viscosity ratio.

Equation 2-19.

$$\frac{\phi_{11}}{\phi_{12}} = \frac{\eta(\dot{\gamma})_1}{\eta(\dot{\gamma})_2}$$

Most of the researchers have acknowledged that Equation 2-18 and Equation 2-19 are valid for predicting the phase inversion concentration in many binary blend systems with a viscosity ratio near unity(Mekhilef & Verhoogt, 1996; Miles & Zurek, 1988a). It has been demonstrated that they are invalid for the ones that exhibit viscoelastic asymmetry between the melt components(Favis & Chalifoux, 1988).

Some other studies (Everaert, Aerts, & Groeninckx, 1999; Ho, Wu, & Su, 1990) developed Equation 2-18 and added excess factors for given blend systems to correlate their results with a semi-empirical model. A model was derived by Metelkin et al. (Metelkin & Blekht, 1984) based on theory of filament instability described by Tomotika (Tomotika, 1935a) in terms of viscosity ratio:

Equation 2-20.

$$\phi_{i2} = \frac{1}{1 + \lambda f(\lambda)}$$

where λ is viscosity ratio and $f(\lambda)$ is defined as :

Equation 2-21.

$$f(\lambda) = 1.25 \log(\lambda) + 1.81(\log(\lambda))^2$$

with λ being the viscosity ratio of the blend components at the blending shear rate. Again all of these equations can predict the phase inversion point with a very good accuracy when both components have approximately equal viscosity. Results of samples with high viscosity ratio demonstrate that these models are unable to predict the phase inversion point and significant errors appear. For such cases, some authors used the percolation threshold definition to develop an equation based on maximum packing volume fraction. Utracki (Utracki, 1991) proposed a model based on theory for mono-dispersed hard spheres (Krieger & Dougherty, 1959).

Equation 2-22.

$$\phi_{i2} = \frac{\phi_m + (1 - \phi_m) \left(\frac{\eta_1}{\eta_2} \right)^{\frac{1}{[\eta]\phi_m}}}{\left(\frac{\eta_1}{\eta_2} \right)^{\frac{1}{[\eta]\phi_m}} + 1}$$

where ϕ_{i2} is the phase inversion point, ϕ_m is the maximum packing volume fraction, $[\eta]$ is intrinsic viscosity, and indices refer to components. For polymer blends, ϕ_m is defined as $\phi_m = 1 - \phi_c$, where ϕ_c stands for the percolation threshold and amounts to 0.156 for dispersions of spheres. The definition of the percolation threshold is explained in detail in the next sections. This equation explains that the addition of the first component to second one leads to an increase

in the respective blend viscosity until, at the phase inversion point, the maximum viscosity is reached.

Luciani et al.(Luciani & Jarrin, 1996), based on Tomotika's theory and the relative stability of networks created by coalescence, developed the following equation:

Equation 2-23.

$$\phi_{12} = \frac{\left(\frac{\eta_1}{\eta_2}\right)^2 \Omega^2 \left(\frac{\eta_1}{\eta_2}\right)}{\left(\frac{\eta_1}{\eta_2}\right)^2 \Omega^2 \left(\frac{\eta_1}{\eta_2}\right) + \Omega^2 \left(\frac{1}{\frac{\eta_1}{\eta_2}}\right)}$$

where $\Omega\left(\frac{\eta_1}{\eta_2}, \lambda\right)$ is a complex function of both the viscosity ratio and observed wavelength of the distortion λ in Tomotika's equation.

The other semi-empirical model which accounts for the viscous properties of the polymers was proposed by Willemse et al.(Willemse, de Boer, van Dam, & Gotsis, 1998) based on geometrical requirements for the formation of co-continuous structures:

Equation 2-24.

$$\frac{1}{\phi_d} = 1.38 + 0.0213 \left(\frac{\eta_m \dot{\gamma}}{\sigma} R_0 \right)^{4.2}$$

where η_m is matrix phase viscosity, R_0 is the initial radius of the droplet before deformation into a cylinder, and σ is interfacial tension. This equation can determine the composition range over which co-continuity exists and gives the lower limit of continuity for component 1 and upper limit for component 2.

Steinmann et al.(Steinmann, Gronski, & Friedrich, 2002) derived the following equation point, assuming that phase inversion occurs at maximum shape relaxation times of domains of components:

Equation 2-25.

$$\phi_{2I} = \frac{1}{\left(\frac{\eta_1}{\eta_2}\right)^{\frac{1}{z}} + 1}$$

where the parameter z is dependent on the blend system and is evaluated experimentally for each system.

Some other researchers focused on the elasticity or used it along with viscosity to predict the phase inversion composition. The first approach based on the elasticity ratio was described by Van Oene (Vanoene, 1972). He defined an equation to describe interfacial tension under dynamic conditions adding an elastic properties term to interfacial tension under static conditions:

Equation 2-26.
$$\gamma_{eff} = \gamma + \frac{d}{12} [(N_2)_d - (N_2)_m]$$

where γ_{eff} is the effective interfacial tension under dynamic conditions, d represents droplet diameter, γ is the static interfacial tension and $(N_2)_d$, $(N_2)_m$ are the second normal stress functions of the dispersed and matrix phases, respectively.

Considering that the storage modulus G'_i and $\tan \delta$ represent the elasticity of phase i , Bourry and Favis (Bourry & Favis, 1998a) introduced elasticity into the understanding of phase inversion.

Equation 2-27.
$$\frac{\phi_{11}}{\phi_{12}} = \frac{G'_2(\omega)}{G'_1(\omega)}$$

Equation 2-28.
$$\frac{\phi_{11}}{\phi_{12}} = \frac{\tan \delta_1(\omega)}{\tan \delta_2(\omega)}$$

where $\delta_i = \frac{G''_i}{G'_i}$. It was reported (Bourry & Favis, 1998a) that these formulas are in much better

agreement with experimental data than other equations based only on viscous effects, particularly at high shear rates. Steinmann et al. (Steinmann, et al., 2001) compared some of the mentioned approaches and found that the factors are still inadequate to predict the phase inversion point. Consequently, they developed a semi-empirical equation based on elasticity ratio

$\Psi_{eff.G'}$:

Equation 2-29.
$$\phi_{11} = -0.34 \log(\Psi_{eff.G'}) + 0.67$$

As reviewed above, numerous models have been proposed but to date none of them are able to predict the phase inversion composition for all binary polymer blends.

One of the most important applications of co-continuous blends is the fabrication of continuous conductive parts in the blend. Several works have been done in this area to decrease the percolation threshold of conductive polymers by making a network of conductive polymer in another phase. As conductivity of the blend corresponds to the continuity of the conductive polymer, the percolation threshold of continuity of the conductive component can be measured by showing the percolation threshold of conductivity of the blend. Zilberman et al. (Zilberman, Siegmann, & Narkis, 2000d) compared the conductivity of several binary blends such as PANI/LLDPE, PANI/CoPA and PANI/(PS/DOP) (Figure 2-1). A detailed study of binary conductive polymer blends will be conducted in the next sections.

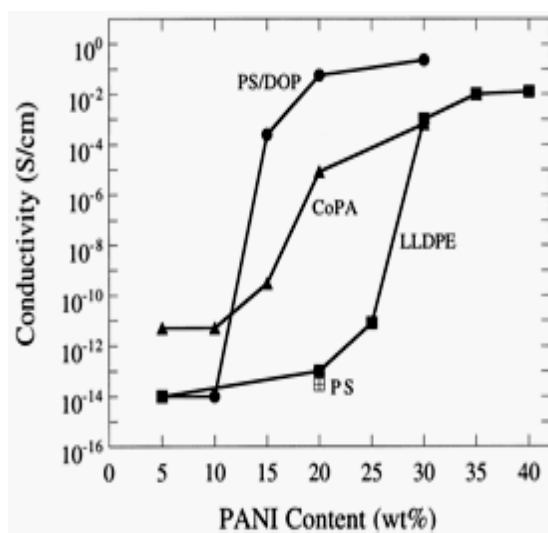


Figure 2-1. Electrical conductivity versus PANI content of polymer/PANI binary blends (Zilberman, et al., 2000d).

2.1.2.1.2 Interfacial Modification of Binary Blends

Compatibilizing agents (surfactants) have been long used with mixtures of low molecular weight molecules. The earliest and simplest kind is soap made by boiling fats together with plant ashes, which dates back to 2800 B.C. and was industrially developed in 1920's. The term of

“compatibilization” was suggested by Gaylord in the 1960s for the method used to decrease the interfacial tension between polymer pairs and the blend shows more stable morphology(N. G. Gaylord, 1969; N. G. Gaylord, ,Vol.142,P.76,(ACS,Washington,1975). 1975).

Compatibility between phases is enhanced using a block copolymer with particular physically or chemically compatible segments with each of the blend components. Block copolymers are designed for binding two components together. They stay at the interface and either part of their molecular chain has physical or chemical interaction with each component of the blend. The main effect of addition of an interfacial agent on the morphology of an immiscible blend is to reduce the particle size and to narrow the particle-size distribution(Hoganand & Banks, 1958; Matos, Favis, & Lomellini, 1995; Sarazin & Favis, 2003) (Figure 2-2).

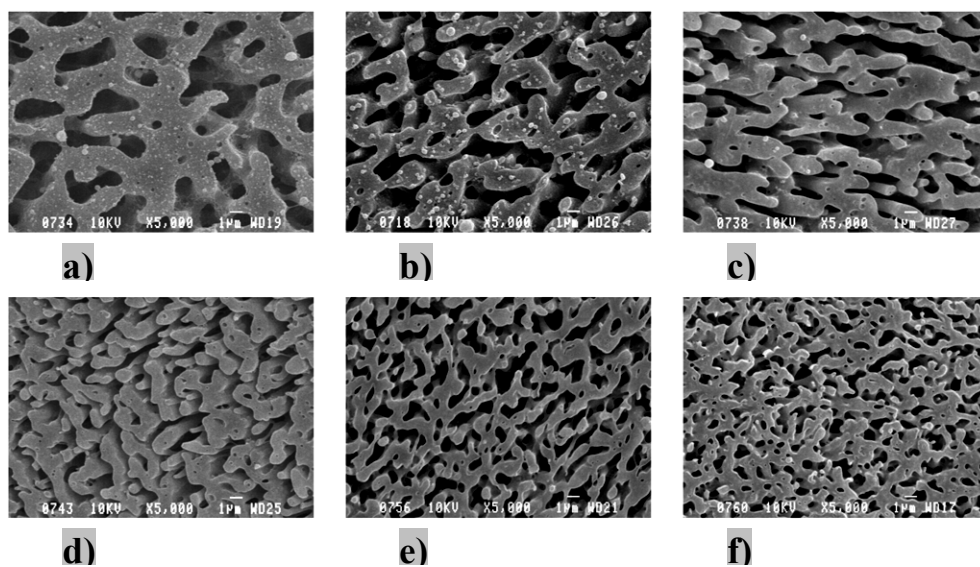


Figure 2-2. Action of the diblock copolymer to reduce the pore size for 50/50 PLLA/PS blends at copolymer concentrations of (a) 2.5%, (b) 5%, (c) 8%, (d) 12%, (e) 15%, and (f) 20%. Copolymer concentration shown is based on the weight of polystyrene. The white bar indicates 1 micron(Sarazin & Favis, 2003).

Both reduction of coalescence and decrease in interfacial tension results in reduction of particle size after interfacial modification. Sundararaj et al.(Sundararaj & Macosko, 1995) showed suppression of coalescence happens when two droplets with a layer of diblock or graft copolymer at the interface are less likely to coalesce due to formation of a shell of copolymer molecule around droplets.

2.1.2.2 Ternary Polymer Blends

Mathematical models derived from physical considerations have been successfully used to predict and explain several observed morphologies of immiscible ternary polymer blends. Harkin used thermodynamic properties, such as surface and interfacial tensions of the components, to express the tendency of liquid to spontaneously spread across a solid or liquid substrate (Harkins & Feldman, 1922). The first comprehensive study on a ternary liquid mixture was carried out by Torza and Mason (Torza & Mason, 1970). They used modified Harkins Spreading Theory to analyze interfacial energy differences between the liquid components. Hobbs et al. (Hobbs, Dekkers, & Watkins, 1988) followed their work and employed this method to predict and interpret composite-droplet morphology of ternary polymer blends. The modified Harkins equation can be written as:

Equation 2-30.
$$\lambda_{ij} = \gamma_{jk} - \gamma_{ik} - \gamma_{ij}$$

λ_{ij} is defined as the spreading coefficient giving the tendency of component (i) to encapsulate or spread onto component (j) in the matrix of component (k). γ_{ij} , γ_{jk} , and γ_{ik} are the interfacial tensions of the different polymer pairs. Two different morphologies can be obtained, depending on the values of the spreading coefficients, as spreading is predicted to occur only for positive values of λ_{ij} . In other words, a positive value of one of the spreading coefficients such as λ_{ij} indicates wetting of phase j by phase i. This case is called complete wetting morphology and is shown in Figure 2-3. The other possible prediction is partial wetting in which all spreading coefficients have negative values. In this morphology all phases have interfaces with each other (Figure 2-3).

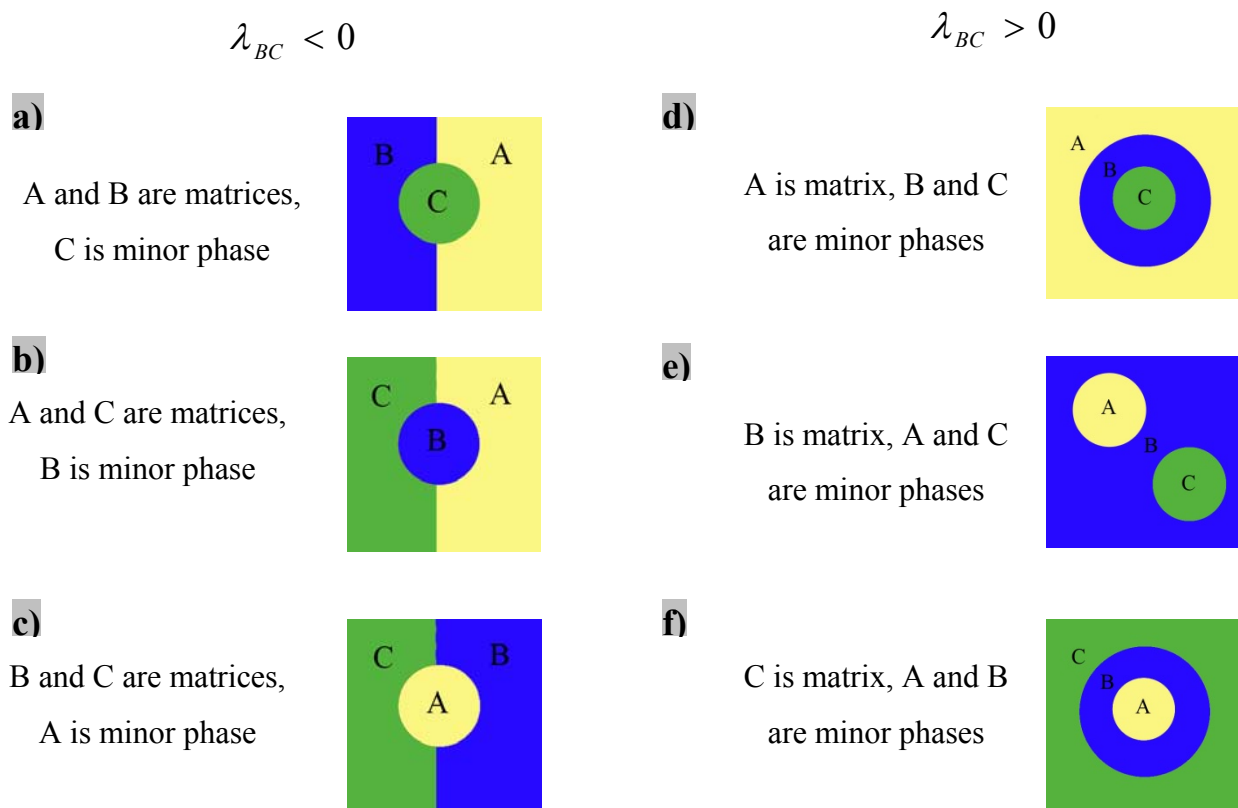


Figure 2-3. a), b), c) Ternary blends with partial wetting case, and d), e), f) ternary blends with complete wetting case

A phenomenological model suggested by Guo et al. (Guo, Gvozdic, & Meier, 1997; Guo, Packirisamy, Gvozdic, & Meier, 1997) was used to predict the morphology of ternary and quaternary blends. They used interfacial area associated with interfacial tension and derived an expression for the free energy of mixing of a multiphase blend. The free energy calculation is written as:

Equation 2-31.

$$G = \sum_i n_i \mu_i + \sum_{i \neq j} A_i \gamma_{ij}$$

where μ_i is the chemical potential of component i, n_i is the number of moles, A_i is the interfacial area, and γ_{ij} is the interfacial tension between components i and j. Thus, the phase structure of a polymer blend can be predicted by comparing the Gibbs free energies of the different structures. In their work on a HDPE/PS/PMMA blend, numerous conditions were assumed to simplify the study such as equal value of the first term of the equation for all types of morphology. For further simplification, they assumed that numbers of droplets of minor phases were equal to each other, which lead to a big error.

The second term is simplified further and rewritten as:

$$\text{Equation 2-32.} \quad \left(\sum A_i \gamma_{ij} \right)_{B+C} = (4\pi)^{1/3} \left[n_B^{1/3} x^{2/3} \gamma_{AB} + n_C^{1/3} \gamma_{AC} \right] (3V_c)^{2/3}$$

$$\text{Equation 2-33.} \quad \left(\sum A_i \gamma_{ij} \right)_{B/C} = (4\pi)^{1/3} \left[n_B^{1/3} (1+x)^{2/3} \gamma_{AB} + n_C^{1/3} \gamma_{BC} \right] (3V_c)^{2/3}$$

$$\text{Equation 2-34.} \quad \left(\sum A_i \gamma_{ij} \right)_{C/B} = (4\pi)^{1/3} \left[n_B^{1/3} x^{2/3} \gamma_{BC} + n_C^{1/3} (1+x)^{2/3} \gamma_{AC} \right] (3V_c)^{2/3}$$

where V_i is the volume fraction of phase I, $x = \frac{V_B}{V_C}$, n_B and n_C are numbers of particles of B and C phases. The most stable morphology is predicted by calculation of the values of $(\sum A_i \gamma_{ij})$ which correspond to the value of the Gibbs energy of mixing.

Obviously, the Harkins equation and the Guo model are purely thermodynamic equations in which some other factors influencing the morphology, such as rheological parameters, have not been considered. Although in measuring interfacial tensions of polymer pairs by various methods such as the breaking thread and pendent drop, viscosities of the components are taken into account, the effect of elasticity is still neglected. In the method developed by Guo to calculate the free energy compared to Harkins equation, concentration of components is also contributed to determine the kind of morphology as well and it is more modified. Researchers use both the spreading coefficients and the minimal free energy surface model to predict the morphologies of polymer blends (Guo, Gvozdic, et al., 1997; Guo, Packirisamy, et al., 1997; Hara & Sauer, 1998; Hobbs, et al., 1988; Horiuchi, Matchariyakul, Yase, & Kitano, 1997; Nauman & He, 2001;

Reignier & Favis, 2000, 2003a; Reignier, Favis, & Heuzey, 2003; Tchomakov, Favis, Huneault, Champagne, & Tofan, 2004; Urashita, Kawakatsu, & Doi, 2000).

It has been observed that the rheological properties of the two minor phases can play a role in the final morphology of ternary polymer blends, most notably through viscosity effects (Gupta, 1993; Luzinov, Pagnouille, & Jerome, 2000; Nemirovski, Siegmann, & Narkis, 1995; Tchomakov, et al., 2004), and elasticity ratio effects (Legros, Carreau, Favis, & Michel, 1997; Vanoene, 1972). The effect of the viscosity ratio is still controversial amongst the authors. Some authors did not observe any influence of the viscosity ratio on the type of morphology (Reignier, et al., 2003; Tchomakov, et al., 2004), while some observed encapsulation of the higher viscosity component by the component of lower viscosity (Nemirovski, et al., 1995), and others observed a contrary result (Gupta, 1993).

Van Oene (Vanoene, 1972) showed that under conditions of dynamic flow, the difference in elasticity between the phases can contribute to the interfacial tension. A dynamic interfacial tension, which can be quite different from the static interfacial tension, can have a significant impact on the final morphology. He developed an expression for the interfacial tension in flow and defined a term proportional to the difference between a second normal stress function in this equation (Equation 26)

2.1.2.2.1 Composite Droplet Morphology

Another interesting morphology observed in multiphase polymer blends is the composite droplets morphology. In this particular morphology, a dispersed phase (B), in a matrix of (A), encapsulates a third phase (C).

There are two main causes for sub-inclusion formation: 1) Thermodynamic effect: to minimize the surface free energy of a blend (Guo, Packirisamy, et al., 1997; Hobbs, et al., 1988) and 2) Rheological effect: the entrapment of the sub-inclusions in a more viscous phase near the phase inversion region (Favis & Chalifoux, 1988).

Reignier et al. (Reignier & Favis, 2000, 2003a, 2003b; Reignier, et al., 2003) showed that in a ternary blend comprised of PMMA, PS, and HDPE, when HDPE is the matrix, the blend exhibits

composite droplet formation constituted of a well-segregated PMMA core and PS shell (Figure 2-4Ia, 2-4Ib, and 2-4Ic).

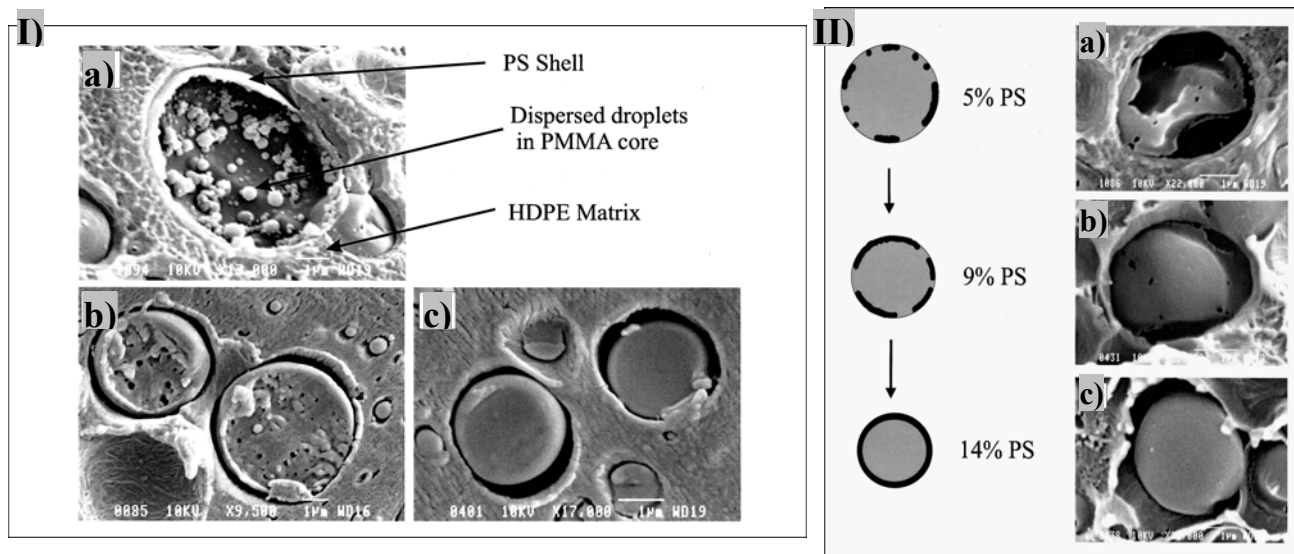


Figure 2-4. SEM micrographs of the 80 (HDPE) /20 (PS/PMMA) I) a) fracture surface etched with acetic acid for 2 min, 14%PS/86%H-PMMA; b) microtomed surface etched 24 h with cyclohexane, 9%PS/91%H-PMMA; and c) microtomed surface etched 24 h with cyclohexane, 9%PS/91%L-PMMA, II) Evolution of the shell formation process with increasing PS content (vol. % based on the dispersed phase) for the 80(HDPE)/20(PS/L-PMMA)(cryofractured samples after being etched for 10 s with acetic acid).

It was explained that the thickness of the PS shell can be controlled by changing the relative amount of PS and PMMA. They also showed the evolution of the shell formation process with increasing PS content in a ternary HDPE/PS/PMMA blend (Reignier & Favis, 2003a) (Figure 2-4IIa, 2-4IIb, and 2-4IIc). They also found (Reignier & Favis, 2000) that after two minutes of mixing, approximately all of the PMMA is encapsulated within the PS dispersed phase and morphology becomes stabilized after that.

Harrats et al. (Harrats, Omonov, & Groeninckx, 2005) reported encapsulation of the PP phase between the PS and PA6 phases (Figures 2-5a and 2-5b). They found this against the prediction of the Harkins equation, whereas the interfacial tension values of $\gamma_{PA6/PS}=13.72$ mN/m, $\gamma_{PA6/PP}=13.64$ mN/m, and $\gamma_{PP/PS}=2.26$ mN/m demonstrated partial wetting case. They did not

measure the interfacial tension of tensions. The harmonic mean equation, as mentioned earlier, is a method to calculate the interfacial tension between two polymers based on their surface tension and polarity (Equation 16).

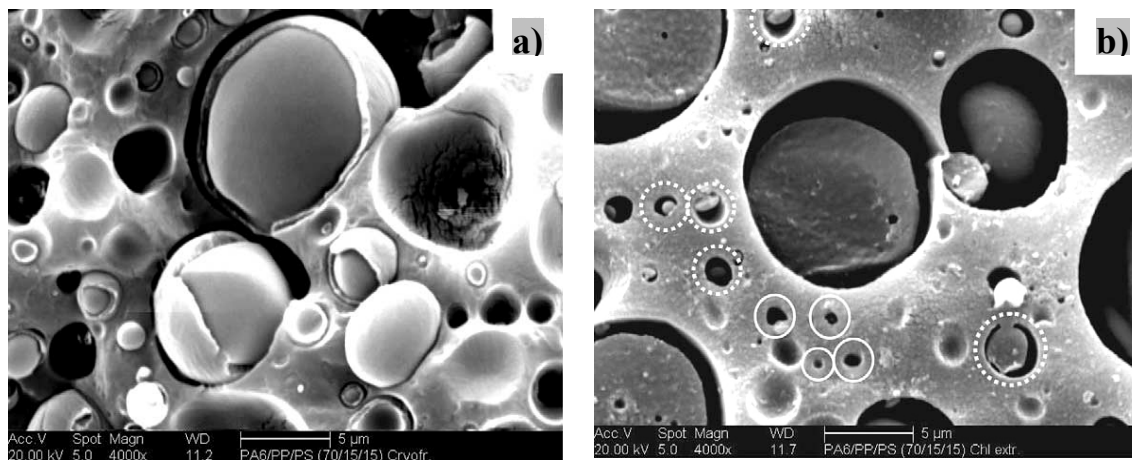


Figure 2-5. SEM micrograph of 70PA6/15PP/15PS blends: (a) cryofractured and (b) chloroform extracted surfaces.(Harrats, et al., 2005)

They claimed that the concept of spreading theory fails in their case because “the development of the phase morphologies in polymer melt depends also on other key factors such as the viscosity and elasticity of the blend. The use of the interfacial tension alone for the prediction of the type of phase morphologies in immiscible polymer melt can be successful in blend components having closer melt viscosities.”

Reignier et al.(Reignier, et al., 2003) studied the effect of different factors on the composite droplet formation. They showed the influence of elasticity on composite droplet formation by introducing the dynamic interfacial tension term taken from VanOene(Vanoene, 1972) in the free energy model developed by Guo et al.(Guo, Packirisamy, et al., 1997), and developed new equations for the interfacial free energies in conditions of dynamic mixing:

$$\text{Equation 2-35.} \quad \left(\sum A_i \gamma_{ij} \right)_{B+C} = 4\pi R_i^2 \left[\gamma_{BA} + \frac{R_i}{6} (N_{1,B} - N_{1,A}) \right] + 4\pi R_i^2 \left[\gamma_{CA} + \frac{R_i}{6} (N_{1,C} - N_{1,A}) \right]$$

$$\text{Equation 2-36.} \quad \left(\sum A_i \gamma_{ij} \right)_{B/C} = 4\pi R_e^2 \left[\gamma_{BA} + \frac{R_e}{6} (N_{1,B} - N_{1,A}) \right] + 4\pi R_i^2 \left[\gamma_{CB} + \frac{R_i}{6} (N_{1,C} - N_{1,B}) \right]$$

$$\text{Equation 2-37.} \quad \left(\sum A_i \gamma_{ij} \right)_{C/B} = 4\pi R_e^2 \left[\gamma_{CA} + \frac{R_e}{6} (N_{1,C} - N_{1,A}) \right] + 4\pi R_i^2 \left[\gamma_{BC} + \frac{R_i}{6} (N_{1,B} - N_{1,C}) \right]$$

Normal stress differences for the phases A, B, and C are referred to by N_1 , γ_{ij} is the interfacial tension between the components i and j, and the internal and external radius of the core-shell droplets are shown by R_i and R_e , respectively. Reignier et al.(Reignier, et al., 2003) indicated that the viscosity ratio estimated at a constant shear stress rather than at a constant shear rate is accurate to study the effect of viscosity ratio on the morphology because shear stress is more continuous at the interface between the dispersed phase and the matrix phase.

The effect of molecular weight of phases on the encapsulation process was investigated(Reignier, et al., 2003). The equilibrium morphology for HDPE/low molecular weight PS/low molecular weight PMMA illustrates that PS encapsulates PMMA (Figure 2-6a). When components were replaced by high molecular weight PS and high molecular weight PMMA, an inversion in encapsulation occurred and PMMA encapsulated PS (Figure 2-6b). They related this discrepancy to the high viscosity of PS that does not allow PMMA to be encapsulated. Finally, considering all the observations, they concluded that interfacial energy reduction is the main driving force controlling encapsulation effects and that the viscosity ratio and the absolute viscosity have little influence on encapsulation phenomena in composite droplets.

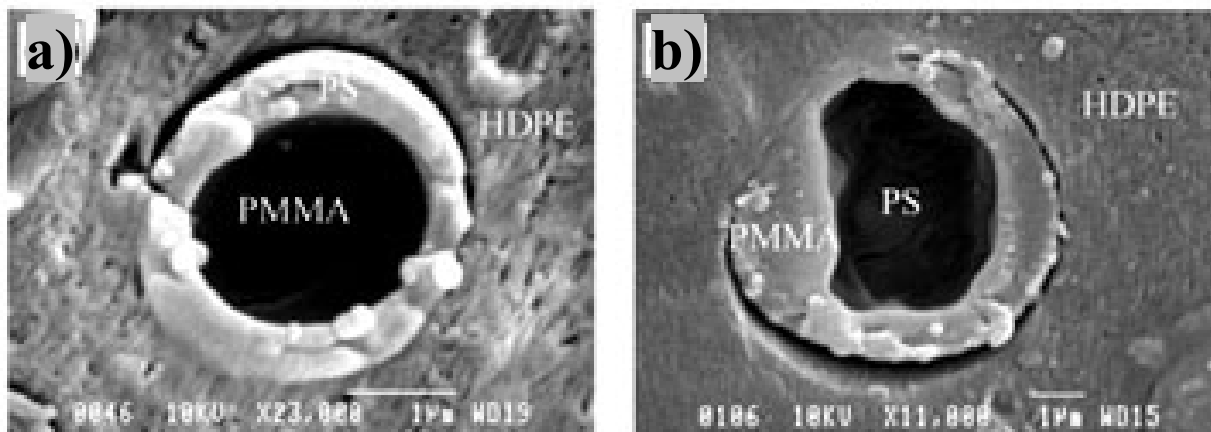


Figure 2-6. Dependence of the composite dispersed morphology on PS and PMMA molecular weights. SEM photomicrographs of (a) HDPE/L-PS/L-PMMA; PMMA is extracted by acetic acid and (b) HDPE/H-PS/H-PMMA; PS is extracted by cyclohexane. The white bar denotes 1 μm (Reignier, et al., 2003).

This section showed that many parameters can affect the simplest morphology of ternary polymer blends, which is composite droplet morphology. The question is: which theory can correctly predict the morphology, and which theory can give similar results to reality in the fastest time? In some work, different theories mentioned above are compared by (Valera, Morita, & Demarquette, 2006) work. In this work, the morphology of the PMMA/PP/PS ternary blend with different compositions was comprehensively studied. PMMA, PS, and PP are selected as the matrix and the composition of the minor phases was changed to find which model is able to predict a wide range of compositions. It has been reported that the predictions of the minimal surface free energy theory were verified by experimental observations only when PS was the matrix, and in the other cases the minimal surface free energy theory was unsuccessful to predict the morphology. The spreading coefficient model and the dynamic interfacial tension model can predict most of the experimental results.

Finally, it is concluded that the fastest way to predict the morphology of the ternary polymer blend with a great accuracy still remains the spreading coefficients.

2.1.2.2.2 Double-Percolated Systems

Zhang et al. (J. Zhang, et al., 2007) showed that through a combination of composite droplet and co-continuous blend morphology preparation methodologies, a continuous shell structure of one component was situated at the interface of a co-continuous structure of two other phases. In a composite-droplet structure with composite droplets of PMMA in PS, if the amount of HDPE is decreased while the quantity of the PMMA is increased, a co-continuous network of HDPE and PMMA is formed while the PS forms a continuous sheath structure at the HDPE/PMMA interface (Figure 2-7a). In this kind of morphology, it is possible to have a co-continuous structure of one component using a very small amount of that component. The percolation threshold is significantly decreased and continuity development increases as compared to classical blends. This is verified by gravimetric measurement, as shown in Figure 2-7b. As it is illustrated, the percolation threshold of the PS phase in a HDPE/PS blend and that of the PMMA phase in a HDPE/PMMA blend are 15% and 20%, respectively. The percolation threshold of PS sharply decreases when it is situated at the interface of HDPE and PMMA, whereas at concentrations as low as 3%, 70% continuity is observed.

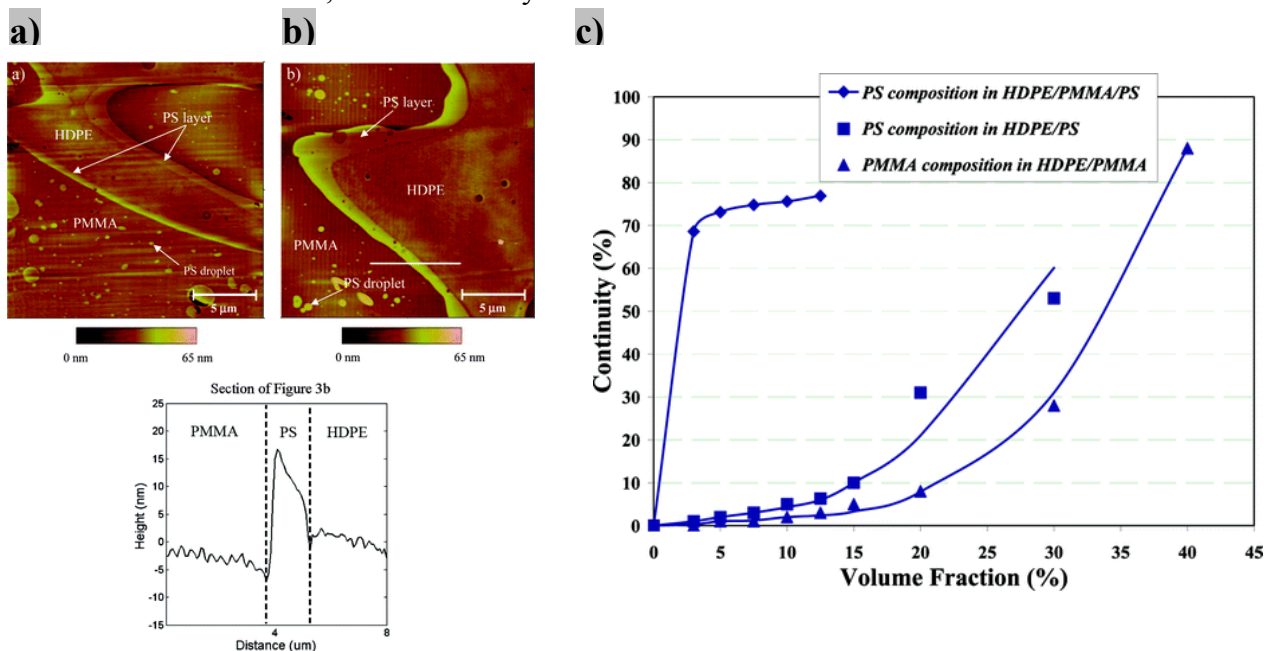


Figure 2-7. a, b) FIB-AFM images of HDPE/PS/PMMA ternary blends. The white line in Figure 7b indicates the section analyzed below, and c) Continuity of PS or PMMA as a function of the composition using the solvent dissolution technique (Zhang, et al., 2007)

Omonov et al. found double percolated structures for ternary 40PA6/30PP/30PS (Figure 2-8a) and 40PA6/(25/5)(PP/PP-MA2)/(25/5)(PS/SMA2) (Figure 2-8b) blends. In this work, the observed results were opposite to the prediction of spreading theory, which is partial wetting. They found that despite the negative values of spreading coefficients, a complete wetting case with PA6 phase at the interface is observed. The gravimetric measurements for all phases showed that for 40PA6/30PP/30PS, all phases have more than 97% continuity while PA6 separates the PP and PS phases. Figure 2-8b shows that addition of a compatibilizing agent to the sample does not change the location of phases. It only reduces phase sizes, but PA6 still remains at the interface of the two other phases.

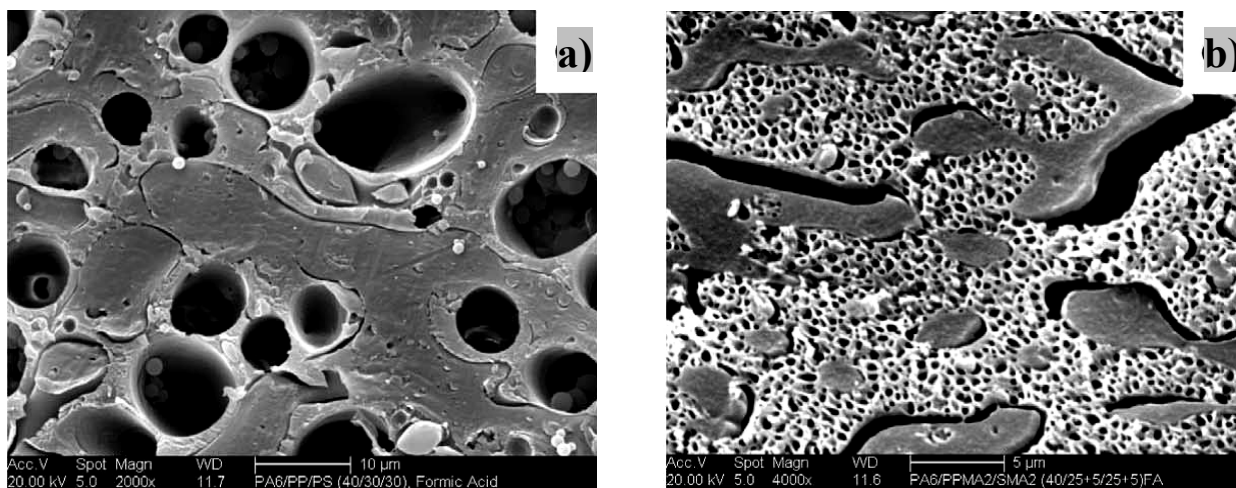


Figure 2-8. Scanning electron micrograph of a) 40PA6/30PP/30PS; formic acid extracted surfaces, and b) 40PA6/(25/5)(PP/PP-MA2)/(25/5)(PS/SMA2); formic acid extracted surfaces (Harrats, et al., 2005)

One of the most important applications of double-percolated structures is the preparation of conductive polymer blends. Since locating the conductive phase at the interface decreases the percolation threshold of continuity of the middle phase, it is predicted that the percolation threshold of conductivity of the blend is reduced significantly. Narkis et al. (Narkis et al., 2000b; Zilberman, Siegmann, & Narkis, 1998, 2000a, 2000b) studied various polymer blends consisting of two immiscible thermoplastic polymers and PANI and tried to locate PANI at the interface of two other polymers, but they were not successful. They showed that for CoPA/LLDPE/PANI (Figure 2-9) and (PS/DOP)/LLDPE/PANI (Figure 2-10), changing the concentration of the

middle phase has an effect on the continuity and conductivity of the PANI, which is the inner phase. It is noted that as PANI is not the middle phase, the percolation threshold is not reached at lower concentrations of PANI such as 10%, and a higher amount of PANI is required(Zilberman, et al., 2000b). A detailed review on the double percolated morphologies is presented in the next sections.

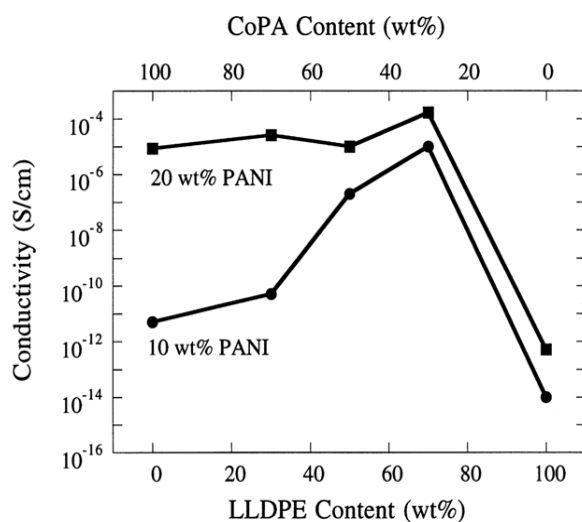


Figure 2-9. Electrical conductivity versus LLDPE content for CoPA/LLDPE/PANI ternary blends containing 10 and 20 wt% PANI(Zilberman, et al., 2000b)

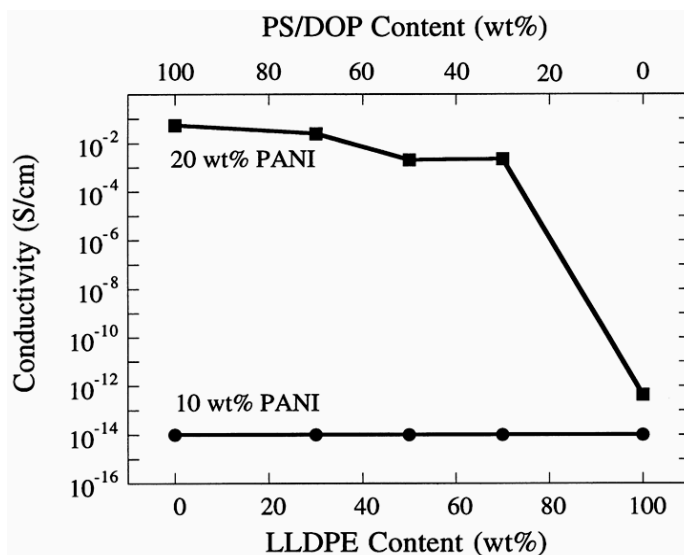


Figure 2-10. Electrical conductivity versus LLDPE content for (PS/DOP)/LLDPE/PANI blends containing 10 and 20 wt% PANI(Zilberman, et al., 2000b)

2.1.2.2.3 Effect of Composition on Ternary Blends with Complete Wetting Morphology

In the case of complete wetting, one phase situates at the interface of two other phases and separates them from each other. By varying the composition, three different cases can be formed. Guo et al. (Guo, Packirisamy, et al., 1997) showed that in a HDPE/PS/PMMA ternary blend, PS always separates HDPE and PMMA phases for various compositions. They showed that when HDPE is the matrix and PS and PMMA are the minor components, the PMMA phase is encapsulated by the PS phase (Figure 2-11a).

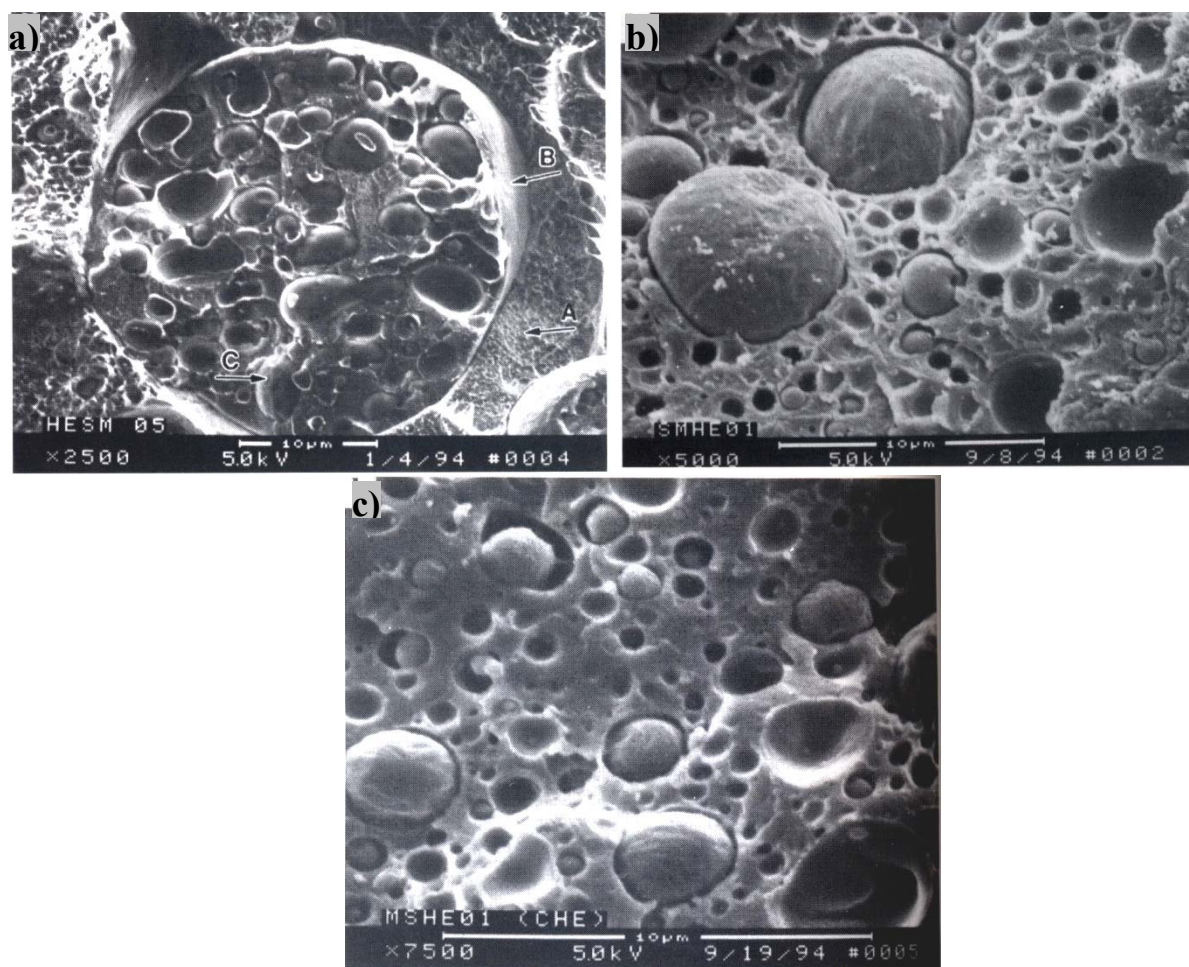


Figure 2-11. a) 70%HDPE/15%PS/15%PMMA, b) 15%PMMA/70%PS/15%HDPE(PMMA extracted fracture surface), and c) 70%PMMA/15%PS/15%HDPE (PS extracted fracture surface) (Guo, Packirisamy, et al., 1997)

When PS is the matrix with PMMA and HDPE minor phases, separate dispersions of HDPE and PMMA have the lowest interfacial free energy (Figure 2-11b). Finally, when PMMA is the major phase and PS and PMMA are minor components, the HDPE is encapsulated in the PS phase (Figure 2-11c).

2.1.2.2.4 Interfacially Modified Ternary Polymer Blends

As mentioned above, the Harkins theory can predict whether the morphology of a ternary blend is complete wetting or partial wetting. This theory is based on the interfacial tension of polymer pairs. Hence, by changing the interfacial tension between two polymers via addition of interfacial modifier, the prediction of the morphology by Harkins can toggle between the complete wetting case and the partial wetting case. Another effect of interfacial modifier is that in a partial wetting case, one phase moves from one phase to the other phase, thus creating more interfacial area. Guo et al. (Guo, Packirisamy, et al., 1997) showed that in a ternary polymer blend of 70/10/20 HDPE/PS/PP, all three phases have interface with each other (Figure 2-12a). This is predicted by the Harkins equation, as interfacial tension values of $\gamma_{PE/PS}=5.9$ mN/m, $\gamma_{PE/PP}=1.1$ mN/m, and $\gamma_{PP/PS}=5.1$ mN/m show three negative spreading coefficients. A blend without interfacial modifier represents more interfacial area between the PS phase and the PP phase (Figure 2-12a). Addition of 0.5% PS/PE diblock copolymer shows movement of the major part of the PS phases to HDPE (complete wetting case), and also more PS droplets at the interface move to the HDPE phase (Figure 2-12b).

The other effect of interfacial modifier on the blend, as previously discussed, is increasing interfacial area between phases. Therefore, addition of diblock copolymer to the blend results in a decrease of the droplet size. Figure 2-12c shows that addition of 2% PS/PE copolymer to 70/10/20 HDPE/PS/PP results in smaller droplet sizes in both the partial and complete wetting cases.

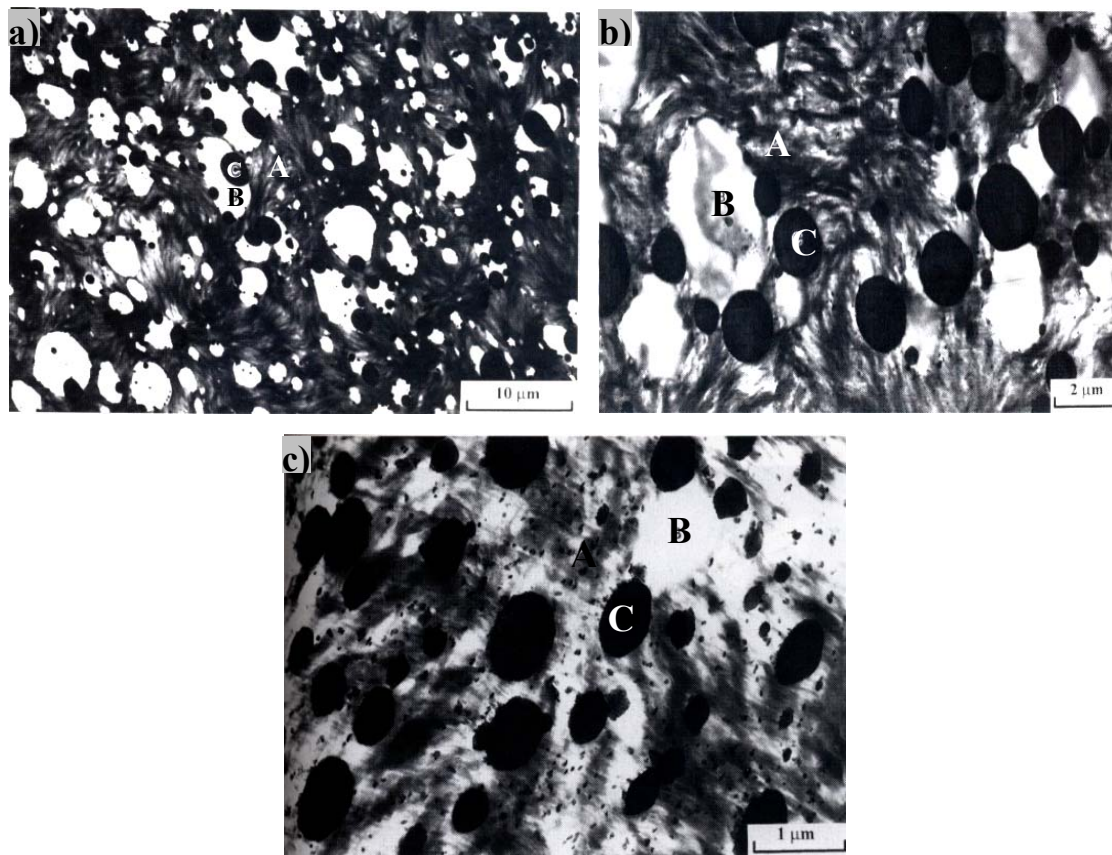


Figure 2-12. SEM photomicrograph of a) 70%HDPE(A)/20%PP(B)/10%PS(C), b) 70%HDPE(A)/20%PP(B)/10%PS(C) + 0.5% S-E block copolymer, and c) 70%HDPE(A)/20%PP(B)/10%PS(C) + 2% S-E block copolymer(Guo, Packirisamy, et al., 1997)

2.1.2.3 Quaternary Polymer Blend Systems

A few works have been performed to predict and analyze the morphology of quaternary blend systems(Guo, Gvozdic, et al., 1997; Virgilio, Desjardins, et al., 2009). Guo et al.(Guo, Gvozdic, et al., 1997) calculated the value of χ_{12} for various cases of a quaternary blend comprised of PP, HDPE, PS, and PMMA. They showed, as predicted when PP is the matrix, that a structure of (PE+PS/PMMA) is observed where the PMMA phase is encapsulated by the PS phase and the PE particles are dispersed separately in the matrix (Figure 2-13a).

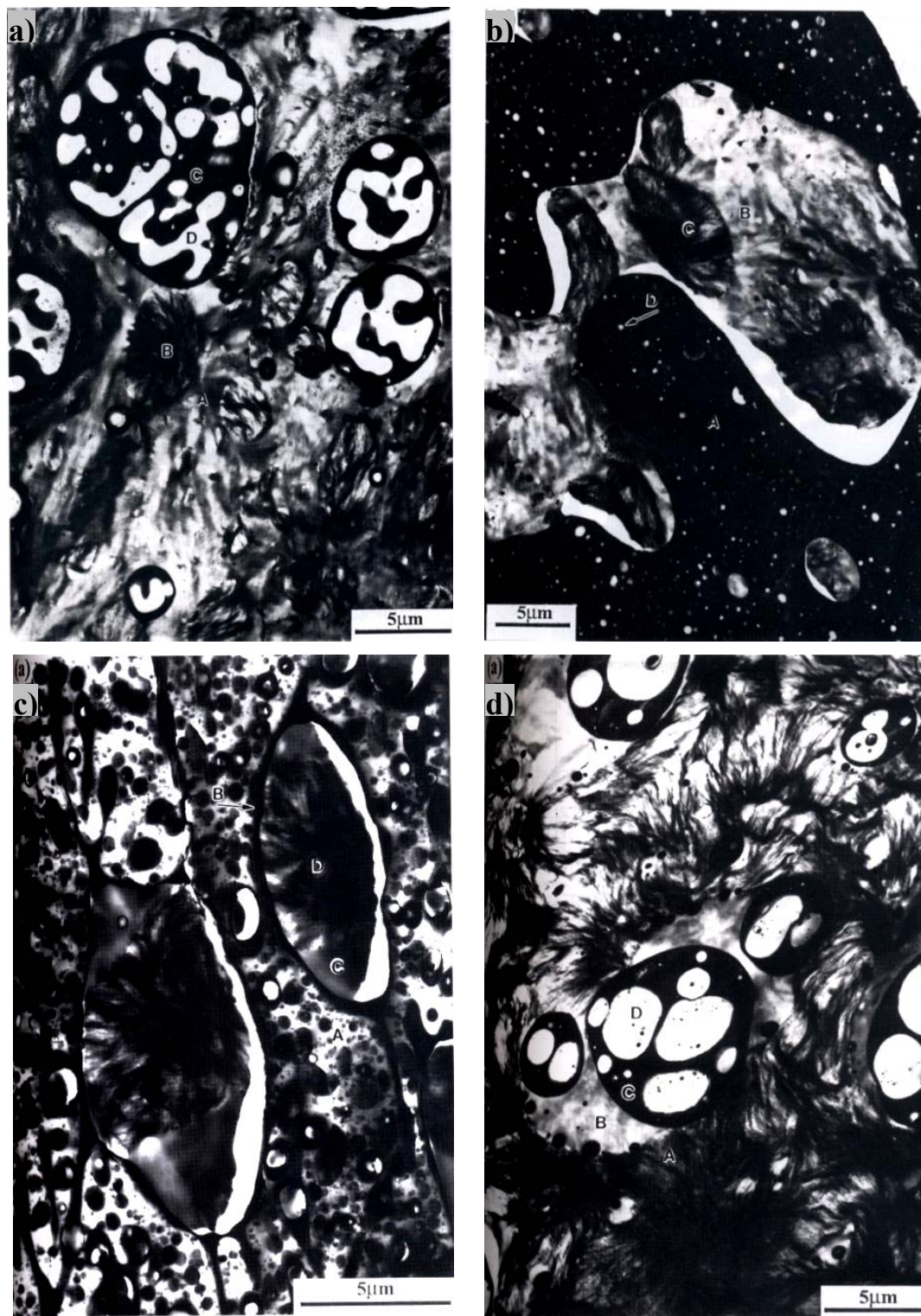


Figure 2-13. SEM photomicrograph of a) 10%PMMA(D)/10%PS(C)/60%PP(A)/20%HDPE(B),
 b) 10%PMMA(D)/60%PS(A)/20%PP(B)/10%HDPE(C),
 c) 60%PMMA(A)/20%PS(B)/10%PP(C)/10%HDPE(D), and
 d) 10%PMMA(D)/10%PS(C)/20%PP(B)/60%HDPE(A)(Guo, Gvozdic, et al., 1997)

In the case where PS is the matrix, the value of interfacial energy results in a (PMMA+PP/HDPE) structure, in which HDPE is encapsulated by PP and PMMA is separately dispersed in the matrix (Figure 2-13b). For PMMA and HDPE matrices, structures of (PS/PP/HDPE) (Figure 2-13c) and (PP/PS/PMMA) (Figure 2-13d) were predicted and observed, respectively.

2.1.3 Porous Polymeric Substrates Prepared by Melt-Blending

Highly controlled polymeric co-continuous structures have been fabricated in our group (J. Li & Favis, 2001b; Jianming Li, Ma, & Favis, 2002; Sarazin & Favis, 2003) through a melt-blending process of immiscible polymers followed by selective solvent extraction. As mentioned before, in a binary immiscible polymer blend, two possible morphologies can be formed: dispersed droplet/matrix and co-continuous morphologies. Binary polymer blends comprised of polymer 1 and polymer 2 in the co-continuity range lead to a co-continuous morphology at concentrations above the percolation threshold. The dual phase region is located at concentrations above the percolation threshold, where phase inversion determines the area that two fully interconnected phases through a continuous pathway exist. Etching one of the components by selective solvent extraction leads to a fully interconnected porous substrate. The greatest advantage of this method compared to other techniques used for generating interconnected porous polymer substrates, such as solvent casting/particulate leaching or gas foaming, is the ability to control porosity and pore distribution, and internal surface area.

2.1.3.1 Controlling the Pore Size in the Substrate

There are a few ways to control the pore sizes of porous samples prepared via melt-blending. Pore size and extent of continuity can be controlled through composition, interfacial modification, and static annealing. Interfacial modification in a blend is employed to achieve

substantially reduced pore sizes, and annealing of the multi-component is used to increase the phase sizes of porous material. It has been observed that for a constant void volume, a range of pore diameters from 0.9 to 72 μm can be obtained (Sarazin & Favis, 2003).

2.1.3.1.1 Coarsening of Binary and Ternary Polymeric Systems

In some works, large porous media are needed for facilitating penetration of the solution through the empty interconnected network of a porous substrate. In order to perform controlled annealing, the sample must be in contact with hot press surfaces for a certain time. In this case, a temperature gradient, which is defined as the change in temperature over the change in distance from hot surfaces, is present throughout the samples. At each point in the sample (x,y,z) in time t , the temperature is $T(z,t)$. By increasing temperature, the magnitude of gradient rises and T equals $T(z,t)$ until it reaches the set temperature. At this point the gradient is no longer a function of time and just changes in height. It is concluded that for thick samples (larger than 0.5cm thickness), the annealing method is not a suitable technique to fabricate porous substrates with uniform pore sizes.

In a detailed work about annealing of immiscible co-continuous blends, Zhenhua et al. (Zhenhua Yuan, 2005) proposed that the driving force for the coarsening process during static annealing is a capillary pressure effect. Siggia (Siggia, 1979) explained that although capillary pressure is proportional to the interfacial tension, it is inversely proportional to the rod thickness. It was described that in a blend, thin part structures with small cross-sections generate capillary forces larger than thick parts with large cross-sections. It demonstrates a force gradient from thin parts to thick parts and a continuous merging of thin parts toward the thick ones resulted from the difference in capillary pressure throughout the co-continuous structure (Figure 2-14).

Hence, there are a lot of thin rods or branches attached to thick rods which continuously feed them. Important factors in coarsening were reported as temperature and time of the annealing, interfacial tension, and zero shear viscosity of components. Increasing the time and temperature of annealing results in increasing the droplet motions and coalescence of droplets, which leads to average domain size growth and also size distribution growth (Willemsse, Ramaker, van Dam, &

Posthuma de Boer, 1999) (Kumin & Chang Dae, 1996). Linear time dependence was observed in the coarsening of immiscible co-continuous blends as shown by experimental pore size growth at a constant temperature of 200°C in Figure 2-15. Sarazin et al. (Sarazin & Favis, 2003; Sarazin, Roy, & Favis, 2004) showed that for a binary blend of PLLA and two typical polymers, domain growth is more rapid at a higher temperature over a longer time.

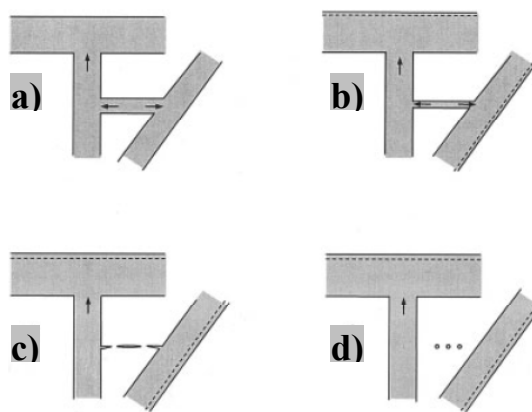


Figure 2-14. Coarsening process in co-continuous structure upon annealing. (a) the thin rod merges/flows into thick ones at both sides, the thick rod merges into a much thicker one at the same time; (b) the thin rod becomes thinner during the merging process; (c) the thin rod breaks/splits; and (d) the residual parts retract/shrink to the thick rods. (Yuan, 2005)

Veenstra et al. (Harm Veenstra, Van Dam, & Posthuma de Boer, 2000) described a relationship between coarsening and the fiber retraction process. They showed the evolution of a polymer rod to a sphere in a polymer matrix during the annealing process. However, this mechanism is unable to explain some facts about coarsening and is not in agreement with experimental data (Zhenhua Yuan, 2005).

Reignier et al. (Reignier & Favis, 2000) investigated static coalescence for a composite droplet morphology in a ternary blend. A similar mechanism governed by the same methodology for coalescence of each phase in binary blend and ternary blend was found. They set the temperature at 200°C and observed that core-core and shell-shell coalescence occurred from 2 min to 90 min. They reported that the only difference is that the ternary blend showed a dual coalescence process, first between subinclusions within composite droplets and second between composite

droplets. The results indicate that due to forces and coalescence, each phase joins with same phase, and thus phase sizes become larger. In other words, a complete transition from multiple subinclusion particles within a given shell to a core-shell structure is observed. It can be said that this process is performed similarly to the case of binary blends, as thin parts of each component are being pushed to thick parts of the same component due to capillary forces, which results in an increase in average pore size.

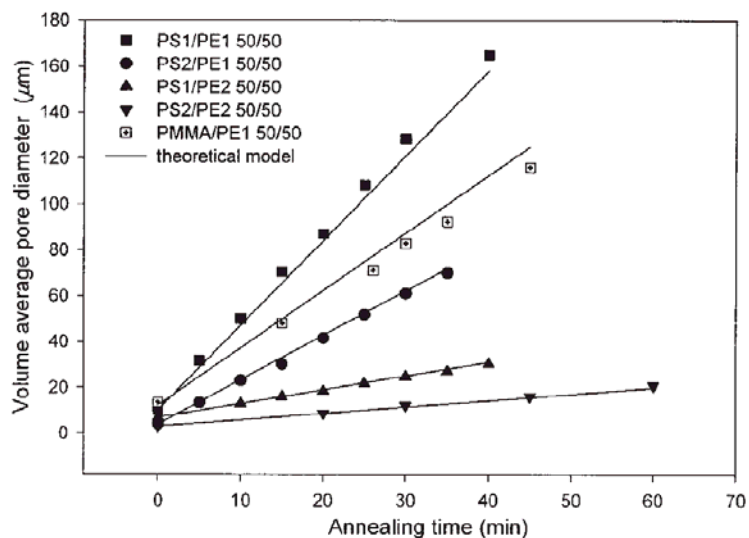


Figure 2-15. Experimental pore size growth (points) with the theoretical model (solid lines) for different blends annealed at 200°C. (Yuan, 2005)

2.2 Percolation Theory

The behavior of the connected clusters in a random graph in mathematics is described by the percolation theory. The main concept of the percolation theory is the existence of a percolation threshold. Percolation threshold is a mathematical term defined as the formation of long-range connectivity in random systems. Percolation threshold in engineering and material science deals with fluid flow and similar processes which concern the movement and filtering of fluids through porous media. One question that arises is whether a liquid poured on top of a porous material is able to make its way from the top to the bottom. From a mathematical point of view, a regular

lattice, such as square lattice, with a random network by randomly occupying sites (vertices) or bonds (edges) with a statistically independent probability is imagined (Figure 2-16).

If it is examined as an infinite network corresponding to Kolmogorov's zero-one law, for a given P , the probability that an infinite cluster exists is either zero or one. There is a critical P (since this probability is increasing) below which the probability is always 0 and above which the probability is always 1. This critical amount P_c is called the percolation threshold, which if we start out at $P = 0$ and randomly create connections, P_c is defined as a point at which a spanning cluster first appears. It means that for P greater than P_c , a spanning cluster always exists, although some isolated, non-spanning clusters can be present, and for P less than P_c , there are only isolated clusters (Stauffer & Aharony, 1994a).

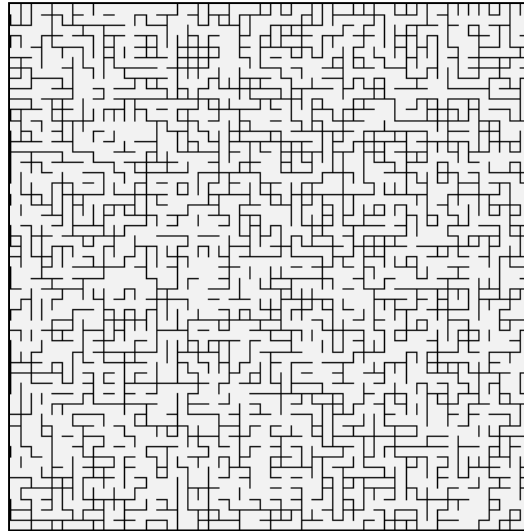


Figure 2-16. Detail of a bond percolation on the square lattice in two dimensions with percolation probability $p=0.51$ (Stauffer & Aharony, 1994b)

P_c may be calculated theoretically in some cases such as for a square lattice in two-dimensions where the percolation threshold has a value of 0.5. For triangular and honeycomb bonds, (P_c) will be respectively as follows:

Equation 2-38.
$$P_c = 2 \sin\left(\frac{\pi}{18}\right)$$

Equation 2-39.
$$P_c = 1 - 2 \sin\left(\frac{\pi}{18}\right)$$

Calculation of P_c for a square lattice was an open question for more than 20 years and was finally resolved by Harry Kesten. For three-dimensional systems, P_c 's are unknown and cannot be calculated for now, although the most interesting thing to do is not calculating the P_c .

The percolation threshold has a significant application in universality systems. For example, Utracki et al.(Utracki, 1991) used the percolation threshold to predict the phase inversion point based on emulsion theory as follows:

Equation 2-40.
$$\frac{\eta_1}{\eta_2} = \left(\frac{\phi_m - \phi_2}{\phi_m - \phi_1} \right)^{[\eta]\phi_m}$$

In this model, ϕ_m and η refer to the volume fraction of the component at percolation threshold and intrinsic viscosity, respectively.

The universality principle describes that the value of P_c is connected to the local structure of the graph, while the behavior of clusters below, at and above P_c are invariants of the local structure, and therefore, in some sense are more natural quantities to consider.

2.2.1 Universality Systems

Systems which tend to be chaotic often have a large number of interacting parts. They are called universality systems. Systems display universality in a scaling limit, when a large number of interacting parts come together. As a matter of fact, universality originated in the study of phase transitions in a statistical science, especially in statistical mechanics. The transformation of a thermodynamic system from one phase to another is a phase transition. When the properties of a material change in a dramatic way, a phase transition happens. For example, when a magnet is heated, its magnetism is lost. In this case, the phase transition is characterized by the

magnetization, which is a function of a parameter of the system, such as the temperature. A system's critical point is the value of the parameter at which the system has a phase transition. For a given parameter, such as (ϕ) , with a critical value of (ϕ_c) , the order parameter (a) is approximated by the following equation:

Equation 2-41.
$$a = a_0(\phi - \phi_c)^t$$

The exponent t is a critical exponent of the system and its value is dependent on the dimensions of the lattice (Grimmett, 1999). For a monodispersed distribution of spheres, a value of 0.156 is predicted for onset of the percolation threshold by percolation theory, which has been verified by several works.

For example, in the case of an electrically conductive polymer with filler, the effect of filler loading on the composite resistivity follows a nearly universal pattern regardless of which fillers are chosen.

2.3 Conductive Materials

In modern society, a life without electronics cannot be imagined. All materials under normal conditions have some resistance to flowing charges. The electrical resistance of a material is defined by Ohm's law as the ratio of the voltage (V) applied to the electric current (I) which flows through it. A resistance formula is:

$$R = \frac{V}{I}$$

There are three main groups of materials from an electrical point of view: conductors, semiconductors, and insulators. Materials containing movable charges of electricity are called conductors. These mobile charges are forced to move when an electric potential difference is applied across separate points on a conductor. The measure of the ability of a conductor to carry electric current is conductivity, which is defined as the ratio of the amount of charges passing through a unit area of the conductor per second, divided by the electric field intensity.

Equivalently, it is the inverse of the electrical resistivity, with units in Siemens per meter. Therefore, it can be written as:

Equation 2-42
$$R = \frac{\rho l}{A}$$

where R is resistance, ρ is resistivity, l is length, and A is cross sectional area.

Devices made from semiconductor materials are the foundation of modern electronics, including radio, computers, telephones, and many other devices. Semiconductor devices include transistors, solar cells, many kinds of diodes including the light-emitting diode, the silicon controlled rectifier, and digital and analog integrated circuits. In semiconductors, electrical conductivity is controlled over a wide range, either dynamically or permanently. These materials generally have an intermediate conductivity (Figure 2-17) which varies under different conditions such as specific frequencies in AC, light, temperature and electric field. Insulators are non-conducting materials as they lack mobile charges.

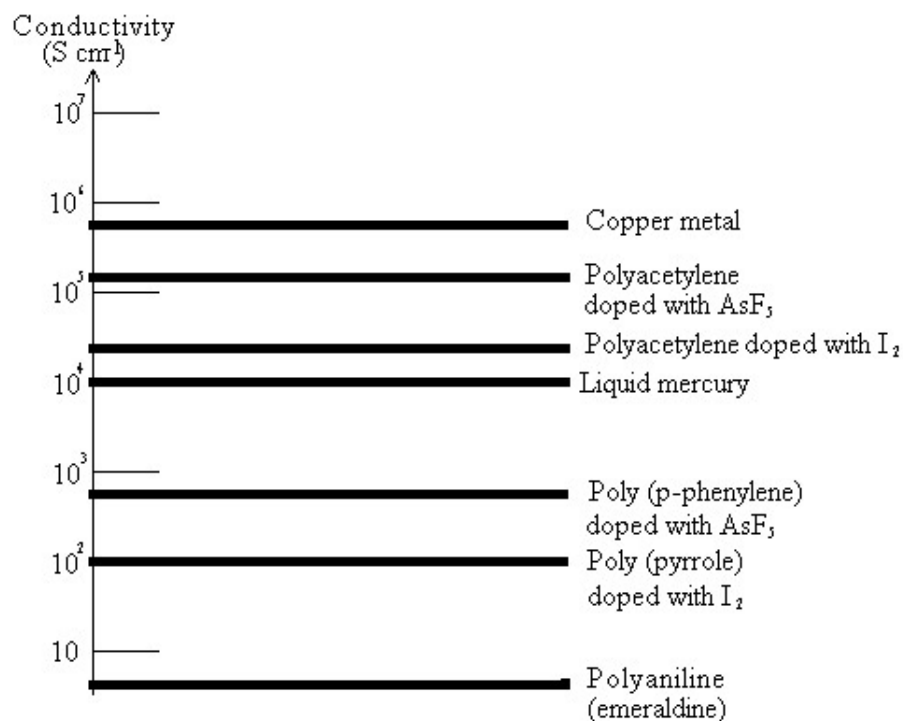


Figure 2-17. Logarithmic conductivity ladder locating some metals and conducting polymers(Pratt, 2001)

Polymers have long been thought of and applied as insulators. Moreover, some observed electrical conduction in polymers was generally regarded as an undesirable phenomenon. With the discovery in 1960 of intrinsically conducting polymers (ICPs), a new class of electronically conducting polymers in the partially oxidized state was surprisingly discovered. In metals and semiconductors such as silicon, free electrons and holes are the charges that are responsible for the current. The Nobel Prize in Chemistry in 2000 “for the discovery and development of electronically conductive polymers” was received by Alan J. Heeger, Alan J. MacDiarmid and Hideki Shirakawa (Chiang, Drury, et al., 1978; Chiang et al., 1977; Chiang, Park, et al., 1978).

2.3.1 Electrically Conductive Polymers and Composites

Generally, four types of electrically conductive polymer system with different degrees of conductivity have been recognized (Wise, Wnek, Trantolo, Cooper, & Gresser, 1997).

1. The most widely used conducting polymeric systems where an insulating polymer matrix is filled with particulate or fibrous conductive fillers such as metal powder, carbon black, or carbon nanotubes to impart high conductivity.
2. Ionically conducting polymers are electrically conductive because of the movement of ions present in the system. For example mobility of lithium ions in polyethylene oxide is behind the electrical conductivity in this system.
3. Redox polymers containing immobilized redox centers (electroactive centers) can conduct charge by electron transfer from one center to another through the well known “hopping” mechanism. During conduction, electrons tunnel from one redox center to another through an insulating barrier. The systems need to have a large number of redox centers to increase the probability of such tunneling.
4. Intrinsically conducting polymers are conjugated polymers consisting of alternating single and double bonds, creating an extended π -network. The movement of electrons within this π -framework is the source of conductivity. However, dopant is required to increase the level of conductivity for this type of polymers.

2.3.1.1 Conducting Polymer Composite Materials (CPCM)

The development of efficient conductive polymer composites materials(CPCMs) remains an important endeavor in light of growing energy concerns. Conductive and anti-static compounds have been commercially prepared for more than 80 years. A CPCM consists of a random distribution of conducting filler throughout an insulating polymer; this is of interest for several application fields. It is crucial to choose a suitable filler-polymer pair in the production of CPCM. A good balance between filler-polymer and filler-filler interactions can lead to the formation of a continuous network, but filler particles tend to stick together if the filler-filler interactions dominate and aggregates rather than forming network of particle-contacting chains. On the other hand, a good adhesion between polymer and filler results in an insulating layer around the filler particles and prevents formation of current-conducting chains. Many conductive polymer composites exhibit percolation characteristics(Chung, Sabo, & Pica, 1982; Flandin, Bréchet, & Cavallé, 2001).

The most universal conducting filler for this purpose is carbon black, because dispersion of conducting carbon black particles in synthetic polymers is a very efficient way of providing them with semi-conductive and antistatic properties. From the economical and technical viewpoint, decreasing the carbon black percolation threshold as much as possible in the blend is desirable. Consequently, the percolation theory is the most adequate for modelling conductivity of CPCM.

It has been observed that insulator-conductor transition in polymer-filler composites depend on the aggregation(Masao Sumita, Kayaki, & Miyasaka, 1986), size, size distribution, structure and porosity of the conducting particles(Verhelst, Wolthuis, Voet, Ehrburger, & Donnet, 1977), on rheological properties of polymer components(Miyasaka et al., 1982b), and on processing conditions.

The curve of conductivity versus filler concentration is S-shaped (Figure 2-18), which clearly demonstrates a relatively narrow filler loading range during which a small increase in loading will result in a drastic increase in conductivity. This change implies some sudden changes in the dispersing state of conductive particles at a critical point (percolation threshold), i.e. the coagulation of particles to form networks which facilitates the electrical conduction through the composites. Figure 2-18 shows the conductivity of a thermoset system of multiwall-nanotube/

epoxy as a function of nanotube weight fraction. Consequently, insulator to conductor transition is attributed to the critical amount of filler necessary to build up a continuous conductive network, resulting in a tremendous change in the electrical conductivity (Du et al., 2004).

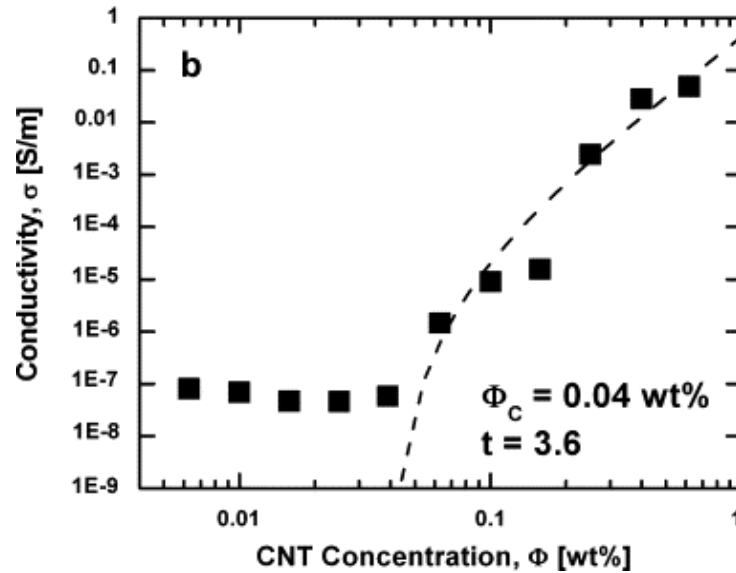


Figure 2-18. Simultaneous measurement of the nanocomposite (MWCNT/epoxy) electrical conductivity as function of the nanotube weight fraction, performed in the liquid state prior to curing at 0.1 s^{-1} and $20 \text{ }^\circ\text{C}$. The rheological percolation threshold is located at $0.1 \text{ wt}\%$ and the electrical one at $0.04 \text{ wt}\%$ (Du, et al., 2004).

Since the polymer blends containing conductive filler with continuous structures are universality systems, the conductivity value for filler loading fractions higher than the filler percolation threshold can be calculated with regards to the critical concentration of conductive material (percolation threshold) p_c by the following scaling law (Kirkpatrick, 1973; Stauffer & Aharony, 1994b).

Equation 2-43.
$$\sigma \propto (p - p_c)^t$$

Equation 2-44.
$$\sigma = \sigma_c (p - p_c)^t$$

where p is the volume fraction of the conducting phase above the percolation threshold, p_c is the percolation threshold, σ is conductivity of sample at given volume fraction of p , and σ_c is the conductivity of the sample at the percolation threshold. The conductivity exponent t generally reflects the dimensionality of the system with values typically around 1.3 and 2.0 for two and three-dimensions, respectively (Clerc, Giraud, Laugier, & Luck, 1990). Gubbels et al. found that in a polystyrene (PS)/ polyethylene (PE)/ carbon black (CB) system, t is 2.0 when CB is dispersed within the amorphous phase of pure PE. Its value becomes 1.3 when CB is at the interface of a PE/PS blend with dual-phase continuity (Gubbels, Blacher, et al., 2002; Gubbels, Jerome, et al., 2002). Al-Saleh et al. (Al-Saleh & Sundararaj, 2008) showed that selective localization of CB at the interface of PS/PP blend is possible by introducing SBS copolymer that can selectively localize at the interface and for which CB has the highest affinity. Addition of 5% SBS resulted in reduction of percolation threshold to less than 1%.

The classical percolation theory (Equation 2-44) applied to conductive polymer composite systems must meet some definite conditions. First, the system should be randomly distributed, and secondly, particles must be spherical, monodisperse and have an isotropic conductivity. If one or all of these conditions are not fulfilled, the theoretical value will deviate far from the realistic one. For example, Carmona et al. (Carmona, Prudhon, & Barreau, 1984) reported that in short fiber-epoxy resin composites, the exponent $t = 3.0 \pm 0.6$ when the length of fibers ranges between 1.15 mm and 2.85 mm.

A simplified view of percolation transition is depicted in Figure 2-19. At low filler loadings the conductive particles act like conductive islands in a sea of electrically insulating resin. Since electrons moving through the composite still encounter the insulating polymer, little or no change in conductivity is observed. Addition of further conductive material leads to the conductive particles being more crowded and more likely to come into contact with each other. Finally, at the percolation threshold, the first complete cluster from the bottom to the top of the sample is generated.

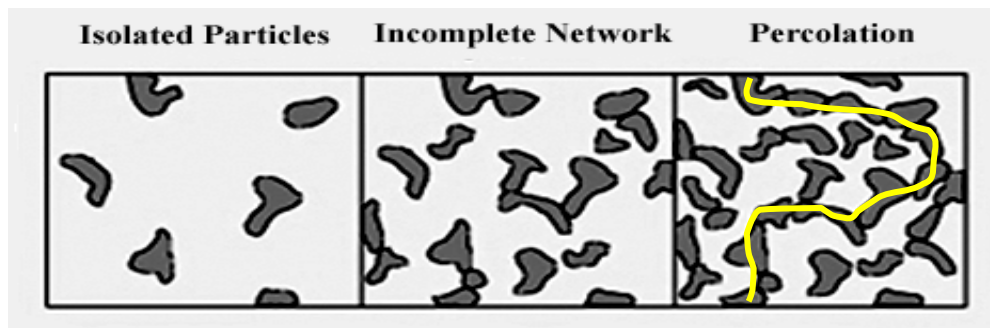


Figure 2-19. Approaching the percolation threshold in a binary blend

Thereby, continuous chains or networks of conductive material through sample are formed. An electrical charge can now pass through the conductive composite or blend via this network without encountering the low conductivity of the polymer resin. Introducing further conductive material loading beyond the percolation threshold does not greatly increase the conductivity of this material (Bhattacharya, 1986).

2.3.1.1.1 Parameters Influencing the Percolation Threshold of Conductive Fillers

There are several ways to decrease the percolation threshold of conductive filler concentration in polymeric matrices, which are mainly based on the use of additives, the polymer properties, the optimization of processing conditions, and the size, distribution and porosity of the filler (Smuckler & Finnerty, 1974; Verhelst, Wolthuis, Voet, Ehrburger, & Donnet, 1977). Therefore, varying these factors can cause strong deviations from the percolation theory. Several important factors influencing the percolation threshold in conductive polymer composites are as follows:

- **Type and Shape of Conductive fillers**

The shape of the particle plays a critical role in where (at what filler volume) percolation occurs. The more structured or elaborately shaped the particle, the more likely it is to contact a nearest neighbor and form a continuous network. Perfectly spherical fillers, which arguably have the least elaborate and least structured shape, can require as much as 40% loading in order to reach

the percolation threshold. As compared in Figures 2-20a and 2-20b, by using high aspect ratio fillers such as conductive fibers/wires, the conductivity of the polymer composite can be achieved at a much lower filler loading level (Figure 2-20c).

Carbon-black particles are more irregularly shaped and often have long branches reaching out from the main body of the particle. These moderately structured fillers can require anywhere from 5 to 35% loading to reach the percolation threshold (Sichel, 1982). In carbon black filled nitrile rubber composite, the percolation threshold lies in between 20% and 35%, while for a short carbon fiber filled composite it ranges from 10% to 20% (Pramanik, Khastgir, & Saha, 1992). Highly shaped fillers such as carbon or stainless-steel fibers may be present in as little as a few percent by volume in order to achieve low resistance. Gelves et al. (Gelves, Lin, Sundararaj, & Haber, 2006) used silver and copper nanowires with a diameter of 25 nm and aspect ratios of up to 200 and 400, respectively. Electrical percolation thresholds of 0.5-0.75 vol.% for silver nanowires and 0.25-0.75 vol.% for copper nanowires in PS nanocomposites were found.

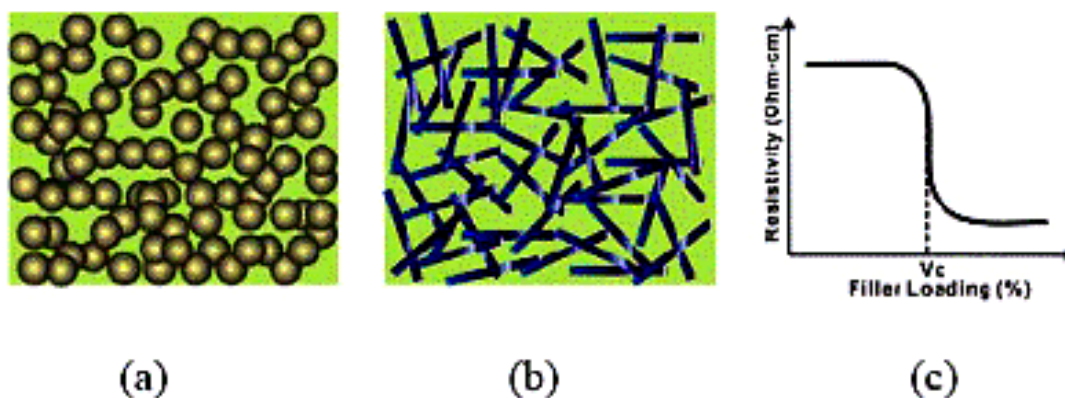


Figure 2-20. Schematic illustrations of conductivity establishment for polymer composites with (a) spherical fillers, (b) high aspect ratio fillers (fiber/wire) and (c) percolation threshold (V_c) in a resistivity vs. filler loading plot (Wong, 2003-2008)

Lin et al. (Lin, Gelves, Haber, Potschke, & Sundararaj, 2008) reported an electrical percolation threshold between 1 and 2 vol.% for polystyrene/copper nanowire nanocomposites. The nanowires have a diameter of around 25 nm and an average length of $1.29 \pm 0.83 \mu\text{m}$. A very low percolation threshold of high aspect ratio fillers for silver nanotubes is shown in Figure 2-21.

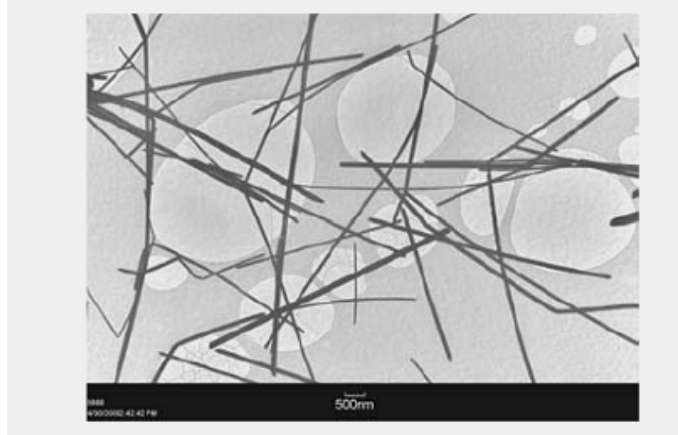


Figure 2-21. Transmission electron micrograph of silver nanowires(Wong, 2003-2008)

- **Polymer Polarity**

Some studies(Miyasaka et al., 1982a) revealed that the polymer polarity may be related to the percolation threshold; that is the higher the polarity of a given polymer, the larger the percolation threshold is. As well, a correlation between the surface tension of the polymer and the percolation threshold was found(Johnson, Kendall, & Roberts, 1971): the larger the surface tension, the larger is the percolation threshold.

- **Polymer Viscosity**

Percolation threshold is limited by increasing the viscosity of the polymer(Sau, Chaki, & Khastgir, 1997), since high viscosity of the polymer results in high amount of breakdown and degradation of the structure of carbon black owing to the high shearing action experienced during mixing. Consequently, the formation of a conductive network throughout the matrix is delayed and occurs at a higher concentration(Sau, Chaki, & Khastgir, 1998).

- **Polymer Crystallization**

High-density polyethylene loaded with conductive carbon black showed that the carbon black aggregates tend to concentrate in amorphous regions. A major part of the carbon black aggregates in a semi-crystalline system are located in amorphous regions. Lower percolation

threshold concentrations are obtained in semi-crystalline systems compared to amorphous polymers due to geometrical restriction of the conductive pathway(Narkis & Vaxman, 1984).

- **Polymer Blend Morphology**

Another approach to reduce the percolation threshold of conductive fillers relies on the selective localization of conductive phase particles in multiphase polymeric materials in one of the phases or better yet at the interface of binary co-continuous blends(Gubbels et al., 1995). A percolation threshold of 0.5 vol.% of carbon black was reported by compression molding of a mixture of carbon black and polystyrene powders(Klason & Kubát, 1975). Although the carbon black particles do not penetrate the polystyrene phase and remain essentially located at the interface between polystyrene particles, this method suffers from poor mechanical properties and reproducibility. Gubbels et al.(Gubbels, Blacher, et al., 2002; Gubbels, Jerome, et al., 2002) succeeded in fabricating a multiphase material with low percolation of carbon black particles in polymers by selectively localizing carbon black percolation threshold of conducting polymer lowers owing to double percolated structure(Levon, Margolina, & Patashinsky, 2002; Sumita et al., 1992). The percolation threshold of the poly(ethylene-co-vinyl acetate) (EVA)/high density polyethylene (HDPE)/ carbon black (CB) blend is at a significantly lower carbon content than the individually filled HDPE or EVA(Foulger, 1999). Similar results were obtained for polypropylene/nylon/CB(Tchoudakov, Breuer, Narkis, & Siegmann, 1996).

The effect of the PE continuity fraction on the CB content is illustrated in Figure 2-22. Double percolation is at the origin of this situation(Calberg et al., 1999):

- 1) Percolation of the polymer phases and thus of their interface.
- 2) Percolation of the conducting particles in one phase or at the interface.

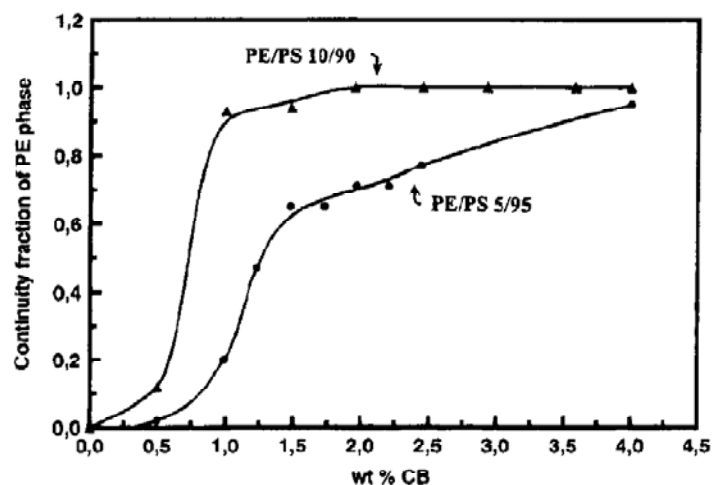


Figure 2-22: Dependence of PE continuity fraction on the CB content in 5/95 and 10/90

Jerome et al. (Gubbels, Blacher, et al., 2002; Gubbels, Jerome, et al., 2002) conducted studies with different binary blends, such as PE/PS and PS/PMMA, to investigate the influence of parameters on the percolation threshold and extend the dual percolation concept to other binary blends.

Jerome and co-workers found that due to thermodynamic forces governing the system and filler aggregation, the classical theory of percolation (Equation 2-44) can not account even qualitatively for most of the experimental data. For instance, the experimental t exponent is quite different from the theoretical values and depends strongly on the morphology of the blend. Hence, the theory needs to be modified. It was observed that for PE/PS blend, carbon black was accumulated at the polymer interface as the result of a kinetic control leading to unstable systems, but in PS/PMMA, due to the more polar polymer component (PMMA vs. PE), the interfacial localization of CB particles was appropriately improved (Calberg, et al., 1999) (Figure 2-23).

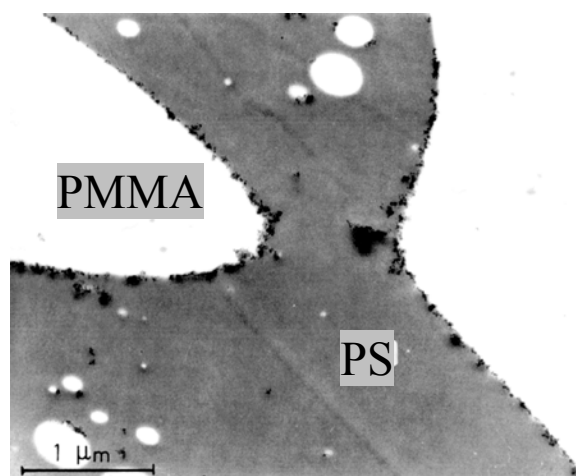


Figure 2-23. TEM micrograph of a 50/50 PS/PMMA blend filled with 2 wt% CB.

2.3.1.1.2 Percolation Threshold of Carbon-Nanotube Polymer Composites

Figure 2-24 clearly shows a large spread in the number of investigations for polymer/carbon nanotubes in different polymer matrices. Figure 2-24 also shows the minimum observed percolation thresholds ϕ_c together with the number of publications for each polymer matrix. This study shows that for all $\phi_c > 0.2$ wt% of carbon nanotubes, no more than two papers could be exploited. This finding supports the belief that with optimized dispersion methods a percolation threshold $\phi_c \approx 0.1$ wt% might be obtainable for nearly any CNT/polymer system (Bauhofer & Kovacs, 2009).

2.3.1.1.3 Disadvantages of Conductive Fillers, Especially Carbon Black

The great majority of commercial resins are compounded with conductive fillers to create conductive composites. The most commonly used composite is 15–30% carbon black in polymer to make containers, trays, bags, work surfaces, wrist straps, etc.

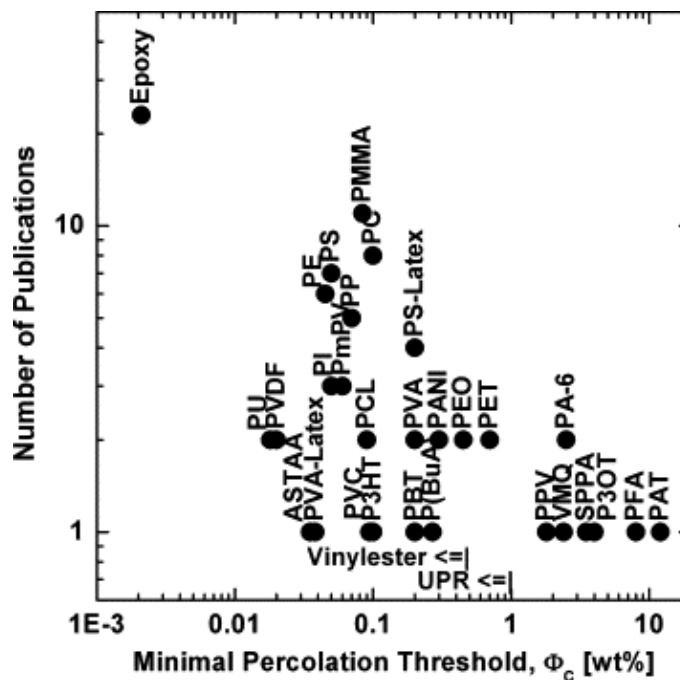


Figure 2-24. Plot of the total number of publications per polymer system versus the minimum percolation threshold achieved with the respective system (Bauhofer & Kovacs, 2009).

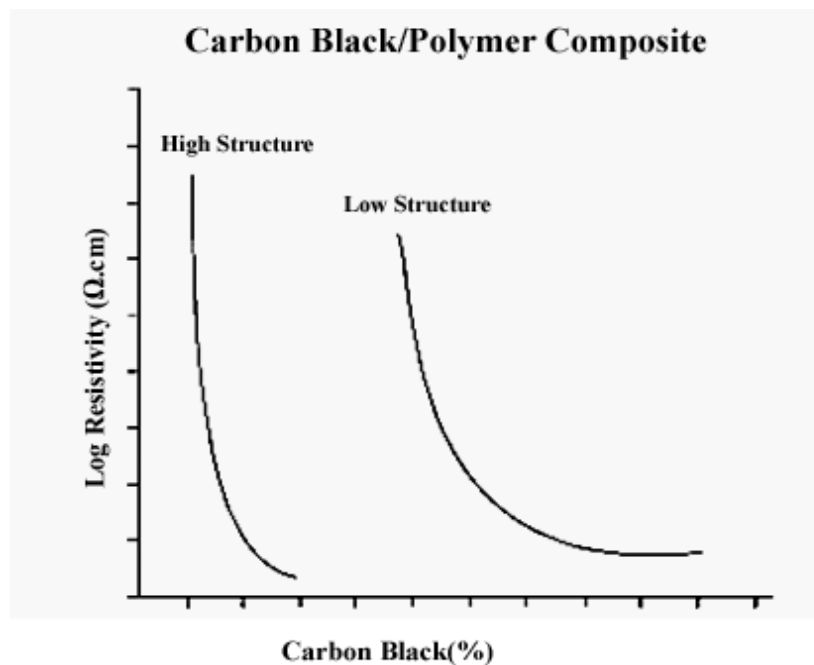


Figure 2-25. Resistivity of carbon black/polymer composite as a function of carbon black volume fraction (Rosner, 2000)

Although polymer and carbon-black composites are versatile, relatively inexpensive, and permanently conductive, there are several disadvantages related to the use of carbon black. The possibility of contamination of clean-room environments by shedding of carbon particles, a process known as sloughing, makes it unusable in many areas. Also, the level of conductivity for a particular resin is hard to control because of the steepness of the percolation curve (Figure 2-25). Thereby, resistivity levels ranging from 10^6 to $10^9\Omega$ are hard to reach, and also other conductivity values are not completely reproducible.

2.3.1.2 Intrinsically Conductive Polymers

Applications of conductive polymers have been extended during the last years, with the emphasis being to make better, smaller and faster electronic instruments. A few years ago, semiconductor silicon was the only material used to fabricate almost all electronic devices. Around 16 million bits of information can be stored by an advanced silicon chip in an area of less than 1 cm^2 , although a practical limit to the density of stored information in a chip exists. With further decreasing of the size, overheating occurs and electronic components do not work properly. To overcome this limitation, it has been suggested to use conductive polymers as a conventional semiconductor. Moreover, polymers have the advantages of flexibility, lightweight, high chemical inertness, corrosion resistivity, and ease of processing.

Intrinsically conductive polymers have caused a dramatic change in polymer architecture. A key property of a conductive polymer is the presence of conjugated double bonds along the backbone of the polymer. A regular chemical bond (C–C) occurs when two atoms share a pair of electrons. Such sharing of electrons allows atoms to bind together and keeps molecules from flying apart. A double bond denoted as (C=C) occurs when the atoms share an extra pair of electrons. Conjugation occurs when there are single and double bonds alternating along the polymer chain in a π -conjugated system of the conductive polymers (Gerard, Chaubey, & Malhotra, 2002; Inzelt, Pineri, Schultze, & Vorotyntsev, 2000; Pron & Rannou, 2002). Consequently, electrically conducting polymers are composed of macromolecules having fully conjugated sequences of double bonds along the chains. It implies that in intrinsically conductive polymers, the polymer

chain provides the conductive path for the electrons. π -electrons are responsible for the unusual electronic properties of these polymers, such as low ionization potential, low energy optical transition, electron conductivity and high electron affinity.

The conductivity of a polymer can be significantly increased by doping it with oxidative/reductive substituents or by donor/acceptor radicals. For example, Shirakawa et al. reported a conductivity increase of 9 to 13 orders of magnitude for doped polyacetylene (PA). Doping inorganic materials such as silicon involves substitution of atoms and is completely different from doping organic polymers. Conductive polymers are doped with oxidizing or reducing agents and chemicals that remove electrons from or add electrons to the polymer. A simple explanation is that the oxidation or reduction changes the electronic structure of the polymer so that it can conduct electricity. The degree of conductivity in the doping process is related to many factors, including the polymeric structure, degree of doping, and type of dopant. The “doped” form of polyacetylene had a conductivity of 10^5 Siemens per meter, which was higher than that of any previously known polymer. As a comparison, silver and copper have conductivity of 10^8 S m⁻¹.

One of the most important domains still at the foreground of research activity in electrochemistry is preparation, characterization and application of electrochemically active, electronically conducting polymeric systems. From a practical standpoint, the first generation of intrinsically conductive polymers did not achieve great commercial success. These polymers tended to be insoluble, unprocessable, and extremely sensitive to environmental conditions.

The genesis of the field can be traced back to the mid 1970's when polyacetylene was reportedly prepared by accident by Shirakawa(Ito, Shirakawa, & Ikeda, 1996) as the first polymer capable of conducting electricity. Polythiazyl (SN)_x discovered in 1975, was one of the pioneering conjugated polymers which showed conductivity around 0.29 K(Greene, Street, & Suter, 1975). Shirakawa et al.(Shirakawa, Louis, MacDiarmid, Chiang, & Heeger, 1977) in 1977 established the idea of using polymers for electrical conducting goals when the iodine-doped trans-polyacetylene, (CH)_x, exhibited a conductivity of 10^3 S/cm. After the appearance of the first organic conductive materials, other conducting polymers were synthesized, such as polyaniline (PANI), polypyrrole (PPY), poly *p*-phenylene (PPP), polythiophene (PT), and polyfuran (PFU), which are shown in Figure 2-26. Researchers started to work in this area and could tune the

conductivity of these polymers for various applications from the insulating regime to the superconducting regime, using different methods of chemical modification, and especially doping.

During the last decade, conductive polymers have found applications in a wide variety of fields of technology and science, such as biosensors for coupling of electron transfer, antistatic coating, development of individual electronic devices, gas sensors, electrochromic windows, preparation of pH or reference electrodes, corrosion protection, and whole integrated circuits.

At present, conductive polymers are extensively used in novel technologies involving electrochromic, electroluminescent and optoelectric devices such as light emitting diodes (LEDs) or flat-panel light emitting displays, electronically conductive fibers and wires, solar cells, solid capacitors, and Schottky barrier diodes (Galal, Atta, & Mark Jr, 1998; Kumar & Sharma, 1998).

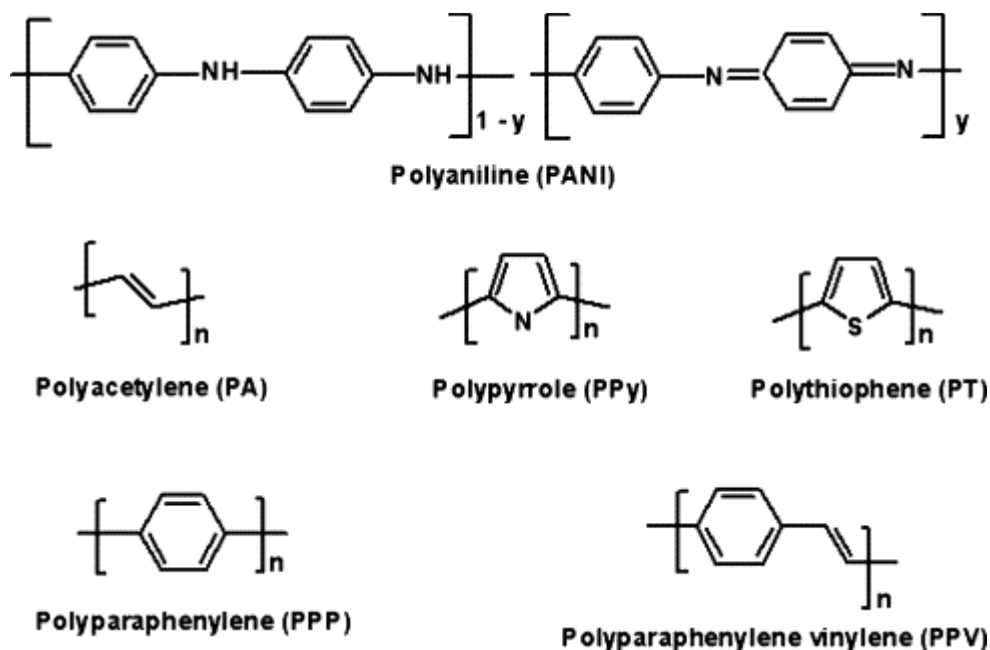


Figure 2-26. The structure of a number of intrinsically conducting polymers (ICP).

2.3.1.2.1 Polyaniline

One of the most technologically promising electrically conductive polymers is polyaniline, due to its good environmental stability(Huang, D., & MacDiarmid, 1986), ease of synthesis, versatile processability and stable conductivity in relation with other conductive polymers. Investigations by Macdiarmid et al.(Macdiarmid et al., 1985) in the mid-1980's resulted in the discovery of electrical conductivity for the emeraldine salt of polyaniline, which led to an explosion of interest in this fascinating polymer. Polyaniline is known to be crystalline, and a highly conducting state is accomplished by simple protonation of the imine nitrogen atoms in the emeraldine base backbone. Only one form of polyaniline, called the emeraldine salt, is electrically conducting. The main disadvantage of all intrinsically conductive polymers, including PANI, is its limited melt-processability. Addition of zinc compound to doped-PANI made some complex allowed a method to tailor the processability of sulfonic acid-doped PANI(Hartikainen et al., 2001; Ruokolainen et al., 2000). It has been observed that for polymer blends containing PANI, a range of conductivity between 10^{-10} S cm⁻¹ to 10^{-1} S cm⁻¹ (melt processing) and 10^{-10} S cm⁻¹ to 10 S cm⁻¹ (solution processing) can be achieved(Panipol, 2000). There are several dopants belonging to the sulfonic acid group for PANI, such as dinonylnaphthalenedisulfonic acid (DNNDISA). Among the sulfonic acids, camphor-10-sulfonic acid (CSA) is much used for this purpose due to high solubility of PANI-CSA in m-cresol(Vikki et al., 1996). A soluble PANI-dodecylbenzenesulfonic acid (DBSA) dispersion was synthesized by Kababya et al.(Kababya, Appel, Haba, Titelman, & Schmidt, 1999) showing that DBSA is molecularly miscible with PANI. PANI-DBSA dispersions have been recently used to prepare blends with other commodity plastics(Haba, et al., 2000).

2.3.1.2.1.1 Binary PANI/Polymer or Ternary PANI/Polymer/Polymer Blends

Co-continuous polymer blends of PANI and a variety of classical polymers have been extensively studied to improve mechanical properties of these materials and also to decrease the percolation threshold of the conductive polymers. Polystyrene(PS)(Jousseume, Morsli, & Bonnet, 2002; Jousseume, Morsli, Bonnet, Tesson, & Lefrant, 1998; Won-Jung et al., 2004;

Woo Jin, Won Ho, & Yun Heum, 2003), cellulose acetate(Niziol & Laska, 1999; Planes et al., 1998; Pron, Zagorska, Nicolau, Genoud, & Nechtschein, 1997; Wolter, Banka, Genoud, Pron, & Nechtschein, 1997), polymethyl methacrylate (PMMA)(Angappane, Rajeev Kini, Natarajan, Rangarajan, & Wessling, 2002; Morgan, Foot, & Brooks, 2001), polyethylene (PE), polypropylene (PP), polyamide (PA)(Domenech, Bortoluzzi, Soldi, & Franco, 2002; Jing, Yang, Zheng, & Lan, 1999; Qinghua, Xianhong, Yanhou, Dajun, & Xiabin, 2002; Zhang, Jin, Wang, & Jing, 2001), polyimide (PI)(Liangcai et al., 2001; Moon Gyu & Seung Soon, 2001; Su et al., 1997; Watcharaphalakorn, Ruangchuay, Chotpattananont, Sirivat, & Schwank, 2005), polyvinyl chloride (PVC)(Chipara et al., 1998; Laska, Zak, & Pron, 1997), polyurethane (PU)(Rodrigues & Akcelrud, 2003; Rodrigues, Lisboa-Filho, Mangrich, & Akcelrud, 2005; Yoshikawa, Hino, & Kuramoto, 2006), and a wide variety of thermoplastic elastomers(Dong-Uk, Kitae, Young Chul, Yun Heum, & Jun Young, 2001; Goh, Chan, & Ong, 1998; Ong, Goh, & Chan, 1997) were used, among others. Conductive polymer blends with good mechanical properties and conductivity varying between 10^{-11} and 300 S/cm have been easily fabricated. There are some other reasons for blending PANI with general polymers, such as to increase the stability of conduction. It has been observed that for polymer blends containing PANI, a range of conductivity between 10^{-10} to 10^{-1} S/cm (melt processing) and 10 S/cm (solution processing) can be achieved(Panipol, 2000). Different techniques, including melt-blending, solution blending, in-situ polymerization, and dispersion mixing have been used to prepare binary and ternary PANI/polymer (A)/polymer (B). Each technique has some advantages and some disadvantages. For example, in PS/PANI melt-blend, the percolation threshold of PANI is much higher than that in a PS/PANI blend prepared by dispersion mixing, although it is clear that a binary blend composed of PANI and PS prepared by melt-blending has better mechanical properties than a PS/PANI blend made by dispersion mixing(Segal, et al., 2001). Moreover, Woo et al.(Woo Jin, et al., 2003) reported that PS/PANI blends prepared by an in-situ polymerization technique have a higher conductivity than by the other techniques, such as solution blending. A conductivity value of 0.1 S/cm for 20 wt% of PANI is observed for a PS/PANI blend prepared by in-situ polymerization, due to a better morphology compared with the other methods, such as solution blending. Zilberman et al.(Zilberman, et al., 2000d) reported that for PS/PANI and LLDPE/PANI, the percolation threshold is about 30 wt% PANI. For a binary blend composed of CoPA/PANI, a value of 20 wt% PANI is obtained. They also observed a high-quality conducting PANI network in a

CoPA/LLDPE/PANI blend and a poor-quality PANI network in a (PS+DOP)/LLDPE/PANI blend. They concluded and reported formation of a host matrix containing two co-continuous immiscible thermoplastic polymer phases and developed a model predicting that doped PANI can generate a network at the interface of CoPA/LLDPE blend and disperse in a (PS+DOP)/LLDPE blend due to their solubility properties. Zilberman et al.(Zilberman et al., 1997) measured the stability of conductivity of 80%PS/20%PANI-DBSA blend at 80°C in a vacuum and at 50°C in 60% RH based on exposure time. It was noted that after four hours, the conductivity decreased from 0.25 S/cm to about 0.1 S/cm in both states. Fraysse et al.(Fraysse, Planes, & Dufresne, 2000) could decrease the percolation threshold of PANI sharply in a PANI/PMMA blend prepared by melt dispersion to 0.5 wt% of PANI. TEM micrographs showed that connectivity of the PANI-CSA network in PANI-CSA/PMMA blend decreases rapidly for a volume fraction less than 0.5% (Figures 2-27a and 2-27b)(Reghu et al., 1994; C. Y. Yang, Y. Cao, Paul Smith, & A. J. Heeger, 1993a).

A typical scenario for a percolating medium with “links” (PANI-CSA fibrils), “nodes” ((crossing points of the links), and “blobs” (dense, multiply connected regions)(Stauffer & Aharony, 1994b)) is illustrated in these figures. Numerous links with diameters of about 100-500 Å are clearly exhibited in the sample containing 0.5% PANI-CSA (Figure 2-27a), while rather few links between the nodes and blobs are observed in sample containing 0.25% PANI-CSA (Figure 2-27b). They showed that the relationship between conductivity and volume fraction of PANI-CSA was critically dependent upon the nature of mass distribution among the links, nodes, and blobs in the samples. They found various parameters involved in this distribution including the molecular weight of the polymers, the viscosity of the polyblend solution, the solvent, and the drying temperature.

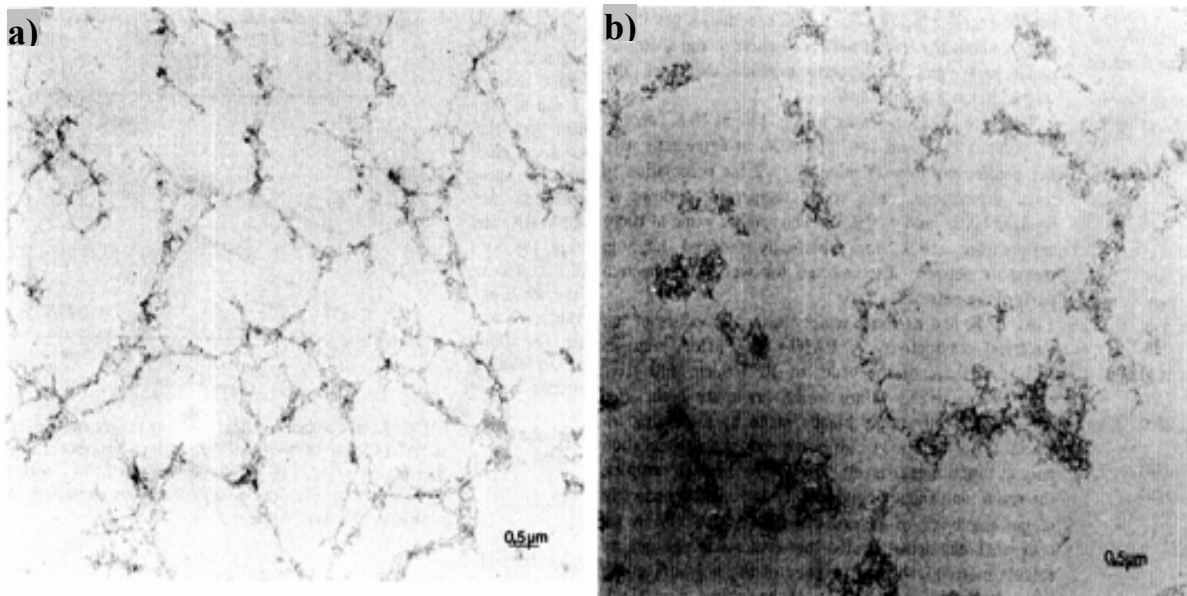


Figure 2-27. Transmission electron micrographs of extracted PANI-CSA/PMMA polyblend films containing (a) Vol% = 0.5% , and (b) Vol% = 0.25% PANI-CSA(Yang, et al., 1993a).

Figure 2-28a depicts the percolation threshold of PANI-CSA in PANI-CSA/PMMA. The scaling law of the percolation theory was applied for linear lines represented in Figure 2-28b to identify the percolation threshold of such a material.

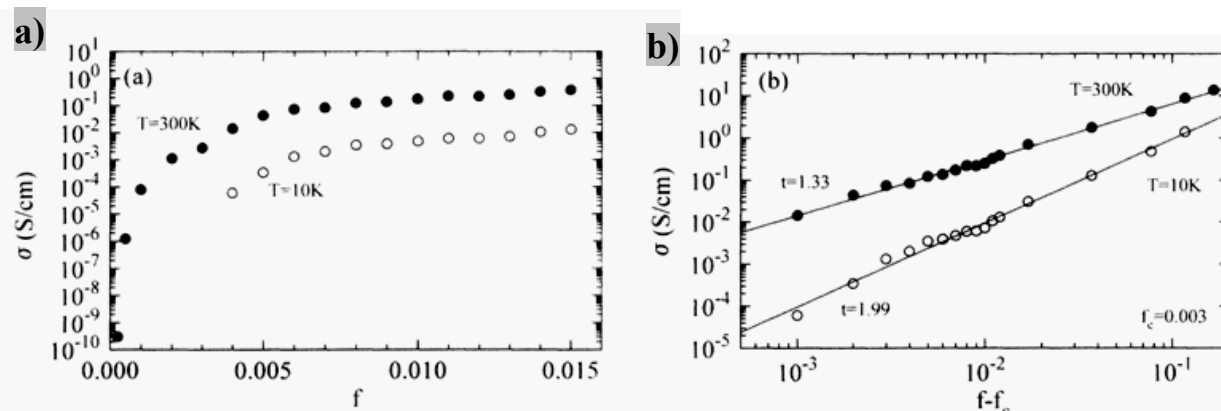


Figure 2-28. a) Conductivity vs volume fraction(f) of PANI-CSA at $T=300\text{K}$ and $T=10\text{K}$, b) conductivity vs $(f-f_c)$ where percolation threshold (f_c) is 0.3%. The solid lines through the points correspond to $t=1.99$ at $T=10\text{K}$ and $t=1.33$ at $T=300\text{K}$ (Yang, et al., 1993a).

Narkis and co-workers extended and developed previous works about melt-blending PANI and other general polymers in order to decrease the percolation threshold and increase mechanical properties (Haba, et al., 2000; Narkis, et al., 2000a; Segal, et al., 2001). They compared dispersion mixing (Figure 2-29a) and melt-blending process (Figure 2-29b) (Narkis, et al., 2000a) and found a percolation threshold of less than 1% for the former case and approximately 20% for latter case.

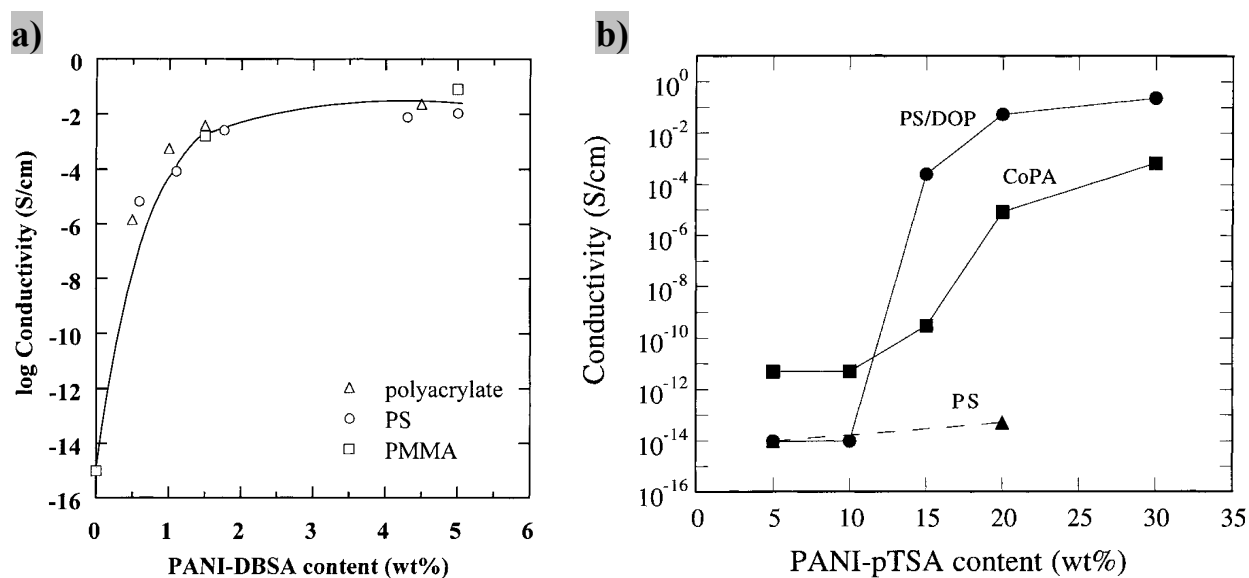


Figure 2-29: Conductivity vs. concentration of PANI/polymer prepared via a) dispersion mixing, b) melt-blending (Narkis, et al., 2000a)

Levon et al. (Levon, Margolina, & Patashinsky, 1993) were the first who suggested utilization of three components instead of two. They introduced the term “double percolated” in a ternary polymer blend consisting of a conductive polymer. Double percolated system was defined as the connectivity in a hierarchical basis of a connected path within a connected path, the last of which is conducting. Narkis et al. (Narkis, et al., 2000a) reported a ternary blend comprised of (PS/DOP)/CoPA/PANI and showed that CoPA situates at the interface. They showed that PANI preferentially locates at the CoPA phase demonstrating a double percolation phenomenon in which PANI is encapsulated by CoPA. The conductivity of the blend as a function of concentration of CoPA was studied (Figure 2-30).

Solvent casting followed by a thermal imidization process was utilized to prepare PANI-DBSA/PI blend. (Han & Im, 1999) It was observed that at a low amount of PANI (about 5 wt%), a good conductivity can be achieved and even has a higher conductivity than pure doped PANI as it is represented in Figure 2-31.

Two recent studies were performed on binary PANI/PVDF blends(Malmonge et al., 2006) (Privalko et al., 2005). The conductivity curves are depicted in Figures 2-32a and 2-32b, representing a percolation threshold of 15 wt% and 3.5 wt%, respectively.

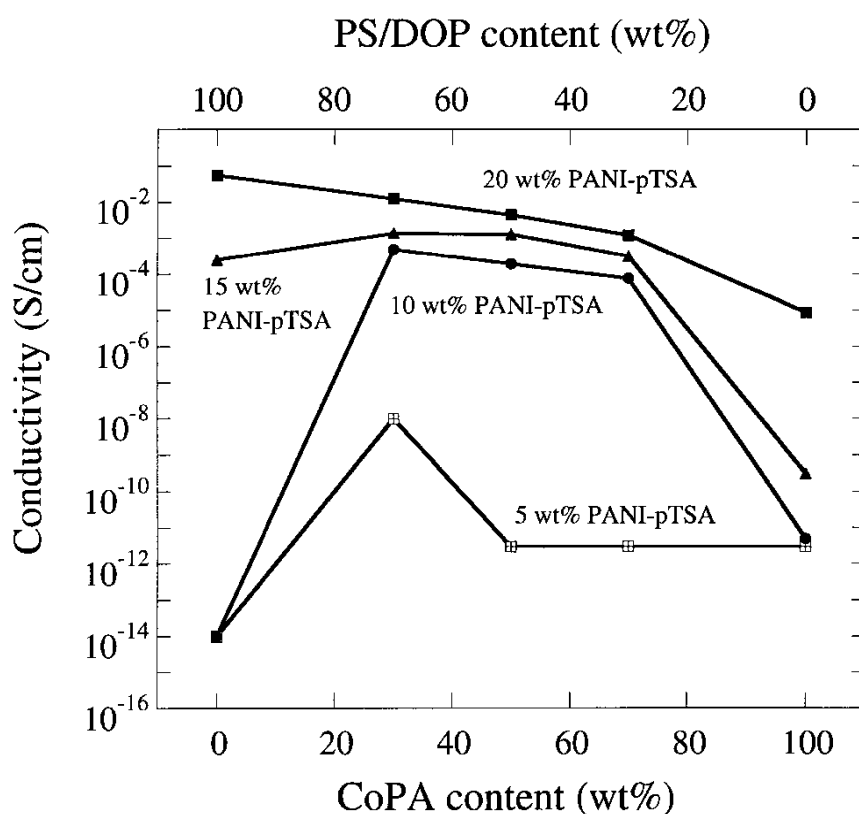


Figure 2-30. Electrical conductivity vs. CoPA content for (PS/DOP)/CoPA/PANI-pTSA blends of various PANI-pTSA contents(Narkis, et al., 2000a)

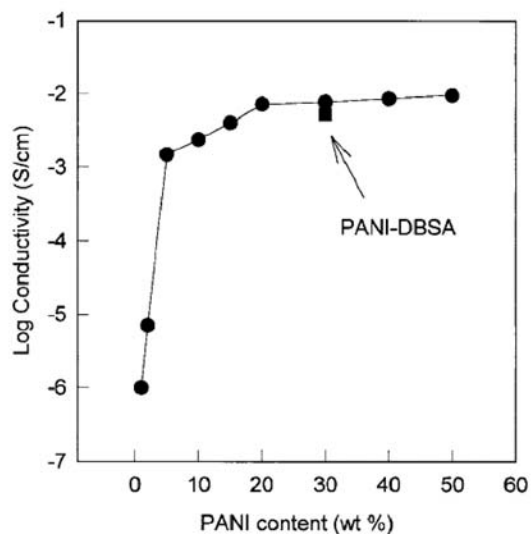


Figure 2-31: Conductivity of PVDF/PANI and pure doped PANI as a function of PANI content(Wt%)

Using the definition of the percolation threshold, it appears that co-continuous structures with various levels of continuity can be formed at various compositions above the percolation threshold. There are several methods to evaluate the percentage of continuity, among which is the relatively simple gravimetric analysis.

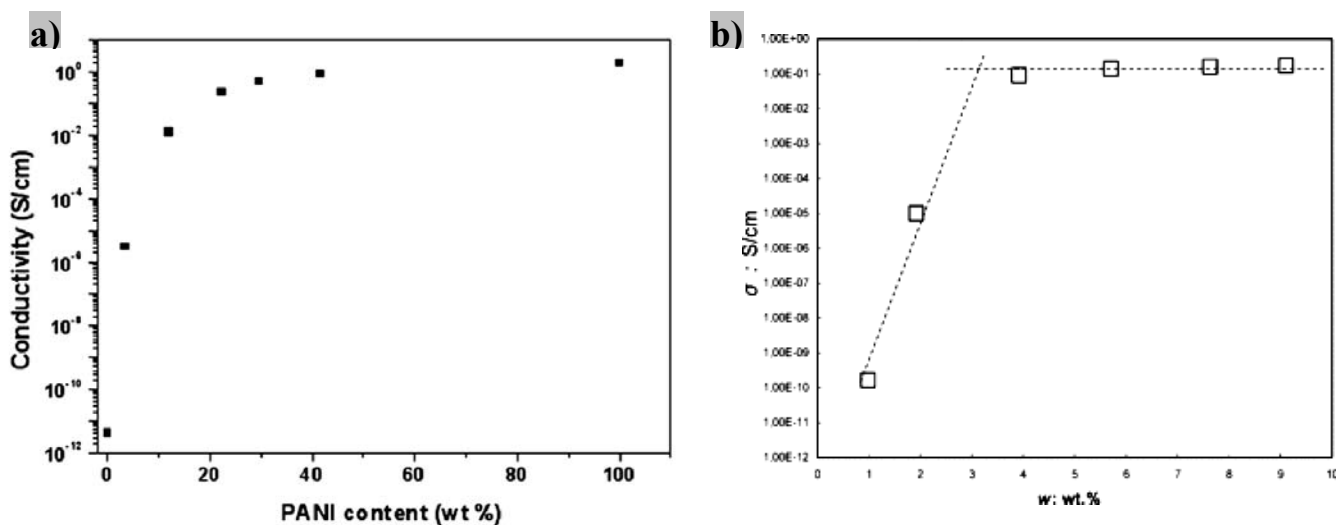


Figure 2-32: Conductivity of PANI/PVDF binary blend based on PANI concentration a) (Malmonge, et al., 2006) and b) (Privalko, et al., 2005)

Co-continuous polymer blends are an interesting and challenging research topic that offer promising opportunities for improving desirable properties. These structures have potential applications in a wide range of fields(Potschke & Paul, 2003), ranging from improvement of physical and mechanical properties(Harm Veenstra et al., 2000) to electrical conductivity(Geuskens, Gielens, Geshef, & Deltour, 1987; Man & Shaw, 2006; Soares et al., 1995) or selective permeability.

2.4 Self-assembly Processes in Material Science

Self-assembly in the classic sense can be defined as the spontaneous and reversible organization of molecular units into ordered structures by non-covalent interactions. Or more simply, self-assembly is defined as the science of things that put themselves together. Hosokawa et al.(Hosokawa, Shimoyama, & Miura, 1996) defined self-assembly as a system in which the following conditions should be met: 1) some bonding forces should be generated; 2) bonding should be selected, 3) moving the parts randomly so that they come together by chance. Campbell et al.(Campbell, Freidinger, Hastings, & Querns, 2002) gave a simpler definition for it which “refers to aggregating of particles into an organized structure without external assistance.” The most straightforward definition was offered by Reif et al.(Reif, Sahu, & Yin, 2006) as a “process in which small objects autonomously associate with each other to form larger complexes”. Finally the most comprehensive definition was presented by Pelesko as “spontaneous formation of organized structures through a stochastic process that involves pre-existing components, is reversible, and can be controlled by proper design of the components, the environment, and the driving force”.

2.4.1 Layer-by-Layer Self-Assembly Technique

Polymer thin films have a great importance in a wide range of technological applications, such as devices with tailored mechanical, physical, chemical, optical, electrical properties or functional coatings. To achieve a well-controlled supramolecular architecture in fabricating

organic thin films, a novel and straightforward method was developed in the last decade (G. Decher & Hong, 1991a; Nicolau, 1985). It was observed (G. Decher & Hong, 1991a) that polyelectrolytes with opposite charges could be assembled in an alternating layer by layer method onto a substrate to generate a sequential multilayer organic thin film (G. Decher, Hong, & Schmitt, 1992b). The potential utility of this method is to obtain thin, uniform electrically conductive films on a variety of substrates, as was shown by Rubner and his group (Cheung, Fou, Ferreira, & Rubner, 1993; Cheung, Fou, & Rubner, 1994; Cheung, Stockton, & Rubner, 1997). It was found that two consecutive layers are strongly interpenetrated, although some researchers believe that the layers are locally interpenetrated and diffusion from one polyanion layer to the neighboring polyanion layer can not occur (Farhat, Yassin, Dubas, & Schlenoff, 1999) but some other authors mention that a network of two co-continuous layers is generated (Cheung, et al., 1997).

In such a film-forming technique, layer-by-layer deposition of different polyelectrolytes with opposite charges is involved to fabricate molecularly controlled ultrathin multilayer films (Tse et al., 2007). Electrostatic interactions are the cause of the adsorption of layers. Kinetic trapping of charge species from solution on the surface can be described as film assembly (Decher, 1997). Repetitive deposition steps provide a precise control over the total thickness of the layers in the range from a few angstroms up to the micrometer range. The LbL technique, unlike other film fabrication processes such as the Langmuir-Blodgett (LB) (Blodgett, 1934; Zasadzinski, Viswanathan, Madsen, Garnaes, & Schwartz, 1994) technique, which requires particular equipment, has no limitation on the type of substrate and charge-bearing species. Consequently, LbL is a simple method and considerably more versatile than other techniques.

Decher et al. (G. Decher & Hong, 1991b) developed the LbL deposition method since it has been extensively used to construct thin films of well-defined thicknesses for a wide variety of applications that can be divided into two categories (Decher & Schlenoff, 2003): 1) tailoring surface interactions, such as corrosion protection (Farhat & Schlenoff, 2002), sensors (Decher, Hong, & Schmitt, 1992a), antibacterial (Rudra, Dave, & Haynie, 2006), antistatic coating for electrophoresis (Graul & Schlenoff, 1999), and biosensing (Yipeng Sun, 1996), and 2) fabrication of surface base devices such as electro-optic materials (Fou, Onitsuka, Ferreira, & Rubner, 1996), devices including nanoreactors (Joly et al., 2000), electrochromic windows (DeLongchamp & Hammond, 2001), or even in the area of surface patterning for the deposition of quantum dots

with a polyelectrolyte (Jaffar et al., 2004). In the LbL approach, the adsorption process involves consecutive and alternate deposition of polyelectrolytes including polyanions and polycations driven by electrostatic forces, or other interactions such as hydrogen bonding. Although oppositely charged polyelectrolyte side groups represent a quite powerful attraction, some other types of intermolecular interactions between polyelectrolytes such as van der Waals, dipole-dipole, and ion-dipole, involve chains of polyelectrolyte and molecules of solvent.

Polyelectrolytes or polysalts are similar to both high molecular weight compounds (polymers) and electrolytes (salts). This means that due to electrolyte groups, they are electrically conductive in aqueous solutions and because of macromolecules, their solutions are viscous. In the LbL technique, each step involves dipping of the substrate into an oppositely-charged solution followed by a rinsing step with water. To maintain film growth until the desired thickness or number of bilayers is achieved, alternate dipping is repeated. A stepwise increase of multilayer thickness or film mass with each deposition step is expected. Thickness of each monolayer in this method is dictated by the polymer geometry; also supramolecular structures of alternately charged polymers can be controlled by polymer combination, surface charges, and solution parameters (Decher, 1997). The thickness increment after each deposition, referred to as growth rate, shows a steady state regime of multilayer assembly with several nanometers thickness for each layer.

Decher (Decher & Schlenoff, 2003) mentioned two significant advantages for layer-by-layer assembly method: 1) surface properties of existing objects and devices can be controlled by controlling surface functionality, and 2) thin-film devices can be fabricated in a very controlled way by template-assisted assembly. Properties of devices can be engineered by controlling the spatial arrangement of functionality in multimaterial-layered nanocomposites. There are some more advantages for this technique in comparison with other methods such as its low-cost preparation and its environmental friendliness. Kotov (Kotov, Dekany, & Fendler, 1995) added that by varying the total number of deposited layers, the total thickness of the coating can be controlled with a precision of a few nanometers. Thus, the technique is exceptionally simple, precise, versatile and scale-up friendly.

After showing the deposition of oppositely charged polymer layers, the number of published papers on polyelectrolyte multilayer has grown exponentially. More than 200 published papers

on the topic have been reported in 2000. The number of published papers per year is represented in Figure 2-33(<http://www.chem.fsu.edu/multilayers/>).

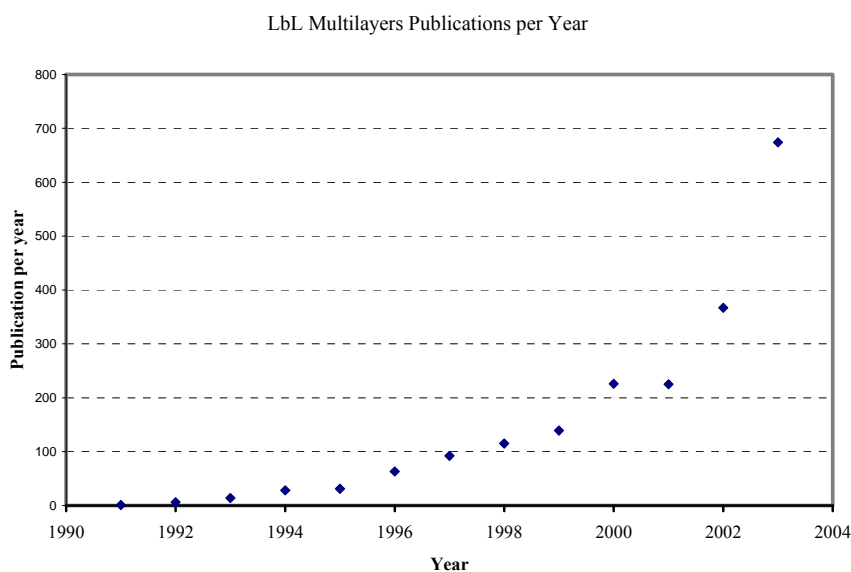


Figure 2-33. LbL multilayers publications per year

Polyelectrolyte is not the only component for the LbL technique as various types of macromolecular species (charged preferred), such as nanoparticles (NPs)(Caruso, Lichtenfeld, Giersig, & Mohwald, 1998; Kotov, et al., 1995), nanowires(R. Gunawidjaja, 2006; Tang, Kotov, & Giersig, 2002), inorganic molecular clusters(Keller, Kim, & Mallouk, 1994), organic dyes(Nicol, Habib-Jiwan, & Jonas, 2003), polypeptides(Lvov, Ariga, Ichinose, & Kunitake, 1995), DNA(Lvov, Decher, & Sukhorukov, 1993), and viruses(Dimitrova, 2007) can be applied as the assembly components. Kotov called the resulting material a nanoparticle-polymer hybrid and explained that by this method, unique properties of monolayers and nanoparticles can be combined with the good mechanical properties of polymers. LbL deposition has practically no limitations on the type of the substrate. Multilayer fabrication by the LbL(Krass, Papastavrou, & Kurth, 2003) assembly technique can use various interactions other than electrostatic interaction, including hydrogen bonding(Stockton & Rubner, 1997), donor/acceptor interactions(Shimazaki, Mitsuishi, Ito, & Yamamoto, 1997), and metal-ion coordination(Krass, et al., 2003). The theoretical description of this theory is quite complex because of the special interactions between the layers. There have been several attempts to model this method(Joanny, 1999; Solis, Cruz, & M., 1999) but they have been inaccurate and certain calculations have not been represented yet.

2.4.1.1 Fabrication of Conductive Multilayers by the LbL Method

Conducting polymers prepared by thin film technology have become increasingly important for electrical and optical applications. Polyaniline is one of the most promising electrically conducting polymers due to ease of synthesis, versatile processability, stable electrical conductivity, and relatively low cost. PANI is used in a wide variety of fields such as chemical sensors (Dan, Yadong, Zhiming, Xiangdong, & Yanrong, 2000; Mathur, Misra, Singh, & Tripathi, 2002), solar cells, light-weight batteries, light emitting diodes, polymer actuators, and corrosion protection agents. Shirakawa et al. (Ito, Shirakawa, & Ikeda, 1974) found that by “doping” polyacetylene, its conductivity is increased by many orders of magnitude. There are two kinds of dopants: electron acceptors (p-type dopants) such as iodine, and electron donors (n-type doping). The use of various concentrations of dopants can vary electrical properties by as much as 18 orders of magnitude, and so conductivity can be controlled in a wide range. The conductivity of the emeraldine base (EB), which is the best representation of polyaniline at ambient temperature, is about 10^{-10} S/cm, while by doping it with different acids and adding sites of (-N=) to EB, emeraldine salt can be formed with a conductivity of about 5 S/cm at the same temperature (Epstein et al., 1986; Ginder, Richter, MacDiarmid, & Epstein, 1987). Ferreira et al. (Ferreira, Cheung, & Rubner, 1994) found that both aqueous and polar organic solutions of positively charged protonated forms of polyaniline and polypyrrole can be prepared, although solubility of PANI in an organic medium such as dimethylacetamide (DMA) is much higher than that in water. Nevertheless, for LbL self assembly, preferred media are aqueous solutions.

The preferential affinity of certain ions for others is an important factor in film growth. In low molar mass compounds, chloride or bromide bind much stronger to the ammonium group than sulfonate does and sodium binds stronger to the sulfonate group than to chloride and bromide. For example, film growth forms smoothly using sodium poly(styrene sulfonate) and poly(N,N,N-trimethyl-2-methacryloyl ethyl ammonium) bromide or poly(diallyldimethyl-ammonium) chloride (Bertrand, 2000).

Rubner's group at MIT investigated both electrostatic and hydrogen-bonded LbL assembly using fully and non-fully ionized polyelectrolyte in solution. They found that the structure of polyelectrolyte multilayer depends on the degree of ionization of the polyelectrolyte. They

succeeded in creating thin films with unique and quite useful properties by using weak polyelectrolytes and tuning charge densities by simple changes in solution pH. It was noted by Cheung and Rubner (Cheung, et al., 1997) that under different pH environments, a weak polyelectrolyte becomes less ionized and so a pH-sensitive trigger can be used to release the charged molecules.

2.4.1.1.1 Charged Polymer Adsorption

In this section, the physical aspects of polymer adsorption are focused. From an architectural point of view, polymers can be divided into linear homopolymers, branched homopolymers, disordered linear heteropolymers, charged polymers or polyelectrolytes, and heteropolymers composed of a backbone and side-chains of different chemical nature (Figure 2-34).

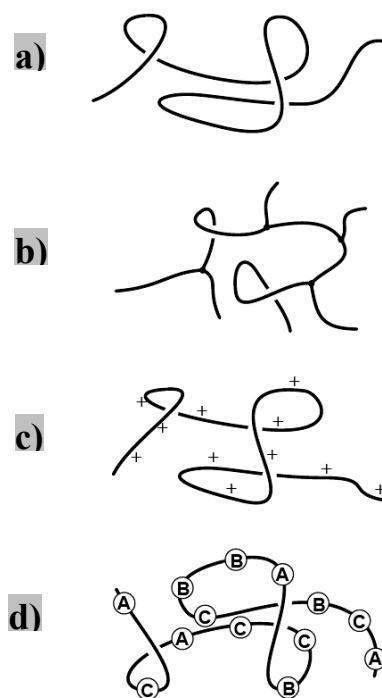


Figure 2-34. Schematic view of different polymer types: (a) linear homopolymers that are the main subject of this review, (b) branched polymers, (c) charged polymers or polyelectrolytes (PEs), and (d) a disordered copolymer with no specific order of the different monomers.

Shapes and sizes of polymer molecules are controlled by the nature of the covalent bonds that bind the atoms of the molecule together. Generally, polymer molecules in a particular kind of solution or in a melt state have a coil shape which is called a random coil. Solvent affinity also affects the conformation of polymers associated with polymer architecture. Therefore, a random conformation is usually found for an uncharged linear polymer chain in solution. In the case of polyelectrolytes, charge also has a significant influence, as charged linear polyelectrolyte chains repel each other due to coulomb repulsion, which causes the chain to adopt a more expanded rigid-rod-like conformation. Persistence length is defined as a characterization factor for stiffness on macromolecule chains. It is the length over which the normalized bond vectors at different locations on the chain are correlated. It can also be described as an estimate for the typical radius of curvature of chains.

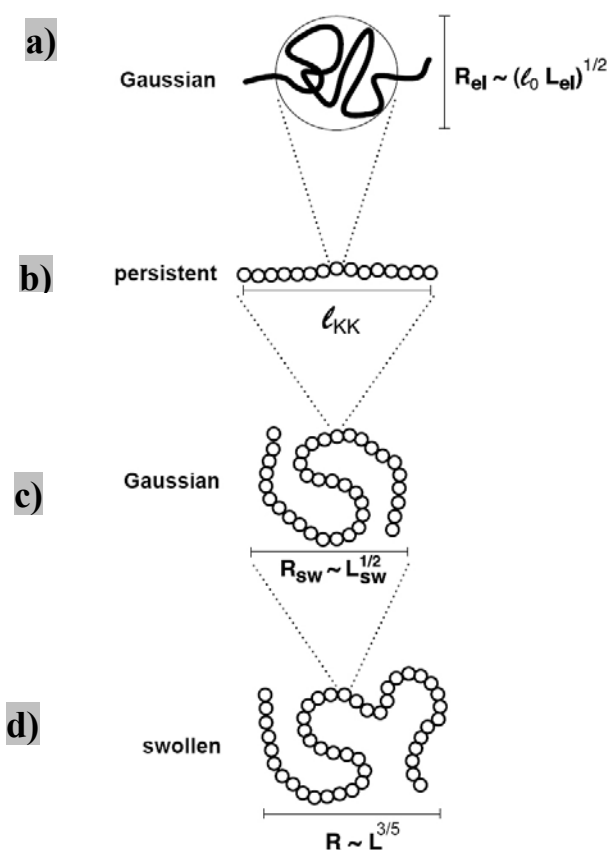


Figure 2-35. Schematic view of the four scaling ranges in the Gaussian-persistent regime (Netz & Andelman, 2003)

Addition of salt to the solution of polyelectrolyte will cause screening of the charges and collapse of the rod polyelectrolyte chain occurs, favoring a more conventional conformation, essentially identical to a neutral chain in good solvent. Another way to control the charge of each monomer for weak polyelectrolytes, including polyacids and polybases, is adjusting the pH of the solution. Consequently, it is concluded that due to chain stiffness and electrostatic repulsion between monomers in a polyelectrolyte, the effective persistence length is increased compared to uncharged polymers. Figure 2-35 shows a schematic view of the four scaling ranges in a Gaussian-persistent regime for a polyelectrolyte structure.

As seen, on scales as small as a Gaussian blob of size R_{el} , each blob contains a segment of length L_{el} . Within these blobs, electrostatic interactions are not so effective. Chain stiffening is caused because of electrostatic repulsions on larger length scales. On a scale larger than R_{el} , Gaussian (electrostatic) blobs are aligned linearly due to electrostatic repulsion.

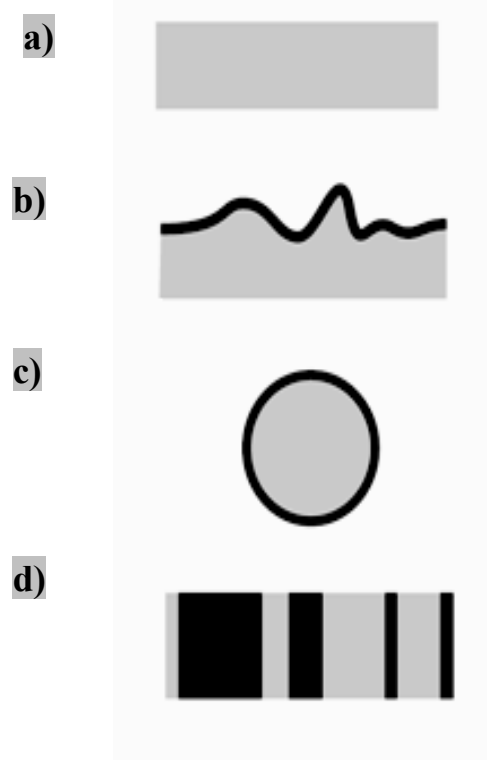
2.4.1.1.2 Polymer Adsorption on the Surface

The choice of substrates has so far been dominated by their convenience for particular analytical methods. Glass and quartz, because of their transparency, are the most suitable materials for utilization of optical microscopy and UV-spectroscopy. Silicon wafer enables X-ray reflectivity studies, ellipsometric studies, and IR-spectroscopic investigations. Gold-coated surfaces are well suited for electrochemical studies, surface plasmon resonance (SPR) investigations, and studies by quartz crystal microbalance (QCM). If the interaction between the solvent and the surface is less favorable than that between the polymer and the surface, the polymer will adsorb from the solution onto the substrate surface. Charged polystyrene sulfonate (PSS), which is soluble in water, has the ability to adsorb onto various hydrophobic surfaces because of the equilibrium adsorption, where the concentration of monomers of the polymer in the bulk solution is less than their concentration close to the substrate surface (Klitzing et al., 1999). In the opposite case, when the interaction between solvent and surface is more favorable than the interaction between monomers of polymer and surface, the entropy of mixing will cause a depletion of

macromolecules from the substrate. Depletion of polystyrene, soluble in toluene, from a mica substrate is an example of this case(Luckham & Klein, 1985).

The type of surface and its internal structure significantly affects the adsorption process. The potential of the surface can be either short-range, influencing on monomers which are in direct contact with or close to the surface, or it can be long-range, affecting on farther monomers through van der Waals or electrostatic interactions. Various possible substrates include: 1) a flat and homogeneous substrate (Figure 2-36a), 2) rough and corrugated surfaces (Figure 2-36b), 3) a curved surface or spherical substrate in which curvature effects can be neglected if the radius of curvature is much larger than the polyelectrolyte size (Figure 2-36c), 4) some other particular surfaces, including chemically non-homogeneous substrates, interfaces of two immiscible liquids, or surfaces with internal degrees of freedom like surfactant monolayers (Figure 2-36d).

Figure 2-36. Different possibilities of substrates: (a) the prototype, a flat, homogeneous substrate; (b) a corrugated, rough substrate. Note that experimentally, every substrate exhibits a certain degree of roughness on some length scale; (c) a spherical adsorption substrate, such as a colloidal particle. If the colloidal radius is much larger than the polymer size, curvature effects (which means the deviation from the planar geometry) can be neglected; (d) a flat but chemically heterogeneous substrate;



Adsorption of polymers on the substrate can be performed through various mechanisms such as grafting of an end-functionalized polymer via a chemical or physical bond. One of the most influencing parameters on adsorption characteristics is polymer topology. Adsorption of star polymers and ring polymers, investigated by some research groups, have been found to be

different from that of linear homopolymers (Stratouras & Kosmas, 1992; Van Lent, Scheutjens, & Cosgrove, 1987). As mentioned before, due to the increase of polymer concentration close to the surface, polymer chains adsorb to the substrate. In an adsorption process of a linear homopolymer, all monomers have the same interaction with the substrate, but some distinguished sections of adsorption are still observed (Figure 2-37). An adsorbed single polymer chain can be divided into three sections, consisting of trains, which are monomers bound to the surface, loops, which are a number of unattached monomers between trains, and tails, which are end sections that can form dangling sections.

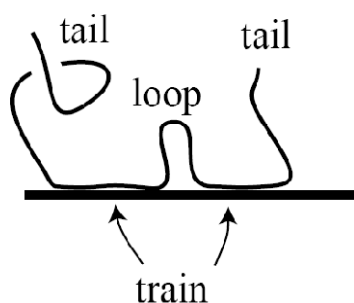


Figure 2-37. The ‘tail’, ‘train’ and ‘loop’ sections of the adsorbing chain

2.4.1.1.3 Adsorption of Polyelectrolytes on the Surface of a Substrate

Generally, there are two factors determining adsorption behavior for a neutral polymer chain. The first factor is reduction of conformational states of the polymer at the substrate. The second one is substrate-monomers interactions (Israelachvili, 1992) that depend on the solvent, the chemical nature of the monomer, and the substrate material. Attractive or repulsive van der Waals interactions exist between the substrate and polymer monomers. It is observed that for strongly attractive potentials or low temperatures, the adsorption between polymer and surface is very strong and the thickness of the adsorbed layer is small (Figure 2-38a). Conversely, at high temperatures or if the attractive potentials are weak, a weakly adsorbed layer is anticipated while a diffuse layer thickness, much larger than in the previous case, is observed (Figure 2-38b).

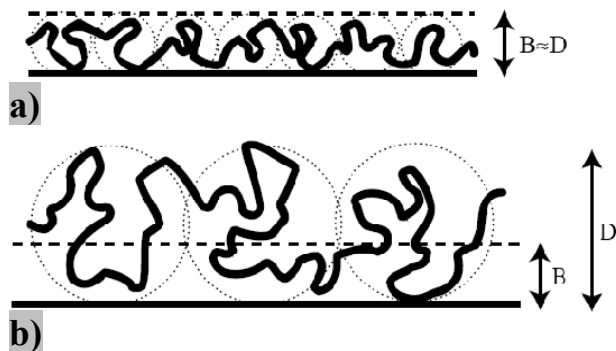


Figure 2-38. Schematic drawing of single-chain adsorption. (a) In the limit of strong coupling, and (b) in the case of weak coupling

Therefore, adsorption behavior of a neutral polymer chain is a result of a competition between the attractive potential and entropic repulsion. The former tries to bind the monomers to the substrate surface and the latter tries to maximize entropy.

In the case of the adsorption of a single semi-flexible polyelectrolyte on an oppositely charged substrate, the adsorption process is a result of a balance between electrostatic repulsion of charged monomers, which leads to chain stiffening, and electrostatic attraction between substrate surface and polymer chain. It is much more complicated than the corresponding adsorption of neutral polymers because the driving force in this case is electrostatic potential. Due to electrical charges of polyelectrolytes, flexibility of the polyelectrolyte chains becomes an important factor in the adsorption of polyelectrolyte to the surface. In order to measure flexibility of a polyelectrolyte, the persistence length is defined. Flexible chains have low persistence lengths while inflexible or rigid ones have high persistence lengths. Light scattering or viscosity measurements are performed to measure persistence length of polymers in dilute solutions.

For charged polymers (polyelectrolytes) in the bulk, the effective persistence length is increased due to electrostatic repulsion between monomers. Polyelectrolyte conformation is governed by intra-chain Coulombic repulsion between charged monomers. Expansion of chain structure due to increase of the persistence length is represented in Figures 39a, 39b, and 39c.

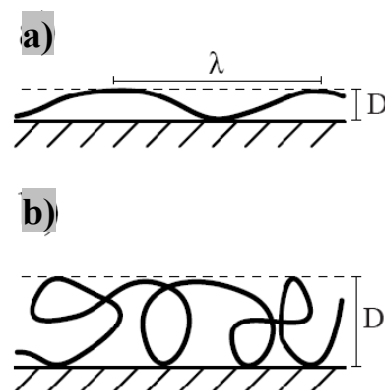
In comparison with neutral polymers, this electrostatic repulsion results in a more extended and swollen conformation (Figure 2-39c).



Figure 2-39. Macromolecule with a) small persistence length, b) medium persistence length, and c) large persistence length

In the adsorption of a single polyelectrolyte chain on the surface, confinement in the adsorbed layer causes an entropic repulsion. If the effective persistence length of the polymer is much larger than the thickness of the adsorbed layer, an extended chain on the surface is observed (Figure 2-40a). In contrast, a random coil with many loops within the adsorbed layer is generated if the effective persistence length is smaller than layer thickness.

Figure 2-40. Schematic picture of a) the adsorbed polymer layer when the effective persistence length is large, (b) Adsorbed layer for the case when the persistence length is small. In this case the polymer forms a random coil with many loops



Consequently, electrostatic interactions play a major role in the adsorption of polyelectrolytes. Other important parameters affecting electrostatic interactions, besides the charged monomers, are the surface charge density, or surface potential in the case of conducting surfaces, the concentration of salt in the solution, or ionic strength of low molecular weight electrolyte, and the pH of the solution.

2.4.1.1.4 Various Mechanisms of Film Growth

Understanding how the multilayers are structured and what governs their assembly is of great importance for tuning their physico-chemical properties.

Two main modes of growth of polyelectrolyte multilayer films, namely linear and non-linear (supralinear or sublinear), have been recognized. The extent of deposited polyelectrolyte per adsorption step for consecutive steps distinguishes the two modes. Generally, strong polyelectrolytes with high charge densities and low ionic strength result in a linear growth. In this case, polyelectrolytes from the solution interact mostly with constituents of the film surface and less with more deeply buried molecules. In linear growth, combination of different techniques such as ellipsometry, SPM, X-ray and neutron reflectivity led researchers to establish a three zone model of the multilayer films(Decher, 1997; Ladam et al., 2000). The first zone consists of the first few polyelectrolyte layers being deposited close to the substrate surface. Typically, the amount of adsorbed polymer per deposition cycle increases during the initial 1 to 5 deposition cycles, and then approaches a constant value(Gero Decher, Lvov, & Schmitt, 1994; Lvov & Decher, 1994). It was observed that for poorly charged surfaces, this transition regime can even stretch over much more than 5 deposition cycles(Kotov et al., 1997; Lutt, Fitzsimmons, & DeQuan, 1998). The thickness per layer in this zone is smaller than in the second zone. The second zone is the bulk film, which contains interpenetrating layers of polyelectrolytes. Due to the proximity of the outer part of the multilayer, the local properties vary because of the solution environment and the increase in surface roughness(Decher, 1997). The third zone is comprised of one or a few polyelectrolyte layers close to the multilayer surface, including a diffuse double layer of counterions to maintain overall electroneutrality(Ladam, et al., 2000).

On the contrary, the mechanism of exponential buildup processes is not clearly understood. The first suggestion for the phenomenon was an increase in film roughness with the number of deposited layers. Later experiments(Picart et al., 2002) suggested that non-linear (exponential) growth results from diffusion of polyelectrolyte molecules inward and outward from a film, while the film thickness is proportional to the amount of migrating polyion. The inward polyelectrolyte diffusion step causes supralinear growth and is favored by a non-homogeneous multilayer (Lavalle et al., 2002). Deposition of poly(L-lysine) (PLL) in the presence of a

polyanion such as hyaluronan (HA)(Picart, Ladam, et al., 2001) or poly(L-glutamic acid) (PGA)(Lavalle, et al., 2002) revealed that PLL chains diffuse in and out of the film during buildup. At the subsequent rinsing step, some of these free chains entrapped in the multilayer diffuse outward from the film but lots of chains still remain inside. In the next step, these remaining free chains were brought into contact with polyanions (HA or PGA) in solution. Due to electrostatic interactions between them, free PLL chains diffuse out of the film, resulting in the formation of PLL/polyanion complexes at the outer layer of the film. The amount of PLL chains that diffuse out of the multilayer in presence of the polyanion in solution determines the thickness of the new forming layer on top of the multilayer. The ability of the polyelectrolytes to diffuse inward and outward of the films (mostly seen for weak polyelectrolytes) can lead to an exponential growth system rather than a linear one. Film roughness is also increased with layer number due to charge mismatch between the polyanions and polycations, demonstrating more non-linear behavior(Bertrand, 2000). Hence, weak polyelectrolytes can display linear or exponential growth, but strong ones always show linear behavior.

2.4.1.1.5 Effect of Polyelectrolyte Concentration on Multilayers

The available amount of polymer to be adsorbed is greater in solutions with higher polymer concentration than in solutions with lower polymer concentration, which leads to greater adsorption(Ferreira & Rubner, 1995). The main reason for greater adsorption in higher concentration solutions is the presence of more anchor sites, including loops and tails, on the substrate surface. This forces molecules to adopt a more compact orientation because of the severe competition of the polymeric chains. In lower polymer concentration solutions, there is less competition, and thus polymer chains straighten out, resulting in thinner layers and smaller adsorption. It was shown(Cheung, et al., 1997) that the bilayer thickness of polyaniline/PSS has an average value between 12 Å and 36 Å (Table 1), which increases by a factor of about three when the polyanion (PSS) solution concentration increases from 10^{-4} to 10^{-2} M.

2.4.1.1.6 Effect of Molecular Weight on Multilayers

Similar growth mode and thickness have been observed for conventional polyelectrolytes with various molecular weights such as poly(ethyleneimine) and poly(styrenesulfonate) (PSS). Conventional or common polyelectrolytes refer to polyelectrolytes having been studied extensively and available from commercial sources such as PSS, poly(acrylic acid) (PAA), poly(diallyldimethylammonium chloride) (PDADMAC), and poly(allylamine hydrochloride) (PAH).

Although previous research shows little effect of molecular weight on the polyelectrolyte thickness, the length of the chains can influence the process in several ways. First, the possibility of association of a long chain in solution to a formed layer is much higher than for a shorter one. In other words, an adsorbed shorter chain can provide fewer binding sites than longer ones because they are poorly suited to multilayer film assembly. Secondly, shorter chains are also more prone to be released from the multilayer to the solution under conditions of overcompensation.

Cheung et al.(Cheung, et al., 1997) reported similar multilayer thicknesses in a wide range of molecular weights of poly(styrene sulfonic) acid, ranging from 5000 to 1000000.

Table 2-1. Relationship between concentration of the Polyanion and thickness of the Monolayers in L-b-L deposition technique(Cheung, et al., 1997)

Concentration (M)	Thickness per bilayer (Å)
0.0001	12
0.001	20
0.005	28
0.01	36

2.4.1.1.7 Effect of Salt on Multilayers

The presence of salt has a subtle effect. It screens the monomer-monomer repulsive interactions, leading to enhancement of adsorption, because the interaction between the non-charged surface and the chain does not have an electrostatic component.

Multilayers are fabricated using salt-containing or salt-free solution. Salt concentration has also been taken into account as the most important factor in multilayer thickness (Decher, 1997; Decher & Schmitt, 1992). In salt-containing solutions, the salt ions of opposite charge (counterions) are drawn to the charged object and form a loosely bound counterion cloud around it. They effectively reduce or screen the charge of the object. The effective electrostatic interaction between two charges in the presence of salt ions is governed by Debye-Huckle law. There are two scenarios for charge balance in a system with and without salt, as shown in Figure 2-41.

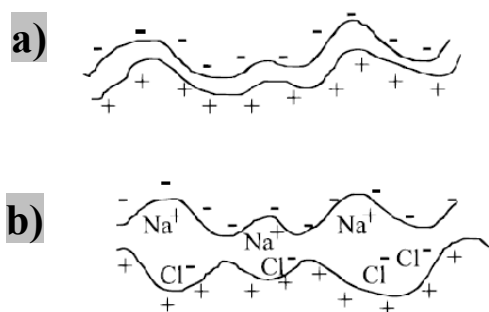


Figure 2-41. Deposition of layer in LbL process a) in the absence of salt and b) in the presence of salt

In the salt-free case, a positively charged polyelectrolyte is balanced by a negatively charged one. In an alternative mechanism, for a salt-containing system, charged polyelectrolytes are balanced by salt counterions derived from the bathing solution and construct multilayers. Thereby, multilayers containing salt ions are thicker, less interpenetrating, and chains have a high degree of mobility, leading to less stable structures.

Schlenoff et al. (Dubas & Schlenoff, 2001a; Schlenoff & Dubas, 2001) performed sequential adsorption of polyelectrolytes in the presence of various concentrations of salt (NaCl) from 0 to 1M. They reported that for strong polyelectrolytes, addition of further salt to the solution results

in swelling of the multilayer, and excess charge can be spread more efficiently into the multilayer surface. Due to the increase in the salt concentration, the surface charge increases for PSS/PDADMAC multilayers (Figure 2-42).

The surface charge depends on the last adsorbed layer, allowing a degree of control over surface and interface properties. In this case, charge overcompensation is the key to multilayer construction. The last-added polymer charge compensates the previous layer at the multilayer surface by a factor of ϕ . Polymer charges within the bulk of the multilayer balance with a 1:1 stoichiometry-termed intrinsic charge compensation if $\phi=1$ and equal ϕ for both positive and negative polymers. Hence, a value of $\phi-1$ represents an overcompensation factor. Normally, the phenomenon of overcompensation of the surface charge occurs when polyelectrolyte chains deposited on the multilayer surface compensate the previous layer charge while it has extra charge to compensate the next deposited layer. In other words, overcompensation can be described for a polyelectrolyte adsorbing on an oppositely charged surface as an overcharging created during repeating of alternating positive and negative dipping. The overcompensation has a maximum value at the multilayer surface and decreases towards the substrate surface. The level of overcompensation at the multilayer/solution interface decreases in an exponential fashion from the interface into the multilayer, representing a characteristic length of decay.

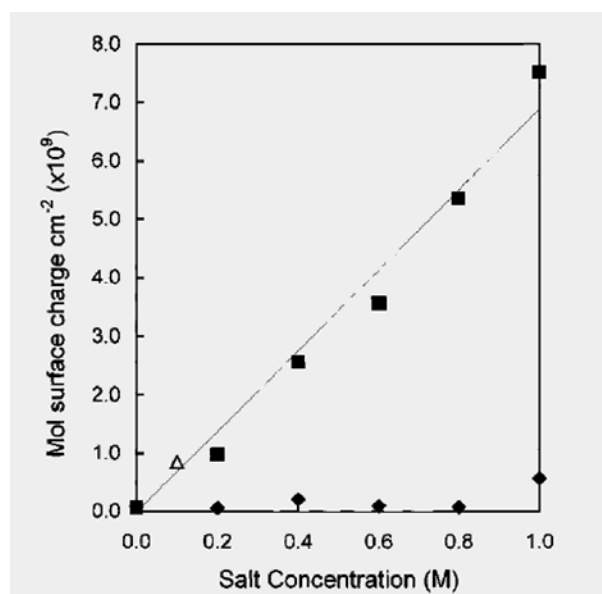


Figure 2-42. Surface charge in LbL process as a function of salt concentration (Schlenoff & Dubas, 2001)

2.4.1.1.8 Overcompensation of the Multilayer/Solution Interface

The charged surface, after each new polyelectrolyte deposition, is the driving force for buildup of multilayers in a linear growth system. In the case of exponentially growing films, at the end of each step, on the outer surface of the multilayer (multilayer/solution interface), an extra charge (overcompensation) appears, which is responsible for the non-linear growth of thickness.

There are two reasons for overcompensation at the interface of multilayer and solution: overcompensation due to diffusion of polyelectrolytes in and out of the multilayer (Lavalle, et al., 2002; Lavalle et al., 2004) and overcompensation due to addition of salt in solutions (Dubas & Schlenoff, 2001a, 2001c; Schlenoff & Dubas, 2001).

2.4.1.1.8.1 Overcompensation due to Diffusion of Polyelectrolytes inside Multilayers

Lavalle et al. (Lavalle, et al., 2002) proposed a model based on AFM observations for overcompensation on multilayer surfaces due to diffusion of polyelectrolytes inward and outward throughout the multilayer film, leading to exponential growth. Later, they verified their idea by means of confocal laser scanning microscopy (CLSM), optical waveguide lightmode spectroscopy (OWLS), and quartz crystal microbalance (QCM) (Picart, et al., 2002). They reported that in a PGA/PLL system, if the outer layer is PLL, two kinds of PLL chains in the film were defined. The first population consists of chains which have formed the multilayer by being strongly involved in interactions with PGA. The second one consists of some mobile chains which are weakly bonded to the polyelectrolyte structure in the film construction. The latter chains can diffuse within the film and are responsible for excess charge of multilayer (overcompensation), which must be compensated by counterions. Dipping the multilayer in a solution of PGA in the next step results in a strong interaction between the PGA chains and the first population of PLL chains located at the surface, to form the outermost layer. At the same time, mobile PLL chains in the interior of the multilayer slowly diffuse outward. When these chains reach the surface, an extra reaction between them and PGA chains present in the solution occurs and an extra layer of PLL/PGA is formed. These neutral complexes are weakly anchored

on the previously formed layer, establishing a larger structure. At this step, while most of the PLL chains have diffused out onto the surface, free mobile PGA chains present in the solution start to diffuse into the multilayer. This time, charge overcompensation is the result of an excess amount of PGA chains in solution. Again, free PGA chains diffuse out, and these processes repeat themselves alternately, resulting in a continuous film reconstruction and leading to an increase in the thickness of the multilayers. Part of the free chains of either polyelectrolyte come out during the rinsing step with a free aqueous solution. The increase of thickness at each step is proportional to the mass of PGA/PLL complexes that form on the surface of the multilayer, which are proportional to the free mobile PLL or PGA chains with weak bonds, that can easily diffuse out of the film.

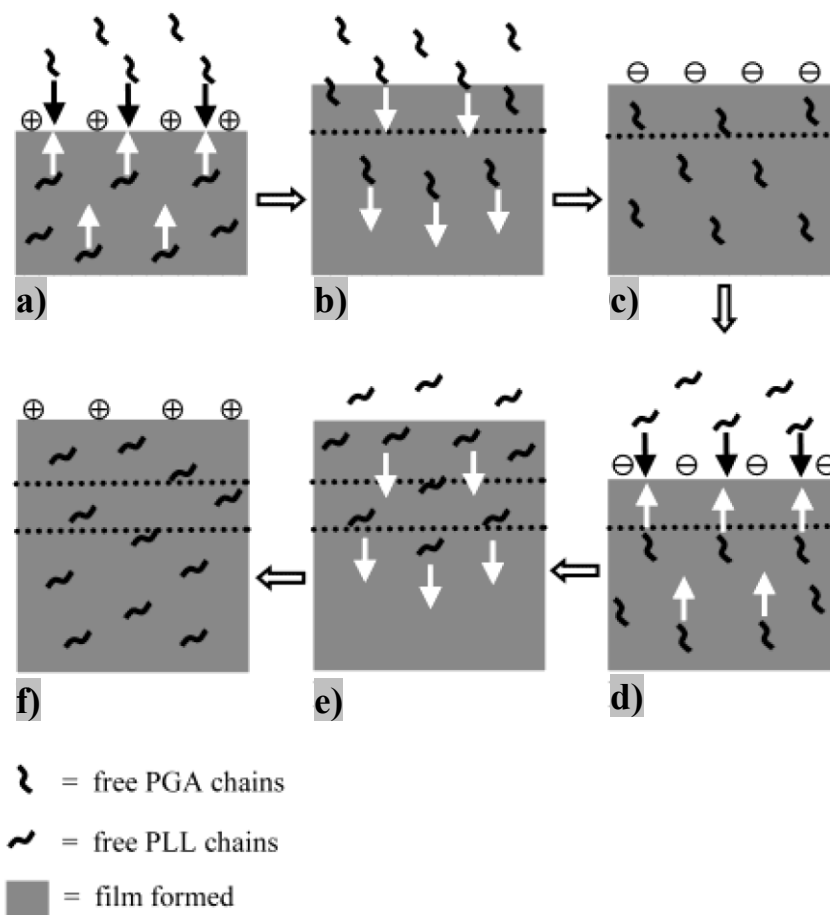


Figure 2-43. Penetration of polyelectrolyte chain inward and outward of a multilayer film

Some other polyanion/polycation systems showing linear evolution in thickness increment generate denser multilayer structures and avoid polyelectrolyte diffusion inside the film. Two

important factors determining the growth regime of a system are ionic strength and pH of the solution. Varying these parameters can change a linear growth regime for a given system to an exponential system(Lavalle, et al., 2002).

2.4.1.1.8.2 Overcompensation due to the Addition of Salt

In the second case, salt concentration is responsible for overcompensation of the multilayer surface. Salt concentration of the solution used for deposition has been found to be the most important variable determining mass deposited and multilayer thickness(G. Decher, 1997). Ion exchange phenomena in multilayers occur and displace small salt counterions by charged polymer segments. Displacement of salt ions and polymer charge pairs compensates any excess surface charge. Salt counterion profile visualizes overcompensation gradient as the excess polymer charge is balanced by small salt ions(Na^+ or Cl^-)(Klitzing & Moehwald, 1995). At low-salt concentrations, the surface charge is completely compensated by the polymer charge. In the absence of salt, the excess surface charge vanishes since the electrostatic free energy diverges. At high-salt concentration, the salt compensates some of the surface charge, resulting in a decrease in the amount of adsorbed polymer.

This has been described in detail for two cases: a strong polyelectrolyte system (PSS/PDADMAC)(Schlenoff & Dubas, 2001) and a weak polyacid (PAA/PDADMAC)(Dubas & Schlenoff, 2001a), which exhibits gradual dissociation. In both cases, adsorbed amount is determined by the surface charge due to salt concentration. In the former case, a constant surface charge during multilayer buildup for strongly dissociated polyelectrolytes was observed. In this mechanism, on each step the level of overcompensation is constant and proportional to a steady-state thickness increment, and only the surface charge signs reverse. Addition of salt to the solution increases the overcompensation charge. In the case of strong polyelectrolyte systems, overcompensation is related to salt concentration and proportional excess charge penetration into multilayer controls the film growth.

Addition of salt within the polyelectrolyte solution causes an ion exchange process and polymer/polymer ion pairs are forced apart. At this step, small salt counterions displace charged polymer segments and make polymers highly swollen because of the water of hydration which is brought in with the salt. In this case, it is required to have a few polymer/polymer ion pairs that

are barely sufficient to hold the polyelectrolyte complex together. If the interaction of the polymer/polymer ion is not strong enough, the polymer chains are sufficiently extrinsically compensated by salt counterions, resulting in an inadequate intrinsic interaction to form and build polyelectrolyte multilayers. When salt ions swell the polyelectrolyte at the surface, some additional polymer adds to the surface of the multilayer due to the concentrated charges in that area. Thus, the surface charge of the multilayer becomes overcompensated and the sign of the surface charge reverses. Consequently, this causes an inversion of the population of surface counterions from anions to cations or vice-versa. This step allows the oppositely charged polymer to deposit on the surface. Figure 2-44 represents two oppositely charged polyelectrolytes when extrinsic compensation occurs by addition of salt. It shows swelling of the multilayer due to the added ions.

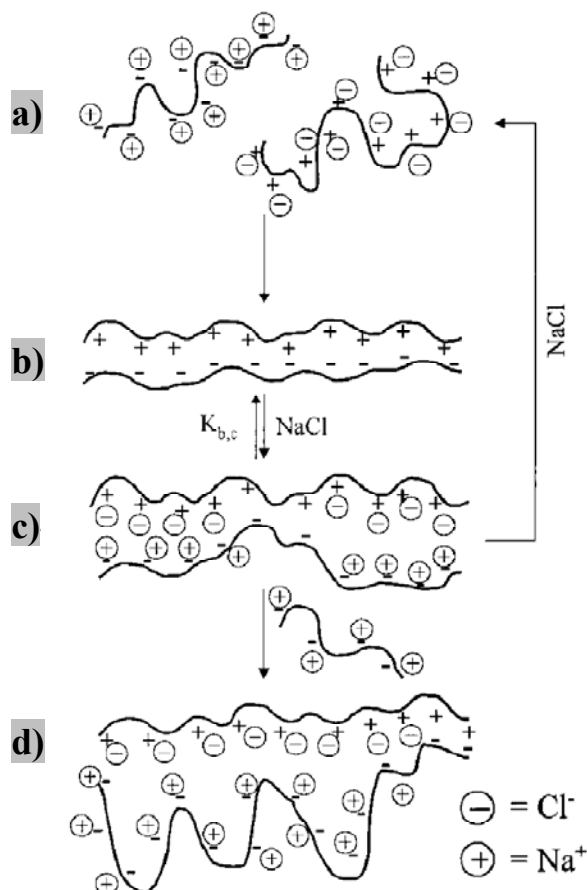


Figure 2-44. Displacement of polyelectrolyte ions with salt counter-ions

As shown in Figure 2-44, swelling and overcompensation steps occur simultaneously during construction of the multilayer, while in the case of high salt concentration, deconstruction of polyanion/polycation is observed.

As more salt is added, the multilayer swells more and excess charge can be spread into the multilayer surface to a point where all the polymer/polymer ion pairings are forced apart and intrinsic compensation is no longer enough to keep the multilayer together. The critical salt concentration for strong polyelectrolytes is much larger than for weak polyelectrolytes. It can be said that further addition of salt can neutralize and thus dissociate weak polyelectrolytes at a lower salt concentration (Dubas & Schlenoff, 1999). For example, the critical amount of NaCl for PSS/PDADMAC is 3.5M, while for a weak polyacid like PAA with a molecular weight of 84500 and a pH of 11, its value is 0.3M (Dubas & Schlenoff, 2001a). Salt can easily swell weak polyelectrolytes in the multilayer structure, like PAA/PDADMAC, and consequently give more deposited mass on the surface while it is less stable than films constructed by strong polyelectrolyte swollen due to salt, such as PSS/PDADMAC.

Some models (Schlenoff, Ly, & Li, 1998) have been developed for the overcompensation at the surface resulting of polymer excess charge due to the presence of salt. It is concluded that salt causes the swelling of the polyelectrolytes and relieves some of the steric repulsive interactions leading to enhanced degrees of freedom. It allows a wider range for the distribution of excess charges and a greater thickness increment per layer. Lefaux et al. (Lefaux, Zimmerman, Dobrynin, & Mather, 2004) studied the dependence of multilayer growth rate on the solution ionic strength by the spin assembly method. UV-Vis and AFM showed that the growth rate of polymer surface coverage increases rapidly with salt concentration up to 0.1M, and that at a higher concentration of salt a constant value or plateau is reached.

Another important effect of salt on multilayer thickness growth is that the addition of salt results in an enhancement of screening and serves to decrease polymer/surface interactions, permitting more chain loops and tails formation.

2.4.1.1.9 LbL Deposition on Curved Surfaces

Numerous investigations for adsorption of polymer on rough and corrugated (Blunt, Barford, & Ball, 1989) or sinusoidal (Hone, Ji, & Pincus, 1987) substrate surfaces have been performed. The first investigations on macroscopically curved bodies was carried out by Alexander (Alexander, 1977). Of considerable interest is the adsorption of strongly charged polymers on oppositely charged spheres (Golestanian & Sens, 1999; Gurovitch & Sens, 1999; Wallin & Linse, 1996) and cylinders (Kunze & Netz, 2002; Odijk, 1980). It has been found that when the radius of the curved surface is much larger than the polymer size, this effect can be neglected. But when the polymer size is large enough, surface curvature has a great effect on polyelectrolyte adsorption on the substrate, whereas the electrostatic energy of the adsorbed polyelectrolyte layer depends strongly on curvature. Very small spherical substrates need a large amount of electrostatic energy to bend a charged polymer around them (Mateescu, Jeppesen, & Pincus, 1999; Nguyen & Shklovskii, 2001). Curvature disfavors adsorption of long, strongly charged polyelectrolytes at too low salt concentration, due to self-repulsion of the charged chains.

2.4.1.1.10 Effect of Roughness on the Multilayer Thickness

The adsorbed polymer layer can be described in terms of loop and tail size distributions (Figure 2-37). It has been observed that the thickness of the adsorbed layer increases with an increase in the adsorption of loopy structures, leading to the deposition of correspondingly large amounts of polyelectrolyte. The relative weight of loops and tails in an adsorbed layer is a measure of entanglement of free polymers to this layer. Loops due to binding to the substrate at both ends are more prone to entanglements than tails. On the other hand, polymer loops dangling from the surface into the solution may entangle with free chains. Consequently, loop size distribution governs coupling between the bulk and the interface (Adjari et al., 1994). The monomers close to the wall mainly belong to loops, whereas the external part of the layer is mostly built up by the tails. This fold-forming of polymer chains (loops and tails) leads to an increase in film roughness. As the polymer concentration increases, the film surface roughness increases due to entangling more polymer chains to loops and tails. Surface roughness is also enhanced by

increasing the pH value due to a decrease in electrostatic repulsion and the prevention of molecular packing when the pH is raised (Braga, Paterno, Lima, Fonseca, & de Andrade, 2008). It can be concluded that the increase of loops and tails is proportional to the increase of surface roughness and adsorbed layer thickness.

2.4.1.1.11 Important Views on PANI/PSS LbL Adsorption

General aspects: Rubner et al. (Cheung, et al., 1997) reported that adsorption of polyaniline onto a negatively charged surface occurs very rapidly. For the most concentrated solution, it took 5 min to reach complete adsorption, and in case of the least concentrated solution (around 10^{-4} M) it took approximately 25 min. It was also mentioned that even for adsorption process as long as 24 hrs, no additional net adsorption was observed. Adsorption of bilayers of PANI/PSS has a linear rate and is independent of the number of layers deposited onto the substrate surface.

Undoped and partially doped polyaniline can be dissolved in a wide variety of solvents, but doped polyaniline can be dissolved only in very strong solvents such as chromic acid. The poor nature of PANI-solvent interactions favors the spontaneous adsorption of polyaniline chains onto a variety of quite different substrates, including both hydrophilic and hydrophobic surfaces. It also demonstrates a significant aggregation of the polyaniline chains after 1-2 weeks. The film deposition process is very sensitive; films made by three different operators at the same conditions revealed three completely different thickness of PANI (Braga, et al., 2008).

pH: The pH of the solution has a crucial influence on the stability of the solutions, doping and the adsorption process. A polyaniline solution is not stable for more than a couple of hours. No deposited layers have been observed by alternately dipping the substrate into a neutral polyaniline solution and a poly(styrene sulfonic) acid solution. The lower pH of a polyaniline solution has more positive charges because of the protonic acid doping, resulting in an increase of polyaniline adsorption by a factor of around 1.5. Consequently, a higher electrostatic repulsion is made between charges of polyelectrolytes such as PANI (Ferreira & Rubner, 1995). Polymer chains according to this electrostatic repulsion tend to straighten out and improve molecular packing. For this reason, a small number of PANI chains can approach the substrate surface and the amount of polymer adsorbed decreases. On the contrary, raising the pH results in a decrease

in electrostatic repulsion and an enhancement of the amount of adsorbed polymer (Mattoso et al., 2005; Raposo & Oliveira Jr, 2002). Several studies (Cheung, et al., 1997; M. K. Ram, M. Salerno, M. Adami, P. Faraci, & C. Nicolini, 1999) did not succeed in assembling PANI/PSS films in the presence of PANI in its neutral state.

Conductivity of PANI/PSS: some researchers have reported that with an increase of the number of adsorbed PANI/PSS bilayers, electrical conductivity of the multilayer increases until a saturation plateau is reached around the 13th bilayer or the 25th layer (Braga, et al., 2008; Paloheimo, Laakso, Isotalo, & Stubb, 1995). Further deposition of layers showed no more increase in the film's electrical conductivity.

2.4.1.1.12 Characterization Techniques for LbL Deposited Layers

Commonly used methods used to characterize the internal structure of the multilayer and film thickness could not be used in this research due to several limitations. Special techniques such as UV-Vis, ellipsometry (Schwarz, Eichhorn, Wischerhoff, & Laschewsky, 1999), quartz crystal microbalance (QCM) (Baba, Kaneko, & Advincula, 1999), streaming potential measurements (SPM) (Schwarz, et al., 1999), atomic force microscopy (AFM) (Caruso, Furlong, Ariga, Ichinose, & Kunitake, 1998), gravimetric measurement (Roy, et al., 2006), and x-ray and neutron reflectivity (Schmitt et al., 1993) have been utilized to measure thickness or mass deposited on the surface of each layer. Although the most commonly used method is UV-Vis, measurement of light absorbance is impossible due to the black color of the PANI solution. .

As well, ellipsometry is one of the most appropriate techniques for showing the growth rate. As the technique works with the reflection of emitted light, it is limited for substrates with curved surfaces.

CHAPTER 3 - ORGANIZATION OF THE ARTICLES

To achieve the main objective of this work, an elegant technique to reduce the continuity and/or electrical percolation threshold of a conductive polymer is developed by increasing the number of continuous structures in polymer blends. Polyaniline and four other commercial polymers with specific surface tensions, polarity and interfacial tensions are precisely selected. The interfacial tensions between various components show a range from 1 mN/m for PVDF/PMMA to 26.9 mN/m for PANI/HDPE.

Morphological sample characterization is performed by both SEM and FIB-AFM techniques. The polymer blends are prepared in a melt-blending process in an internal mixer at 50 rpm for 8 min at 200°C. Selective solvent extraction of phases either assists in better detection of phases in order to collect qualitative data, or is employed to produce porous samples. Combination of FIB treatment and AFM technique allows us to clearly distinguish the phases based on the topographical contrast formed by the difference in FIB etching rate of materials. In order to study the effect of viscosity ratio on the ternary blends, both low molecular weight and high molecular weight poly(methyl methacrylate) are selected. Fully interconnected porous materials are used as substrates for alternate deposition of PSS and PANI.

In the first step, three components, namely high density polyethylene (HDPE), polystyrene (PS), and poly(methyl methacrylate) (PMMA), are carefully chosen to satisfy the thermodynamic conditions. The positive spreading coefficient of PS over PMMA predicts that the PS phase situates at the interface of the HDPE and PMMA phases, and a complete wetting case occurs. Experimental results confirms the prediction of the morphology by the spreading theory as the identification of the phases can be clearly seen by the topographical heights induced by FIB etching and subsequently quantified by AFM analysis in the topographical mode.

Addition of fourth phase (PVDF) to the ternary blend with complete wetting of HDPE/PS/PMMA, provided that the entire set of thermodynamic spreading equations is satisfied, results in hierarchically ordered phases of HDPE|PS|PMMA|PVDF. The Harkins spreading theory predicts a hierarchically ordered structure of HDPE|PS|PMMA|PVDF|PANI by addition of PANI to a quaternary HDPE|PS|PMMA|PVDF blend. Experimental results show a very good consistency between these predictions and qualitative results.

After a theoretical determination of the order of all phases, controlling the composition of phases allows us to generate novel morphologies such as onion morphology and multi-percolated structures. SEM micrographs confirm onion morphology for a quaternary HDPE/PS/PMMA/PVDF blend with a matrix of HDPE and PVDF droplets encapsulated by first-shell PMMA encapsulated by second-shell PS. Changing the composition of phases, controls the evolution of the morphology from an onion structure to a multi-percolated one. It illustrates that in a multi-percolated structure, all phases are fully interconnected and interpenetrated. In order to quantitatively find the precise region of multi-percolation, solvent extraction followed by a gravimetric measurement was used to obtain the percent continuity of each phase. Addition of PANI to highly continuous quaternary blend of HDPE/PS/PMMA/PVDF demonstrates a quadruple-percolated morphology with the order of phases as HDPE/PS/PMMA/PVDF/PANI. As PANI situates as the inner phase, even at low concentration it is forced to spread between other percolated phases.

In another part of the first paper, the effect of the addition of PS-co-PMMA to quinary HDPE/PS/PMMA/PVDF/PANI blend with a quadruple-percolated structure is studied. Addition of a compatibilizing agent of two adjacent phases (PS and PMMA) demonstrates phase reduction of PS and PMMA in the blend. Since all phases are assembled in a hierarchically ordered manner, reduction of the phase size of two layers forces the other assembled layers to decrease in size. The first paper evaluates the effect of the number of the phases in a multi-percolated structure. Ternary, quaternary, quinary, and 6-component blends containing 5% PANI are prepared. The results indicate that increasing the number of components reduces the conductivity percolation threshold of all phases including PANI due to geometrical restriction of the phases. In order to spread the PANI, at least four components in the multi-percolated structure are required. Addition of a further number of phases increases conductivity correspondent to continuity of PANI only slightly.

In the second paper, through development of multi-percolated morphology associated with a layer-by-layer (LbL) approach, a novel 3D porous polymeric conducting device (PPCD) is generated. This technique allows for the percolation threshold concentration of polyaniline conductive polymer (PANI) to be reduced to values as low as 0.19%. A fully interconnected porous HDPE substrate with ultra low surface area is prepared by generating double- and triple-percolated systems followed by annealing and selective solvent extraction of phases. As

discussed above, HDPE, PS, PMMA, and PVDF components are shown to produce a multi-percolated structure with hierarchically ordered phases, since the interfacial tensions of the various pairs satisfy the positive conditions of the Harkins equation sets. Ternary blends and quaternary blends are prepared. After quiescent annealing, a substantial increase in the average phase size is observed. Selective solvent extraction of multi-percolated structures results in preparation of substrates with higher void volume. Hence, a fully interconnected porous HDPE substrate of low surface area is prepared by employing double- and triple-percolated morphology. The extra-large pores of HDPE substrates also facilitates the penetration of the polyaniline (PANI)/poly(styrene sulfonate) (PSS) solution inward to the interconnected porous area. Up to thirty-eight PSS and PANI layers are deposited on the internal surface of the 3-dimensional porous polymeric substrate, revealing an inter-diffused network conformation. Microstructural information collected by SEM and AFM depicts a relatively thick polyelectrolyte multilayer as wide as 5.5 μm for 38 layers of PSS and PANI on the surface of the porous HDPE substrate with a void volume of 66%. The mass deposition profile of PANI/PSS as a function of layer numbers demonstrates an unusual non-linear growth with an oscillatory behavior. The oscillating deposition indicates that PSS and PANI polyelectrolytes diffuse in the previously deposited layers. Like chains make contact with other like chains, and consequently, an inter-diffused network of PANI and PSS is generated. Since salt is generally added in procedures involving LbL deposition, the effect of the addition of 1 molar NaCl salt to the PSS polyanion in the multilayer construction is studied.

Conductivity measurements show that the percolation threshold of PANI in porous devices is achieved at a maximum of 8 layers. This corresponds to 0.19 wt.% PANI for a porous substrate made of 33% HDPE/33% PS/33% PVDF and 0.28 wt.% for a porous substrate generated from 33% HDPE/33% PMMA/33% PVDF. It is found that sample conductivity increases by increasing the number of deposited PSS/PANI layers until a conductivity saturation plateau is reached after 32 deposited layers. Compression of porous samples can be employed as another control parameter to achieve a wide range of conductivities in these conductive porous devices.

In the last paper, ternary HDPE/PS/PMMA blends with various compositions of components represent a complete wetting case with the development of a thermodynamically stable PS layer between the HDPE and PMMA. Four thermodynamically stable sub-classes of morphologies exist for HDPE/PS/PMMA, depending on the composition of phases: a) matrix/core-shell

dispersed phase (60/10/30 HDPE/PS/PMMA); b) tri-continuous (40/25/25 HDPE/PS/PMMA); c) bi-continuous/dispersed phase (50/25/25 HDPE/PS/PMMA); d) matrix/two separate dispersed phases (20/60/20). Solvent extraction/gravimetry is used to examine the extent of continuity of the components. Increasing the concentration of the core phase in the matrix/core-shell morphology results in the coalescence of core phases which leads to the formation of a tri-continuous morphology. Tri-continuous structures can be classified into two categories: type I and type II. The bi-continuous/dispersed phase morphology consists in a co-continuous structure for two phases with the third phase present as a dispersed phase.

A triangular composition/morphology diagram comprised of various compositions of HDPE/PS/PMMA is prepared to better understand the composition dependence of the various morphological states for complete wetting and their inter-conversion. This diagram demonstrates the concentration regimes for various morphological regions. These regions are detected by a combination of both SEM and FIB-AFM and through the use of selective extraction/gravimetric analysis as a quantitative technique to detect inversion points. Triangular continuity plots are introduced to show the continuity of the PS and PMMA phases respectively. It is found that in a ternary blend, percolation threshold becomes a line due to simultaneously changing the concentration of the two other phases in blend. Two compositional lines, or schemes, across the 3-axes triangular diagram which traverse multiple morphological states, are selected to study the effect of the concentration of the inner (HDPE) and middle (PS) phases on the morphology of the middle phase and the effect of the composition of the inner phase (HDPE) and the outer phase (PMMA) on the morphology of the middle phase (PS).

It is shown that extreme changes in the viscosity of the PMMA phase (L-PMMA and H-PMMA) in a PS/HDPE/PMMA blend of constant composition still results in morphological structures where the PS separates HDPE and PMMA. In both the L-PMMA case and the H-PMMA case, the morphological classification of the bi-continuous/dispersed PMMA phase is unchanged. It is found that the scale of the resulting morphological structures has been significantly modified by the viscosity of the PMMA, as the system attempts to respond to the dramatically reduced interfacial area of the H-PMMA droplets. It is also found that the composition, interfacial tension, and viscosity ratio play an important role in determining the phase size in ternary polymer blends.

CHAPTER 4 - LOW PERCOLATION THRESHOLD CONDUCTIVE DEVICE DERIVED FROM A FIVE-COMPONENT POLYMER BLEND

4.1 Abstract

In this work we report on the preparation of a solid, 3D, low percolation threshold conductive device prepared through the control of multiple encapsulation and multiple percolation effects in a 5 component polymer blend system through melt processing. Conductive polyaniline (PANI) is situated in the core of the 5 component continuous system comprised of high-density polyethylene(HDPE), polystyrene(PS), poly(methyl methacrylate)(PMMA) and poly(vinylidene fluoride)(PVDF) and, in this fashion, its percolation threshold can be reduced to below 5%. The approach used here is thermodynamically controlled and is described by Harkins spreading theory. In this work the detailed morphology and continuity diagrams of binary, ternary, quaternary and finally quinary systems are progressively studied in order to systematically demonstrate the concentration regimes resulting in the formation of these novel multiple-encapsulated morphological structures. Initially, onion-type dispersed phase structures are prepared and it is shown that through the control of the composition of the inner and outer layers the morphology can be transformed to a hierarchical-self-assembled, multi-percolated structure. The influence of a copolymer on selected pairs in the encapsulated structure is also examined. The conductivity of the quinary blend system can be increased from 10^{-15} S cm⁻¹ (pure PE) to 10^5 S cm⁻¹ at 5 % PANI and up to 10^{-3} S cm⁻¹ for 10% PANI. These are the highest conductivity values ever reported for these PANI concentrations in melt processed systems.

4.2 Introduction

Over the last 30 years the polymer-polymer blending of conventional polymers has received significant attention since these materials can result in highly synergistic property sets. Although a vast number of studies have been devoted to the study of immiscible polymer blends and of the

dispersed phase-matrix, fibrillar, and co-continuous morphologies, relatively few studies have focused on the fundamentals of three or more components with complex morphologies (Moussaif & Jérôme, 1999; Reignier & Favis, 2000, 2003a; J. Zhang, et al., 2007).

Ternary A/B/C systems can exist in two possible states. One is known as complete wetting and the other is partial wetting. Complete wetting can result in B and C droplets individually dispersed in an A matrix. It can also result in the case where one B or C phase completely engulfs the other in a matrix of A. In this latter case, the minimization of interfacial free energy occurs when, for example, phase B is situated at the interface of, and completely wets, phases A and C (Figure 4-1a). In the partial wetting state, all three phases have an interface with each other (Figure 4-1b). In such a case intact droplets of B, for example, can be placed at an A/C interface. Recently some very novel structures have been generated via partial wetting (Virgilio, Desjardins, et al., 2009; Virgilio, Marc-Aurele, & Favis, 2009).

Strict thermodynamic conditions need to be met in order to have either discrete phases, encapsulated structures or partial wetting. Torza and Mason (Torza & Mason, 1970) and then Hobbs et al. (Hobbs, et al., 1988) employed a modified Harkins spreading theory (Equation 4-1) to predict whether the morphology of a ternary blend is dominated by complete wetting or is partial wetting.

Equation 4-1.

$$\lambda_{12} = \gamma_{23} - \gamma_{13} - \gamma_{12}$$

where λ is the spreading coefficient, γ represents the interfacial tension for various polymer pairs where the sub-indexes refer to each component. If one of the spreading coefficients such as λ_{12} has a positive value, a complete wetting case occurs in which phase 1 separates phases 2 and 3 (Figure 4-1a). In another case, where all spreading coefficients have negative values, the system demonstrates a partial wetting case in which all phases have contact with each other (Figure 4-1b). It has been shown that Harkins equation is, on the whole, a good criterion to predict the position of phases in ternary polymer blends (Reignier & Favis, 2000, 2003b; Virgilio, Desjardins, et al., 2009; Zhang, et al., 2007). As the number of phases increases to four however, it is difficult to determine the morphology by such a simple model. To date, there is no equation

or model which predicts where the phases will situate in a multi-blend system comprising more than three phases.

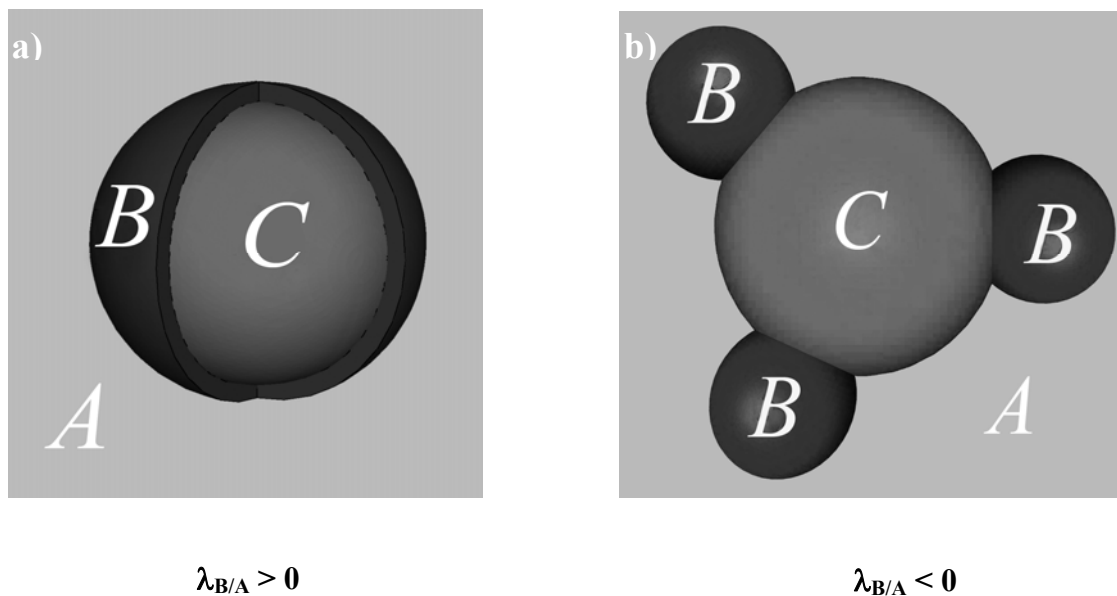


Figure 4-1. Schematic representation of (a) the complete wetting case where phase B spreads between, and fully separates, phases A and C and (b) the partial wetting case all phases are in contact with each other

Co-continuous morphologies represent the special case where, in an A/B system, both components are fully continuous within the blend. This type of system is referred to as a single-percolated structure. Recently (Zhang, et al., 2007; Zilberman, et al., 1998, 2000d), some papers are examining the potential of double percolated structures by locating a phase with a specific characteristic at the interface of two other continuous phases. For example, Zhang et al. (Zhang, et al., 2007) by employing Harkins equation and controlling the composition of phases, developed a double-percolated structure in which polystyrene was situated at the interface of high-density polyethylene and poly(methylmethacrylate). All three phases were shown to be fully continuous.

The most well-known utilization of a double-percolated morphology is locating intrinsically conductive particles or polymers at the interface of binary blend of common polymers to produce a conductive polymer composite (Anand, Palaniappan, & Sathyanarayana, 1998; A. Bhattacharya & De, 1999; Pud, Ogurtsov, Korzhenko, & Shapoval, 2003). Classic percolation theory is

usually utilized to explain the transition from discontinuous phase behavior to continuous phases. In conductive materials, this transition point is defined as the critical concentration of conductive phase required to build up a first conductive pathway and is referred to as the percolation threshold. The percolation threshold is generally defined as the onset of long-range connectivity in random systems. By employing a double percolated structure, the percolation threshold of the middle phase sharply decreases as its presence is limited only to the interface. The conductivity of a conductor-insulator blend near the percolation threshold point is calculated by the following equation:

Equation 4-2.
$$\sigma = \sigma_0 (p - p_c)^t$$

where σ_0 is the conductivity at the percolation threshold point, σ is the conductivity of the blend, p is the concentration of the conductive material, p_c is the percolation threshold concentration, and t is a dimensionless index.

The classic percolation threshold for a random dispersion of hard-core spheres in a matrix in three dimensions is approximately 16 volume percent (Scher & Zallen, 1970). Restricting the dispersed phase spatially, for example in interfacial tension driven structures such as a double-percolated morphology, can significantly reduce the percolation threshold of that phase. In that case the particles or polymer components can be precisely located at the interface leading to dramatic reductions in the percolation threshold value (Gubbels, et al., 1995; Gubbels et al., 1994; Zhang, et al., 2007). In other words, by controlling the morphology of the blend and restricting the pathways of the components, the percolation threshold deviates from the standard value of percolation threshold in a random system predicted by percolation theory. Moreover, using the same approach, controlling the morphology of the system can also influence the behavior of conductive systems. Confining the pathways of a conductive material in a multiphase system can result in high conductivities at low concentration of conductive material. The dimensionless index t in Equation 4-2 represents the effect of the morphology of the system on the conductivity behavior. This has already been shown to be possible for conductive systems where the conductive phase was selectively localized in the multiphase blend and consequently the

concentration threshold for the onset of electrical conductivity was significantly decreased (Anand, et al., 1998).

In the case of conductive fillers, both the size and shape of the particles influence the percolation threshold. Typically the percolation threshold ranges from 10-40% volume fraction of the conductive filler (Jagur-Grodzinski, 2002). It has also been theoretically and experimentally observed that for polymer blends including a dispersed metal (Bridge & Tee, 1990) or carbon black (Carmona, 1989) phase, that the percolation threshold depends on the aspect ratio of the filler and it decreases when the ratio of the length to the diameter increases (Munson-McGee, 1991). Gubbels et al. reported a percolation threshold as low as 3 weight percent carbon black when it is localized in one phase of a binary blend consisting of 45% polyethylene and 55% polystyrene (Gubbels, et al., 1995; Gubbels, et al., 1994). Then, they showed that localization of carbon black at the interface of a co-continuous PE/PS blend exhibits a sharp reduction in the percolation threshold value to 0.5 wt%. Blends consisting of conductive material prepared slightly above the percolation threshold have low conductivity. The most difficult part is preparing the conductive blend near the percolation threshold with reproducible conductive results. Sumita et al. (Sumita, Sakata, Asai, Miyasaka, & Nakagawa, 1991) employed the methodology of spreading coefficient to develop a criterion to determine the conditions of localization of carbon black at the interface.

After the discovery of doped polyacetylene and its metal-like behavior, research shifted from carbon black to intrinsically conductive polymer blends (ICP). By replacing the inorganic semiconductors in conventional device structures with a semiconducting polymer, the basic application of these materials has already been demonstrated (Burroughes, Jones, & Friend, 1988). They can store information and energy, and are capable of performing intelligent functions. The most amenable conductive polymer to solution processing and melt-processing (Paul, Vijayanathan, & Pillai, 1999) is polyaniline (PANI). Investigations by Macdiarmid et al. (Macdiarmid, et al., 1985), which resulted in the discovery of electrical conductivity for the emeraldine salt of polyaniline, led to an explosion of interest in this fascinating polymer. The emeraldine base of PANI is soluble in a few strong acids (Andreatta, Cao, Chiang, Heeger, & Smith, 1988). Various dopants were utilized to induce melt-processability in PANI. The main disadvantage of all intrinsically conductive polymers including PANI is its limited melt-processability. The addition of zinc compound to doped-PANI complex

allows for a method to tailor the processability of sulfonic acid-doped PANI(Hartikainen, et al., 2001; Ruokolainen, et al., 2000). It has been observed that for polymer blends containing PANI, a range of conductivity between 10^{-10} S cm⁻¹ to 10^{-1} S cm⁻¹ (melt processing) and 10^{-10} S cm⁻¹ to 10 S cm⁻¹ (solution processing) can be achieved(Panipol, 2000).

The blending of PANI with a variety of classical polymers to improve the mechanical properties of PANI and also to decrease the percolation threshold of the conductive polymers has been extensively studied. Conductive binary polymer blends can demonstrate good mechanical properties with conductivity varying from 10^{-11} S cm⁻¹ (almost insulating) to 300 S cm⁻¹. It should be noted that different techniques including melt-blending, solution blending, in-situ polymerization, and dispersion mixing have different influence on PANI morphology and subsequently on properties. For instance, in the case of a PS/PANI blend, although melt-blending results in a higher PANI percolation threshold than dispersion mixing, a significant improvement in mechanical properties is achieved via the melt blending approach(Segal, et al., 2001). Most studies of polymer blends containing PANI have been performed in solution and only a few melt-blending studies have been reported(Ikkala et al., 1995; Narkis, Zilberman, & Siegmann, 1997; Shacklette, et al., 1993; Zilberman, et al., 1997). Polystyrene(PS)(Woo Jin, et al., 2003), Cellulose acetate(Planes, et al., 1998), Polymethylmethacrylate(PMMA)(Morgan, et al., 2001), Polyethylene(PE), Polypropylene(PP), Polyamide(PA)(Qinghua, et al., 2002), Polyimide(PI)(Moon Gyu & Seung Soon, 2001), Polyvinyl chloride(PVC)(Chipara, et al., 1998), Polyurethane(PU)(Rodrigues & Akcelrud, 2003), and a wide variety of thermoplastic elastomers(Dong-Uk, et al., 2001; Ong, et al., 1997) have been blended with PANI using a variety of techniques other than melt-blending(Ikkala, et al., 1995; Narkis, et al., 1997; Segal, et al., 2001; Shacklette, et al., 1993; Zilberman, et al., 1997).

A conductivity value of 0.1 S cm⁻¹ for 20 wt% of PANI is observed for PS/PANI blend prepared by in-situ polymerization(Woo Jin, et al., 2003). Using a polymer solution blending approach, Cao et al.(Cao, Smith, & Heeger, 1992) developed a processing method for a host polymer of PMMA and polyaniline optimally doped with camphor sulfonic acid. Using this method the value of electrical conductivity could be increased to 1 S cm⁻¹ for loading levels of polyaniline as low as 0.3% (vol/vol)(Yang, Y. Cao, P. Smith, & Heeger, 1993b). The solution blending of PANI and its derivatives with poly(vinylidene fluoride)(PVDF) have attracted significant interest due to some of the special properties of PVDF, namely, excellent mechanical properties,

chemical and weathering resistance, piezo-electric properties and good flexibility (Bliznyuk et al., 2005; Privalko, et al., 2005). Fraysse et al (Fraysse, et al., 2000) were able to decrease the percolation threshold of PANI sharply in a PANI/PMMA solution blend to 0.5 wt% of PANI. Although the above methods using in-situ polymerization and polymer solution blending can result in very low percolation thresholds of conductive polymer, they suffer from serious disadvantages such as poor mechanical properties. In addition, clearly the environmental and health related issues associated with solvents and solvent removal are critical concerns. A melt blending approach, from this point of view, is potentially a much more robust and environmentally friendly approach.

In the case of melt-processing, Shacklette et al. (Shacklette, et al., 1993) reported percolation thresholds in a range of 6-10% for PANI dispersed in polar polymers such as polycaprolactone and poly(ethylene terephthalate glycol). Zilberman et al. (Zilberman, et al., 2000d) have reported percolation thresholds of PS/PANI and linear low-density polyethylene (LLDPE)/PANI of about 30 wt% of PANI. They reported a lower percolation value of 20 wt% PANI for the binary blend composed of CoPA/PANI.

Levon et al. (Levon, et al., 1993) were the first to suggest the concept of double percolation in a ternary polymer blend consisting of a conductive polymer. This double percolated system was comprised of a connected path within a connected path, the latter of which is conducting. Zilberman et al. (Zilberman, et al., 2000d) observed a high-quality conductive PANI network in a CoPA/LLDPE/PANI ternary blend and a poor-quality PANI network in a (PS+DOP)/LLDPE/PANI blend. Narkis and coworkers (Haba, et al., 2000; Narkis, et al., 2000a; Segal, et al., 2001) extended and developed these previous works by blending PANI with other homopolymers via different methods mostly by using the methodology of a double percolated morphology to decrease the percolation threshold and increase mechanical properties. They showed that for several melt processed PANI/polymer blends, the conductivity results reveal a percolation threshold of approximately 20%. That work also shows that, in ternary blends consisting of PANI and two immiscible polymers, the PANI is preferentially located in one of the constituting polymers. They found that PANI always prefers to locate in one phase rather than situating at the interface (Zilberman, et al., 2000d). In all previous works performed on PANI, the percolation threshold concentration of PANI was determined based on the onset of increase in the conductivity as a function of composition. In most of those cases, the sample

conductivity at the percolation threshold point is between $10^{-11} \text{ S cm}^{-1}$ and $10^{-9} \text{ S cm}^{-1}$. In order to have higher conductivity values, higher concentrations of PANI are required.

This work reports on the development of onion morphology and multi-percolated morphologies in HDPE/PS/PMMA/PVDF/PANI blends in which all phases are assembled hierarchically in order. The overall objective is to lower the percolation threshold conductivity value of PANI to the lowest possible value. The required thermodynamic conditions to obtain these structures will be examined. The effect of the number of components, phase composition and the influence of an interfacial modifier on the conductivity of the blends will be examined.

4.3 Experimental Methods

4.3.1 Materials

Commercial HDPE, PS, PMMA, processable PANI, and fluorene polymer(PVDF) were examined in this work. The main characteristics of the materials used in this study are represented in Table 4-1. Cyclohexane, acetic acid, dimethylformamide(DMF), and chromic acid were used to extract or dissolve the selected phases.

PANI was purchased from Panipol Ltd, in the form of cylindrical compressed pellets with a composition of about 25 weight % polyaniline salt and 75 weight % of a zinc compound to modify its processability. The specific conductivity of this material is about 5 S cm^{-1} .

Table 4-1. Material Characteristics

Material	Supplier	Commercial Code	Mw×10 ⁻³ (g/mol)	$\eta^* \times 10^{-3}$ at 25 rad s ⁻¹ (Pa.s)	Density (g/cm ³) at 20 °C	Density (g/cm ³) at 200 °C
Poly(methyl methacrylate)	Aldrich	-	12	0.04 ^a	1.19	1
Polystyrene	Dow	615APR	290	1.5	1.04	0.97
High density Polyethylene	Dow	-	79	0.72	0.98	0.85
Polyaniline	Panipol	CX	-	0.11 ^b	-	1.07
Polyvinylidene fluoride	Arkema	Kynar Flex	-	1.4 ^c	-	1.6
PS-co-PMMA (40% Styrene)	-	-	100-150	34 ^d	-	0.98

^a reported by Reignier et al.(Reignier & Favis, 2000)

^b viscosity measured at 180°C

^c zero shear viscosity of PVDF is 902000 Pa.s at 190°C calculated by Carreau-Yasuda model

^d zero shear viscosity (Pa.s) at 190°C

4.3.2 Rheological Analysis

The rheological characterization of the neat polymers was measured using a Bohlin constant stress rheometer (CSM) in the dynamic mode. PS, PMMA, HDPE, and PVDF are known to follow the Cox-Mertz equation(Cox & Merz, 1958), consequently, the applied frequency can be considered as the shear rate and the complex viscosity as the steady shear viscosity. Measurements were carried out at 190 °C under a nitrogen atmosphere. The complex viscosity of the pure homopolymers are plotted as a function of frequency in Figure 4-2. The viscosity of homopolymers at 25 s⁻¹ are reported in Table 4-1. All polymers show shear-thinning behavior and the Carreau-Yasuda model(Yasuda, Armstrong, & Cohen, 1981) was used to determine the zero-shear viscosity of PVDF.

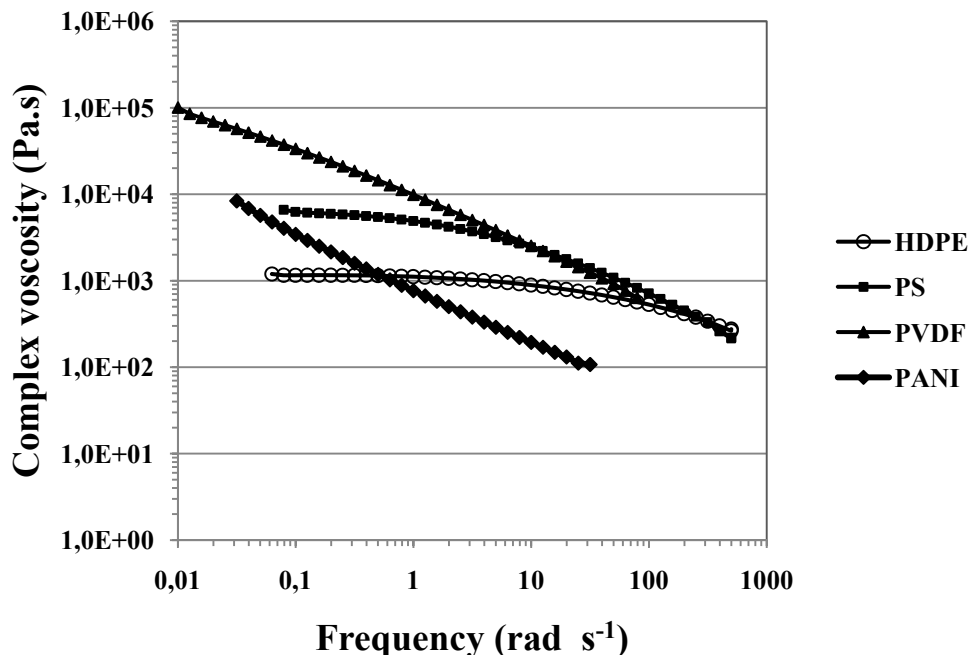


Figure 4-2. Complex viscosity as a function of frequency at 190°C for the homopolymers. The complex viscosity of PANI is at 180°C.

4.3.3 Sample Preparation

Various blends were prepared via melt-blending under a flow of dry nitrogen in a 30mL Brabender operating at a set temperature of 200 °C and 50 rpm. The maximum shear rate at this speed is close to 25 s⁻¹.(Philippe Lavalle, et al., 2004) The real temperature achieved by the end of mixing experiment was approximately 185°C. A value of 0.7 fill factor was selected and thus after converting the volume to the mass and weighing the material, the mixing chamber was filled to 70% of its total volume. A concentration of 0.2 weight percent of Irganox antioxidant supplied by CIBA was added to the mixture to reduce the thermal oxidation of the components. All the blends were mixed for 8 min. After average 2 min mixing time the torque achieves a constant plateau value. After mixing, the samples were immediately cut from the mass and quenched in a cold water bath to freeze-in the morphology.

In order to produce disk-shaped samples of 2.5cm diameter and 1.2mm thickness for conductivity testing, a hot press was employed. The press is heated to 200°C and the mould is

filled with blend pellets. To facilitate the de-molding of the material, two sheets of Teflon are inserted between the plaques. The total molding cycle takes 8min under a nitrogen purge gas. A large cold press was employed after hot press to decrease the temperature sharply to avoid annealing of the sample.

4.3.4 Solvent Extraction

A solvent extraction/gravimetric method was used to obtain quantitative data on the extent of continuity of the phases. Selective solvents were used to extract the specimens of various masses at room temperature. The volume of the components before and after extraction is measured by weighing the sample and converting the weight to volume(Equation 4-3). As a primary advantage, solvent extraction is an absolute measurement and is also a straightforward technique to detect the existence of co-continuous microstructures when the components are soluble in specific solvents.

Equation 4-3.

$$\%Cocontinuity = \frac{\sum_n V_{initial} - \sum_n V_{final}}{\sum_n V_{initial}}$$

Where $V_{initial}$ and V_{final} are the volume of one component present in the sample before and after extraction calculated by weighing the sample and converting it to the volume. The degree of continuity represents the fraction of a phase that is continuous. Samples in which each phase has a degree of continuity of 1.0 are completely continuous. The reported value is the average of several samples and the average error for high continuity levels is $\pm 5\%$ and for low continuity levels is $\pm 3\%$. Cyclohexane, acetic acid, and chromic acid were utilized as selective solvents for polystyrene, polymethyl methacrylate, and polyaniline, respectively and DMF extraction was performed to dissolve PS, PMMA, and PVDF altogether.

4.3.5 Characterization of Phase Morphology

4.3.5.1 Microtoming and Scanning Electron Microscopy (SEM)

The specimens were cut and microtomed to a plane face under liquid nitrogen using a microtome (Leica-Jung RM 2065) equipped with a glass knife and a cryochamber type (LN 21). After the appropriate chemical treatment at room temperature with selective solvents (acetic acid for PMMA, cyclohexane for PS, chromic acid for PANI, and DMF for all three of PVDF, PMMA, and PS) to remove one or several of the components, the sample surface was coated with a gold/palladium by plasma deposition. A JEOL JSM 840 scanning electron microscope, operated at a voltage of 10 keV to 12 keV, was used to obtain photomicrographs of the sample surface.

4.3.5.2 Focused Ion Beam (FIB), Atomic Force Microscopy (AFM)

A FIB/AFM technique was used to examine the PE/PS/PMMA blend. After cryomicrotoming of the specimens using a glass knife to obtain perfectly flat surface, samples were coated with a gold-palladium alloy. The surface of the samples was then treated and etched using a Hitachi focused ion beam FIB-2000A operated at 30 keV gallium beam. FIB uses a focused beam of gallium ions which are accelerated to energy of 5-50 kiloelectronvolts. Using an electrostatic lens, ion beam can be focused on a very small spot, resulting in a high resolution because of the small emitting area. In this work, a 0.8 nA beam current and a dwell time at 3 μ s was applied in order to remove approximately 3-4 μ m of the surface. Milling was carried out parallel to the observed surface. Since each polymer component has a different interaction with the gallium beam, this approach induces topological differences and hence increases the contrast between components. The milled surface of the specimen was then examined by a scanning probe microscope dimension (AFM) with a Nanoscope IIIa controlled in topological mode. The atomic force microscope measures topography with a force probe. Silicon tips with spring constant of 40 N/m and a resonant frequency of around 300 kHz was employed.

4.3.6 Conductivity Measurements

DC electrical measurements were performed through the vertical thickness of the substrate at ambient temperatures using a Keithley electrometer model 6517. The sample is placed between two sample holders and a DC voltage is applied using two point probe equipment. The setup works at a voltage range of 0-1000V and an ammeter range of 0-20mA. To standardize equal pressure for all samples, a 5lb load was applied on the sample holders. Cylindrical specimens with a thickness of 1.2mm and a radius of 1.25cm were tested in dry air. Although the top and bottom surfaces of the samples are flat, two graphite sheets covered the surface of the sample in order to ensure good contact of the sample surface and electrodes. The electrical conductivity of the samples varied over a wide range from 10^{-12}S cm^{-1} to 10^{-1}S cm^{-1} . The average % error in the conductivity measurements is ± 0.2 orders of magnitude.

4.4 Results and Discussions

4.4.1 Reducing the Percolation Threshold of PANI in a Multi-component Polymer Blend

The principal objective of this work is to control the morphology of a multi-component polymer blend in order to significantly reduce the percolation threshold of the conductive PANI component. The first question to be addressed is where does the PANI need to be located in the blend system?

In recent work, Zhang et al. (J. Zhang, et al., 2007) demonstrated that the percolation threshold of one component could be reduced to values as low as three percent by preparing a ternary blend and situating that phase at the interface of two other co-continuous phases. In Figure 4-3a, it is shown that polystyrene situates at the interface of PE and PMMA and the ordering of the phases can be directly related to Harkins spreading theory. In Figure 4-3a, the identification of the phases can be clearly seen by the topographical heights induced by FIB etching and subsequently quantified by AFM analysis in the topographical mode. Previous work showed that PMMA is

less etched than HDPE which is less etched than PS (Virgilio, Favis, Pepin, Desjardins, & L'Esperance, 2005a). The positive spreading coefficient of PS over PMMA ($\lambda_{PS/PMMA}$) with a value of 2.6 mN/m predicts the development of a thermodynamically stable PS layer between the PE and PMMA phases and is a direct result of the very high interfacial tension of PMMA and HDPE ($\gamma_{HDPE/PMMA} = 8.4$ mN/m).

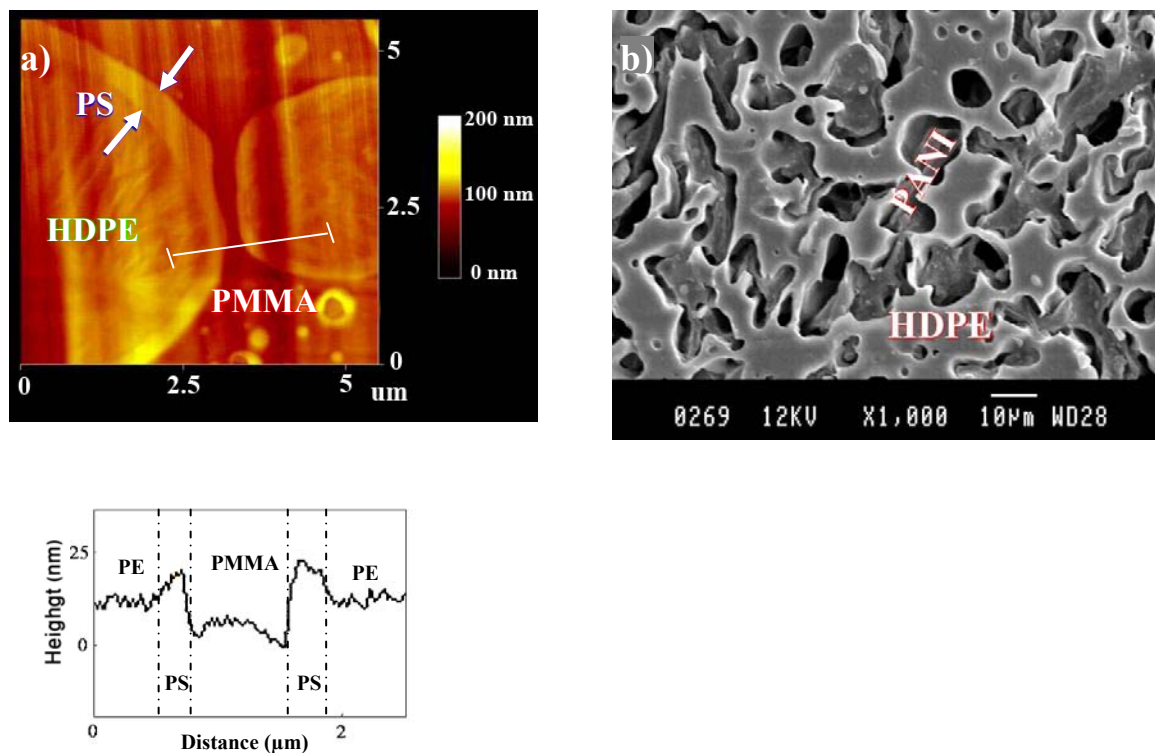


Figure 4-3. a) FIB-AFM image of the composite-droplet morphology of 30/10/60 HDPE/PS/PMMA showing PS as a layer separating HDPE and PMMA. Scan size is $5\mu\text{m} \times 5\mu\text{m}$. The bar to the right of the FIB/AFM micrograph indicates the colours associated with the topographical height in nm. The white line in the image indicates the section analyzed below, and b) SEM micrograph of a 45/10/45 HDPE/PVDF/PANI blend after extraction of the PVDF phase by DMF. The voids show that PVDF was present as a layer separating HDPE and PANI.

Table 4-2 represents the surface tension and polarity of the various polymers being used in the harmonic mean equation (Wu, 1982) for interfacial tension. Table 4-3 shows a range of interfacial tension values of polymer pairs, including PANI with other polymers, estimated using the harmonic mean equation. A number of these interfacial tensions were also measured

experimentally in this research group and they show a good correlation with the harmonic mean data (Table 4-3).

Table 4-2. Surface Tension, Polar Contribution, Dispersive Contribution, Polarity, and Rate of Surface Tension per Temperature for Homopolymers

Polymers	γ (mN/m) at 20°C	γ (mN/m) at 200°C	γ^p (mN/m) at 200°C	γ^d (mN/m) at 200°C	Polarity, X^p	$(-d\gamma/dT)$ (mN/m-deg)
HDPE ^a	35.7	25.4	0	25.4	0	0.057
PS ^a	40.7	27.7	4.6	23.1	0.167	0.072
PMMA ^a	41.1	27.4	7.7	19.7	0.28	0.076
PVDF ^b	33.2	22.9	8.7	14.2	0.376	0.057
PANI ^c	55.6	40.3	24.6	15.7	0.612	0.085

^a From ref. (Wu, 1982), ^b From ref. (Baradie & Shoichet, 2003), ^c Measured by contact angle method

Table 4-3. Theoretical and Experimental Interfacial Tension for Polymer Pairs

Theoretical data(Harmonic mean equation) γ (mN/m)				Experimental datay (mN/m)	
PS/HDPE	4.7	PMMA/HDPE	8.4	PS/HDPE ^a	5.1
PMMA/PS	1.1	PANI/HDPE	26.9	PMMA/PS ^a	2.4
PVDF/HDPE	11.9	PVDF/PMMA	1	PMMA/HDPE ^b	8.5
PVDF/PS	3.4	PVDF/PANI	7.7		
PANI/PMMA	9.3	PANI/PS	15.1		

^a From ref. (Reignier & Favis, 2000), ^b Measured by breaking thread method

The harmonic mean equation approach is a classic approach for estimating the interfacial tension of polymer pairs and has been used widely in a number of studies(Wu, 1982). It can be seen that, compared to other polymer pairs, mixtures with PANI result in exceptionally high interfacial tensions. It thus follows from spreading theory that PANI will not be driven to encapsulate other polymers in a multi-component blend, rather it will tend to be encapsulated by virtually every other polymer species. For example, in a ternary HDPE/PVDF/PANI blend, a positive spreading coefficient value of 7.3 mN/m for $\lambda_{\text{PVDF/PANI}}$ predicts encapsulation of PANI by PVDF as confirmed in Figure 4-3b. In that figure, the voids left by the extracted PVDF can be clearly seen to show that PVDF formed an interlayer between HDPE and PANI.

By increasing the number of components in a multi-percolated structure, the percolation threshold of all phases sharply decreases. Thus, a unique approach to achieve a low percolation threshold conductive PANI device would be to prepare a multiple percolated blend system with PANI as the innermost phase. In this work we will examine the progressive morphological development of highly continuous multi-component structures by first examining the development of multi-encapsulated ternary to quinary droplets which are referred to here as *onion* morphologies. Then, the required conditions for transformation of the onion morphology to continuous multi-percolated morphologies and the conductivity of those systems are examined.

4.4.2 Self-Assembled Onion Morphology and the Hierarchical Ordering of Phases

Typically, in the literature, a core/shell morphology is used to describe a droplet comprised of one phase encapsulated by another single phase. Here, we use the term onion morphology, schematically shown in Figure 4-4, to describe a multi-phase, multi-encapsulated dispersed droplet structure. In other words, a polymeric droplet phase comprised of layers of different polymers assembled concentrically. Figure 4-4 shows schematically the progression from a matrix-droplet(Figure 4-4a) to a core/shell(Figure 4-4b) and finally two cases of onion morphology(Figures 4-4c and 4-4d).

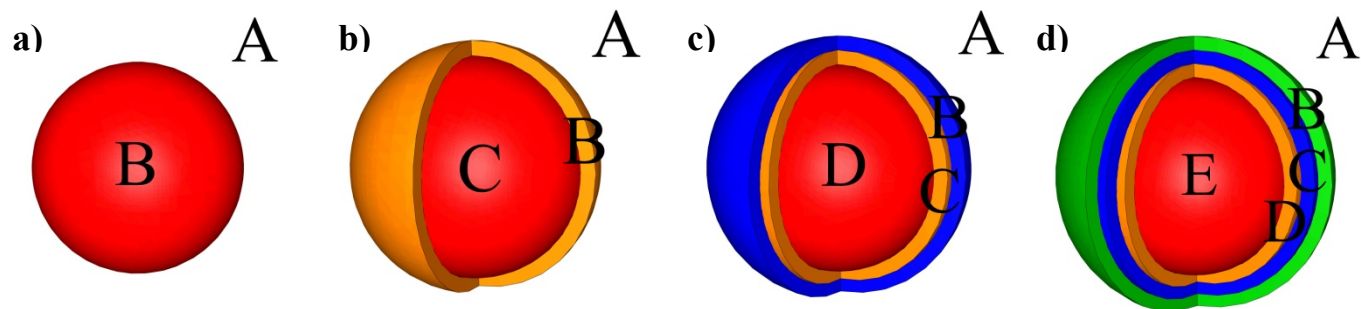


Figure 4-4. Schematic illustration of various encapsulated structures, a) dispersed phase B in matrix A, b) core-shell morphology B/C in matrix A, c) quaternary onion morphology B/C/D in matrix A, and d) quinary onion morphology B/C/D/E in matrix A.

The thermodynamic conditions to obtain such onion structures for a given n -component blend is that the spreading coefficients of each of three selected components out of n components should satisfy the complete wetting case in Harkins equation. At the same time, the order of phases in each selected ternary blend should be consistent with the order of the phases situated in the multi-blend. This implies that for a core/shell structure, as there are only three phases in the blend system, only one set of Harkins equation needs to be examined. In the case of a quaternary blend system with an onion structure, a combination of three out of four which is equal to four systems of Harkins equation should be evaluated. Finally in this study, ten systems of Harkins equation (equivalent to three out of five components) should be evaluated for a quinary blend system, which in the present work is comprised of HDPE, PS, PMMA, PVDF, and PANI. Both the interfacial tensions and the spreading coefficients for these ten binary pairs are shown in Tables 4-3 and Table 4-4, respectively.

The first four ternary blends in Table 4-4 indicate that in a quaternary blend comprised of an HDPE matrix with PS, PMMA, and PANI, the order of components from outer to inner should be: HDPE|PS|PMMA|PVDF. Using the data from Tables 4-3 and 4-4 it is also predicted that various other quaternary mixtures should assemble hierarchically as follows: HDPE|PS|PMMA|PANI (see spreading coefficients 1,4,5 and 8 from Table 4-4); HDPE|PMMA|PVDF|PANI (spreading coefficients 3,5,7 and 10); HDPE|PS|PVDF|PANI

(spreading coefficients 2, 6, 7, and 9); and PS|PMMA|PVDF|PANI (spreading coefficients 4, 8,9, and 10. Finally, from the above, the quinary blend should have the hierarchical ordering of HDPE|PS|PMMA|PVDF|PANI.

Table 4-4. Spreading Coefficients in Different Ternary Blends and Predicted Order of Phases in Blends

	Spreading coefficients λ (mN/m)	Ternary blend and order of phases in the blend		Spreading coefficients λ (mN/m)	Ternary blend and order of phases in the blend
1	$\lambda_{PS/PMMA} = 2.6$ mN/m	HDPE PS PMMA	6	$\lambda_{PS/PANI} = 7.1$ mN/m	HDPE PS PANI
2	$\lambda_{PS/PVDF} = 3.8$ mN/m	HDPE PS PVDF	7	$\lambda_{PVDF/PANI} = 7.3$ mN/m	HDPE PVDF PANI
3	$\lambda_{PMMA/PVDF} = 2.5$ mN/m	HDPE PMMA PVDF	8	$\lambda_{PMMA/PANI} = 4.7$ mN/m	PS PMMA PANI
4	$\lambda_{PMMA/PVDF} = 1.3$ mN/m	PS PMMA PVDF	9	$\lambda_{PVDF/PANI} = 4$ mN/m	PS PVDF PANI
5	$\lambda_{PMMA/PANI} = 9.2$ mN/m	HDPE PMMA PANI	10	$\lambda_{PVDF/PANI} = 0.6$ mN/m	PMMA PVDF PANI

After a theoretical determination of the order of all phases, morphology experiments for the binary, ternary, and quaternary blends comprised of the previously mentioned components confirm the theoretical ordering. Some examples are shown in Figure 4-5. The binary blend of 80/20 PMMA/PS with matrix-droplet morphology is shown in Figure 4-5a. A ternary blend of 30/10/60 HDPE/PS/PMMA blends has already been shown in Figure 4-3a and confirms the situation of PS at the interface of PE and PMMA which corresponds to the positive value of $\lambda_{PS/PMMA}$ (2.6 mN/m) (Case 1 from Table 4-4) as already discussed. Another ternary blend of 60/20/20 HDPE/PMMA/PVDF is shown in Figure 4-5b. In that case the PMMA has been selectively extracted showing clearly a core/shell structure where PMMA is the shell and PVDF is the core. This HDPE/PMMA/PVDF ternary blend corresponds to $\lambda_{PMMA/PVDF}$ (2.5 mN/m) (Case 3 from Table 4-4) which predicts an encapsulation of PMMA about PVDF. The morphology observed for a quaternary blend of 50/20/10/20 HDPE/PS/PMMA/PVDF, shown in Figure 4-5c, is also consistent with the theoretical ordering discussed above. Figure 4-5c shows the onion-like

microstructure of the quaternary blend after selective dissolution of PMMA. The selective dissolution of PMMA allows for the clear identification of the other phases. There is a core of PVDF encapsulated in a first shell of PMMA, encapsulated in second shell of PS, all of which are encapsulated by the HDPE matrix.

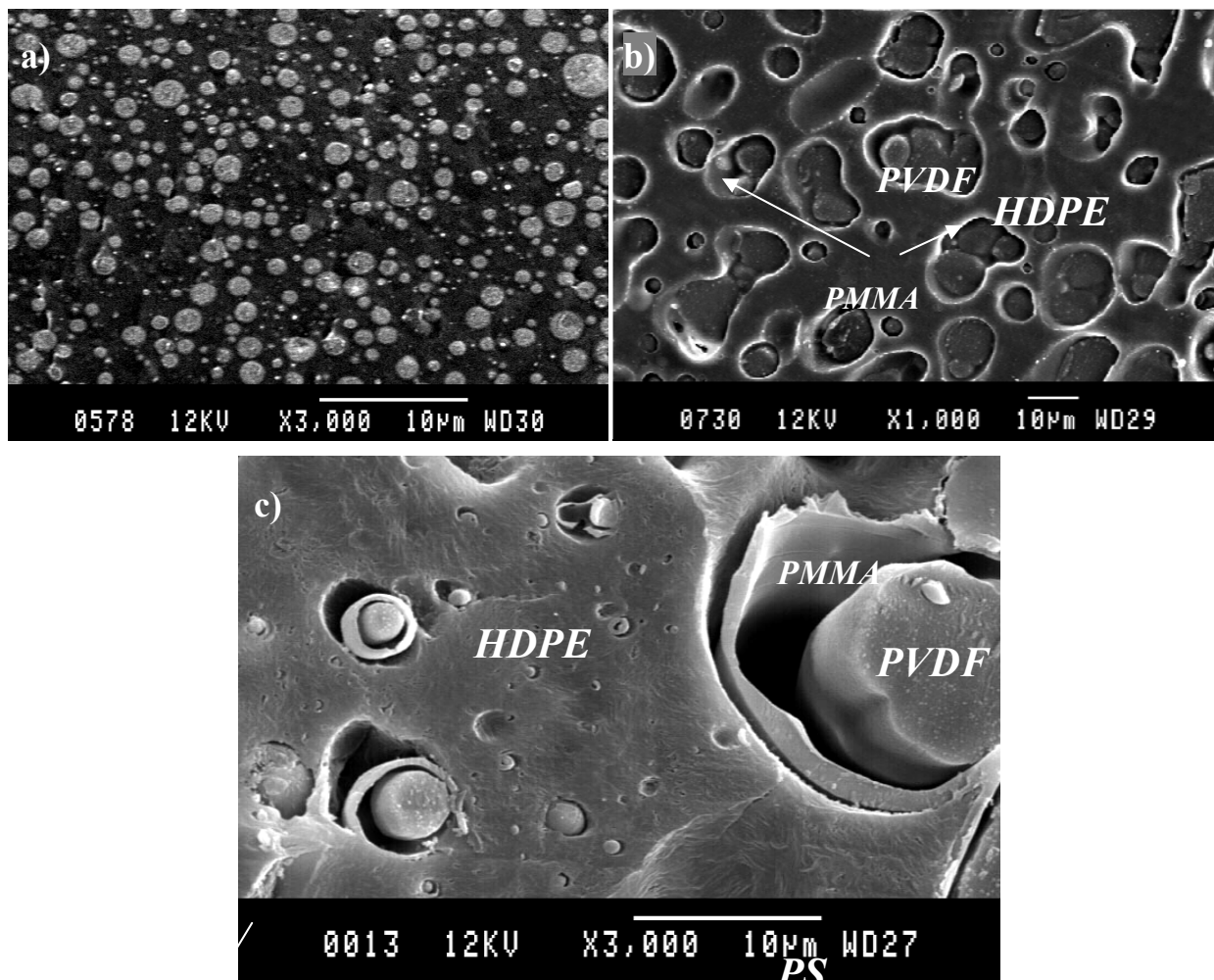


Figure 4-5. SEM micrograph of a) matrix-droplet morphology of 80/20 PMMA/PS, b) PVDF core-PMMA shell morphology in an HDPE matrix for 60/20/20 HDPE/PMMA/PVDF (PMMA extracted), and c) onion morphology in an HDPE matrix for 60/13/13/13 HDPE/PS/PMMA/PVDF (PMMA extracted)

Theoretically, the addition of PANI as a fifth component to the quaternary blend above, creates a five-component onion droplet structure with PANI as the inner phase and HDPE as the matrix.

Since it is difficult to isolate the position of PANI in a 5 component blend system, a ternary blend of HDPE/PVDF/PANI, already shown in Figure 4-3b was prepared. The morphology of this blend, after selective extraction of the PVDF, clearly shows the localization of PVDF at the interface of HDPE and PANI which is a result of the very high spreading coefficient of PVDF over PANI, $\lambda_{\text{PVDF/PANI}}$ (7.3 mN/m). These data on the PE/PVDF/PANI blends as well as the discussion related to the other ternary and quaternary blend systems above would tend to confirm the ordering of phases in the quinary system as HDPE|PS|PMMA|PVDF|PANI as was predicted from Harkins spreading theory.

Although detecting the position of each phase in a five-component onion structure by microscopy techniques is very difficult, the morphology of 50/10/20/10/10 HDPE/PMMA/PS/PVDF/PANI blend after selective extraction of one or several phases is represented in Figure 4-6. Figure 4-6a depicts the continuous structure of HDPE after extraction of all other phases. Empty spherical areas observed in the matrix of HDPE represent onion domains containing various phases. The selective extraction of PS (Figure 4-6b) and PMMA (Figure 4-6c) phases from the blend verifies them as two layers of an onion. Figure 4-6d shows the same blend where phases PS and PMMA have been extracted together demonstrating a wider empty area, indicating the successive situation of PS and PMMA phases. The extracted area in Figure 4-6d separates two major phases which are the matrix of HDPE and droplet-in-droplet of PANI-in-PVDF. All of the above confirms the hierarchical ordering of HDPE|PS|PMMA|PVDF|PANI in the quinary blend.

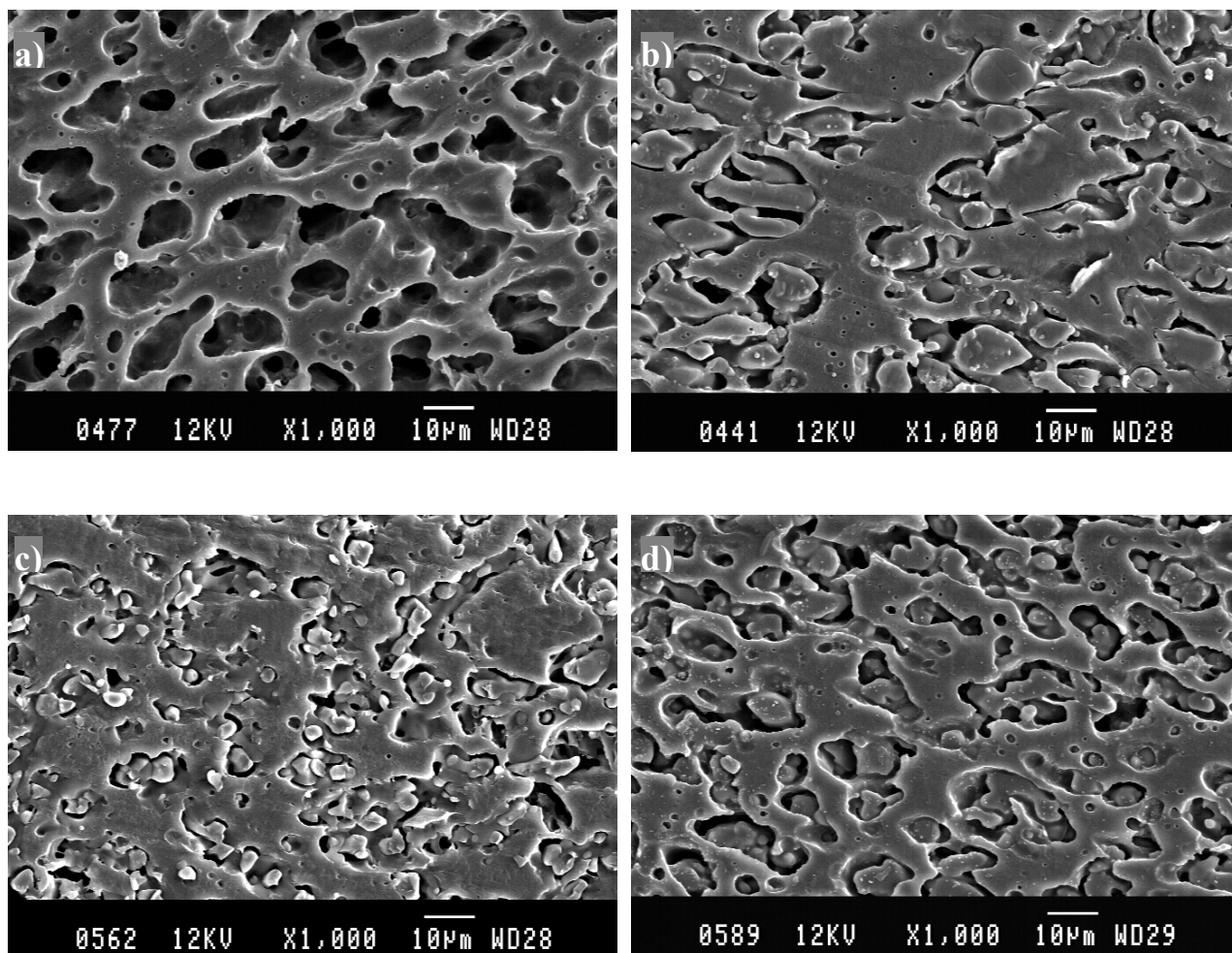


Figure 4-6. SEM micrographs of 50/10/20/10/10 HDPE/PMMA/PS/PVDF/PANI after extraction of (a) all phases except HDPE, (b) PS by cyclohexane (c) PMMA by acetic acid, and (d) PS and PMMA by combining cyclohexane and acetic acid

4.4.3 Generating Highly Continuous (Multiple-Percolated) Quaternary Polymer Blends

In this part of the work the composition range required to achieve multiple percolation for quaternary HDPE/PS/PMMA/PVDF blends, where all phases are continuous and percolated through the system, will be determined. In such a case, not only does the typical percolation threshold of the multiphase blend decrease due to the increased number of components, but also

the specific percolation threshold of each of the individual phases (middle, inner, and outer) significantly decreases.

The most critical phases in HDPE/PS/PMMA/PVDF are the first(HDPE) and last(PVDF) phases. Changing the ratio of these two phases, while maintaining the concentration of the middle phases controls the evolution of the morphology from an onion structure to a multi-percolated one. It has been shown in previous work from this laboratory(Reignier, et al., 2003) that composite droplets with a core/shell morphology can experience coalescence and still maintain the hierarchical order after coalescence. Figure 4-7a-e, which shows quaternary HDPE/PS/PMMA/PVDF blends of concentrations of 60/13/13/13(onion morphology), 50/17/17/17, and 30/15/15/40(multi-percolated morphology), illustrates that the hierarchical order is maintained as the morphology transits from an onion structure to more elongated structures through to a multi-percolated one. Figure 4-7e shows unambiguously, after the selective extraction of the PMMA phase, that highly ordered multipercolated morphology is obtained for 30HDPE/15PS/15PMMA/40PVDF with a hierarchical ordering of HDPE/PS/PMMA/PVDF.

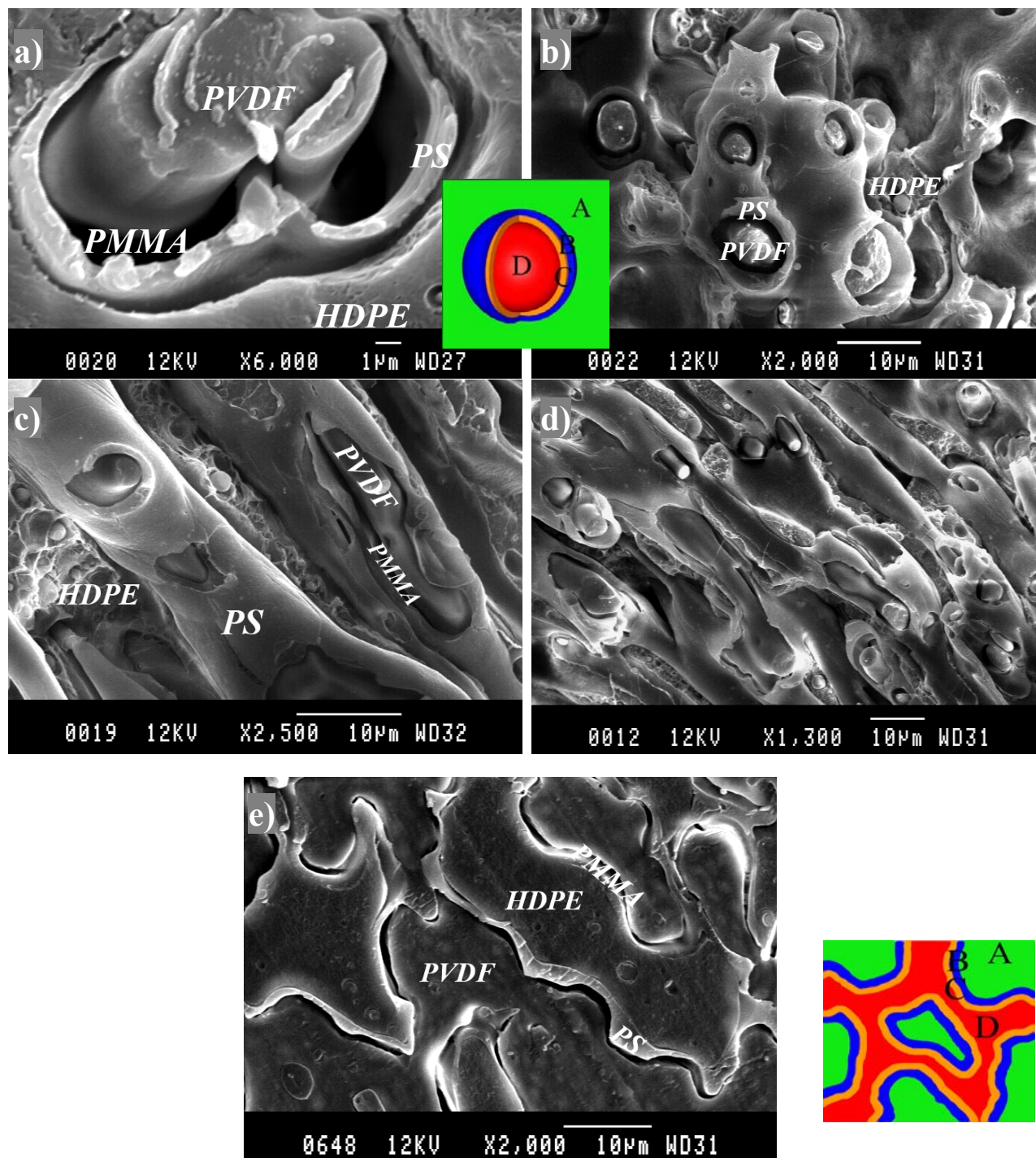


Figure 4-7. SEM micrographs and schematics of HDPE/PS/PMMA/PVDF after extraction of PMMA by acetic acid for a) and b) onion morphology in an HDPE matrix for 60/13/13/13, c) and d) more elongated morphology of 50/17/17/17, and e) triple-percolated morphology of 30/15/15/40 (microtomed surface). The voids show that PMMA is present as a layer separating PS and PVDF.

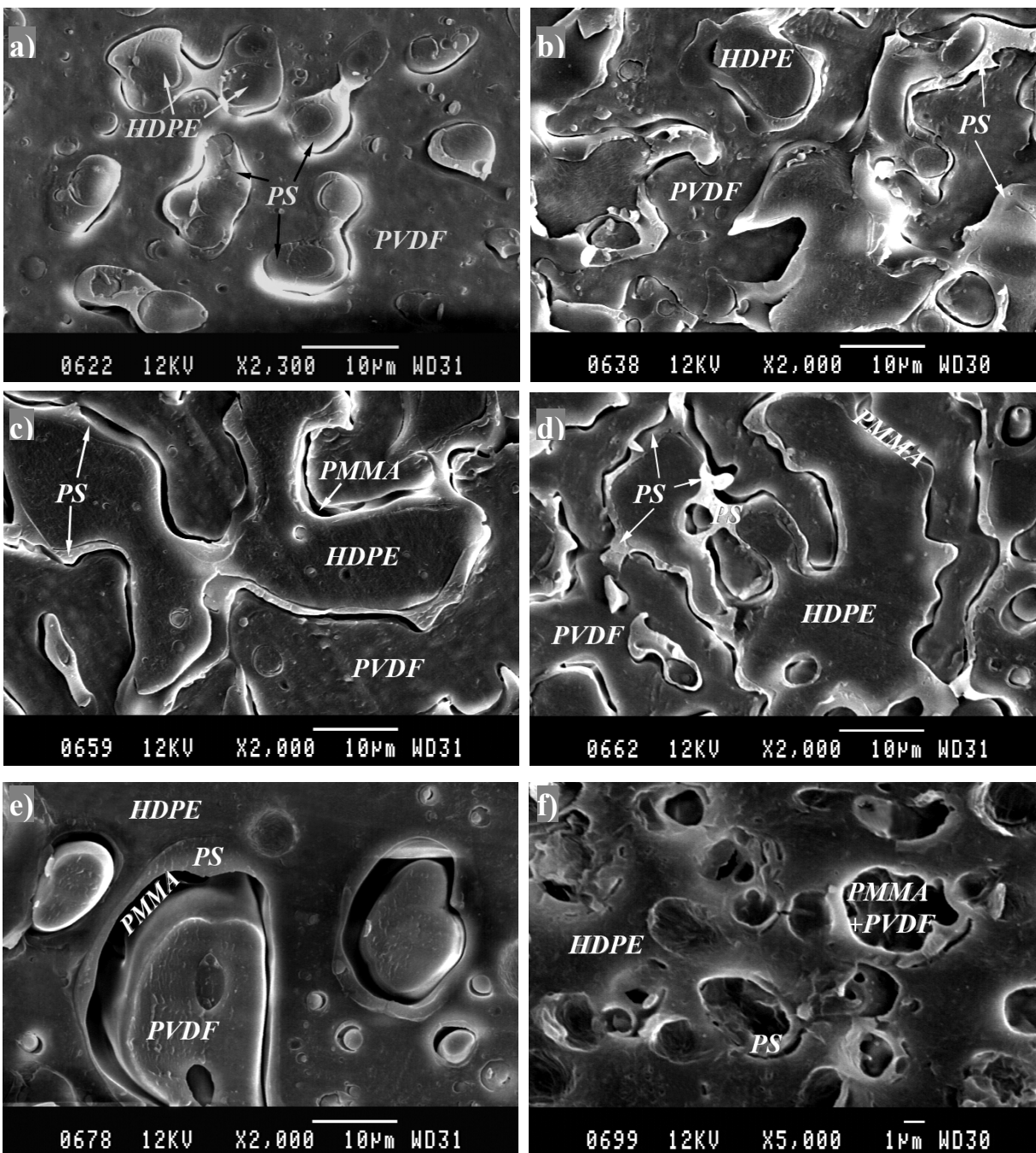


Figure 4-8. SEM micrographs of various quaternary HDPE/PS/PMMA/PVDF blends after microtoming and extraction of the PMMA phase; (a) 10/15/15/60, (b) 20/15/15/50, (c) 30/15/15/40, (d) 40/15/15/30, (e) 50/15/15/20, (f) 60/15/15/10.

Uniform layers of PS and PMMA situated in the middle of a quaternary blend of HDPE/PS/PMMA/PVDF are found at concentrations levels of 15% for each respectively. In order to determine the range of multi-percolated regions in the quaternary HDPE/PS/PMMA/PVDF blend, the composition ratio of HDPE and PVDF is varied from 10/15/15/60 HDPE/PS/PMMA/PVDF to 60/15/15/10 HDPE/PS/PMMA/PVDF while the composition of PS and PMMA is maintained at 15% (Figure 4-8).

Figure 4-8 illustrates the morphologies obtained and in all cases PMMA has been extracted by acetic acid to distinguish it from HDPE, PS, and PVDF in the blend. Hence, PMMA can be recognized as void areas separating the continuous parts of the PS layer attached to HDPE and continuous PVDF. When the composition of HDPE is as low as 10% and 20%, droplets of HDPE encapsulated by the PS phase are detected, and both are encapsulated by PMMA in a matrix of PVDF (Figure 4-8a and Figure 4-8b). The opposite behavior is encountered when the PVDF phase has concentrations as low as 10% and 20%, demonstrating droplets of PVDF encapsulated by PMMA phase where both are encapsulated by PS within a HDPE matrix (Figure 4-8e and Figure 4-8f). A comparison of 10/15/15/60 HDPE/PS/PMMA/PVDF (Figure 4-8a) and 60/15/15/10 HDPE/PS/PMMA/PVDF (Figure 4-8f) reveals that, although the order of phases does not change, the onion morphology is reversed depending on whether the inner phase or outer phase is the matrix. As the concentration of HDPE or PVDF further increases and reaches 30%, droplets of those phases coalesce and continuous structures of the respective phase forms. Blends of 30/15/15/40 HDPE/PS/PMMA/PVDF and 40/15/15/30 HDPE/PS/PMMA/PVDF show two continuous phases of HDPE and PVDF while continuous PS and PMMA phases are situated at the interface (Figure 4-8c and Figure 4-8d).

In order to find the precise region of multi-percolation quantitatively, solvent extraction followed by a gravimetric measurement was used to obtain the percentage continuity of each phase as a function of volume fraction of HDPE in the quaternary blend of HDPE/PS/PMMA/PVDF (Figure 4-9). Note that in Figure 4-9 the concentrations of PS and PMMA are both held at 15%, while the combined concentration of HDPE plus PVDF is always held at 70%. In Figure 4-9, the x axis refers to the % concentration of HDPE in HDPE plus PVDF. Thus 100% HDPE refers to the 70HDPE/15PS/15PMMA blend while 50% HDPE refers to the 35HDPE/15PS/15PMMA/35PVDF blend.

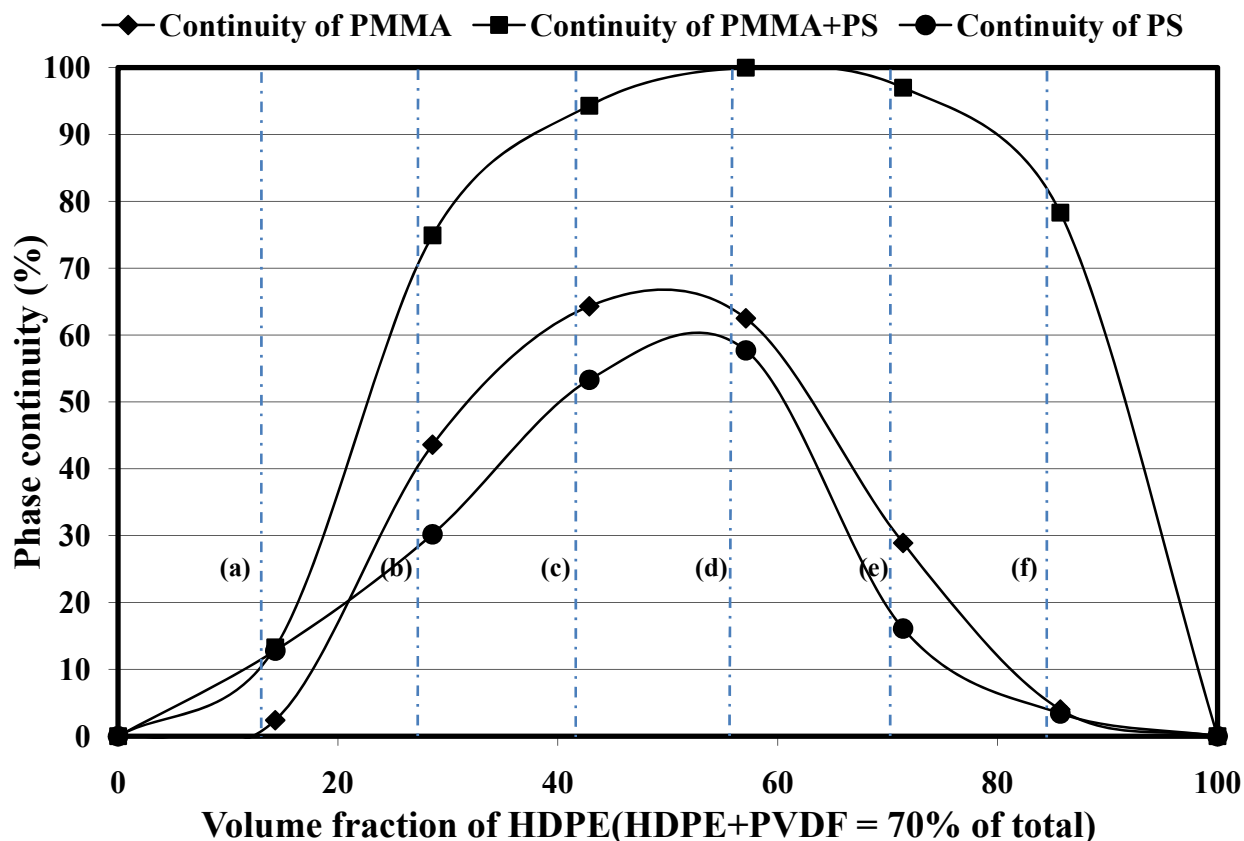


Figure 4-9. Continuity level of PS, PMMA, and PS+PMMA obtained by solvent extraction/gravimetry for 6 blends comprised of HDPE/PS/PMMA/PVDF; (a) 10/15/15/60, (b) 20/15/15/50, (c) 30/15/15/40, (d) 40/15/15/30, (e) 50/15/15/20, (f) 60/15/15/10.

Selective extraction associated with gravimetric measurements was carried out to obtain the continuity levels of PS, PMMA, and PS+PMMA in order to determine the concentrations where the phases are continuous. The continuity of HDPE and PVDF were estimated based on SEM photomicrographs at various compositions. Gravimetric results exhibit a low level of continuity (ranging from five to fifteen percent) for all phases in a 10/15/15/60 HDPE/PS/PMMA/PVDF onion morphology. Increasing the concentration of HDPE to 20 parts in the blend with PVDF at 50 (28.6% HDPE on the x-axis) yields a hierarchical-layered morphology with an HDPE core where the continuity of PS and PMMA reaches levels of 30% and 43%, respectively. Further increasing the HDPE concentration results in a maximum continuity of all phases for blends of 30/15/15/40 HDPE/PS/PMMA/PVDF and 40/15/15/30 HDPE/PS/PMMA/PVDF (Figure 4-9). If

the concentration of HDPE is increased further, an inverse behavior is observed where PVDF becomes the core and HDPE becomes the matrix. In this case, for the blend containing 50HDPE/15PS/15PMMA/20PVDF, the continuity of middle phases including PS and PMMA becomes 15% and 30%, respectively. Figure 4-9 shows that when the concentration of HDPE is increased up to 60 parts in the blend, the continuity of PS and PMMA becomes less than five percent.

4.4.4 Generating Highly Continuous Quinary Polymer Blends

In this part of the work, the addition of a fifth component to the highly continuous quaternary blends ranging from 30/15/15/30 to 40/15/15/30 HDPE/PS/PMMA/PVDF, selected from the previous section, is examined.

Ten percent PANI is added to a quaternary blend of HDPE/PS/PMMA/PVDF within the region of multi-percolation resulting in the formation of a five-component blend of 30/15/15/30/10 HDPE/PS/PMMA/PVDF/PANI (Figure 4-10). Figure 4-10a shows the continuous HDPE phase after the removal of all other phases. The selective extraction of PMMA and PS reveals a perfectly homogeneous continuous network for those phases in the blend (Figure 4-10b and Figure 4-10c). The extraction of both PS and PMMA phases together separates the multi-blend into two inter-diffused continuous structures where one of them is a continuous HDPE phase and the other is a continuous PANI and PVDF phase (Figure 4-10d). It also illustrates that continuous networks of PS and PMMA are adjacent to each other. In Figure 4-10e, the network of PANI which has been extracted by chromic acid is clearly detected.

In order to unambiguously illustrate that PANI forms a network morphology, blends of 25/25/25/25 PS/PMMA/PVDF/PANI and 15/20/15/25/25 PS/PS-co-PMMA/PMMA/PVDF/PANI are prepared. The influence of the addition of a PS-co-PMMA copolymer on the segregation of phases is discussed in a following section in detail. After the extraction of all phases except PANI and followed by a freeze-drying process, a network of PANI with very thin walls remains, as represented in Figure 4-11. Freeze-drying is carried out to prevent of shrinkage of the PANI network.

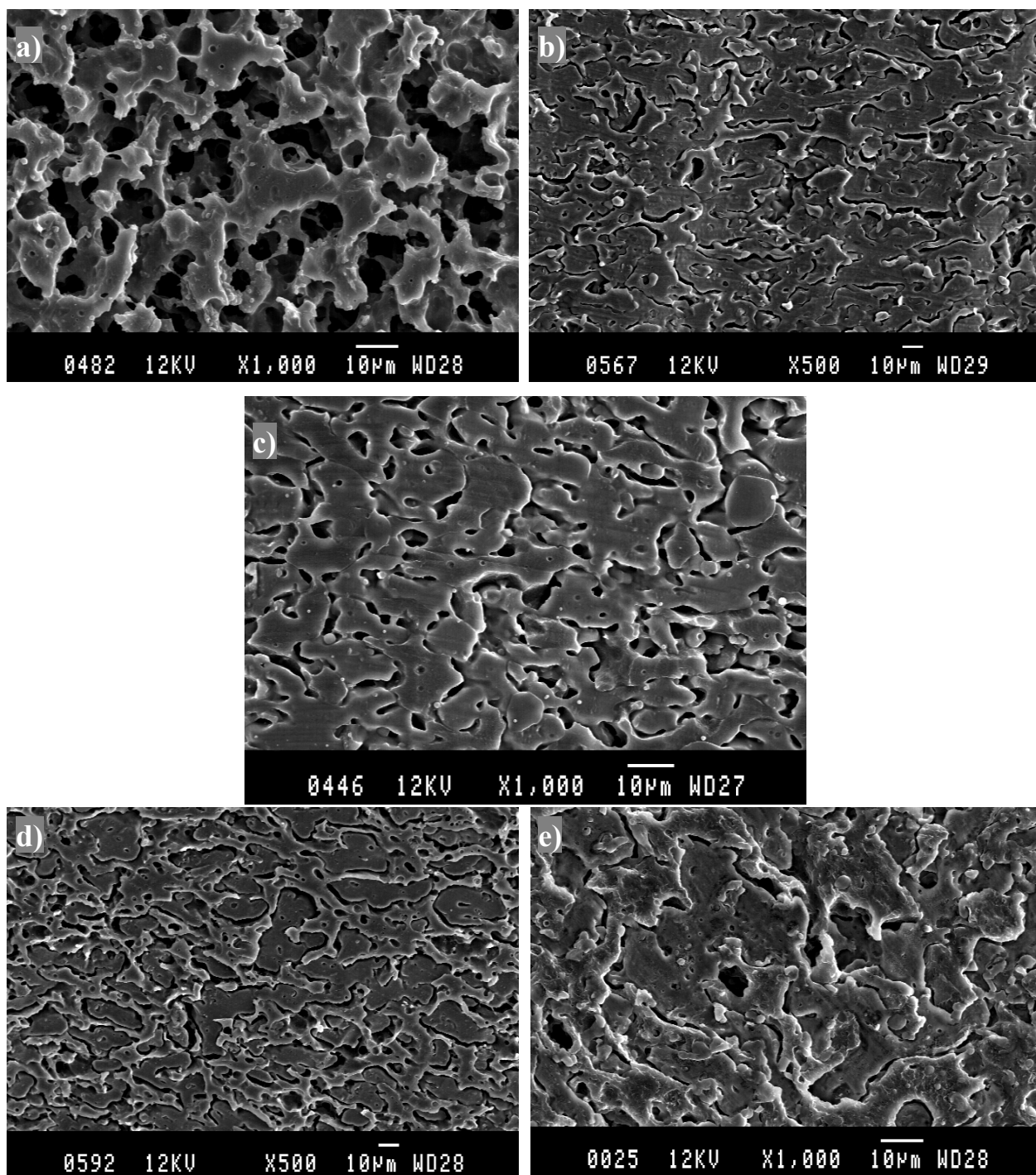


Figure 4-10. SEM micrographs of the multi-percolated 30/15/15/30/10 blend comprised of HDPE/PS/PMMA/PVDF/PANI after extraction of (a) all phases except HDPE, (b) PMMA by acetic acid (c) PS by cyclohexane, (d) PS and PMMA by combining cyclohexane and acetic acid, and (e) PANI by chromic acid

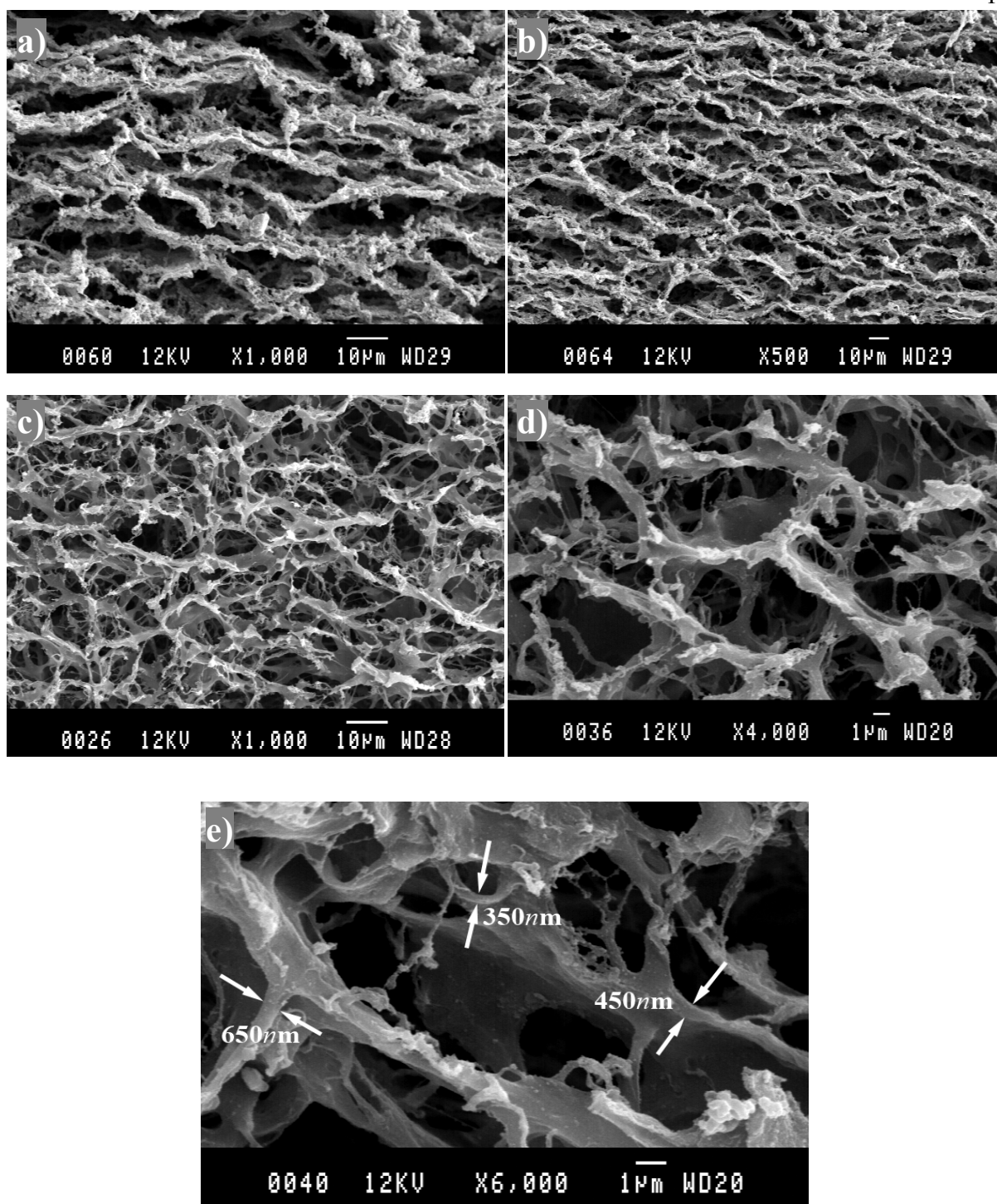


Figure 4-11. SEM micrographs of a), b) continuous PANI network of quaternary 25/25/25/25 PS/PMMA/PVDF/PANI blend after extraction of all phases by DMF followed by a freeze drying process, and c, d, e) continuous PANI network derived from a 15/20/15/25/25 PS/PS-co-PMMA/PMMA/PVDF/PANI blend after extraction of all phases by DMF followed by freeze drying process. The thickness of the PANI network walls are shown in Figure 4-11e.

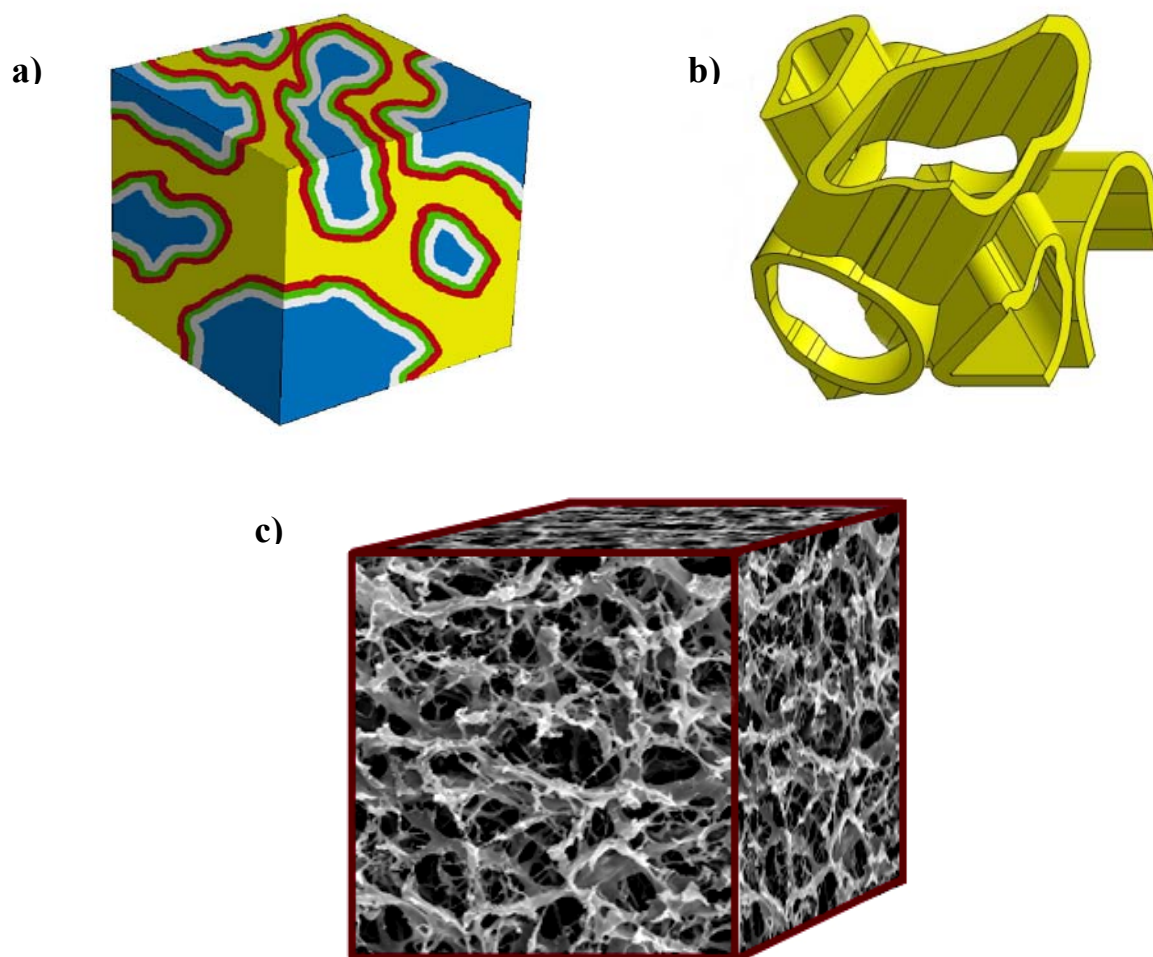


Figure 4-12. a) Schematic representation of quinary multi-percolated morphology, the yellow phase is PANI, the blue phase is HDPE, and all other phases are located between them, b) schematic of a PANI network obtained after removal of all phases except PANI, and c) a 3D image constructed from 2D SEM images of the interconnected PANI network in the quinary 15/20/15/25/25 PS/PS-co-PMMA/PMMA/PVDF/PANI blend after extraction of all other phases.

This figure clearly confirms that in a triple-percolated structure with PANI as the inner phase, PANI will spread. As shown in Figure 4-11e, the PANI network in a multi-percolated structure has branches with very thin walls. The range of thicknesses of the wall in this structure range from a few hundred nanometers to 700 nanometers. Another important point that should be taken into account is the actual content of pure PANI in the blends. The PANI used in this work is

melt-processable and contains 25 wt% pure PANI and 75 wt% zinc compound. This indicates that the real volume of pure PANI present in the blends is less than reported volume fraction in these blends.

A schematic representation for such a 5-component multi-percolated structure is shown in Figure 4-12a. The yellow phase represents PANI which, after removal of all other phases by selective solvents, demonstrates an interconnected network as schematically shown in Figure 4-12b. Figure 4-12c illustrates the 15/20/15/25/25 PS/PS-co-PMMA/PMMA/PVDF/PANI blend after extraction of all phases except PANI, clearly indicating that a complete PANI network is attained.

4.4.5 The Effect of Diblock Copolymer on the Morphology and Conductivity of Multiple-Percolated Blend Systems

The addition of a PS-co-PMMA copolymer to a PS/PMMA/PVDF/PANI multi-percolated structure results in a decrease of the size of the PS and PMMA phases. Such a decrease in the size of two adjacent phases results in corresponding smaller phase sizes for the other phases involved in the multi-encapsulated structure. This can be used as an additional parameter to control morphology and conductivity.

Figure 4-13 depicts two multi-percolated quaternary blends, one without modifier (30/30/30/10 PS/PMMA/PVDF/PANI) and the other with modifier (20/20/20/30/10 PS/PS-co-PMMA/PMMA/PVDF/PANI). In both cases, the composition of all the phases is identical. Figure 4-13a and Figure 4-13b compare samples with and without a copolymer, respectively, after extraction of both PS and PMMA phases using cyclohexane and acetic acid, respectively. The addition of PS-co-PMMA to the multi-percolated PS/PMMA/PVDF/PANI blend clearly reduces the sizes of all the phases.

Figures 4-13c and 4-13d examine the effect of added copolymer on the phase size of PANI alone where PANI is removed using chromic acid. These micrographs show that the PANI phase size is significantly smaller after addition of PS-co-PMMA. Thus, the addition of a copolymer

specific to two adjacent phases in a multi-encapsulated system results in a reduction of all phase sizes in the encapsulated system.

Figure 4-11 shows the effect of copolymer more clearly on the PANI network structure after removal of all other components followed by a freeze drying step. Two blends are considered, one without copolymer, 25/25/25/25 PS/PMMA/PVDF/PANI (Figure 4-11a and b), and one containing copolymer, 15/20/15/25/25 PS/PS-co-PMMA/PMMA/PVDF/PANI (Figure 4-11c, d, and e). The micrographs demonstrate that, in the presence of copolymer, the PANI network is finer and more uniform with homogeneous branches distributed throughout the sample.

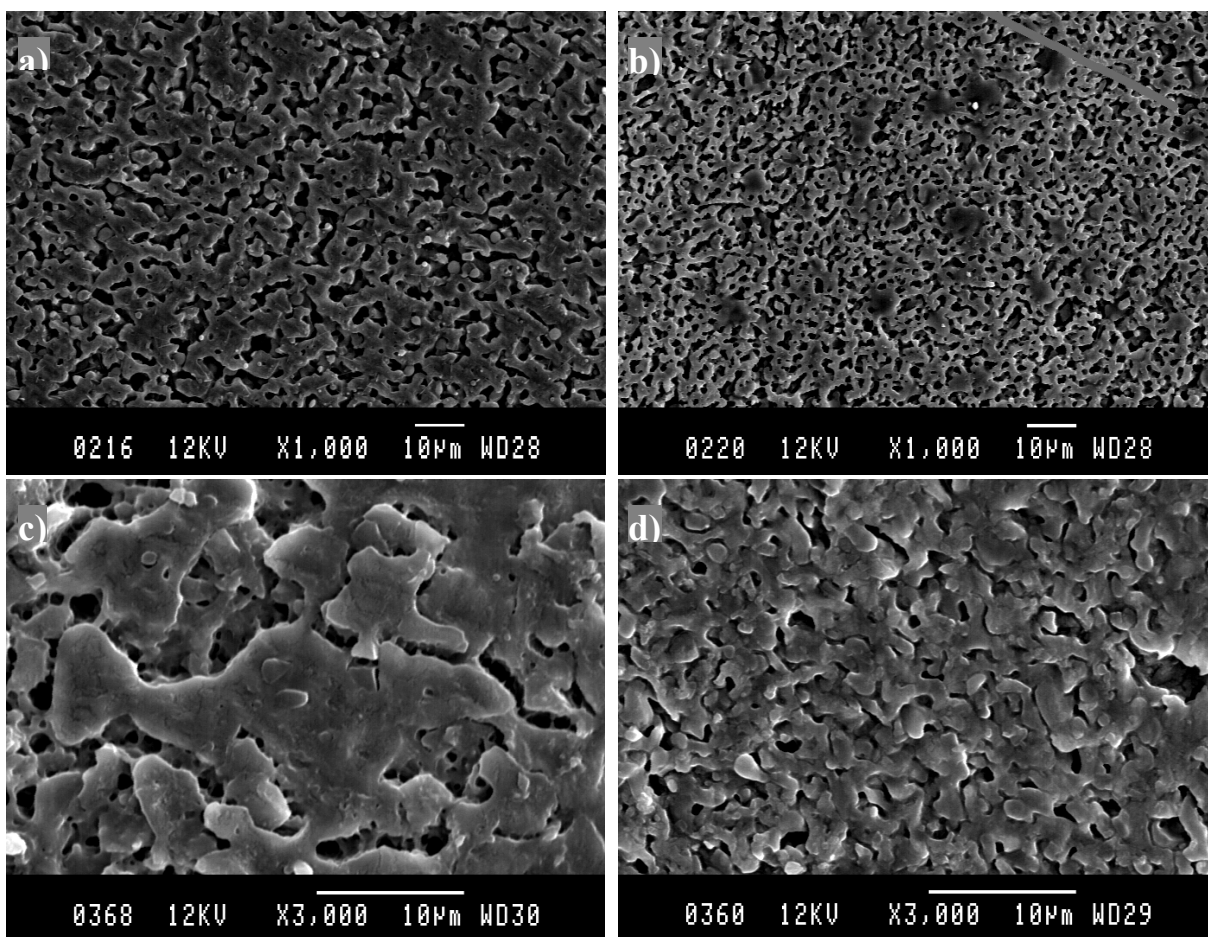


Figure 4-13. SEM micrograph of a) 30/30/30/10 PMMA/PS/PVDF/PANI blend after extraction of PS and PMMA, b) 20/20/20/30/10 PS/PS-co-PMMA/PMMA/PVDF/PANI after extraction of PS and PMMA, c) 30/30/30/10 PMMA/PS/PVDF/PANI blend after extraction of PANI by chromic acid, and d) 20/20/20/30/10 PS/PS-co-PMMA/PMMA/PVDF/PANI after extraction of PANI by chromic acid

One question that should be addressed is whether the addition of a PS-co-PMMA interfacial modifier would be expected to theoretically affect the hierarchical order in these blend systems. Table 4-3 shows a very low value of interfacial tension of $\gamma_{PS/PMMA}=1.1$ mN/m. If after addition of copolymer, $\gamma_{PS/PMMA}$ decreases to the lowest possible value close to zero, all ternary blends comprised of both PS and PMMA in the blend still show positive spreading coefficient values. These results imply that the positive values of $\lambda_{PS/PMMA}$ in HDPE|PS|PMMA, $\lambda_{PMMA/PVDF}$ in PS|PMMA|PVDF, and $\lambda_{PMMA/PANI}$ in PS|PMMA|PANI result in three complete wetting cases with the same order of phases as before the addition of copolymer.

4.4.6 The Effect of the Number of Components of Multi-Percolated Structures on Conductivity

In this section the effect of the number of the components in multi-percolated structures on the conductivity, where PANI phase situated as the innermost phase, is investigated as a function of volume fraction of PANI (Figure 4-14).

The percolation threshold for a conductive material is the concentration at which the first connected pathway of conductive polymer forms in the blend. Conductivity data thus provides a tool as powerful as solvent gravimetry to determine percolation thresholds for a conductive substance. In a blend containing conductive material can be used for both conductivity and continuity. It implies that the concentration at which the first connected pathway of conductive polymer in the blend forms, both conductivity and continuity values sharply increase resulting in percolation threshold. Hence, conductivity percolation threshold corresponds to continuity percolation threshold of sample. In an onion morphology with the PANI phase located at the core of a dispersed phase with low connectivity, the conductivity would be expected to be low. Figure 4-14 shows samples with multi-percolated structures constituting various numbers of components. The concentration of each sample is represented in Table 4-5.

Table 4-5. Number of Components and Compositions of Samples Shown in Figure 4-14

Sample	Number of components	PANI	PS	PVDF	PMMA	HDPE	PS-co-PMMA
A	3	5	50	—	45	—	—
B	4	5	15	45	—	35	—
C	5	5	20	35	20	20	—
D	6	5	16	20	15	35	9
E	3	10	45	—	45	—	—
F	4	10	30	30	30	—	—
G	5	10	20	20	20	30	—
H	5	10	20	30	20	—	20
I	3	20	40	—	40	—	—
J	5	20	20	20	20	20	—
K	6	20	15	20	12	20	13
L	4	25	25	25	25	—	—
M	5	25	15	25	15	—	20
N	3	33.3	—	33.3	—	33.3	—
O	2	50	50	—	—	—	—

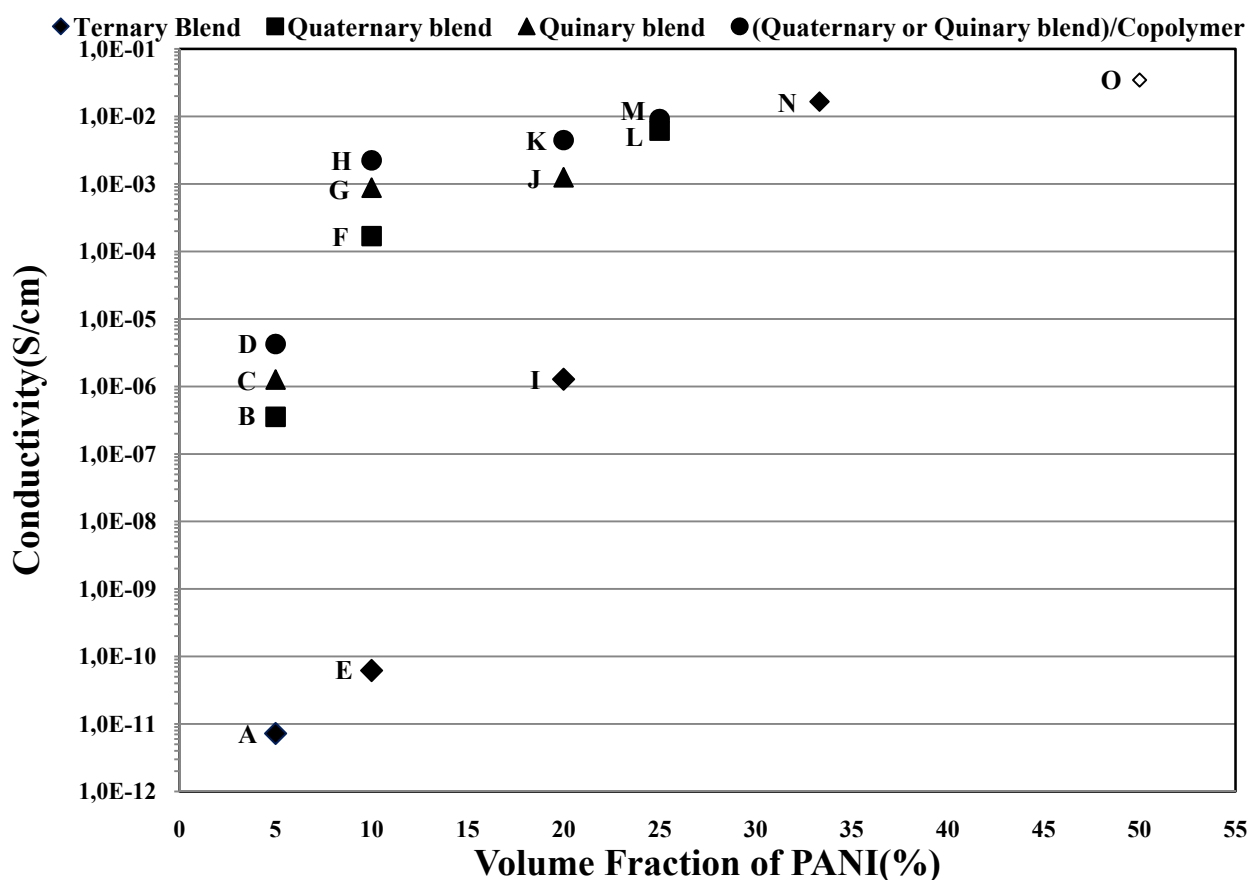


Figure 4-14. Conductivity of multi-percolated blends of ternary, quaternary, quinary, as well as interfacially modified quaternary and quinary systems as a function of the volume fraction of PANI. Note that point O is a co-continuous binary blend of PS and PANI.

In Figure 4-14, samples A, B, C, and D represent ternary, quaternary, five-component, and six-component polymer blends all containing five percent PANI. In all samples, the composition of all phases, other than PANI, have been selected to be in the multi-percolated region (Table 4-5). Sample (A) is a ternary blend of 5/45/50 PANI/PMMA/PS in which PMMA is at the interface. Due to the low amount of PANI (5%) in this sample, droplets of PANI are encapsulated by the PMMA phase. The very low conductivity value of almost 10^{-11} S cm^{-1} indicates that no connected conductive pathway forms in this sample. In order to spread the PANI at least four components in the multi-percolated structure are required. In sample (B), five percent of PANI is present in a quaternary blend with a composition of 35/15/45/5 HDPE/PS/PVDF/PANI. In this blend, due to the geometrical restrictions imposed on PANI, a continuous PANI phase forms a

network and the percolation threshold of PANI is achieved as seen by the conductivity value of $3.5 \times 10^{-7} \text{ S cm}^{-1}$. Although the percolation threshold is defined as a transition state and occurs at different conductivity values, typically its value is between $10^{-11} \text{ S cm}^{-1}$ and $10^{-9} \text{ S cm}^{-1}$. The relatively high conductivity value of $3.5 \times 10^{-7} \text{ S cm}^{-1}$ for sample (B) shows that percolation threshold has in fact been reached at a significantly lower concentration than 5% PANI.

Sample (C) is a quinary blend containing 5% PANI comprised of HDPE/PS/PMMA/PVDF/PANI. This system attains an even higher conductivity value of $1.2 \times 10^{-6} \text{ S cm}^{-1}$ thus corresponding to a lower percolation threshold due to the further geometrical restrictions imposed by the additional phase.

Sample (D) represents a blend with five components and a di-block copolymer of adjacent PS and PMMA phases in the blend. Since the PS and PMMA phases are located beside each other, the addition of their copolymer to a blend results in the size of the PS and PMMA phases being decreased (compare Figures 4-13a and 4-13b). This reduction of size in the PS and PMMA phases carries over to other phases including PANI. The highest conductivity value for blend containing 5% PANI is obtained for sample (D) with a value of $4.2 \times 10^{-6} \text{ S cm}^{-1}$.

The 5% percolation threshold value for PANI reported above is the lowest ever obtained in a melt processed multi-component system. Moreover, as discussed earlier, since the PANI sample used here is a mixture of 25% PANI and 75% zinc compound, the actual concentration of pure PANI at this percolation threshold value is less than 5%.

Points (E), (F), and (G) represent ternary, quaternary, and five-component blends, each of which contains 10% PANI. Point (H) is a quaternary blend containing a copolymer of PS and PMMA. Although the extent of PANI is ten percent in these cases and higher conductivity values are obtained for blends compared to samples containing 5%, a similar behavior in increasing the conductivity value with multi-percolated samples is observed. Higher concentration of PANI in the samples containing 10% PANI results in more connected pathways of PANI in the sample yielding a higher conductivity range from $6.2 \times 10^{-11} \text{ S cm}^{-1}$ for ternary to $2.2 \times 10^{-3} \text{ S cm}^{-1}$ for the quaternary blend plus copolymer.

Ternary, five-component, and six-component samples denoted as (I), (J), and (K), respectively, having 20% PANI are blended. Sample (I) shows a high conductive value of $2.2 \times 10^{-3} \text{ S cm}^{-1}$ for the ternary blend indicating that although the PANI is encapsulated by the middle

phase(PMMA), the concentration of PANI is high enough (20 vol%) to create a random network inside the PMMA. This implies that at a high concentration of PANI, the effect of the morphology of the system on the conductivity is less important. At those higher concentrations, random connected pathways form in the system for all morphologies. But morphology is still affective whereas samples (J) and (K) comprising of more components represent higher conductivity values of $1.2 \times 10^{-3} \text{ S cm}^{-1}$ and $4.5 \times 10^{-3} \text{ S cm}^{-1}$. Samples L and M in Figure 4-14 with 25% PANI demonstrate that 25% of PANI in the sample is sufficient to completely diminish the effect of morphology on conductivity and random networks of PANI form everywhere in the sample. Even at higher concentrations of PANI no significant increase in conductivity for the blend is observed as random pathways saturate the sample. Since the PANI concentration and morphology of the phases in these samples have no affect on the conductivity, even ternary(sample N) and binary(sample O) blends show the maximum conductivity and plateau behavior.

4.5 Conclusions

We have used polyaniline as a conductive polymer to prepare a solid, 3D, low percolation threshold conductive device through the control of multiple encapsulation and multiple percolation effects in a 5 component PE/PS/PMMA/PVDF/PANI polymer blend system through melt processing. The percolation threshold in the multi-component polymer blend is shown to be sensitive to the morphological continuity of the various encapsulated phase networks. PANI is situated in the core of the multiple network system due to its high surface tension and polarity and, in this way its percolation threshold can be reduced to less than 5%. The detailed morphology and continuity diagrams of binary, ternary, quaternary and finally quinary systems are progressively studied in order to systematically demonstrate the concentration regimes resulting in the formation of these novel multiple-encapsulated morphological structures. First, an onion-type morphology of HDPE/PS/PMMA/PVDF is prepared which is comprised of an HDPE matrix with a multiple-component polymeric droplet phase consisting of a PS shell, a PMMA middle layer and PVDF in the core. The order of phases in this concentrically organized onion morphology is thermodynamically controlled and is described by Harkins spreading

theory. Through the control of the composition of the inner(HDPE) and outer(PVDF) layers in the onion structure, the morphology can be transformed to a highly elongated onion morphology and subsequently to a multi-percolated structure in which all HDPE, PS, PMMA, and PVDF phases are continuous and percolated throughout the system. It is shown that the addition of PANI results in a 5-component multi-encapsulated, multi-percolated blend with the PANI situated in the core of the system. The addition of an interfacial modifier for the PS and PMMA components results in the diminished phase sizes of those particular components which, due to the encapsulated nature of the morphology, has the effect of reducing the phase size for all other phases as well. The conductivity is measured for a wide range of the above systems as a function of the number of phases and as a function of the PANI concentration. It is shown that increasing the number of components in the blend with a multi-percolated structure from ternary to quaternary to quinary and finally to an interfacially modified quinary blend results in a several orders of magnitude increase in the conductivity of the system. In this way, the percolation threshold of the PANI can be reduced to below 5 vol%. The conductivity of the quinary blend system, for example, can be increased from 10^{-15} S cm⁻¹ (pure PE) to 10^{-5} S cm⁻¹ at 5 % PANI and up to 10^{-3} S cm⁻¹ for 10% PANI. These are the highest conductivity values ever reported for these PANI concentrations in melt processed systems.

4.6 Acknowledgements

The authors express appreciation to the Natural Sciences and Engineering Research Council of Canada for supporting this work. They also thank F. Normandin from the *Institut des matériaux industriels* for his assistance with the conductivity measurements of the samples.

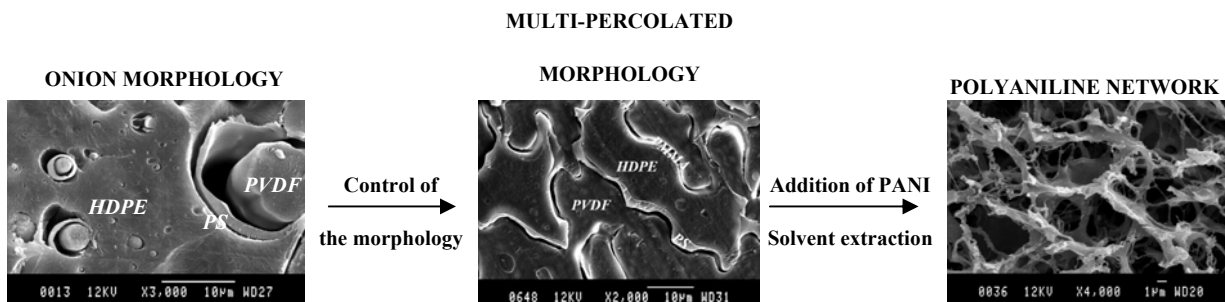
4.1. References

- (1) Moussaif, N.; Jérôme, R. *Polymer* **1999**, *40*, 3919.
- (2) Reignier, J.; Favis, B. D. *Macromolecules* **2000**, *33*, 6998.
- (3) Reignier, J.; Favis, B. D. *AIChE Journal* **2003**, *49*, 1014.
- (4) Zhang, J.; Ravati, S.; Virgilio, N.; Favis, B. D. *Macromolecules* **2007**, *40*, 8817.
- (5) Virgilio, N.; Marc-Aurele, C.; Favis, B. D. *Macromolecules* **2009**, *42*, 3405.

- (6) Virgilio, N.; Desjardins, P.; L'Esperance, G.; Favis, B. D. *Macromolecules* **2009**, *42*, 7518.
- (7) Torza, S.; Mason, S. G. *J. Coll. Interface Sci.* **1970**, *33*, 67.
- (8) Hobbs, S. Y.; Dekkers, M. E. J.; Watkins, V. H. *Polymer* **1988**, *29*, 1598.
- (9) Reignier, J.; Favis, B. D. *Polymer* **2003**, *44*, 5061.
- (10) Zilberman, M.; Siegmann, A.; Narkis, M.; 1 ed.; SAMPE: Anaheim, CA, USA, 1998; Vol. 43, p 528.
- (11) Zilberman, M.; Siegmann, A.; Narkis, M. *Journal of Macromolecular Science - Physics* **2000**, *B39*, 333.
- (12) Pud, A.; Ogurtsov, N.; Korzhenko, A.; Shapoval, G. *Progress in Polymer Science (Oxford)* **2003**, *28*, 1701.
- (13) Anand, J.; Palaniappan, S.; Sathyanarayana, D. N. *Progress in Polymer Science (Oxford)* **1998**, *23*, 993.
- (14) Bhattacharya, A.; De, A. *Journal of Macromolecular Science - Reviews in Macromolecular Chemistry and Physics* **1999**, *C39*, 17.
- (15) Scher, H.; Zallen, R. *The Journal of Chemical Physics* **1970**, *53*, 3759.
- (16) Gubbels, F.; Blacher, S.; Vanlathem, E.; Jerome, R.; Deltour, R.; Brouers, F.; Teyssie, P. *Macromolecules* **1995**, *28*, 1559.
- (17) Gubbels, F.; Jerome, R.; Teyssie, P.; Vanlathem, E.; Deltour, R.; Calderone, A.; Parente, V.; Bredas, J. L. *Macromolecules* **1994**, *27*, 1972.
- (18) Jagur-Grodzinski, J. *Polymers for Advanced Technologies* **2002**, *13*, 615.
- (19) Bridge, B.; Tee, H. *International Journal of Electronics* **1990**, *69*, 785.
- (20) Carmona, F. *Physica A: Statistical and Theoretical Physics* **1989**, *157*, 461.
- (21) Munson-McGee, S. H. *Physical Review B (Condensed Matter)* **1991**, *43*, 3331.
- (22) Sumita, M.; Sakata, K.; Asai, S.; Miyasaka, K.; Nakagawa, H. *Polymer Bulletin (Berlin)* **1991**, *25*, 265.
- (23) Burroughes, J. H.; Jones, C. A.; Friend, R. H. *Nature* **1988**, *335*, 137.
- (24) Paul, R. K.; Vijayanathan, V.; Pillai, C. K. S. *Synthetic Metals* **1999**, *104*, 189.
- (25) Macdiarmid, A. G.; Jin-Chih, C.; Halpern, M.; Wu-Song, H.; Shao-Lin, M.; Somasiri, L. D.; Wanqun, W.; Yaniger, S. I. In *Proceedings of the International Conference on the Physics and Chemistry of Low-Dimensional Synthetic Metals (ICSM 84)*, 17-22 June 1984; 1-4 ed. UK, 1985; Vol. 121, p 173.
- (26) Andreatta, A.; Cao, Y.; Chiang, J. C.; Heeger, A. J.; Smith, P. *Synthetic Metals* **1988**, *26*, 383.
- (27) Ruokolainen, J.; Eerikainen, H.; Torkkeli, M.; Serimaa, R.; Jussila, M.; Ikkala, O. *Macromolecules* **2000**, *33*, 9272.
- (28) Hartikainen, J.; Lahtinen, M.; Torkkeli, M.; Serimaa, R.; Valkonen, J.; Rissanen, K.; Ikkala, O. *Macromolecules* **2001**, *34*, 7789.
- (29) Panipol <http://www.azom.com/details.asp?ArticleID=1197> **2000**.
- (30) Segal, E.; Haba, Y.; Narkis, M.; Siegmann, A. *Journal of Polymer Science, Part B: Polymer Physics* **2001**, *39*, 611.
- (31) Shacklette, L. W.; Han, C. C.; Luly, M. H. *Synthetic Metals* **1993**, *57*, 3532.
- (32) Ikkala, O. T.; Laakso, J.; Väkiparta, K.; Virtanen, E.; Ruohonen, H.; Järvinen, H.; Taka, T.; Passiniemi, P.; Österholm, J. E.; Cao, Y.; Andreatta, A.; Smith, P.; Heeger, A. J. *Synthetic Metals* **1995**, *69*, 97.

- (33) Narkis, M.; Zilberman, M.; Siegmann, A. *Polymers for Advanced Technologies* **1997**, *8*, 525.
- (34) Zilberman, M.; Titelman, G. I.; Siegmann, A.; Haba, Y.; Narkis, M.; Alperstein, D. *Journal of Applied Polymer Science* **1997**, *66*, 243.
- (35) Woo Jin, B.; Won Ho, J.; Yun Heum, P. *Synthetic Metals* **2003**, *132*, 239.
- (36) Planes, J.; Wolter, A.; Cheguettine, Y.; Pron, A.; Genoud, F.; Nechtschein, M. *Physical Review B (Condensed Matter)* **1998**, *58*, 7774.
- (37) Morgan, H.; Foot, P. J. S.; Brooks, N. W. *Journal of Materials Science* **2001**, *36*, 5369.
- (38) Qinghua, Z.; Xianhong, W.; Yanhou, G.; Dajun, C.; Xiabin, J. *Journal of Polymer Science, Part B (Polymer Physics)* **2002**, *40*, 2531.
- (39) Moon Gyu, H.; Seung Soon, I. *Polymer* **2001**, *42*, 7449.
- (40) Chipara, M. I.; Munteanu, I.; Notingher, P.; Chipara, M. D.; Reyes Romero, J.; Negreanu, B.; Panaitescu, D.; IEEE: Vasteras, Sweden, 1998, p 372.
- (41) Rodrigues, P. C.; Akcelrud, L. *Polymer* **2003**, *44*, 6891.
- (42) Dong-Uk, C.; Kitae, S.; Young Chul, K.; Yun Heum, P.; Jun Young, L.; Gordon & Breach: Kyoto, Japan, 2001; Vol. 370, p 399.
- (43) Ong, C. H.; Goh, S. H.; Chan, H. S. O. *Polymer Bulletin (Berlin)* **1997**, *39*, 627.
- (44) Cao, Y.; Smith, P.; Heeger, A. J. *Synthetic Metals* **1992**, *48*, 91.
- (45) Yang, C. Y.; Cao, Y.; Smith, P.; Heeger, A. J. *Polymer Preprints, Division of Polymer Chemistry, American Chemical Society* **1993**, *34*, 790.
- (46) Privalko, V. P.; Ponomarenko, S. M.; Privalko, E. G.; Lobkov, S. V.; Rekheta, N. A.; Pud, A. A.; Bandurenko, A. S.; Shapoval, G. S. *Journal of Macromolecular Science - Physics* **2005**, *B44*, 749.
- (47) Bliznyuk, V. N.; Baig, A.; Singamaneni, S.; Pud, A. A.; Fatyeyeva, K. Y.; Shapoval, G. S. *Polymer* **2005**, *46*, 11728.
- (48) Fraysse, J.; Planes, J.; Dufresne, A.; Taylor and Francis Inc.: Poznan, 2000; Vol. 354, p 511.
- (49) Levon, K.; Margolina, A.; Patashinsky, A. Z. *Macromolecules* **1993**, *26*, 4061.
- (50) Haba, Y.; Segal, E.; Narkis, M.; Titelman, G. I.; Siegmann, A. *Synthetic Metals* **2000**, *110*, 189.
- (51) Narkis, M.; Haba, Y.; Segal, E.; Zilberman, M.; Titelman, G. I.; Siegmann, A. *Polymers for Advanced Technologies* **2000**, *11*, 665.
- (52) Cox, W. P.; Merz, E. H. *Journal of Polymer Science* **1958**, *28*, 619.
- (53) Yasuda, K.; Armstrong, R.; Cohen, R. *Rheologica Acta* **1981**, *20*, 163.
- (54) Virgilio, N.; Favis, B. D.; Pepin, M.-F.; Desjardins, P.; L'Esperance, G. *Macromolecules* **2005**, *38*, 2368.
- (55) Wu, S. *Polymer Interface and Adhesion*; Marcel Dekker Inc.: New York, 1982.
- (56) Baradie, B.; Shoichet, M. S. *Macromolecules* **2003**, *36*, 2343.
- (57) Reignier, J.; Favis, B. D.; Heuzey, M.-C. *Polymer* **2003**, *44*, 49.

Table of Contents



CHAPTER 5 - 3D POROUS POLYMERIC MATERIAL WITH LOW PERCOLATION THRESHOLD OF CONDUCTIVE POLYMER PREPARED USING LBL DEPOSITION

5.1 Abstract

In this work a novel 3D porous polymeric conducting device (PPCD) is derived from multi-percolated polymer blend systems. The work has focused on the preparation of ultra-low surface area porous substrates followed by the deposition of polyaniline conductive polymer (PANI) on the internal porous surface using a layer-by-layer technique. The approach reported here allows for the percolation threshold concentration of polyaniline conductive polymer (PANI) to be reduced to values as low as 0.19%. Furthermore, depending on the amount of PANI deposited, the conductivity of the porous substrate can be controlled from 10^{-15} S cm⁻¹ to 10^{-3} S cm⁻¹.

Ternary and quaternary multi-percolated systems comprised of high-density polyethylene(HDPE), polystyrene(PS), poly(methyl methacrylate)(PMMA) and poly(vinylidene fluoride)(PVDF) are prepared by melt mixing and subsequently annealed in order to obtain large interconnected phases. Selective extraction of PS, PMMA and PVDF result in a fully interconnected porous HDPE substrate of ultra low surface area and highly uniform sized channels. This provides an ideal substrate for subsequent polyaniline(PANI) addition. Using a layer-by-layer(LbL) approach, alternating poly(styrene sulfonate)(PSS)/PANI layers are deposited on the internal surface of the 3-dimensional porous polymer substrate. The PANI and sodium poly(styrene sulfonate)(NaPSS) both adopt an inter-diffused network conformation on the surface. The sequential deposition of PSS and PANI has been studied in detail and the mass deposition profile demonstrates oscillatory behavior following a zigzag-type pattern. The presence of salt in the deposition solution results in a more uniform deposition and more thickly deposited PSS/PANI layers. The conductivity of these samples was measured and the conductivity can be controlled from 10^{-15} S cm⁻¹ to 10^{-5} S cm⁻¹ depending on the number of deposited layers. Applying a load to the substrate can be used as an additional control parameter. Higher loads result in higher conductivity values with values as high as 10^{-3} S cm⁻¹ obtained. The

work described above has focused on very low surface area porous substrates in order to determine the lowest possible percolation threshold values of polyaniline, but high surface area substrates can also be readily prepared using this approach.

5.2 Introduction

One of the main contributions in polymer physics over the last twenty years has been the development of electronic devices consisting of conducting polymers(Contractor et al., 1994; Heywang & Jonas, 1992; Kaneto, Kaneko, Min, & MacDiarmid, 1995; Kraft, Grimsdale, & Holmes, 1998; Roman, Andersson, Yohannes, & Ingañas, 1997; Schmidt, Tegtmeier, & Heitbaum, 1995; Wessling, 1994). This work has led to: the thin film deposition and microstructuring of conducting materials(Heywang & Jonas, 1992); materials for energy technologies(Roman, et al., 1997); electroluminescent and electrochromic devices(Kraft, et al., 1998); membranes and ion exchangers(Schmidt, et al., 1995); corrosion protection(Wessling, 1994); sensors(Contractor, et al., 1994) and artificial muscles(Kaneto, et al., 1995). Electron conductive polymers, which are the result of extended π -conjugation along the polymer backbone, fall into the class of conductive materials exhibiting semi-conducting behaviour. The discovery of polymer light emitting diodes(Burroughes et al., 1990), in particular, has brought considerable attention to the efficacy and lifetime of semiconducting polymer-based electronic devices. The magnitude of the electrical resistivity, or conductivity, determines the application field of the device and these polymeric optoelectronic devices can be classified in a number of different categories including: antistatic applications with a range of 10^{-14} - 10^{-9} S cm^{-1} ; electrostatic dissipation applications with a range of 10^{-9} - 10^{-5} S cm^{-1} ; and semiconducting applications with a range of 10^{-6} - 10^0 S cm^{-1} (Margolis, 1989). By controlling the range of the conductivity, the development of devices such as polymeric photovoltaic devices(Halls et al., 1995), polymer-based lasers(Tessler, Denton, & Friend, 1996), and transistors(Garnier, Hajlaoui, Yassar, & Srivastava, 1994) have received considerable attention recently.

Some of the principal approaches used in the preparation of polymeric conductive devices are the fabrication of ultrathin films by various strategies such as the Langmuir-Blodgett (LB)

technique(Zasadzinski, et al., 1994) and the self-assembled monolayer (SAM) method(Maoz, Frydman, Cohen, & Sagiv, 2000). As well, layer-by-layer(LbL) assembly allows for a high degree of control of material properties and architecture at the nanometer scale(Hammond, 2004; Love, Estroff, Kriebel, Nuzzo, & Whitesides, 2005). In less than 20 years since the introduction of the LbL technique(Decher, et al., 1992a), the electrochemical study of LbL films has grown from theory to functional devices, but, in most cases, thin films of conductive polymer are applied on 2D surfaces. One of the main requirements in this field is to further expand the range and potential of 3D conductive polymeric devices.

In an A/B heterophasic polymer blend, a low concentration of phase A forms droplets in a matrix of phase B. As the concentration is gradually increased the percolation point is reached and the continuity of phase A also increases. Near the phase inversion region a co-continuous morphology is observed(Paul & Barlow, 1980a). A co-continuous morphology is defined as a state where each phase is completely continuous throughout the material. The co-continuous phase structure consists of two fully-interconnected phases which mutually interpenetrate each other(Bourry & Favis, 1998b). The percolation threshold is defined as the formation of long-range connectivity in random systems. Mono-disperse solid droplets typically demonstrate a percolation threshold at values of 0.16 by assuming that the occupation of a site or bond is completely random. A topic of significant interest in heterophasic polymer blends has been to examine the various factors which resulting in significant reductions in the percolation threshold concentration(Gubbels, et al., 1994; Wang & Rubner, 2002). One of the most interesting approaches towards low percolation thresholds is the development of double percolated structures(Levon, et al., 2002; Sumita, et al., 1992). Zhang et al.(Zhang, et al., 2007) reported on a thermodynamically driven double percolated morphology in an HDPE/PS/PMMA blend which was essentially a fully continuous system, PS, encapsulating an already continuous system, PMMA. This type of structure allowed the percolation threshold for the encapsulating polymer to be reduced to well below 3%. This work demonstrated the potential of layering one phase onto another continuous structure as a powerful technique to reducing percolation thresholds.

In a ternary liquid system complete wetting can be described when one phase tends to spontaneously spread on the second phase in the matrix of third phase. For this purpose, Torza and Mason(Torza & Mason, 1970) and then Hobbs et al.(Hobbs, et al., 1988) employed modified Harkins spreading coefficients (λ_{ij}) which is a simple and useful mathematical expression and

thermodynamic explanation to predict the wetting characteristic(phase morphology) of ternary systems.

Equation 5-1
$$\lambda_{ij} = \gamma_{jk} - \gamma_{ik} - \gamma_{ij}$$

λ_{ij} is defined as the spreading coefficient giving the tendency of component (i) to encapsulate or spread onto component (j) in the matrix of component (k). It can also physically be defined as the transition between the non-wet and wet states. γ_{ij} , γ_{ik} and γ_{jk} are the interfacial tensions of the different polymer pairs. A positive value for the spreading coefficient, such as λ_{ij} , determines that phase (i) spreads over phase (j) while negative values for all possible spreading coefficients indicates separately dispersed phases in a continuous matrix.

In co-continuous polymer blends, the solvent extraction of one phase is a route towards porous materials with a fully interconnected porosity. A number of studies have shown that the phase size of co-continuous structures can be closely controlled from about 100 nm to hundreds of microns. The interfacial tension and an annealing step are critical parameters in this regard. One of the most important ways to coarsen, or increase, the phase size of a co-continuous network is melt annealing(Yuan, 2005). It has been shown that the annealing of a PS/PE system could increase the phase size from 0.9 to 72 μm (Sarazin & Favis, 2003). Yuan et al(Yuan, 2005) observed a linear time dependence for the coarsening of immiscible co-continuous blends and proposed a capillary pressure effect as the driving force of the coarsening process during static annealing. Clearly, highly controlled co-continuous morphologies can be converted into highly controlled porous materials through the selective extraction of one of the phases.

The layer-by-layer deposition technique to produce a polyelectrolyte multilayer on the surface of a flat substrate was proposed by Decher et al.(Decher & Hong, 1991b) In the LbL approach, the adsorption process involves consecutive and alternate deposition of positively and negatively charged polyelectrolytes driven by electrostatic forces followed by a rinsing step with water. A number of factors can influence mass deposition by LbL such as: ionic strength(Clark, Montague, & Hammond, 1997), pH of solution(Shiratori & Rubner, 2000), molecular weight of polyelectrolyte(Sui, Salloum, & Schlenoff, 2003), concentration of polyelectrolytes(Ferreira &

Rubner, 1995), and charge density(Schoeler, Kumaraswamy, & Caruso, 2002). Repetitive deposition steps provide a precise control over the total thickness of the layers in the range from a few angstroms up to a few micrometers. The thickness increment after each deposition is referred to as a growth rate which is dictated by polyelectrolyte geometry, surface charges, and solution parameters(Decher, 1997). Some of the most widely used polyelectrolytes are sodium poly(styrene sulfonate), poly(diallyldimethyl-ammonium) chloride, poly(ethyleneimine), poly(allylamine), poly(vinyl sulfate), and poly(acrylic acid). Recent advances in LBL techniques, in the non-conductive area, have demonstrated the possibility of templating multilayers onto 3D scale substrates. Caruso et al. (Caruso, Caruso, & Mohwald, 1998) deposited LBL films onto a colloidal core. Subsequent removal of the core resulted in a thin-film shell. Roy et al. (Roy, et al., 2006) deposited LBL films onto a fully interconnected porous PLLA surface and the subsequent removal of PLLA resulted in a 3D object comprised of a vast nanosheath network of, high surface area and the highest void volume ever reported for a polymeric substrate.

Rubner et al, (Cheung, et al., 1997; Fou & Rubner, 2002) were the first to apply the LbL technique in the field of electronically conductive polymers to construct PSS/PANI bilayers onto thin films in order to prepare a conductive device. Important advances have been made in this area by employing various conjugated polymers such as polyaniline and polypyrrole(Kim et al., 2002; Liang, Cabarcos, Allara, & Wang, 2004; Ram, Salerno, Adami, Faraci, & Nicolini, 1999). Ferreira et al.(Ferreira, et al., 1994) found that the solubility of PANI in an organic media such as dimethylacetamide(DMA) is much higher than that in water. A solution of doped polyaniline generally makes it more difficult to achieve the spontaneous adsorption of polyaniline chains onto a variety hydrophilic and hydrophobic surfaces(Cheung, et al., 1997). The presence of salt in the solutions has a subtle effect. Generally, it screens the monomer-monomer repulsive interactions, leading to enhancement of adsorption(Dautzenberg et al., 1994). Salt can play different roles in polyelectrolyte multilayer(PEM) formation and function, such as controlling the thickness increment of polyelectrolytes, the permeability(Harris & Bruening, 2000), and the stability(Dubas & Schlenoff, 2001b) of the multilayer. Most of the work published so far has revealed an increase in conductivity with an increase of the number of adsorbed PSS/PANI bilayers by measurement of electrical conductivity of LbL films deposited on a flat surface(Braga, et al., 2008; Paloheimo, et al., 1995). In most cases conductivity measured by

four-point probe increases continuously with addition of layers until a saturation plateau is reached around the 13th bilayer or 25th layer.

The principal objective of this work is to prepare a novel 3D porous polymeric conductive device, prepared via the LbL deposition of a conductive polyelectrolyte onto a 3D substrate of fully interconnected porosity generated from a co-continuous polymer blend. The work will involve the preparation of the blends and control of the phase size. Annealing of the co-continuous structure, followed by extraction of the porogen phases will be examined with a view to generating an ultra-low surface area, yet fully interconnected, porous material. Layer-by-layer adsorption of PSS/PANI onto the internal surface of the porous device will be carried out and details such as the growth rate and rate of adsorption and desorption of the polyelectrolytes will be examined. Finally the conductivity will be measured in order to examine the potential of the developed devices.

5.3 Experimental Methods

5.3.1 Materials

Commercial homopolymers were used in this study to prepare the conductive substrate. Poly(methyl-methacrylate) powder of $M_w=12000$ was obtained from Aldrich. High-density polyethylene, HDPE with a molecular weight of $M_w=79000$ was obtained from Petromont and polystyrene, PS with $M_w=290000$ was purchased from Dow Chemical. Polyvinylidene fluoride was obtained from Arkema. The polyelectrolytes used were polyaniline with $M_w=20000$ supplied by Aldrich as a polycation and poly(sodium 4-styrenesulfonate), $M_w=70000$ purchased from Sigma-Aldrich as polyanion. Densities in the melt states were determined via a fully automated PVT(pressure-volume-temperature) equipment supplied by Thermoelectron. Volume variation at controlled temperatures and pressures were determined. Some of the characteristic properties of the homopolymers are reported in Table 5-1.

Table 5-1. Characteristic Properties of Homopolymers

Material	Mw * 10 ⁻³ (g/mol)	Melt Index (g/10min)	$\eta^* \times 10^{-3}$ at 25 rad s ⁻¹ at 190°C (Pa.s)	Density (g/cm ³) at 20 °C	Density (g/cm ³) at 200 °C
Poly(methyl methacrylate)	12	-	0.04 ^a	1.19	1
Polystyrene	290	-	1.5	1.04	0.97
High density Polyethylene	79	8.1	0.72	0.98	0.85
Polyaniline	20	-	-	-	-
Poly(sodium 4-styrenesulfonate)	70	-	-	1.158	-
Polyvinyl difluoride	-	1.5	1.4 ^b	1.77	1.6

^a reported by Reignier et al.(Reignier & Favis, 2000)

^b zero shear viscosity of PVDF is 902,000 Pa.s at 190°C as calculated by the Carreau-Yasuda model

Epofix resin containing 80-100% of Bisphenol-A-diglycidylether with a viscosity of 50cP at 20°C and Epofix hardener containing triethylenetetramine supplied by Struers company were employed to fill the pores of the template after LbL deposition. Sodium chloride 99.5% was purchased from Fluka. Ultrapure water with a resistivity of 18.2MΩ.cm was used in all experiments and was obtained from a Milli-Q plus system Millipore Biocel. For filtration of the PANI solution, glass fiber filters were purchased from millipore with a diameter size of 47mm.

5.3.2 Rheological Analysis

A constant stress rheometer (SR 5000, Rheometric Scientific) equipped with a 25 mm parallel disk geometry was utilized to measure the linear viscoelastic properties of homopolymers containing 0.2% antioxidant. Measurements were carried out using a parallel-plate geometry with a gap of about 1.2 mm. The experiments were carried out under a nitrogen atmosphere at a temperature of 190°C over a frequency range from 0.005 to 79.5 rad s⁻¹. The disc shaped samples

in the rheology tests were compression moulded at 190°C. In order to determine the linear viscoelastic region, a stress sweep test was performed. The Carreau-Yasuda model (Yasuda, et al., 1981) was employed to determine the zero shear viscosity of PVDF.

5.3.3 Substrate Preparation

Multi-component blends were prepared via melt-blending under a flow of dry nitrogen in a 30mL Plasti-Corder internal mixer (Brabender) operating at 200°C and 50 rpm. The maximum shear rate at this speed is close to 25 s⁻¹. The real temperature achieved by the end of mixing experiment was approximately 185°C. After converting the mass to volume (densities presented in Table 5-1), the mixing chamber was filled to 70% of its total volume. All the blends in this study were mixed for 8 min which is more than sufficient to allow the torque to achieve a constant value. Irganox antioxidant, supplied by CIBA, was added to the mixture at a level of 0.2 wt% to reduce the thermal oxidation of the components. After mixing, the samples were immediately cut from the mass and quenched in a cold water bath to freeze-in the morphology. All concentrations have been reported based on the component volume fraction shown in Table 5-2.

Table 5-2. Composition of Polymer Components in Ternary and Quaternary Blends

Samples	HDPE	PS	PMMA	PVDF
A	33.3%	33.3%	0	33.3%
B	33.3%	0	33.3%	33.3%
C	40%	30%	10%	20%
D	40%	10%	40%	10%

5.3.4 Annealing Test

For the annealing experiments a compression molding press was employed. Small pieces of samples were cut from the blend and then sandwiched between two metal plates in a disc-shaped mould. The temperature of both upper and lower plates was set at 200°C. The annealing was carried out under nitrogen in five steps. As a first step, both heating plates of the compression press were brought into contact with the sample pieces without imposing any pressure for 5 minutes, in order to minimize any deformation or flow of the sample. After heating and melting the samples, pressure was applied for 15 minutes. After annealing, the samples were cooled by placing the samples in a large cold press for 3 minutes.

5.3.5 Solvent Extraction

Solvent extraction was used to extract various components and generate porosity in the substrate. Selective solvent extraction also allows for the determination of the % continuity of the different components in the blend system using Equation 5-2. The volume of the components before and after extraction is measured by weighing the sample and converting the weight to volume. As a primary advantage, solvent extraction is an absolute measurement of continuity.

Equation 5-2

$$\%Cocontinuity = \frac{\sum_n V_{initial} - \sum_n V_{final}}{\sum_n V_{initial}}$$

A homogenous blend is assumed when carrying out the selective solvent extraction of the PMMA, PS, and PVDF phases in dimethylformamide(DMF). Volume loss measurements were carried out for one week at room temperature and were used to calculate the extent of continuity of the PMMA, PS, and PVDF phases altogether. $V_{initial}$ and V_{final} are the volume of one component or several components present in the sample before and after extraction calculated by weighing the sample and converting it to the volume. The % continuity represents the fraction of a phase that is continuous.

5.3.6 Layer-by-Layer Deposition

The solid substrate was alternatively immersed for 25min in PSS and PANI solutions with intermediate water rinsing. An aqueous PSS solution of 10 mg/mL buffered to a pH of 2.5 was used as the negative polyelectrolyte solution. The PANI solution was prepared using a procedure by Cheung et al.(Cheung, et al., 1997). A water bath with a pH adjusted to 2.5 was used to remove excess PSS and PANI on the surface of substrate after each dipping. The process was periodically interrupted and samples were dried first under a gentle flow air and then by putting samples in the vacuum oven for 30min prior to weighing.

5.3.7 Filling the Porous Sample with a Resin

A two-component epoxy(Epofix) was used to impregnate the pores of the porous substrates. Epofix resin and Epofix hardener were mixed and stirred carefully for at least 2 minutes by maintaining a mixing ratio of 15 to 2 parts by volume. The mixture was carefully poured into the mould. To eliminate air bubbling during the hardening, the Epovac vacuum impregnation unit was operated for 24h. After evacuating the specimen chamber, the impregnating fluid is then introduced into the chamber under atmospheric pressure by means of a disposable plastic tube.

5.3.8 Characterization and Phase Morphology

5.3.8.1 Microtomy and Scanning Electron Microscopy

Samples were cut and microtomed using a Leica-Jung RM 2065 equipped with a glass knife and a cryochamber type (LN 21). Other samples were fractured under liquid nitrogen known as cryofracture method. After chemical extraction with dimethylformamide to remove all components except HDPE, a JEOL JSM 840 scanning electron microscope was employed to observe the morphology of the samples. Photomicrographs were taken at a range of 5-12keV after coating the surface of the sample with a gold/palladium alloy by plasma deposition.

5.3.8.2 Focused Ion Beam and Atomic Force Microscopy

Cryomicrotoming of the specimens using a glass knife was carried out in order to obtain a perfectly flat surface for subsequent morphology observation. The samples were coated with a gold-palladium alloy. The surface of the samples was then treated and etched using a Hitachi focused ion beam FIB-2000A operated at 30 keV gallium beam. Further details of the FIB preparation are given in Virgilio et al.(Virgilio, et al., 2005a).

Finally, the topography of the sample surface was analyzed by tapping mode AFM using a Dimension 3100 scanning probe microscope equipped with a Nanoscope IIIa control module.

5.3.8.3 Conductivity Measurements

DC electrical measurements were performed through the vertical thickness of the substrate at ambient temperature using a Keithley electrometer model 6517 working at a voltage range of 0-1000V and ammeter range of 0-20mA. In-house software was used to convert the data to conductance. In order to standardize the pressure for all samples, a 5 lb and 10 lb load was applied on the sample holders. Cylindrical specimens with a thickness of 1mm and a radius of 1.25cm were compression moulded and then electrical tests were performed under dry air. Although the top and bottom surfaces of the samples are flat, good contact of the sample surface and electrodes was further ensured by using two graphite sheets which covered the surfaces of the samples.

5.4 Results and Discussion

5.4.1 Multiple-Percolated Morphology with Large Continuous Domain Phases

Since one of the principal objectives of this work is to determine the lowest possible percolation threshold for PANI in a 3D porous polymer conducting device (PPCD), it was necessary to first

prepare a polymer blend structure with large fully interconnected phases. Subsequent extraction of selected phases within that blend would thus allow for the preparation of a very low surface area, fully interconnected, porous polymer substrate (Figure 5-1). As will be shown below, the most effective route towards this is via the preparation of a multi-percolated, multi-component polymer blend.

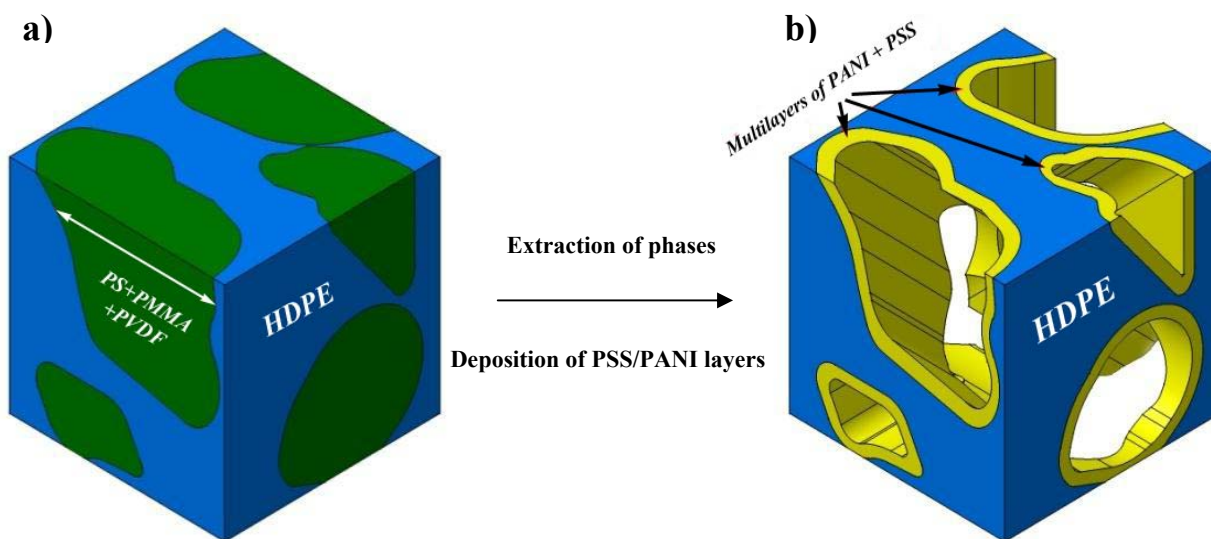


Figure 5-1. 3D schematic showing the approach used to prepare the porous polymeric conducting device via LbL deposition. (a) solid multi-percolated structure comprised of HDPE, PS, PMMA and PVDF after melt blending and annealing; (b) porous polymeric conducting device after extraction of PS, PMMA and PVDF, followed by LbL deposition of PSS and PANI.

Recently (J. Zhang, et al., 2007), it has been shown that a ternary co-continuous (double percolated) morphology could be developed in which hierarchically ordered phases of HDPE/PS/PMMA were generated with all phases fully continuous. It was shown that this phenomenon was governed by the Harkins equation and is a thermodynamically driven process. A positive spreading coefficient of PS over PMMA ($\lambda_{PS/PMMA}$) results in the PS phase locating at the intersection of the HDPE and PMMA phases (Guo, Packirisamy, et al., 1997; Reignier & Favis, 2000). Figure 5-2a illustrates this case where in a 40/20/40 HDPE/PS/PMMA blend, PMMA phase is encapsulated by PS phase in the matrix of HDPE. By controlling the concentration of the phases, a region is determined in which all phases are fully continuous. A 40/10/50 HDPE/PS/PMMA ternary blend is another example of this region where the

composition of PS was controlled to generate a PS shell down to a few hundred *nm* between two continuous PS and PMMA structures (Figure 5-2b). Subsequently, the PS and PMMA phases can be extracted, yielding a fully interconnected porous HDPE substrate of about 60% void volume. This method can be employed to prepare substrates with higher void volume. For instance, in the 40/10/50 HDPE/PS/PMMA ternary blends if one could obtain a selective solvent for HDPE, the combined removal of HDPE and PMMA would yield a highly porous PS substrate of about 90% void volume.

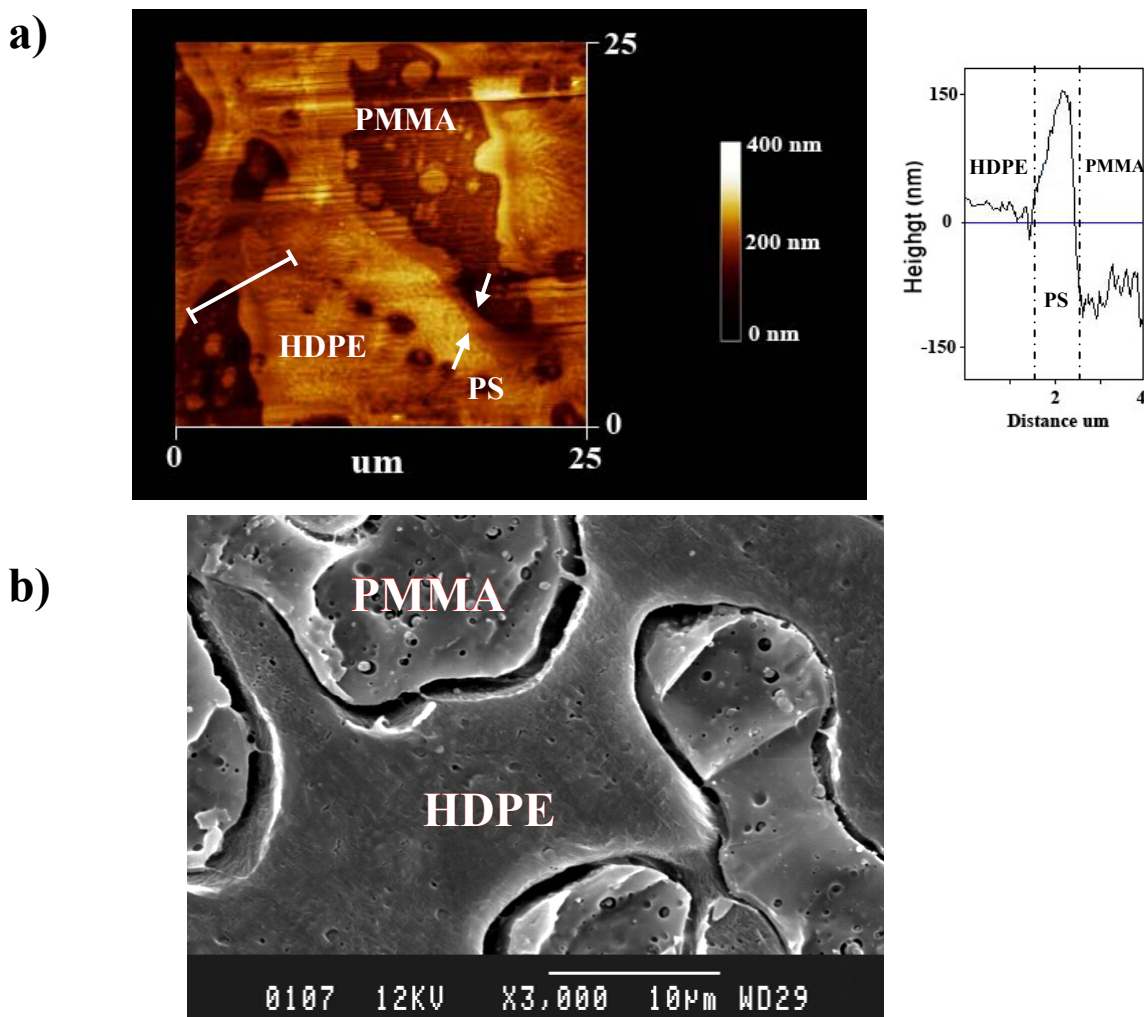


Figure 5-2. (a) FIB-AFM topographic surface image of 40/20/40 HDPE/PS/PMMA. The topographical height vs distance is shown to the right. The white line in the image indicates the trace line used in the height vs distance analysis. and (b) Scanning electron micrograph of 40/10/50 HDPE/PS/PMMA after extraction of the PS phase by cyclohexane

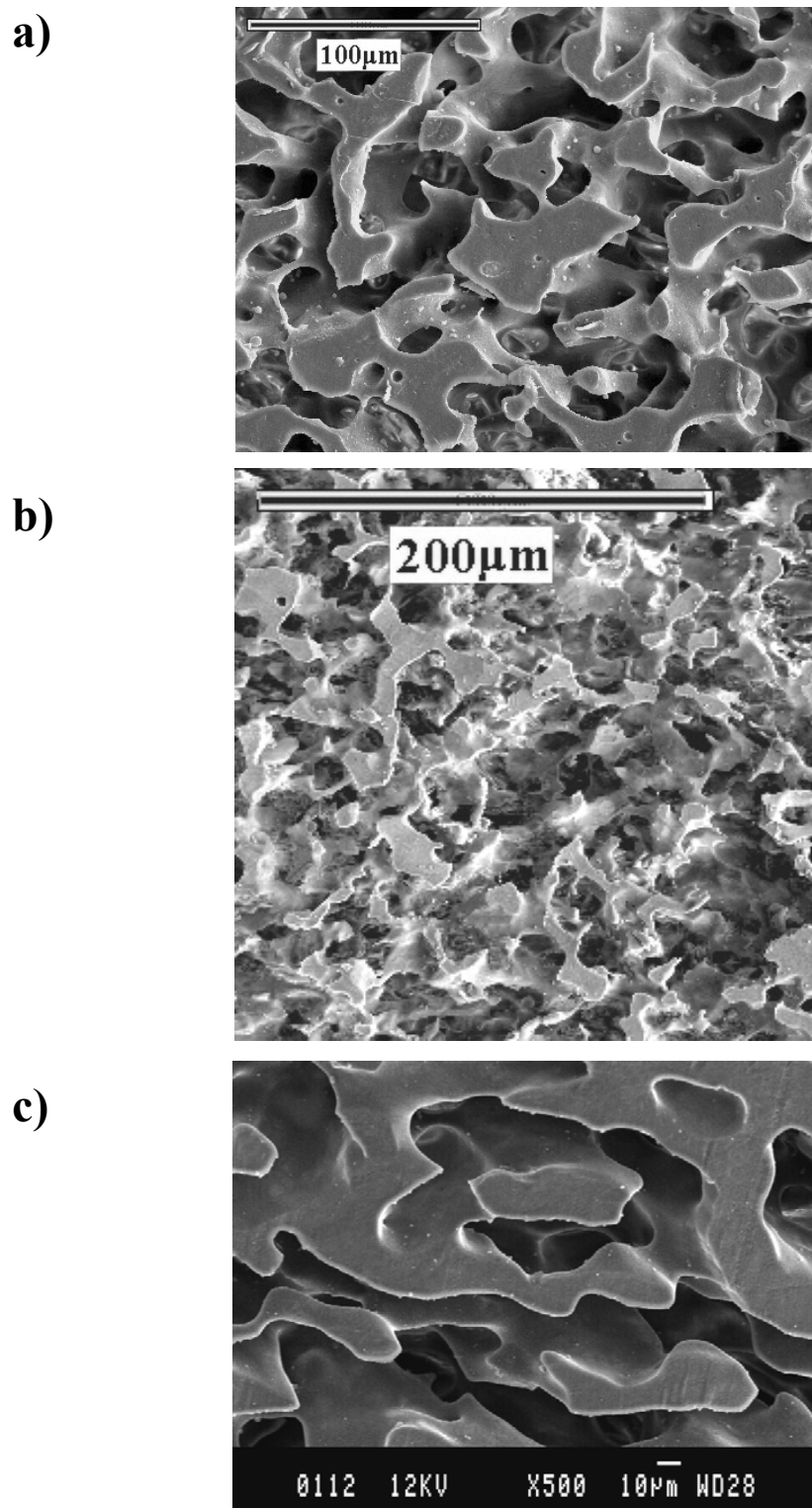


Figure 5-3. Scanning electron micrographs of binary and ternary samples after extraction of all phases (except polyethylene) by DMF for and (a) 33/33/33 HDPE/PMMA/PVDF, (b) 33/67 HDPE/PVDF, and (c) 50/50 HDPE/PVDF

Figure 5-3 illustrates a comparison between binary co-continuous structures (single percolated) and a ternary one (double percolated) and shows that continuous phases can be generated at lower concentrations of each phase in the latter case due to the lower percolation threshold of those phases.

In Figure 5-3a, it is shown that a double percolated HDPE/PMMA/PVDF blend, after PMMA and PVDF extraction, can result in a porous substrate of 33% HDPE which demonstrates a homogeneous, perfectly interconnected structure while a binary blend of 33% HDPE and 67% PVDF yields an imperfect continuous structure of HDPE (Figure 5-3b). Extraction experiments indicate that 98% of the PMMA and PVDF were extracted in the ternary blend proving their high levels of continuity. In the case of the 33%HDPE/67%PVDF binary blend, extraction of PVDF resulted in a value of 108% of material indicating a significant quantity of HDPE present as dispersed entities within the PVDF. The fully continuous binary 50% HDPE/50% PVDF blend is also shown for comparison (Figure 5-3c). Clearly, a double-percolated morphology is a route towards fully continuous phases at low phase concentrations. The subsequent extraction of PMMA and PVDF leaves behind a fully interconnected porous HDPE substrate of low surface area. In this work, as HDPE substrates were exposed to polyelectrolyte solutions, extra-large pores also facilitated the penetration of the solution inward to the interconnected porous area.

The addition of a fourth component to form a quaternary blend with a triple-percolated morphology between adjacent phases is also possible providing that the spreading coefficients of the fourth phase and the engulfed phases satisfy Harkins equations. A more detailed study of the generation of such structures is presented in a separate paper(Ravati & Favis, 2010). A triple-percolated morphology is particularly interesting in the present work since it provides a route towards the generation of porous channels of highly uniform size distribution. Figure 5-4 demonstrates such a structure in which PMMA situates at the interface of PS and PVDF in an HDPE matrix. Thus this triple-percolated morphology follows the order HDPE/PS/PMMA/PVDF (Figures 5-4a and 5-4b). Figures 5-4a and 5-4b represent quaternary blends with the PMMA phase extracted, yielding PS layers engulfed in an HDPE matrix while the PVDF phase remains at the core encapsulated by extracted PMMA. The removal of the PS phase separates HDPE/PS/PMMA/PVDF into two parts: the HDPE matrix and PMMA/PVDF core (Figure 5-4c). These figures unambiguously show that the PS and PMMA phases are situated between HDPE and PVDF, and a hierarchical structure of four different phases is

spontaneously self-assembled. After the removal of all other phases, the final HDPE porous substrate exhibits a continuous structure with large pore sizes and macro-channels of highly uniform distribution. The uniformity of the double-percolated morphology represented in Figure 5-3a and that of the triple-percolated one shown in Figure 5-4d are compared morphologically. The reason for the more uniform structure in the triple-percolated system is the phases are distributed between three interfaces as opposed to be distributed between two interfaces in the double-percolated system. Thus, the triple-percolated structure system appears to form phases which, after extraction, result in a substrate with a more uniform pore size distribution.

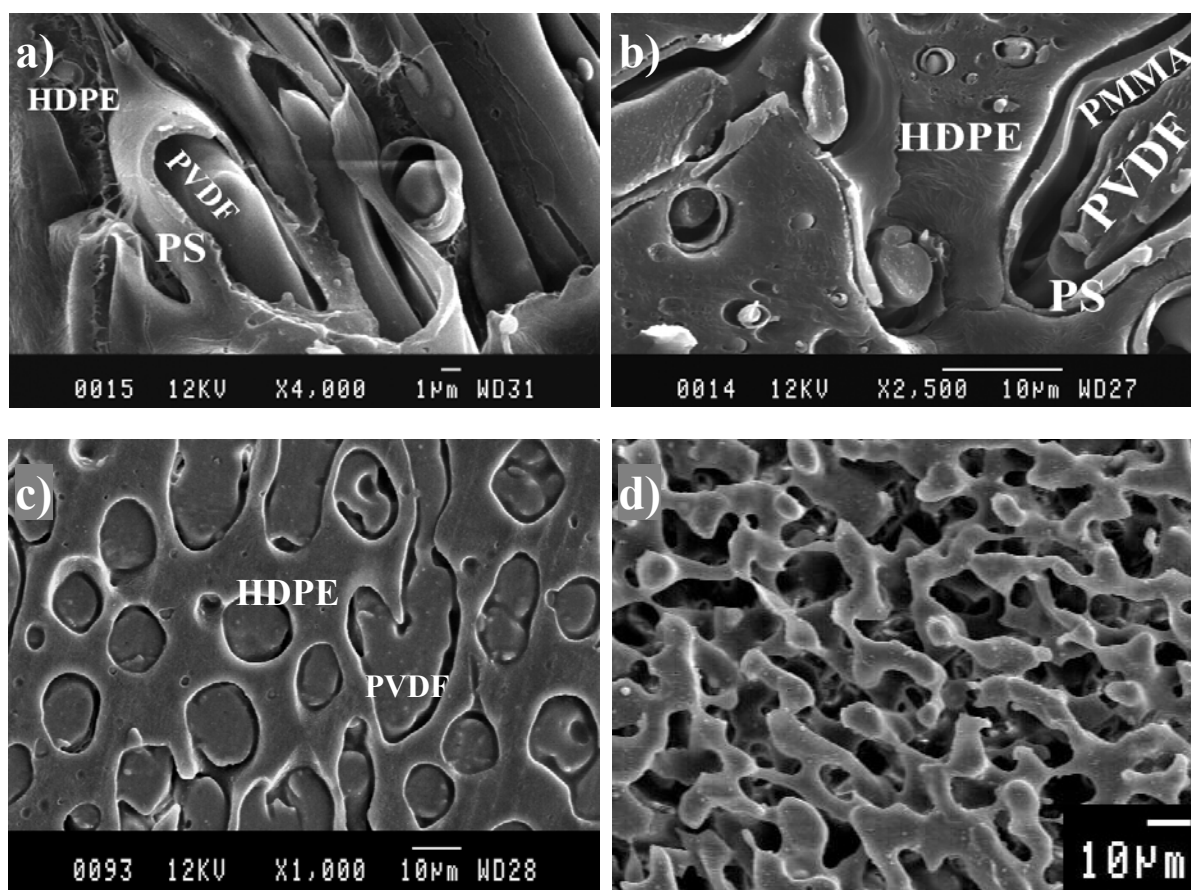


Figure 5-4. Scanning electron micrographs of quaternary polymer blends for various compositions compounded via melt-blending (a) 50/16/16/16 HDPE/PS/PMMA/PVDF after extraction of PMMA by acetic acid, (b) 50/20/10/20 HDPE/PS/PMMA/PVDF after extraction of PMMA by acetic acid, (b) 50/20/10/20 HDPE/PS/PMMA/PVDF after extraction of PS by cyclohexane, and d) 40/10/40/10 HDPE/PS/PMMA/PVDF after extraction of all phases except HDPE

Four samples based on the ternary and quaternary systems of HDPE, PS, PMMA and PVDF will be the principal substrates used in subsequent experiments reported in this paper. These blends are shown in Table 5-2 and are designated as samples A-33%HDPE/33%PS/33%PVDF; B-33%HDPE/33%PMMA/33%PVDF; C-33%HDPE/30%PS/10%PMMA/20%PVDF; and D-33%HDPE/10%PS/40%PMMA/10%PVDF. It is possible to generate porous substrates of an even higher void volume (lower concentration of HDPE), however the mechanical strength of those materials is quite low. Since the study of the effect of load on the conductivity of the sample is also one of the objectives of this work, the above concentrations were selected. These blends effectively allows for the preparation of an ultra low surface area, fully interconnected porous substrate of high void volume.

5.4.2 Annealing the Samples in order to Increase Pore Size

It has been shown in previous work that annealing co-continuous polymer blends is an excellent route towards significantly increasing the phase size and further lowering phase surface area. During this process of static annealing, thin parts of the continuous network merge into larger parts via capillary driving forces(Zhenhua Yuan, 2005).

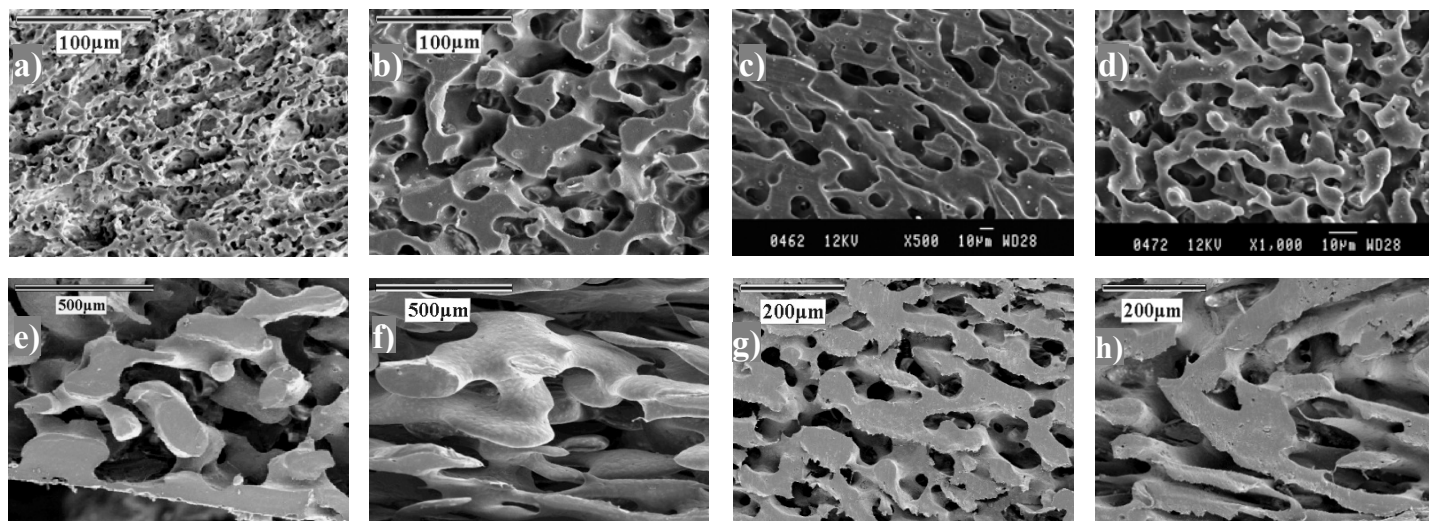


Figure 5-5. Scanning electron microscope images of the morphologies of the porous structures showing the influence of annealing. The top row is without annealing, the bottom row is after annealing. All components have been extracted except HDPE. a),e) Sample (A); b),f) Sample (B); c),g) Sample (C); and d),h) Sample (D).

Double percolated HDPE/PS/PVDF and HDPE/PMMA/PVDF blends and triple-percolated HDPE/PS/PMMA/PVDF were subjected to quiescent annealing for 15 minutes in a compression molding press at very low contact pressures. This operation results in a substantial increase in the average phase size. Figure 5-5 shows the morphology of the blends after annealing and subsequent extraction of all phases except for HDPE. The phase size increase is dramatic and is shown for sample B to increase from approximately 40µm to 500µm as exhibited morphologically in Figures 5-5b and 5-5c. The phase increase before and after annealing for the other samples A, C, and D is also substantial and ranges from 5 to 15 times (Figure 5-5). The results indicate that the coalescence of a multi-percolated system occurs much faster than coalescence in a binary blend. Yuan et al. (Zhenhua Yuan, 2005) reported that, in the best case scenario, a binary blend requires approximately 40 minutes to coarsen from several microns to a phase size of about 160 microns. Consequently, the required annealing time to achieve 400-500 microns is estimated at about two hours of annealing. It is proposed that geometrical restrictions in a multi-percolated system enormously accelerate coalescence effects while still maintaining full continuity of all components.

5.4.3 Continuity and Surface Areas of Substrates

Table 5-3 shows gravimetric data obtained after solvent extraction and demonstrates that in all cases the various phases within the HDPE are fully continuous. The continuity of all extracted phases for both annealed and unannealed samples is higher than 96%. Hence, the 33% volume fraction of HDPE in samples A and B and 40% in samples C and D results in a 67% and 60% void volume respectively after the extraction of all other phases. As well, the effect of annealing on reducing the surface area of the porous substrate is extremely evident as it was below the range which could be measured quantitatively by BET (Table 5-4).

Table 5-3. Continuity of the Porous Morphology With and Without annealing (PS, PMMA and PVDF extracted).

Sample	Continuity of (PS+PMMA+PVDF) no annealing	Continuity of (PS+PMMA+PVDF) with annealing
A	96.6 %	98.3 %
B	98 %	100 %
C	98.3 %	99.3 %
D	96 %	97.4 %

Table 5-4. Surface Area Measurements of Porous Polymer Substrates by BET

Sample	Surface area measured by BET(m ² /g) no annealing	Surface area measured by BET(m ² /g) with annealing
A	1.28	< 0.01
B	0.70	< 0.01
C	0.88	< 0.01
D	0.74	< 0.01

Since the ultra-low surface area values are beyond the range of the BET equipment, the surface area of sample A (morphology shown in Figure 5-5e) was estimated arithmetically. A porous disc-shape sample with a diameter of 2.5-cm and a length of 1-mm is assumed to be comprised of numerous parallel cylinders from top to bottom with a diameter of 175- μm and a length of 1- mm . The diameter of cylinders is obtained from average diameter of HDPE cylindrical rods exhibited in Figure 5-5e. Estimating the number of cylinders and the surface area per cylinder as 6818 and $0.00375\text{m}^2/\text{g}$, respectively, corresponds to a surface area of the porous device of approximately $0.01\text{m}^2/\text{g}$.

Hence, the work to this point has achieved fully interconnected porous substrates (samples A, B, C, and D) of ultra-low surface area (large pores) and a highly uniform pore size. All these samples will be used as substrates for the layer-by-layer deposition of polyaniline in the subsequent parts of this work. Table 5-5 compares the surface area of porous sample A to the surface area of other co-continuous systems and demonstrates that, to our knowledge, this is the lowest surface area, fully interconnected porous polymer material ever presented in the literature. Table 5 also demonstrates the potential of preparing conductive devices from higher surface area co-continuous systems and underlines the versatility of the approach.

Table 5-5. Comparison of Surface Areas Reported in Previous Studies and in the Current Work (last two rows).

porous samples prepared by melt-blending from this laboratory	reported specific surface area measured by BET(m ² /g)
50/50 PLLA/PCL after LbL deposition of PSS/PDADMAC and extraction of both phases(Roy, et al., 2006)	140
50/50 PLLA/PCL after 2h annealing and after LbL deposition of PSS/PDADMAC and extraction of both phases(Roy, et al., 2006)	63
40/60 HDPE/SEB (styrene-ethylene-butylene diblock copolymer)(Jianming Li, et al., 2002)	16
50/50 HDPE/SEB (styrene-ethylene-butylene diblock copolymer)(Jianming Li, et al., 2002)	13.15
50/50 HDPE/SEBS(styrene-ethylene-butylene-styrene triblock copolymer)(J. Li & Favis, 2001a)	8.2
40/60 HDPE/PS after extraction of PS(J. Li & Favis, 2001a)	0.82
33/33/33 HDPE/PMMA/PVDF after extraction of PMMA and PVDF	0.7
33/33/33 HDPE/PMMA/PVDF after 15min annealing and extraction of PMMA and PVDF	≤0.01

5.4.4 Layer-by-Layer Deposition of PSS/PANI

A layer-by-layer deposition technique was used to deposit PSS and PANI alternately on the internal surface of the prepared porous substrate (Figures 5-6a and 5-6b). A PSS polyelectrolyte soluble in water was selected to be deposited first due to its ability to adsorb strongly on hydrophobic surfaces such as HDPE(R. v. Klitzing, et al., 1999). In a subsequent step, a semi-flexible PANI layer is deposited on a PSS layer as a result of a balance between electrostatic repulsion of charged monomers. Up to thirty-eight PSS and PANI layers were deposited. In order to visually examine the multilayer assembly on the surface of the HDPE substrate, the void volumes or empty macro-channels were refilled with epoxy resin.

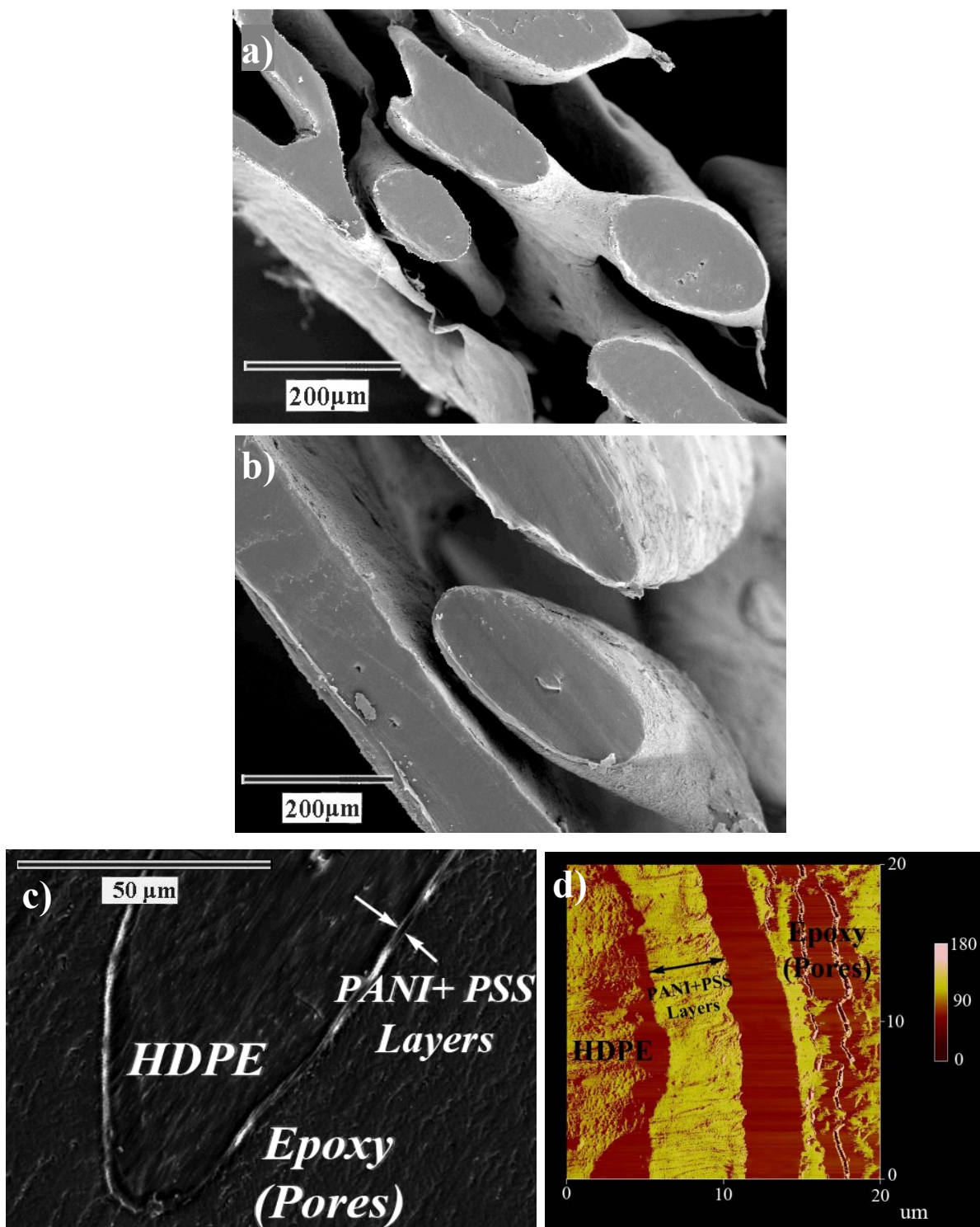


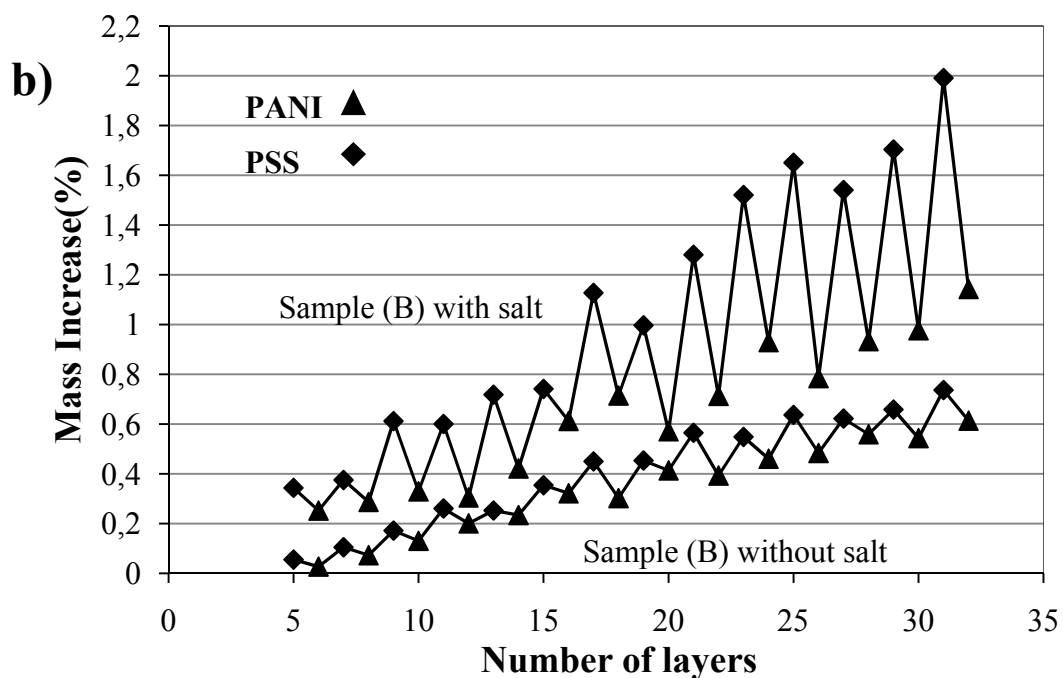
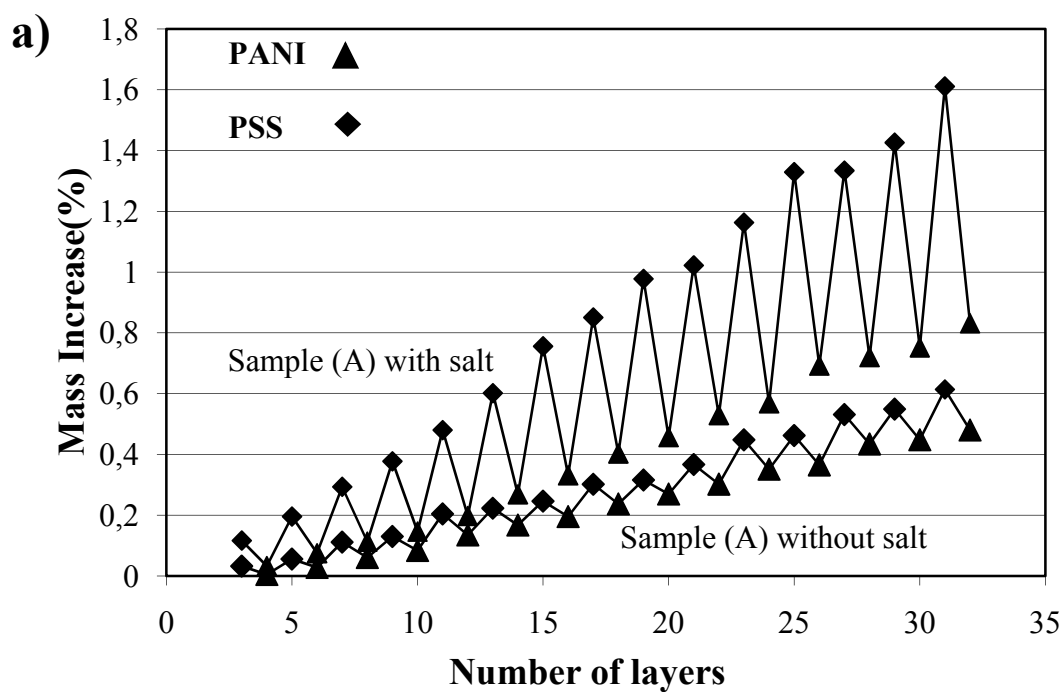
Figure 5-6. a),b) Scanning electron micrographs of the morphology of sample (B) after extraction of PMMA, PVDF and deposition of 38 PSS/PANI layers; c),d) SEM and FIB-AFM of sample(B) after extraction of PMMA, PVDF and deposition of 38 PSS/PANI layers. Pores are filled with epoxy resin.

Microstructural information collected by SEM (Figure 5-6c) and AFM (Figure 5-6d) depicts a relatively thick polyelectrolyte multilayer as wide as $5.5\mu\text{m}$ for 38 layers of PSS and PANI on the surface of the filled sample (B). Picart et al.(Picart, Lavalle, et al., 2001) also reported a very thick multilayer film of $1\mu\text{m}$ for 16 layers. They proposed that this thickness increase can be attributed to a diffusion of polyelectrolyte inwards and outwards in the multilayer during the LbL process. They also reported an exponential growth of layer thickness similar to the mechanism of mass growth in this work.

5.4.5 Mass Deposition Dynamics of PSS/PANI

Although the structural information for the construction of ultra-thin multi-layers is extremely difficult to obtain, gravimetric measurements can interpret the molecular topology of the films that play the most important role in the formation of multi-layers. Figure 5-7 shows the quantification of mass deposition of each layer as measured by gravimetric techniques for various substrates in both the absence and presence of salt. It shows an unusual oscillating behavior of thickness growth. After dipping the substrate in the PSS solution, the deposition mass increases, followed by a decrease in deposition mass in a PANI solution due to the partial removal of a previously adsorbed layer. Some previous works(Dubas & Schlenoff, 2001c; Schoeler, et al., 2002; Tjipto, Quinn, & Caruso, 2007) have also reported on the oscillating behavior of PSS polyelectrolytes due to the partial removal of previously adsorbed layers in subsequent operations. Schoeler et al.(Schoeler, et al., 2002) related the extent of removed material to the critical charge density of the polyelectrolyte. Charge density for a polyelectrolyte is defined as the fraction of monomers in the polymer which are charged. If this fraction is much smaller than 1, the polyelectrolyte is weakly charged. Normally, weak polyelectrolytes tend to demonstrate an oscillating deposition. Dubas et al.(Dubas & Schlenoff, 2001c) concluded that the drawing out of water molecules unassociated with specific ion pairs due to increasing external osmotic pressure is the main reason for the decrease in thickness at low salt concentrations. Tjipto et al.(Tjipto, et al., 2007) related the oscillating behavior of a multilayer formed of poly(4-styrenesulfonic acid-co-maleic acid) and PDADMAC to the heterogeneity and roughness of the samples. Later in this paper it will be shown that all of these explanations are likely responsible for the oscillating deposition observed in this work. The addition of 1 molar

salt to a PSS polyelectrolyte solution magnifies the extent of the oscillation behavior (Figures 5-7a-d) and this will also be discussed in more detail in the next section.



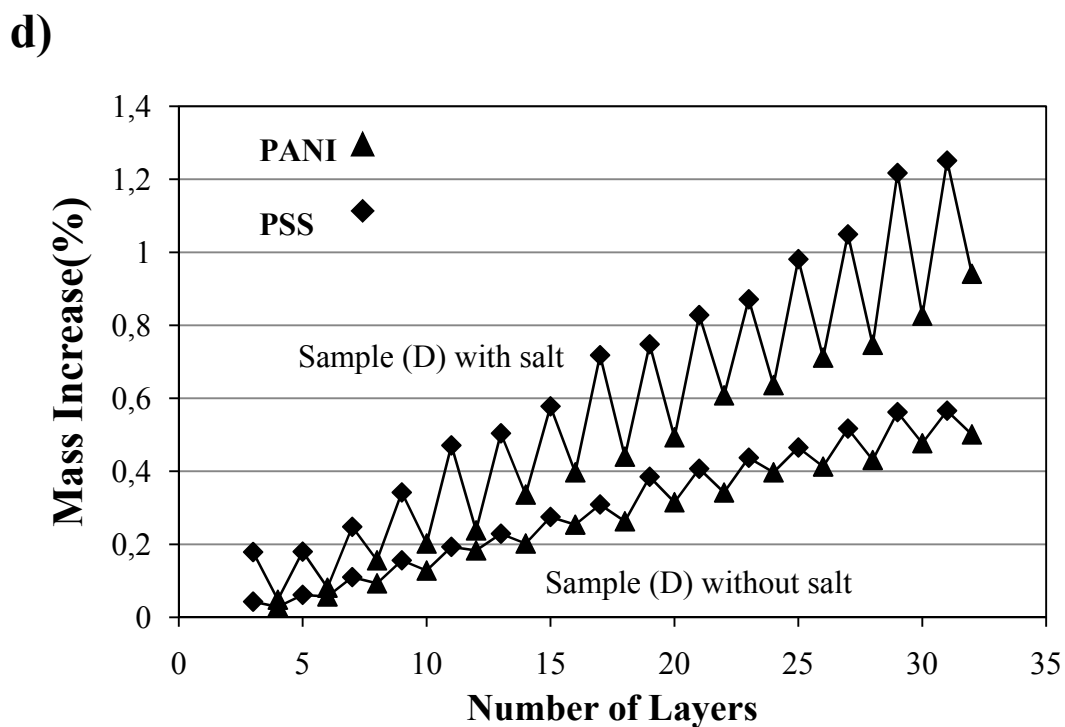
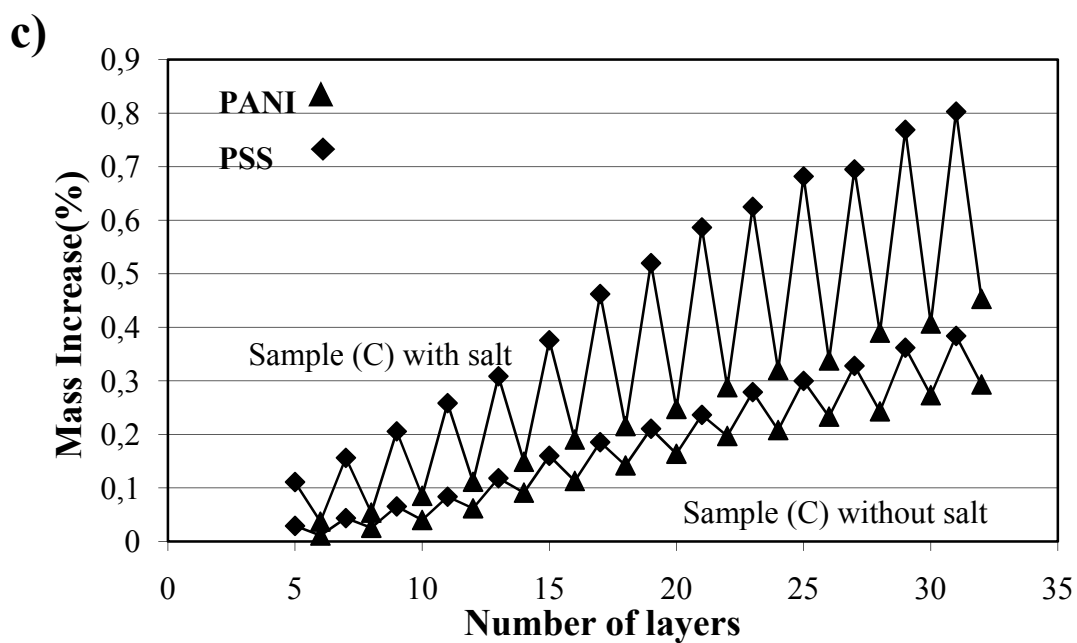


Figure 5-7. Mass increase (%) indicating cumulative deposited mass as a function of number of deposited PSS and PANI layers for solutions containing salt and without salt. a) sample(A); b) sample (B); c) sample(C); and d) sample (D).

A relationship between macropore sizes and mass deposition of layers is found. Approximate average macropore sizes for samples A, B, C and D after annealing are 300 μm , 500 μm , 100 μm , and 150 μm respectively (see Figure 5-5). Figure 5-7 represents the maximum mass deposition for each sample: sample A attains 1.6% after deposition of 31 PSS/PANI layers and 0.82% after deposition of 32 layers. Sample (B) attains 2% and 1.16% after deposition of 31 and 32 layers. Samples C and D attain about 0.8% for 31 layers and 0.5% for 32 layers. These results confirm that larger pore sizes facilitates the penetration of solution and thicker layers constructs

5.1.1. Diffuse Network Structure of PSS/PANI

Lavalle et al.(Lavalle, et al., 2002), using molecular labeling, observed a diffusion of a portion of polyelectrolytes in and out of the film in a nonlinear manner leading to exponential growth. This was observed when one of the polyelectrolytes used was weak as in the current work with PANI. Schlenoff et al.(Dubas & Schlenoff, 2001b; Schlenoff & Dubas, 2001) have reported that the surface charge, propagated and inverted by sequential adsorption steps, is overneutralized (overcompensated) at each step. In that work, the multilayer/solution interface, the charge of the last-added polymer compensates the previous one by a factor ϕ . The opposite polymer charges are in exact stoichiometric ratio for $\phi=1$ yielding a steady-state thickness increment vs layer number. The overcompensation factor, ϕ , can be defined for multilayers when the charge factor has a value higher than 1. Overcompensation leads to excess charge density from the last-added polyelectrolyte, but only at the surface is ϕ “unrestricted” by bulk effects. At increasing length, l , from the interface into the multilayer, the level of overcompensation decreases in an exponential fashion demonstrating an overcompensation gradient(Schlenoff & Dubas, 2001).

The diffusion of a portion of polyelectrolytes in and out of the film in a nonlinear manner leading to exponential growth was proposed as a model for overcompensation(Lavalle, et al., 2002). In this mechanism, the first population was constituted of chains directly interacting with the surface of the multilayer, which are responsible for linearly growing films. The second population was constituted of free chains that diffuse into the multilayer over its whole surface and are responsible for exponential growth. In this study, when a substrate is brought into contact with a charged PSS solution, many free PSS chains paired with hydrated counter-ions in the solution diffuse throughout the film in the x , y , and z directions due to electrostatic interactions.

Following this, the desorption or detachment of some layers is expected in an oppositely charged PANI solution when mobile chains diffuse out. As soon as they reach the surface, an additional reaction occurs between them and the oppositely charged chains available in the solution and an extra layer is formed. In this fashion, a diffuse network structure throughout the deposited thickness is observed in contrast to the formation of discrete polyelectrolyte layers in classic layer-by-layer deposition where strong polyelectrolytes are used.

Based on the above discussion, a schematic representation of film growth has been made to show the progressive formation of multilayers (Figure 5-8). This schematic contrasts with the classic formation of well-separated hierarchical alternating multilayers observed in most work using the LbL approach. In the current work, the oscillating deposition indicates that PSS and PANI polyelectrolytes diffuse into the previously deposited layers. Like chains make contact with other like chains and consequently, an inter-diffused network of PANI and PSS is generated. In a following section, it will be shown that an increase in the conductivity is observed as a function of the number of PSS and PANI layers and it further confirms the formation of a continuous network of PANI interdiffused with PSS. The degree of interconnection of this network becomes more pronounced as the number of deposited layers increases. As well, an increase in the number of deposited layers results in a rougher surface, leading to a further diffusion of free chains.



Figure 5-8. Schematic of exponential growth of PSS/PANI multilayer thickness on the internal surface of the substrate.

5.4.6 The Effect of Salt on the Mass Deposition Growth of PSS/PANI

Salt is generally added in procedures involving LbL deposition. In the absence of salt, charged PSS and PANI in the solution adopt a more expanded rigid, rod-like configuration due to coulomb repulsion (Ha & Thirumalai, 1995). The role of salt is to gradually screen the monomer-monomer repulsive interactions between PSS charges with counter-ions and also bring them

close together. It is interesting to note in Figure 5-7 that the addition of salt significantly increases the oscillation behavior of the mass growth dynamics.

This oscillation behavior can be explained as follows: the number of PSS molecules that diffuse throughout the multilayer and the total concentration of these free chains depend on the electrostatic interaction forces that arise from total overcompensation. Two important parameters influencing the extent of overcompensation are the concentration of added salt and the number of layers. Thus, extra overcompensation is caused by the presence of NaCl in the PSS solution (Klitzing & Moehwald, 1995). As well, the displacement of hydrated small salt counterions and charged polymer segments result in highly swollen polymers as attached water molecules are brought in (Dubas & Schlenoff, 2001c). Jaber et al. (Jaber & Schlenoff, 2007) showed that salt counter-ions can thermodynamically control up to 40% of the mass deposition of the multilayer construction due to this additional water content. Swelling and overcompensation occur simultaneously during the construction of the multilayer in the presence of salt (Dubas & Schlenoff, 2001b), which is involved in the dramatic mass increase of the multilayer.

In a subsequent dipping step in the PANI solution, the electrostatic interaction between the diffused hydrated PSS with PANI chains inside the solution play a major role in the diffusion of free PSS chains out of the multilayer. At this step, in the presence of salt, a significant decrease in mass deposition is detected which is proportional to the mass increase in the previous step (PSS adsorption) as compared to a slight decrease in mass in solutions without salt. Consequently, the amount of thickness growth highly depends on the amount of salt that affects the electrostatic interactions and increases the driving force for diffusion in and out of the multilayer.

Mass deposition growth for the PSS/PANI system in cases where salt is both present and absent, is not linear since a progressive increase of each polyelectrolyte after its deposition is detected (Figure 5-9). As the number of layers increases, the extent of free chains going inward and outward increases exponentially due to increase the amount of overcompensation (Figure 5-9). In other words, at each adsorption step, more PSS is adsorbed than that removed in the previous step, leading to nonlinear layer growth. The rates of increase and decrease of PSS and PANI at

each step corresponding to diffusion in and out of the multilayer is almost double for solutions containing salt (Figure 5-9).

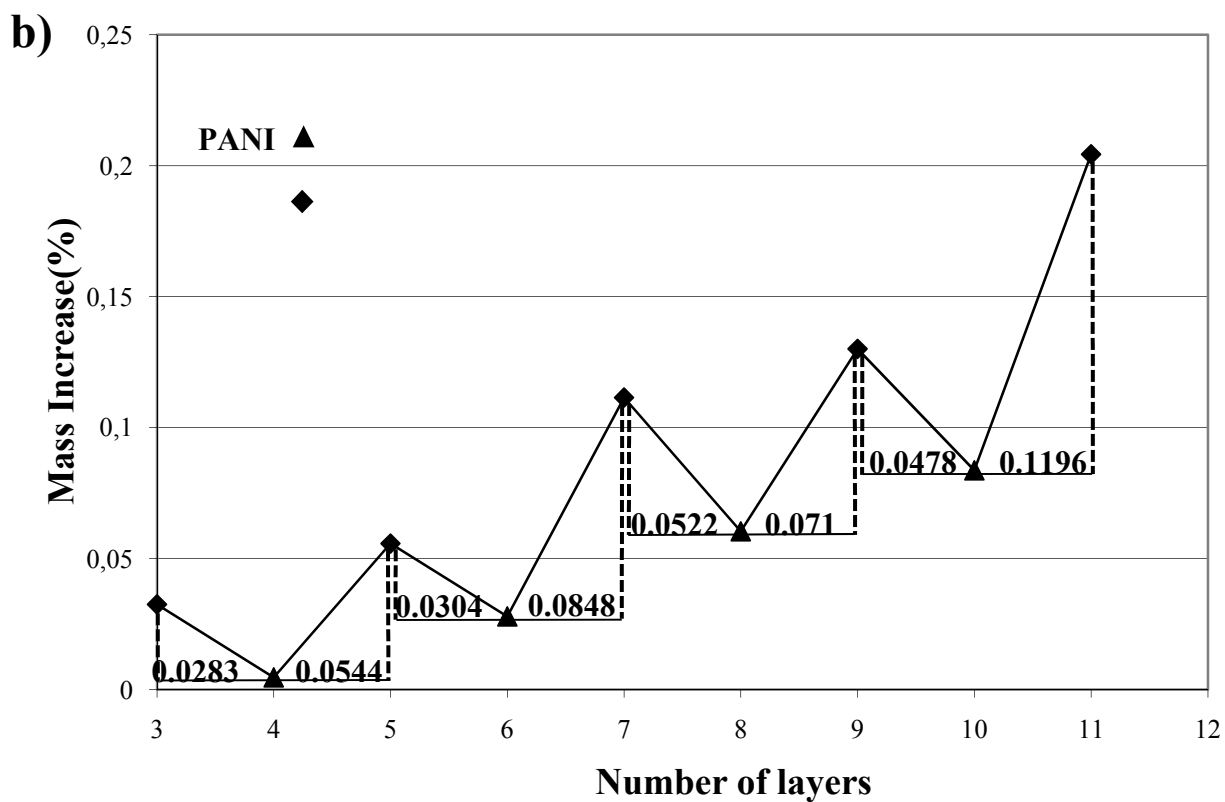
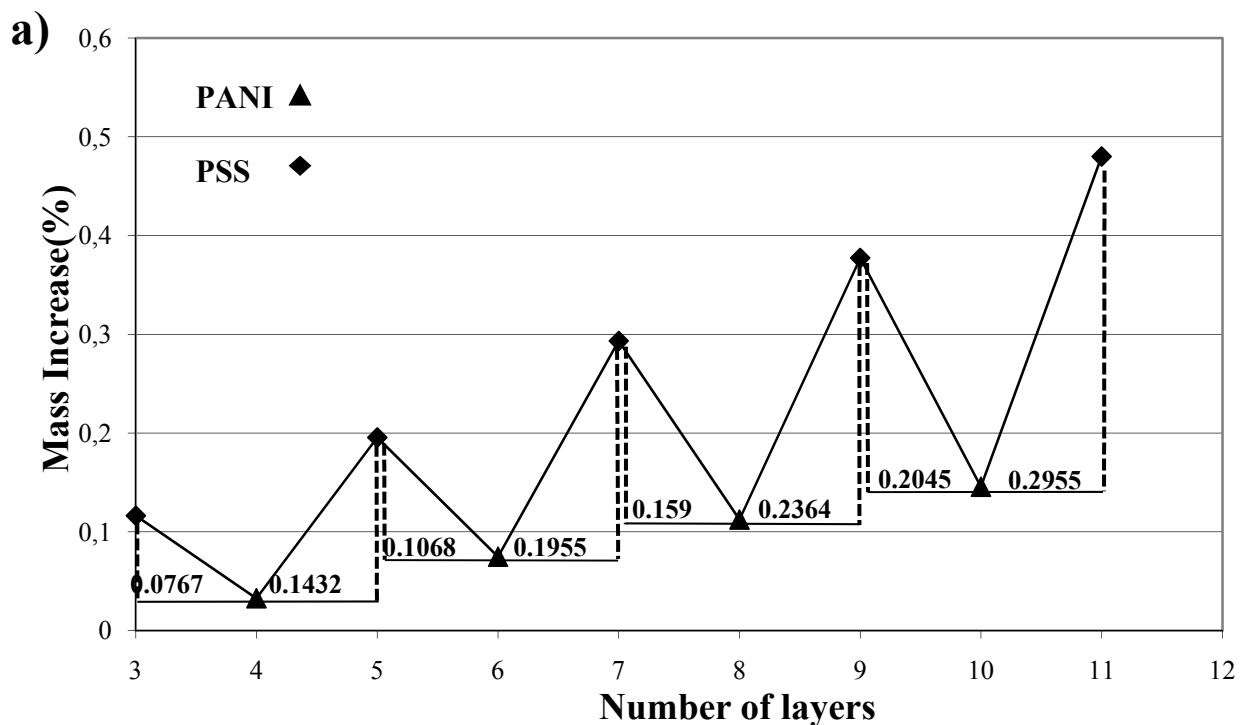


Figure 5-9. Mass increase (%) indicating cumulative deposited mass as a function of number of deposited PSS and PANI layers for sample (A). a) solution containing salt, and b) solution without salt.

5.4.7 Conductivity Measurement of the Conductive Porous Polymer Device

The electrical conductivity of sample A-33%HDPE/33%PS/33%PVDF and sample B-33%HDPE/33%PMMA/33%PVDF was evaluated as a function of the number of deposited PSS and PANI layers. The electrical conductivity of these samples increases by several orders of magnitude as a function of the number of deposited PSS/PANI layers until a saturation plateau is reached at approximately 32 layers (Figure 5-10).

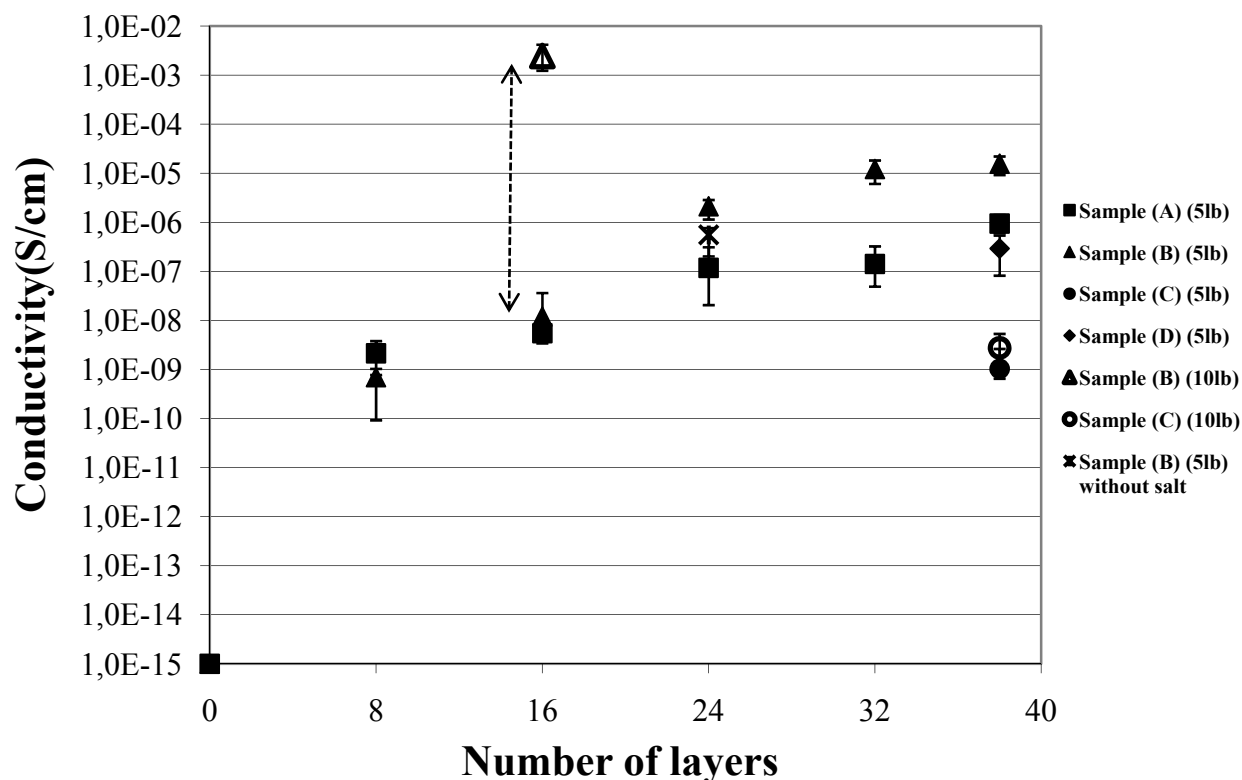


Figure 5-10. Conductivity as a function of the number of deposited layers for various samples at a 5 lb load. The effect of a 10 lb load is shown for two samples as indicated by the arrows.

The percolation threshold of PANI in this porous device is achieved at a maximum of 8 layers. This corresponds to 0.19 wt.% PANI for sample A and 0.28 wt.% for sample B. The conductivity saturation plateau is achieved at 32 layers which corresponds to 0.76% PANI for sample A and 1.1% for sample B. This dependence of conductivity on deposited layers confirms the hypothesis that deposited PSS and PANI form a network type construction as opposed to the formation of discrete PSS and PANI layers. In fact, this network formation allows for the fine tuning of conductivity over several orders of magnitude. Clearly, the deposition of only a few layers results in an incomplete network with disconnections in many parts and demonstrates a limited passage of electricity and thus yields a low conductivity value. By increasing the number of layers to 8 and 16, higher conductivity values are obtained and the conductivity is in the 10^{-9} - 10^{-8} S cm⁻¹ range. As more PANI chains are added they diffuse into the network resulting in a significant increase in network branches. The addition of further layers results in a plateau value for conductivity at approximately 10^{-6} S cm⁻¹ for sample A and 10^{-5} S cm⁻¹ for sample B. Beyond 32 layers, the further addition of PANI has no effect on the conductivity of the device. The conductivity of sample C and D after the deposition of 38 PSS/PANI layers was measured showing the values of 10^{-9} S cm⁻¹ and 3×10^{-7} S cm⁻¹ respectively. The difference in the conductivity values can be dependent on several factors such as pore sizes and pore distribution; however the most important one is the internal surface area of the substrate.

The addition of salt during the LbL process has little influence on the conductivity of the sample as shown in Figure 5-10. Braga et al. (Braga, et al., 2008) and Paloheimo et al. (Paloheimo, et al., 1995) reported that the electrical resistance of PANI/PSS layers with solutions of different polymer concentrations decreases as more layers are adsorbed until a saturation plateau is reached, between the 26th and 30th layer. This closely corresponds with the results observed in this work. It is very likely that the formation of a diffuse network structure in the current study is critical in obtaining high conductivity values. Discrete molecular layers added in a classic LbL protocol using strong polyelectrolytes would have likely resulted in a lower percolation threshold value, but also would not be capable of achieving the high conductivities observed at saturation as seen in this study.

In this work the conductance of the porous samples was converted to conductivity based on the general following equation:

Equation 5-3.
$$\sigma = \frac{Gl}{A}$$

Where G is conductance, A is cross-sectional area, l is length, and σ represents conductivity. As void domains and HDPE have conductivity values of zero and 10^{-15} S cm^{-1} , respectively, a sample including substrates, multilayers and void volumes can be considered as a whole conductive device with certain conductivity. In other words, a sample can be considered as an ultra-porous PANI network. In porous materials, pore geometry (including the pore size and distribution) plays a major role in the conductivity of the material (Solonin & Chernyshev, 1975), as well as the perfection of the contact between the conductive material and the nature of the material filling the pores (Montes, Cuevas, Rodriguez, & Herrera, 2005). A number of theoretical and experimental models have been developed for applying porous-structure parameters, such as volume and pore concentration to calculate conductivity (Lifshitz, Landau, & Pitaevskii, 1984; Skorokhov, 1972). The detailed calculations for the estimation of conductivity using this approach for this type of porous device is described in more detail elsewhere (Ravati, 2010).

5.4.8 Conductivity of the Conductive Porous Polymer Device under Loads

The conductive porous polymer device developed in this study is sensitive to applied compression providing that the void volume percentage is sufficiently high. The compression of sample B of 67 void % under a 10lb load pushes and forces the rods and walls of the substrate to move inward. On the other hand, no deformation in sample C, which has a 60% void volume, is observed. In that case the mechanical strength of the walls of the device is sufficient to resist deformation resulting from the applied load. In the case of sample B, further contact between the walls of the sample after compression results in an increase in the conductivity from 10^{-8} S cm^{-1} up to 0.002 S cm^{-1} as shown in Figure 5-10. This allows for another control parameter to achieve

a wide range of conductivity in these conductive porous devices. It also opens up the potential to develop these devices as load bearing sensors.

5.5 Conclusions

This paper reports on the preparation of a novel 3D porous polymeric conducting device (PPCD) derived from multi-percolated polymer blend systems. The work has focused on the preparation of ultra low surface area porous substrates followed by the deposition of polyaniline conductive polymer (PANI) on the internal porous surface using a layer-by-layer technique. In this way, the percolation threshold of PANI in this porous conductive device can be reduced to a value as low as 0.19%. Furthermore, depending on the amount of PANI deposited, the electrical conductivity of the porous substrate can be controlled over several orders of magnitude from 10^{-15} S cm⁻¹ to 10^{-3} S cm⁻¹.

Ternary and quaternary multi-percolated(hierarchically ordered) systems comprised of high-density polyethylene (HDPE), polystyrene (PS), poly(methyl methacrylate) (PMMA) and poly(vinylidene fluoride) (PVDF) are melt-mixed and subsequently annealed in order to obtain large interconnected phases. Subsequent extraction of PS, PMMA and PVDF within that blend allows for the preparation of a fully interconnected porous HDPE substrate of ultra-low surface area and highly uniform sized channels. This provides an ideal substrate for subsequent polyaniline (PANI) addition. Using a layer-by-layer (LbL) approach, alternating poly(styrene sulfonate) (PSS)/PANI layers are deposited on the internal surface of the 3-dimensional porous polymer substrate. The PANI and sodium poly(styrene sulfonate) (NaPSS) both adopt an inter-diffused network conformation on the surface. The sequential mass deposition of PSS and PANI multilayers has been studied in detail and an oscillating behavior is observed, due primarily to the diffusion of PSS chains both in and out of the multilayer structure. Salt in the deposition solution highly affects the polyelectrolyte construction by allowing for a more uniform deposition and more thickly deposited PSS/PANI layers. The mass deposition growth for the PSS/PANI system in all cases is not linear. Conductivity measurements show that the conductivity of these samples increases from 10^{-15} S cm⁻¹ to 10^{-5} S cm⁻¹ as the number of

deposited PANI layers increases until a saturation plateau is reached at approximately 32 layers. The conductive porous polymer device developed in this study is sensitive to applied compression providing that the void volume percentage is sufficiently high. Higher loads result in higher conductivity values with values as high as 10^{-3} S cm⁻¹ obtained. Although this approach has been demonstrated here for an ultra-low surface area porous substrate, high surface area substrates can also be readily prepared.

5.6 Acknowledgements

The authors express appreciation to the Natural Sciences and Engineering Research Council of Canada for supporting this work. They also thank F. Normandin from the *Institut des matériaux industriels* for his assistance with the conductivity measurements of the samples.

5.7 References

- (1) Heywang, G.; Jonas, F. *Advanced Materials* **1992**, *4*, 116.
- (2) Roman, L. S.; Andersson, M. R.; Yohannes, T.; Inganás, O. *Advanced Materials* **1997**, *9*, 1164.
- (3) Kraft, A.; Grimsdale, Andrew C.; Holmes, Andrew B. *Angewandte Chemie* **1998**, *110*, 416.
- (4) Schmidt, V. M.; Tegtmeier, D.; Heitbaum, J. *Journal of Electroanalytical Chemistry* **1995**, *385*, 149.
- (5) Wessling, B. *Advanced Materials* **1994**, *6*, 226.
- (6) Contractor, A. Q.; Sureshkumar, T. N.; Narayanan, R.; Sukeerthi, S.; Lal, R.; Srinivasa, R. S. *Electrochimica Acta* **1994**, *39*, 1321.
- (7) Kaneto, K.; Kaneko, M.; Min, Y.; MacDiarmid, A. G. *Synthetic Metals* **1995**, *71*, 2211.
- (8) Burroughes, J. H.; Bradley, D. D. C.; Brown, A. R.; Marks, R. N.; Mackay, K.; Friend, R. H.; Burns, P. L.; Holmes, A. B. *Nature* **1990**, *347*, 539.
- (9) Margolis, J. M. *Conductive Polymers and Plastics*; Chapman and Hall: New York, 1989.
- (10) Halls, J. J. M.; Walsh, C. A.; Greenham, N. C.; Marseglia, E. A.; Friend, R. H.; Moratti, S. C.; Holmes, A. B. *Nature* **1995**, *376*, 498.
- (11) Tessler, N.; Denton, G. J.; Friend, R. H. *Nature* **1996**, *382*, 695.
- (12) Garnier, F.; Hajlaoui, R.; Yassar, A.; Srivastava, P. *Science* **1994**, *265*, 1684.
- (13) Zasadzinski, J. A.; Viswanathan, R.; Madsen, L.; Garnaes, J.; Schwartz, D. K. *Science* **1994**, *263*, 1726.
- (14) Maoz, R.; Frydman, E.; Cohen, S. R.; Sagiv, J. *Advanced Materials* **2000**, *12*, 424.

- (15) Love, J. C.; Estroff, L. A.; Kriebel, J. K.; Nuzzo, R. G.; Whitesides, G. M. *Chemical Reviews* **2005**, *105*, 1103.
- (16) Hammond, P. T. *Advanced Materials* **2004**, *16*, 1271.
- (17) Decher, G.; Hong, J. D.; Schmitt, J. *Thin Solid Films* **1992**, *210-211*, 831.
- (18) Paul, D. R.; Barlow, J. W. **1980**, *18*, 109
- (19) Bourry, D.; Favis, B. D. *Journal of Polymer Science Part B: Polymer Physics* **1998**, *36*, 1889.
- (20) Gubbels, F.; Jerome, R.; Teyssie, P.; Vanlathem, E.; Deltour, R.; Calderone, A.; Parente, V.; Bredas, J. L. *Macromolecules* **1994**, *27*, 1972.
- (21) Wang, Y.; Rubner, M. F. *Macromolecules* **2002**, *25*, 3284.
- (22) Sumita, M.; Sakata, K.; Hayakawa, Y.; Asai, S.; Miyasaka, K.; Tanemura, M. *Colloid & Polymer Science* **1992**, *270*, 134.
- (23) Levon, K.; Margolina, A.; Patashinsky, A. Z. *Macromolecules* **2002**, *26*, 4061.
- (24) Zhang, J.; Ravati, S.; Virgilio, N.; Favis, B. D. *Macromolecules* **2007**, *40*, 8817.
- (25) Torza, S.; Mason, S. G. *J. Coll. Interface Sci.* **1970**, *33*, 67.
- (26) Hobbs, S. Y.; Dekkers, M. E. J.; Watkins, V. H. *Polymer* **1988**, *29*, 1598.
- (27) Zhenhua Yuan, B. D. F. *AIChE Journal* **2005**, *51*, 271.
- (28) Sarazin, P.; Favis, B. D. *Biomacromolecules* **2003**, *4*, 1669.
- (29) Decher, G.; Hong, J. D. *European Conference on Organized Organic Thin Films* **1991**, 321.
- (30) Clark, S. L.; Montague, M. F.; Hammond, P. T. *Macromolecules* **1997**, *30*, 7237.
- (31) Shiratori, S. S.; Rubner, M. F. *Macromolecules* **2000**, *33*, 4213.
- (32) Sui, Z.; Salloum, D.; Schlenoff, J. B. *Langmuir* **2003**, *19*, 2491.
- (33) Ferreira, M.; Rubner, M. F. *Macromolecules* **1995**, *28*, 7107.
- (34) Schoeler, B.; Kumaraswamy, G.; Caruso, F. *Macromolecules* **2002**, *35*, 889.
- (35) Decher, G. *Science* **1997**, *277*, 1232.
- (36) Caruso, F.; Caruso, R. A.; Mohwald, H. *Science* **1998**, *282*, 1111.
- (37) Roy, X.; Sarazin, P.; Favis, B. D. *Advanced Materials* **2006**, *18*, 1015.
- (38) Cheung, J. H.; Stockton, W. B.; Rubner, M. F. *Macromolecules* **1997**, *30*, 2712.
- (39) Fou, A. C.; Rubner, M. F. *Macromolecules* **2002**, *28*, 7115.
- (40) Kim, H. S.; Sohn, B. H.; Lee, W.; Lee, J. K.; Choi, S. J.; Kwon, S. J. *Thin Solid Films* **2002**, *419*, 173.
- (41) Liang, Z.; Cabarcos, O. M.; Allara, D. L.; Wang, Q. *Advanced Materials* **2004**, *16*, 823.
- (42) Ram, M. K.; Salerno, M.; Adami, M.; Faraci, P.; Nicolini, C. *Langmuir* **1999**, *15*, 1252.
- (43) Ferreira, M.; Cheung, J. H.; Rubner, M. F. *Thin Solid Films* **1994**, *244*, 806.
- (44) Dautzenberg, H.; Jaeger, W.; Kotz, J.; Phillip, B.; C., S.; Stscherbina, D. *Carl Hanser Verlag: Munich, Germany* **1994**.
- (45) Harris, J. J.; Bruening, M. L. *Langmuir* **2000**, *16*, 2006.
- (46) Dubas, S. T.; Schlenoff, J. B. *Macromolecules* **2001**, *34*, 3736.
- (47) Braga, G. S.; Paterno, L. G.; Lima, J. P. H.; Fonseca, F. J.; de Andrade, A. M. *Materials Science and Engineering C* **2008**, *28*, 555.
- (48) Paloheimo, J.; Laakso, K.; Isotalo, H.; Stubb, H. *Synthetic Metals* **1995**, *68*, 249.
- (49) Reignier, J.; Favis, B. D. *Macromolecules* **2000**, *33*, 6998.
- (50) Yasuda, K.; Armstrong, R.; Cohen, R. *Rheologica Acta* **1981**, *20*, 163.
- (51) Virgilio, N.; Favis, B. D.; Pepin, M.-F.; Desjardins, P.; L'Esperance, G. *Macromolecules* **2005**, *38*, 2368.

- (52) Guo, H. F.; Packirisamy, S.; Gvozdic, N. V.; Meier, D. J. *Polymer* **1997**, *38*, 785.
- (53) Ravati, S.; Favis, B. D. *Macromolecules* **2010**, *Submitted*.
- (54) Li, J.; Ma, P. L.; Favis, B. D. *Macromolecules* **2002**, *35*, 2005.
- (55) Li, J.; Favis, B. D. *Polymer* **2001**, *42*, 5047.
- (56) Klitzing, R. v.; Espert, A.; Asnacios, A.; Hellweg, T.; Colin, A.; Langevin, D. *Colloids and Surfaces A: Physicochemical and Engineering Aspects* **1999**, *149*, 131.
- (57) Picart, C.; Lavallo, P.; Hubert, P.; Cuisinier, F. J. G.; Decher, G.; Schaaf, P.; Voegel, J. C. *Langmuir* **2001**, *17*, 7414.
- (58) Dubas, S. T.; Schlenoff, J. B. *Langmuir* **2001**, *17*, 7725.
- (59) Tjipto, E.; Quinn, J. F.; Caruso, F. *Journal of Polymer Science, Part A (Polymer Chemistry)* **2007**, *45*, 4341.
- (60) Lavallo, P.; Gergely, C.; Cuisinier, F. J. G.; Decher, G.; Schaaf, P.; Voegel, J. C.; Picart, C. *Macromolecules* **2002**, *35*, 4458.
- (61) Schlenoff, J. B.; Dubas, S. T. *Macromolecules* **2001**, *34*, 592.
- (62) Ha, B. Y.; Thirumalai, D. *Macromolecules* **1995**, *28*, 577.
- (63) Klitzing, R.; Moehwald, H. *Langmuir* **1995**, *11*, 3554.
- (64) Jaber, J. A.; Schlenoff, J. B. *Langmuir* **2007**, *23*, 896.
- (65) Solonin, S. M.; Chernyshev, L. I. *Soviet Powder Metallurgy and Metal Ceramics (English translation of Poroshkovaya Metallurgiya)* **1975**, *14*, 806.
- (66) Montes, J. M.; Cuevas, F. G.; Rodriguez, J. A.; Herrera, E. J. *Powder Metallurgy* **2005**, *48*, 343.
- (67) Lifshitz, E. M.; Landau, L. D.; Pitaevskii, L. P. *Electrodynamics of Continuous Media*, 1984; Vol. 8.
- (68) Skorokhov, V. V. *The Rheological Principles of Sintering Theory*; Nauka: Kiev, 1972.
- (69) Ravati, S., École Polytechnique de Montréal, 2010.

CHAPTER 6 - MORPHOLOGICAL STATES FOR A TERNARY POLYMER BLEND DEMONSTRATING COMPLETE WETTING

6.1 Abstract

For the most part, ternary polymer blends demonstrate complete wetting behavior. Conceptually, this is the state where one of the components will always tend to completely separate the other two and from a thermodynamic viewpoint is described as the case where two of the three possible binary spreading coefficients are negative and the other is positive, as defined by Harkins spreading theory. This work examines the complete range of morphological states possible for such a system over the entire ternary composition diagram as prepared by melt mixing. A ternary polymer blend comprised of high-density polyethylene(HDPE), polystyrene(PS), and poly(methyl methacrylate)(PMMA) is selected as a model system demonstrating complete wetting and four sub-categories of morphologies can be identified including: a) matrix/core-shell dispersed phase; b) tri-continuous; c) matrix/two separate dispersed phases;, and d) bi-continuous/dispersed phase morphologies. Electron microscopy as well as a technique based on the combination of focused ion beam irradiation and atomic force microscopy are used to clearly illustrate and identify the various phases. Solvent extraction/gravimetry is used to examine the extent of continuity of the systems so as to effectively identify regions of high continuity. Triangular compositional diagrams are used to distinguish these various morphological regions and the results are interpreted in light of the interfacial tension of the various binary combinations and their subsequent spreading coefficients. The effect of the molecular weight and of viscosity ratio on the phase size of the various structures is also considered.

Keywords: ternary polymer blend, double-percolated morphology, tri-continuous, composite-droplet, co-continuous structure

6.2 Introduction

It is well-known that the morphology of a polymer blend has a significant influence on its properties (Paul & Newman, 1978; Utracki, 1998). For binary immiscible polymer blends, two broad categories of morphology exist: the matrix/dispersed phase structure and the co-continuous morphology (Figure 6-1a) (Favis, 2000; Potschke & Paul, 2003).

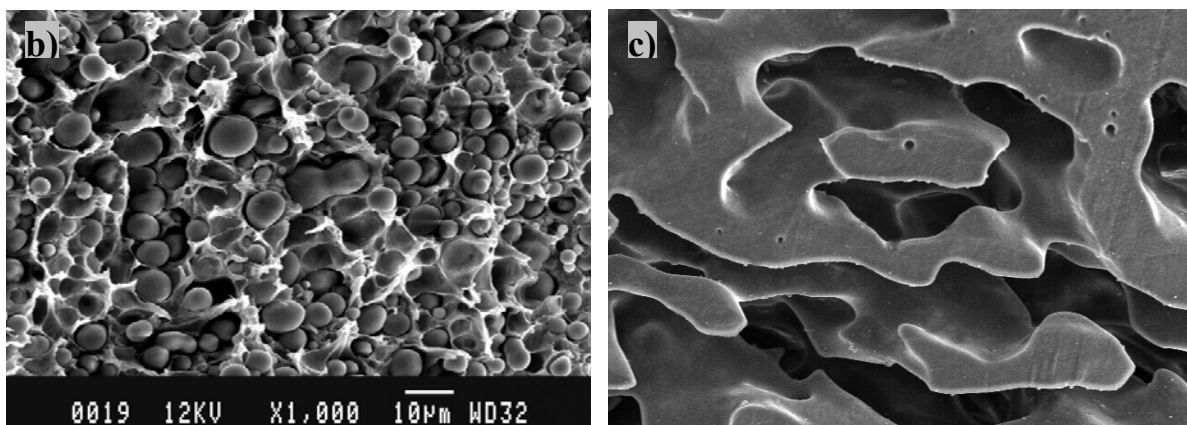
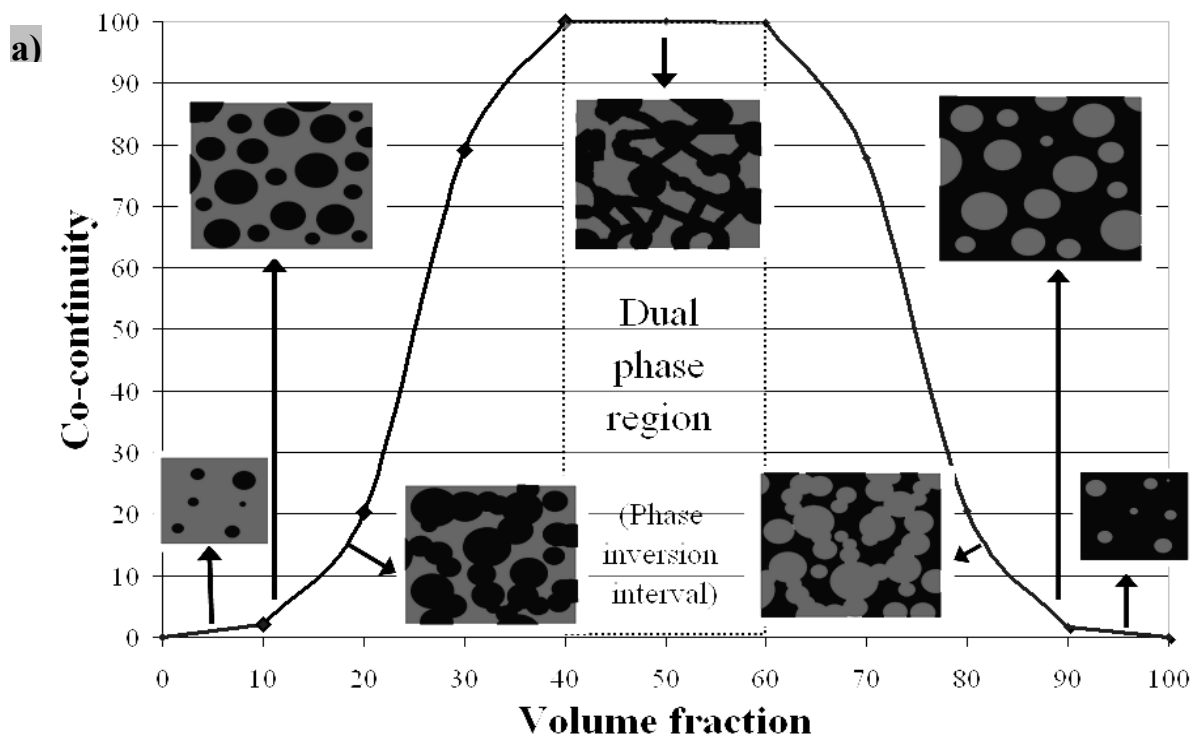


Figure 6-1. (a) schematic representation of the evolution of morphology in a binary blend, (b) matrix/dispersed morphology, and (c) co-continuous morphology

The dispersed phase in a binary polymer blend can take the form of fibers, lamella and A-B-A droplet-in-droplet type structures (Molau & Keskkula, 1966; Reignier & Favis, 2000). In an A/B binary blend, the dispersed phase type structure (Figure 6-1b) is converted to a continuous type structure through an increase in the composition. By increasing the concentration of dispersed phase A, droplets coalesce resulting in a percolation threshold point being reached. This percolation threshold is the first connected pathway in the blend (Figure 6-1a). Classic percolation theory defines the percolation threshold as the onset of long-range connectivity in random systems and it occurs at a volume fraction of 0.156 for a random mono-disperse distribution of spheres (Scher & Zallen, 1970). Through a further increase of minor phase concentration, levels of continuity increase until a fully-interconnected co-continuous morphology is obtained (Figure 6-1c). Co-continuity is defined as the case where each phase is fully continuous in the blend system. Since this often occurs over a concentration range for binary polymer blends, this is also known as the region of dual-phase continuity. Phase inversion is defined as the concentration point where co-continuity converts into a matrix/dispersed phase morphology. It has been reported that the interfacial tension and the viscosity ratio can also influence the position of the region of dual-phase continuity (Jordhamo, et al., 1986; Mekhilef & Verhoogt, 1996).

Much less work has been carried out on the fundamental morphological states present in ternary polymer blends comprised of significant quantities of 3 distinct phases. Recently, some papers have described the morphological behavior of ternary systems with complex morphologies such as A-B-C composite-droplet structures (Reignier & Favis, 2000; Reignier, et al., 2003) and double-percolated morphology (Zhang, et al., 2007).

Complete wetting and partial wetting are two broad categories of morphological states possible for ternary polymer blends. In an A/B/C system, complete wetting describes the case where the most stable thermodynamic state is when one of the phases, say phase B, will always position itself to completely separate phases A and C. In that case phases A and B completely wet each other and phases B and C also completely wet each other. In the case of partial wetting, the most stable thermodynamic state is when there is three-phase contact. In that case, for example, droplets of B will situate at the A/C interface such that all three phases are in contact with each other (Torza & Mason, 1970; Virgilio, Marc-Aurele, et al., 2009). Both complete and partial wetting can be described by spreading theory as defined by Harkins equation. A

modified version of Harkins theory(Harkins & Feldman, 1922) was first reported by Torza et al.(Torza & Mason, 1970). Hobbs et al.(Hobbs, et al., 1988) followed and developed a modified Harkins equation and calculated three spreading coefficients of ternary polymer systems to predict the possible morphological structures as shown in Equation 6-1 :

Equation 6-1
$$\lambda_{ij} = \gamma_{jk} - \gamma_{ik} - \gamma_{ij}$$

where λ_{ij} is defined as the spreading coefficient defining the tendency of component (i) to encapsulate or spread onto component (j) in the matrix of component (k). The interfacial tensions of the various polymer pairs are represented as γ_{ij} , γ_{ik} and γ_{jk} . In a certain ternary blend, 3 different spreading coefficients exist including $\lambda_{ij} = \lambda_{ik}$, $\lambda_{ji} = \lambda_{jk}$, and $\lambda_{ki} = \lambda_{kj}$. A positive value of one of the spreading coefficients indicates that the ternary blend will demonstrate complete wetting behavior as shown in Figure 6-2a. For example, a positive value of λ_{ik} demonstrates that phase (i) spreads over phase (k) leading to a separation of phases (j) and (k) by phase (i) at the interface. A matrix/core-shell dispersed phase structure is an example of complete wetting in which phase B, for example, encapsulates dispersed phase C in a matrix of A. On the other hand, negative values for all three spreading coefficients indicates a partial wetting behavior in which all components have an interface with each other, or all three meet along a common line of three phase contact (Figure 6-2a)(Virgilio, Marc-Aurele, et al., 2009). A number of complex morphologies in ternary HDPE/PS/PMMA blends have been investigated. Reignier et al.(Reignier & Favis, 2000) examined the core-shell morphology of PMMA encapsulated by PS in an HDPE matrix in detail. Zhang et al.(Zhang, et al., 2007) reported on the generation of a double-percolated structure comprised of a PS layer at the HDPE/PMMA interface through the control of the composition of the components. Virgilio et al.(Virgilio, Marc-Aurele, et al., 2009) reported the case of partial wetting for a HDPE/PS/PP blend demonstrating a close-packed droplet array of PS at the interface of HDPE and PP. Guo et al.(Guo, Gvozdic, et al., 1997; Guo, Packirisamy, et al., 1997), studied the morphology of ternary and quaternary blends and proposed a model which includes not only the interfacial tension, but also the interfacial area of the phases. To date, however, the detailed examination of all the possible morphological states over the entire composition range for a ternary polymer blend has not been carried out.

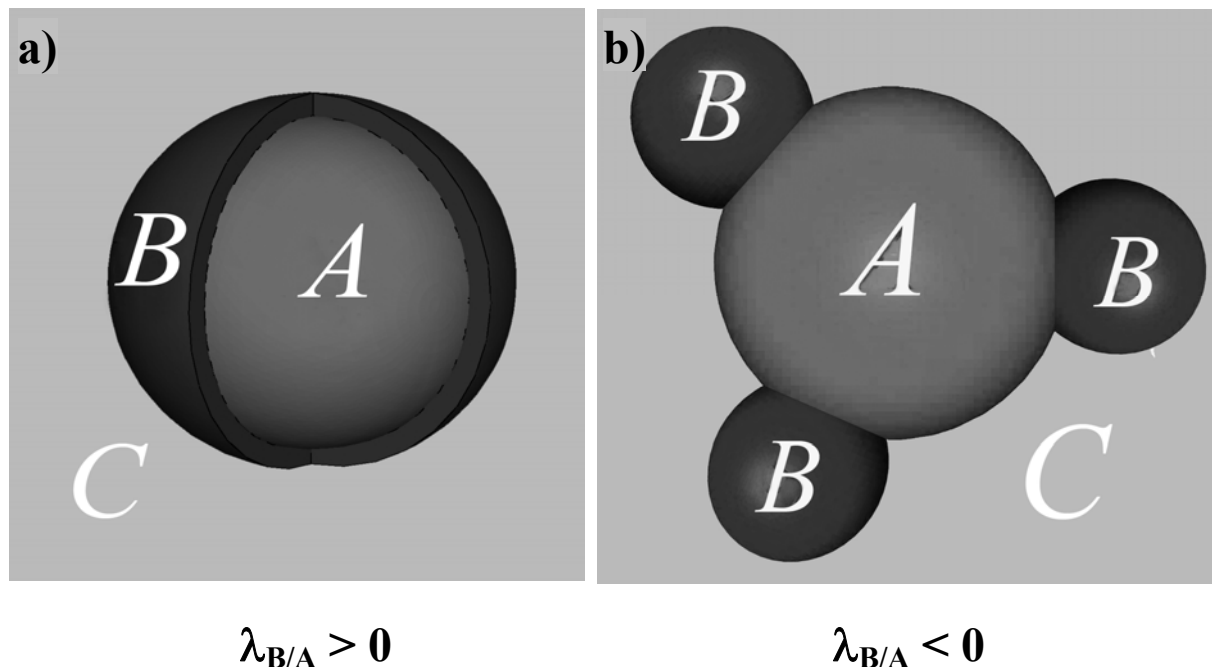


Figure 6-2. Schematic representation of (a) complete wetting: the case that one phase locates between two other phases, and (b) partial wetting: the case that all phases are in contact with each other

The above models employ thermodynamic properties in order to classify the morphology of a ternary blend as complete or partial wetting. Rheological properties also play an important role, particularly with respect to phase size and shape, most notably through viscosity ratio (Gupta, 1993; Luzinov, et al., 2000; Nemirovski, et al., 1995; Tchomakov, et al., 2004), and elasticity ratio effects (Legros, et al., 1997; Vanoene, 1972).

The objective of this work is examined all the possible morphological states for a ternary polymer blend, demonstrating complete wetting, over the entire composition range. A ternary HDPE/PS/PMMA blend will be used as the model system and the morphology will be determined through a combination of electron microscopy, FIB/AFM analysis as well as through the estimation of continuity effects via selective solvent extraction/gravimetry of specific phases. The observed morphologies will be related to spreading theory through a detailed examination of the various interfacial tension values and spreading coefficients.

6.3 Experimental

6.3.1 Materials

Commercial homopolymers of HDPE, PMMA, and PS were used in this study to prepare ternary samples. Low molecular weight poly(methyl methacrylate) and , high molecular weight poly(methyl methacrylate) obtained from Sigma-Aldrich and the high-density polyethylene, HDPE 3000 from Petromont. The L-PMMA was the base resin used in all parts of this work while the H-PMMA was only used in the part discussing the effects of viscosity. Polystyrene, PS 615APR was purchased from Dow Chemical. Some of the characteristics of the homopolymers are reported in Table 6-1.

The interfacial tension values and the Harkins spreading coefficients are tabulated in Table 6-2.

Table 6-1. Material Characteristics

Material	Commercial code	Mw * 10 ⁻³ (g/mol)	Melt Index (g/10min)	η_0 * 10 ⁻³ at 190°C (Pa.s)	$\eta^* \times 10^{-3}$ at 25 rad s ⁻¹ (Pa.s)	Density (g/cm ³) at 20 °C	Density (g/cm ³) at 200 °C
High Density Polyethylene	3000	-	8.1	1.6	0.72	0.98	0.85
Polystyrene	615APR	290	-	5.9	1.5	1.04	0.97
L-Poly(methyl methacrylate)	-	12	-	--	0.04	1.19	1
H-Poly(methyl methacrylate)	182265	996	-	--	7.8	1.2	1.1

Table 6-2. Interfacial Tension of Polymer Pairs from (Reignier & Favis, 2000) and Positive Spreading Coefficient of Ternary Blends

Interfacial tension γ (mN/m)	Positive Spreading Coeff. λ (mN/m)
$\gamma_{\text{HDPE/PMMA}} = 8.6$	$\lambda_{\text{PS/PMMA}} = 2.6$
$\gamma_{\text{PS/PMMA}} = 2.4$	$\lambda_{\text{PMMA/HDPE}} = -5.9$
$\gamma_{\text{PS/HDPE}} = 5.1$	$\lambda_{\text{HDPE/PS}} = -11.3$

6.3.2 Rheological Analysis

The disc-shape samples were compression molded in the hot press at 200°C. A Bohlin constant stress rheometer (CSM) in the dynamic mode equipped with 25 mm parallel disk geometry was utilized to measure the linear viscoelastic properties of homopolymers containing 0.2% antioxidant. All polymers were found to be stable at set temperature in the time sweep test for 8 minutes. After the determination of the viscoelastic region by stress sweep, a frequency sweep allowed for the measure of the zero shear viscosity of each sample. The Carreau-Yasuda model and IRIS Rheo-Hub 2008 software were employed to determine the zero shear viscosity of PEMA. The complex viscosity of pure homopolymers is plotted as a function of frequency in Figure 6-3. The average shear rate in the mixer is approximately 25 s⁻¹ (Reignier, et al., 2003). The zero shear viscosity and the viscosity at 25 s⁻¹ for the various homopolymers are reported in Table 6-1.

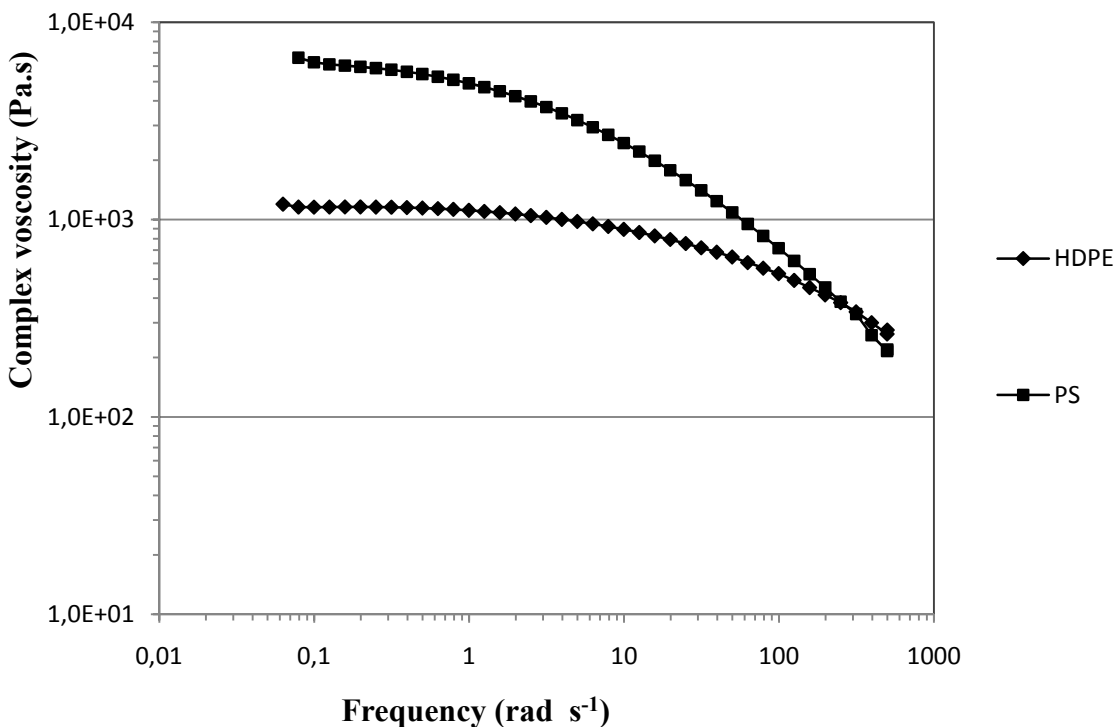


Figure 6-3. Complex viscosity as a function of frequency at 190°C for homopolymers

6.3.3 Sample Preparation

Ternary polymer blends were melt-blended under a flow of dry nitrogen in a 30mL Plasti-Corder internal mixer (Brabender) operating at 200 °C and 50 rpm for 8 minutes. To reduce thermal oxidation of the polymers, 0.2 wt % of Irganox B225 antioxidant from Ciba-Geigy was added to the mixture. The mixing chamber was filled to 70% of its total volume. After mixing, the samples were immediately cut from the mass and quenched in a cold water bath to freeze-in the morphology. All concentrations have been reported based on component volume fraction.

6.3.4 Solvent Extraction

In order to determine the continuity level of components in the blend, a solvent extraction/gravimetric method was performed. It is a fast and straightforward technique to detect

the existence of continuous microstructures with a high accuracy when the components are soluble in specific solvents. In this approach, the volumes of the components before and after extraction are measured by weighing the sample and converting the weight to volume (Equation 6-2).

Equation 6-2

$$\%Cocontinuity = \frac{\sum_n V_{initial} - \sum_n V_{final}}{\sum_n V_{initial}}$$

$V_{initial}$ and V_{final} are the volume of one component or present in the sample, before and after extraction, calculated by weighing the sample and converting it to the volume. The reported value is the average of *%cocontinuity* for several samples and the average error bar for high continuity levels is $\pm 5\%$ and for low continuity levels is $\pm 3\%$. Cyclohexane was utilized as selective solvents for polystyrene and acetic acid for poly(methyl methacrylate).

6.3.5 Characterization of Phase Morphology

6.3.5.1 Microtoming and Scanning Electron Microscopy (SEM)

The specimens were cut and microtomed under liquid nitrogen to a plane face using a microtome (Leica-Jung RM 2065) equipped with a glass knife and a cryochamber type (LN 21). After the appropriate treatment of the sample with selective solvents (acetic acid for PMMA and cyclohexane for PS) to remove one or both of the components, the sample surface was coated with a gold/palladium by plasma deposition. A JEOL JSM 840 scanning electron microscope, operated at a voltage of 10keV to 12keV, was used to obtain photomicrographs of the sample surface.

6.3.5.2 Focused Ion Beam (FIB) and Atomic Force Microscopy (AFM)

After cryomicrotoming the specimens and coating them with a gold-palladium alloy, a Focused Ion Beam (FIB), Atomic Force Microscopy (AFM) technique was used to examine the HDPE/PS/PMMA blend. The surface of the samples was treated and etched using a Hitachi focused ion beam FIB-2000A operating a 30 keV gallium beam. FIB uses a focused beam of gallium ions which are accelerated to energies of 5-50 kiloelectronvolts. Using an electrostatic lens, the ion beam can be focused on a very small spot, resulting in a high resolution because of the small emitting area. In this work, a 0.8 nA beam current and a dwell time of 3 μ s was applied in order to remove approximately 3-4 μ m of the surface. Milling was carried out parallel to the observed surface. Since each polymer component has a different interaction with the gallium beam, this approach induces topological differences and hence increases the contrast between components (Virgilio, et al., 2005a). The milled surface of the specimen was then examined by a scanning probe microscope dimension (AFM) with a Nanoscope IIIa controller in topographical mode. The atomic force microscope measures topography with a force probe. Silicon tips with spring constant of 40 N/m and a resonant frequency of around 300 kHz was employed.

6.4 Results and Discussion

In ternary HDPE/PS/PMMA blends, the very high interfacial tension of PMMA and HDPE ($\gamma_{\text{HDPE/PMMA}} = 8.6$ mN/m) and the low interfacial tension of PS/PMMA ($\gamma_{\text{PS/PMMA}} = 2.4$ mN/m) and HDPE/PS ($\gamma_{\text{HDPE/PS}} = 5.1$ mN/m) results in a positive spreading coefficient of PS over PMMA ($\lambda_{\text{PS/PMMA}}$) with a value of 1.1 mN/m. The other two spreading coefficients are negative and are $\lambda_{\text{PMMA/PS}} = -5.9$ mN/m and $\lambda_{\text{HDPE/PMMA}} = -11.3$ mN/m. This predicts a complete wetting case with the development of a thermodynamically stable PS layer between the PE and PMMA as represented for a ternary 40/20/40 HDPE/PS/PMMA blend as shown in Figure 6-4. In Figure 6-4, the various phases can be clearly identified by the topographical heights induced by FIB etching and subsequently quantified by AFM analysis in the topographical mode. Previous works (Reignier & Favis, 2000, 2003a, 2003b; Reignier, et al., 2003) have shown several sub-morphologies of HDPE/PS/PMMA such as matrix/core-shell morphology and double-percolated

morphology(Zhang, et al., 2007). In the next sections it will be shown that four thermodynamically stable sub-classes of morphologies exist for HDPE/PS/PMMA depending on the composition of phases.

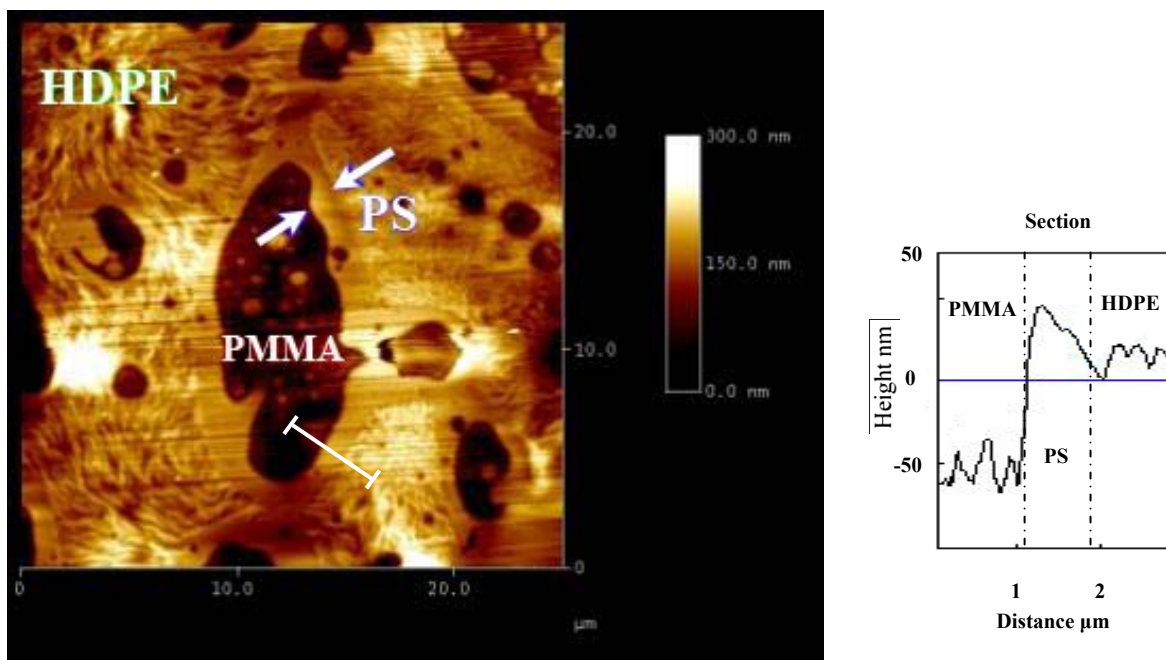
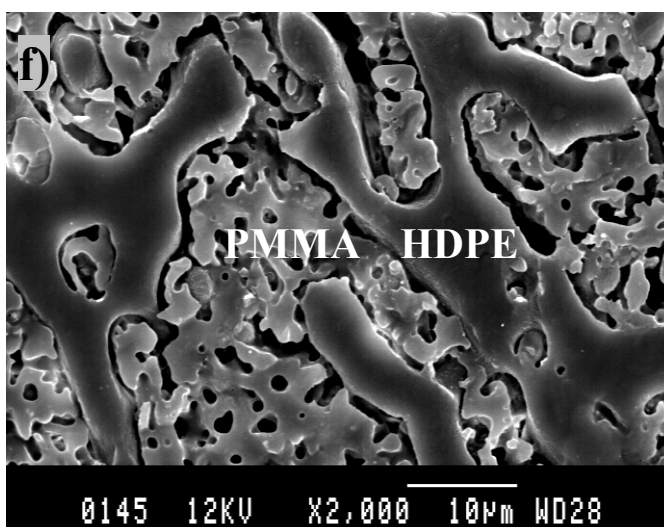
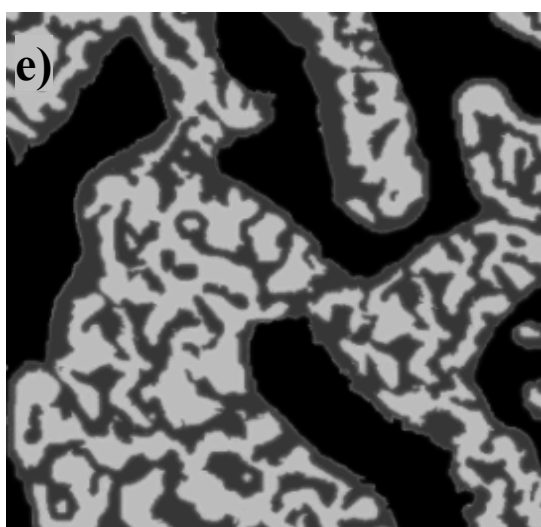
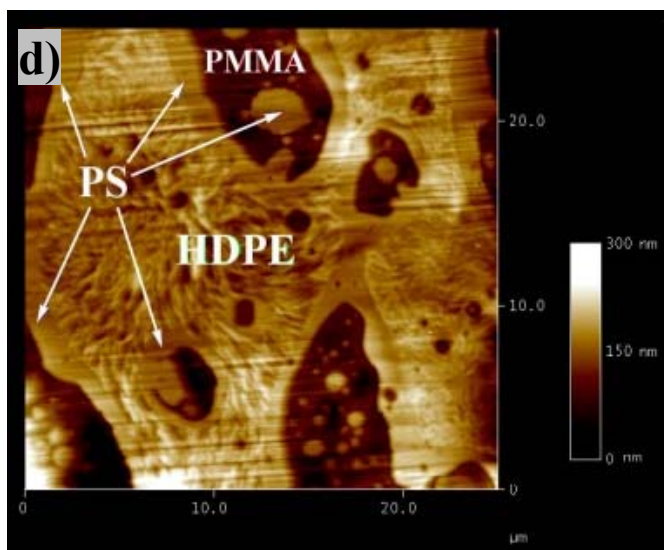
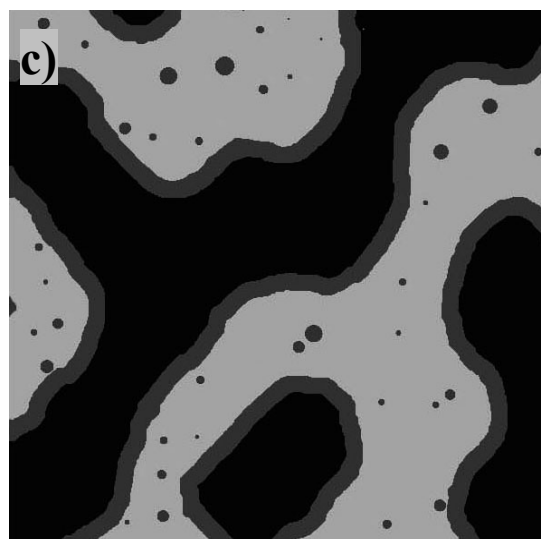
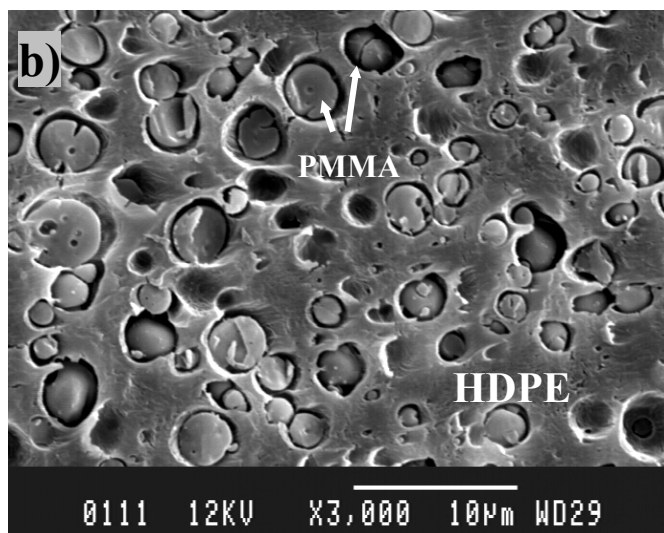
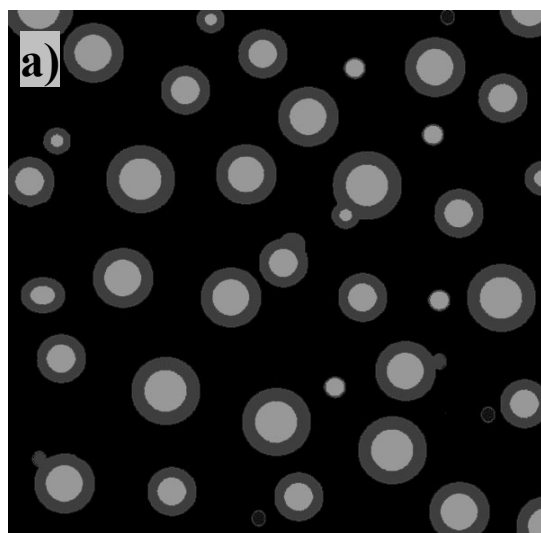


Figure 6-4. FIB-AFM image of complete wetting morphology for ternary 40/20/40 HDPE/PS/PMMA blend showing the layer of PS at the interface of HDPE and PMMA. Scan size is $25\mu\text{m}\times 25\mu\text{m}$. The bar to the right of the FIB/AFM micrograph indicates the colours associated with the topographical height in nm. The white line in the image indicates the section analyzed.

6.4.1 Matrix/Core-Shell Dispersed Phase Morphology

The matrix/core-shell dispersed phase morphology is a well-known sub-morphology for ternary blends. This morphology in a ternary A/B/C blend constitutes droplets of phase A encapsulated by phase B in the matrix of phase C (shown by schematic in Figure 6-5a). A micrograph of this morphology is shown for a ternary 60/10/30 HDPE/PS/PMMA blend comprised of a matrix of HDPE with the PMMA phase present as a core in a PS shell phase(Figure 6-5b).



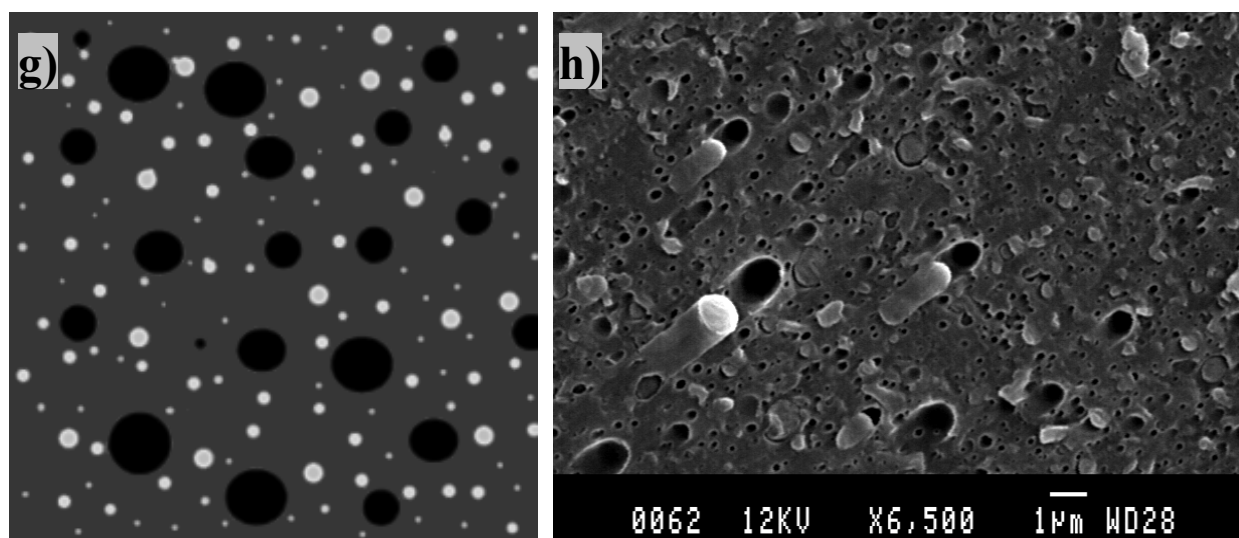


Figure 6-5. (a) Schematic representation of the matrix/core-shell dispersed phase morphology, (b) SEM micrograph of 60/10/30 HDPE/PS/PMMA blend after extraction of PS by cyclohexane, (c) schematic representation of tri-continuous morphology (type I), (d) FIB-AFM image of 40/20/40 HDPE/PS/PMMA showing tri-continuous morphology. Scan size is $25\mu\text{m}\times 25\mu\text{m}$. The bar to the right of the FIB/AFM micrograph indicates the colours associated with the topographical height in nm, (e) schematic representation of tri-continuous(type II), (f) SEM micrograph of 30/30/40 HDPE/PS/PMMA after extraction of PS by cyclohexane, (g) schematic representation of matrix/two separate dispersed phases morphology, and (h) SEM micrograph of 10/80/10 HDPE/PS/PMMA microtomed.

Note that in all schematics black represents the HDPE phase, grey represents the PS phase and white represents the PMMA phase.

6.4.2 Tri-continuous Morphology

In a ternary blend with a matrix/core-shell morphology, increasing the concentration of the core phase results in the coalescence of core phases which leads to the formation of a tri-continuous morphology. In the model ternary HDPE/PS/PMMA blend studied here, as predicted

by Harkins theory, PS will always situate at the interface. Thus, the coalescence of the PMMA cores directly results in the coalescence of PS shells to each other. When the concentration of the PMMA phase becomes high enough to create a continuous network throughout the sample, the PS phase is forced to adopt a continuous form to spread over the PMMA phase (shown by schematic and by micrograph in Figures 6-5c and 6-5d). FIB-AFM characterization of 40/20/40 HDPE/PS/PMMA blend reveals approximately such a morphology (Figure 6-5d). This is a tri-continuous structure or double-percolated morphology and by definition all phases are highly continuous.

Tri-continuous structures can be classified into two categories: type I and type II. The former is shown in Figure 6-5c) and 6-5d), as described above. In that case the PS composition is low enough such that most of the PS situates at the interface, apart from some minor droplet formation in the PMMA. In the Type II case, as the concentration of PS is increased, more isolated droplets are located in the PMMA since the HDPE/PS/PMMA interface is already saturated by PS. These droplets coalesce into elongated structures as the concentration increases until the PS within the PMMA also forms a fully continuous interconnected phase. Such a structure is shown by micrograph and by schematic in Figures 6-5e) and 6-5f) Note that the structure can be described as a co-continuous morphology of PS and PMMA separated by a PS layer from a fully continuous HDPE phase. It should be noted that this morphology is still consistent with Harkins theory as phase B still fully separates phases A and C. In Figure 6-5f) for 30/30/40 HDPE/PS/PMMA the voids left by the selective extraction of PS can be clearly seen to show that PS forms an interlayer between HDPE and PMMA. A fully interpenetrated network of PS and PMMA is also visible.

Hence, tri-continuous type I is transformed to tri-continuous type II by increasing the concentration of the phase separating the other two phases.

6.4.3 Matrix/ Two Separate Dispersed Phases Morphology

Another type of sub-morphology in the complete wetting case of HDPE/PS/PMMA is the matrix with two separate dispersed phases morphology (shown as a schematic in Figure 6-5g). In that

case the grey matrix is PS, with dispersed droplets of PMMA (white) and separate dispersed droplets of HDPE (black). Figure 6-5h shows a micrograph of droplets of PMMA and HDPE phases in a PS matrix. Since it is hard to distinguish PMMA and HDPE droplets, the PMMA is selectively extracted showing voids where the PMMA was located and clearly indicating the presence of HDPE droplets.

6.4.4 Bi-Continuous/Dispersed Phase Morphology

The last case of sub-morphology for HDPE/PS/PMMA is the bi-continuous/dispersed phase morphology comprised of a co-continuous structure for two phases with the third phase present as a dispersed phase. This case is generated when the concentration of the middle separating phase increases resulting in a co-continuous structure of the middle phase with either of the other two phases. The droplets of the third phase are distributed in the middle separating phase (shown as a schematic in Figure 6-6a). Two examples of such a morphology are shown in Figures 6-6b) and 6-6c). 50/40/10 HDPE/PS/PMMA is shown in 6-6b) and it can be seen that the HDPE and PS phases are continuous with droplets of PMMA in the PS phase. 50/25/25 HDPE/PS/PMMA is shown in Figure 6-6c).

In a ternary blend with a bi-continuous/dispersed phase structure increasing the amount of inner dispersed phase and decreasing the extent of continuous outer phase results in an inversion in morphology. In Figures 6-6 d), e) and f), PMMA and PS have a co-continuous structure and HDPE is present as droplets. This inversion can be shown in a comparison of 50/25/25 HDPE/PS/PMMA(Figure 6-6c) where droplets of PMMA can be seen in the PS phase which, in turn, is co-continuous with HDPE, and 10/30/60 HDPE/PS/PMMA(Figure 6-6e) where droplets of HDPE can be seen in PMMA which is co-continuous with PS. The PS phase is extracted in Figure 6-6f for the 10/30/60 HDPE/PS/PMMA clearly showing numerous droplets of HDPE distributed in the PS phase.

Figure 6-7 represents the sub-morphologies in the complete wetting case that can be converted to each other by varying the phase composition.

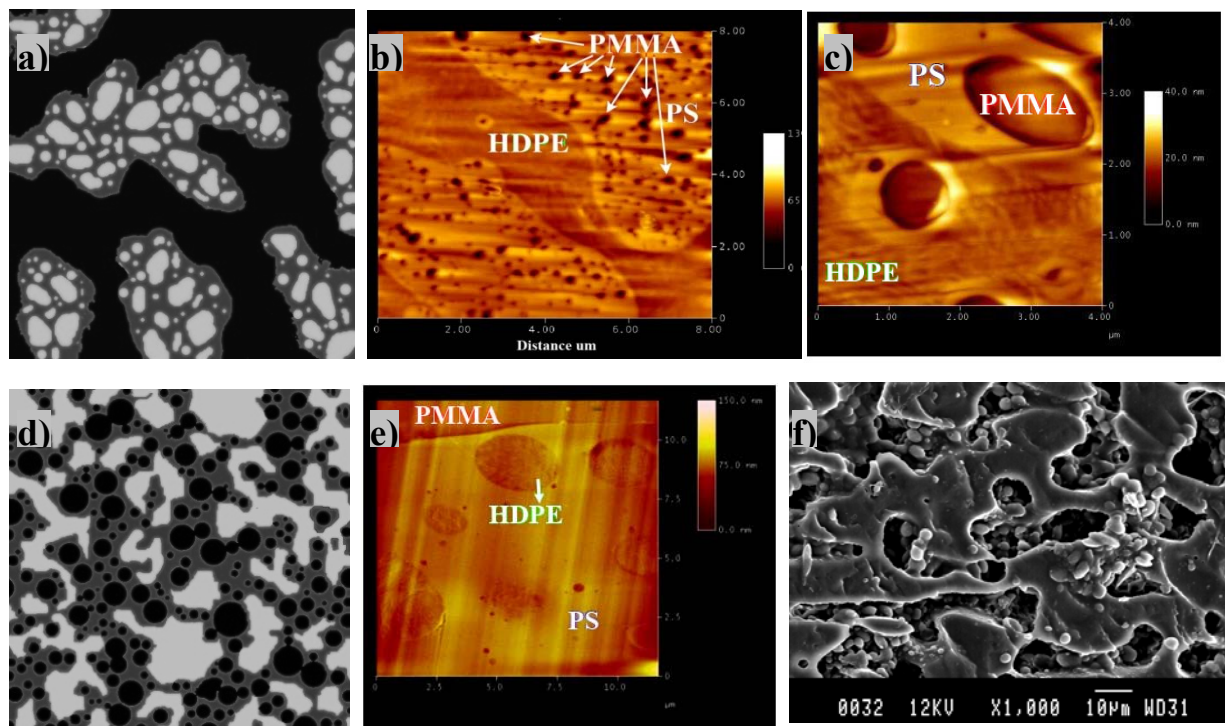


Figure 6-6. a) Schematic representations of bi-continuous/dispersed phase morphology with small droplets of white phase, b) FIB-AFM image of 50/40/10 HDPE/PS/PMMA showing bi-continuous/dispersed phase morphology with small droplets of PMMA. Scan size is $8\mu\text{m}\times 8\mu\text{m}$, (c) FIB-AFM image of 50/25/25 HDPE/PS/PMMA showing bi-continuous/dispersed phase morphology with droplets of PMMA. Scan size is $4\mu\text{m}\times 4\mu\text{m}$, d) schematic representations of bi-continuous-dispersed phase morphology with small droplets of black phase, e) FIB-AFM image of 10/30/60 HDPE/PS/PMMA showing bi-continuous/dispersed phase morphology with droplets of HDPE. Scan size is $11.7\mu\text{m}\times 11.7\mu\text{m}$, and f) SEM micrograph of 10/30/60 HDPE/PS/PMMA after extraction of PS. Small droplets of HDPE are distributed in PS

Note that in the schematics, black represents the HDPE phase, grey represents the PS phase and white represents the PMMA phase.

6.4.5 Triangular Composition/Morphology Diagram

Thirty different samples comprised of various compositions of HDPE/PS/PMMA (Figure 6-8a)) were prepared to better understand the composition dependence of the various morphological

states for complete wetting and their inter-conversion. The various morphological states observed are presented in Figures 6-8b) and 6-8c).

A triangular composition/morphology diagram (Figure 6-8c) was prepared. The sides of the triangle show the volume fraction of HDPE, PS, and PMMA phases ranging from 0% to 100%. The morphologies shown in Figures 6-8b) and 6-8c) will typically be observed in all ternary polymer blends demonstrating complete wetting. However, it should be noted that the boundaries between regions, as shown in Figure 6-8c), could also be influenced by the viscosity of the various phases and this point will be examined in future work. Figure 6-8c) demonstrates the concentration regimes for: a) tricontinuous blends of both type I and type II behavior (Cases I and II in Figure 6-8); b) matrix/separate dispersed phases with PS as matrix phase (Case III); bi-continuous/dispersed phase with HDPE as droplets (Case IV) or with PMMA as droplets (Case V); and matrix/core-shell either with PMMA as matrix (Case VI) or with HDPE as matrix (Case VII). These regions were detected by a combination of both SEM and FIB-AFM and through the use of selective extraction/gravimetric analysis as quantitative technique to detect inversion points.

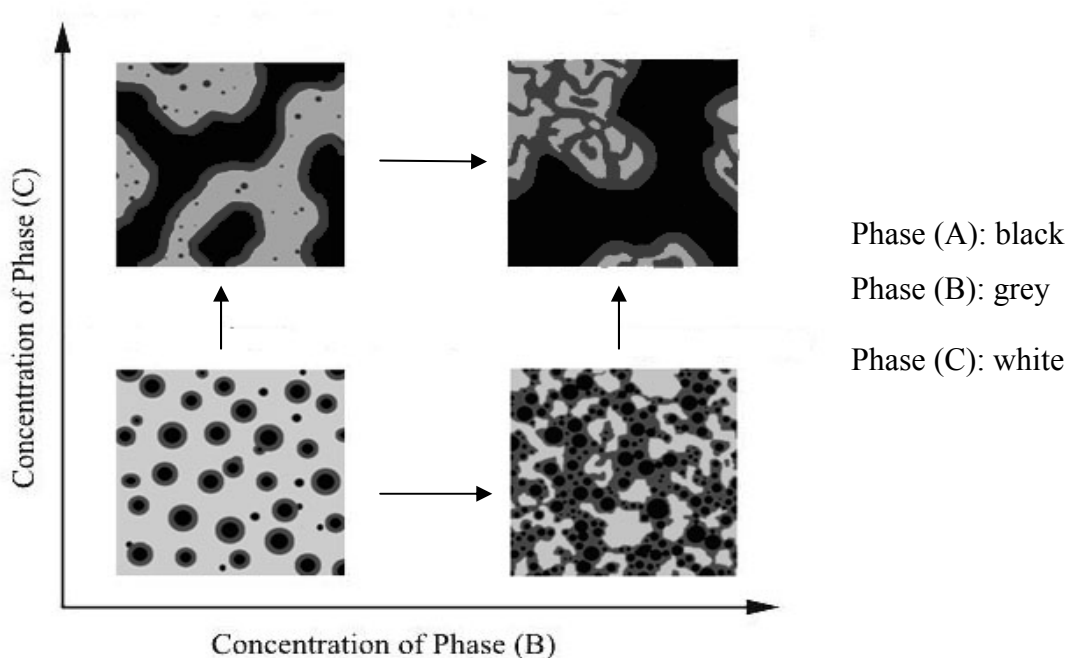
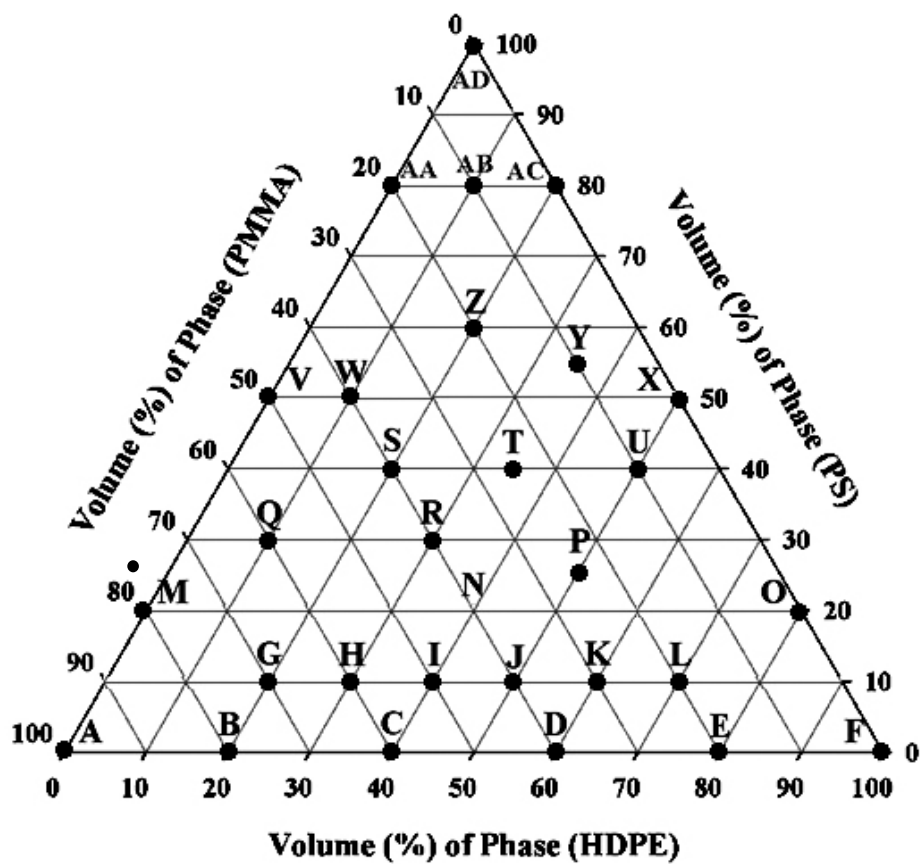
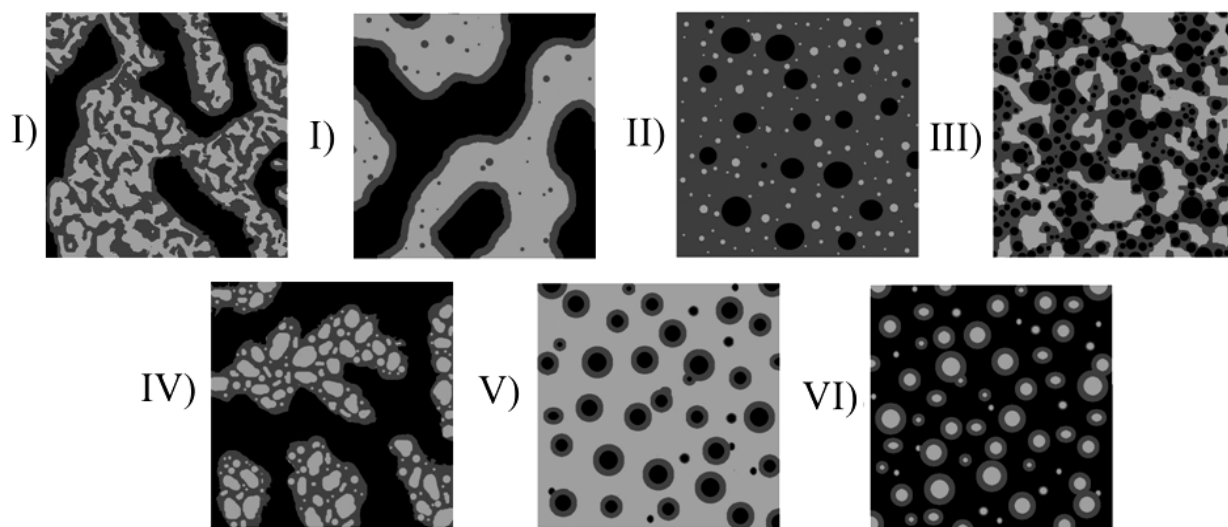


Figure 6-7: Evolution of the morphology in a ternary A/B/C blend demonstrating complete wetting as a function of the concentration of phases B and C. Phase A concentration is held constant.

a)



b)



HDPE : black

PS : grey

PMMA : white

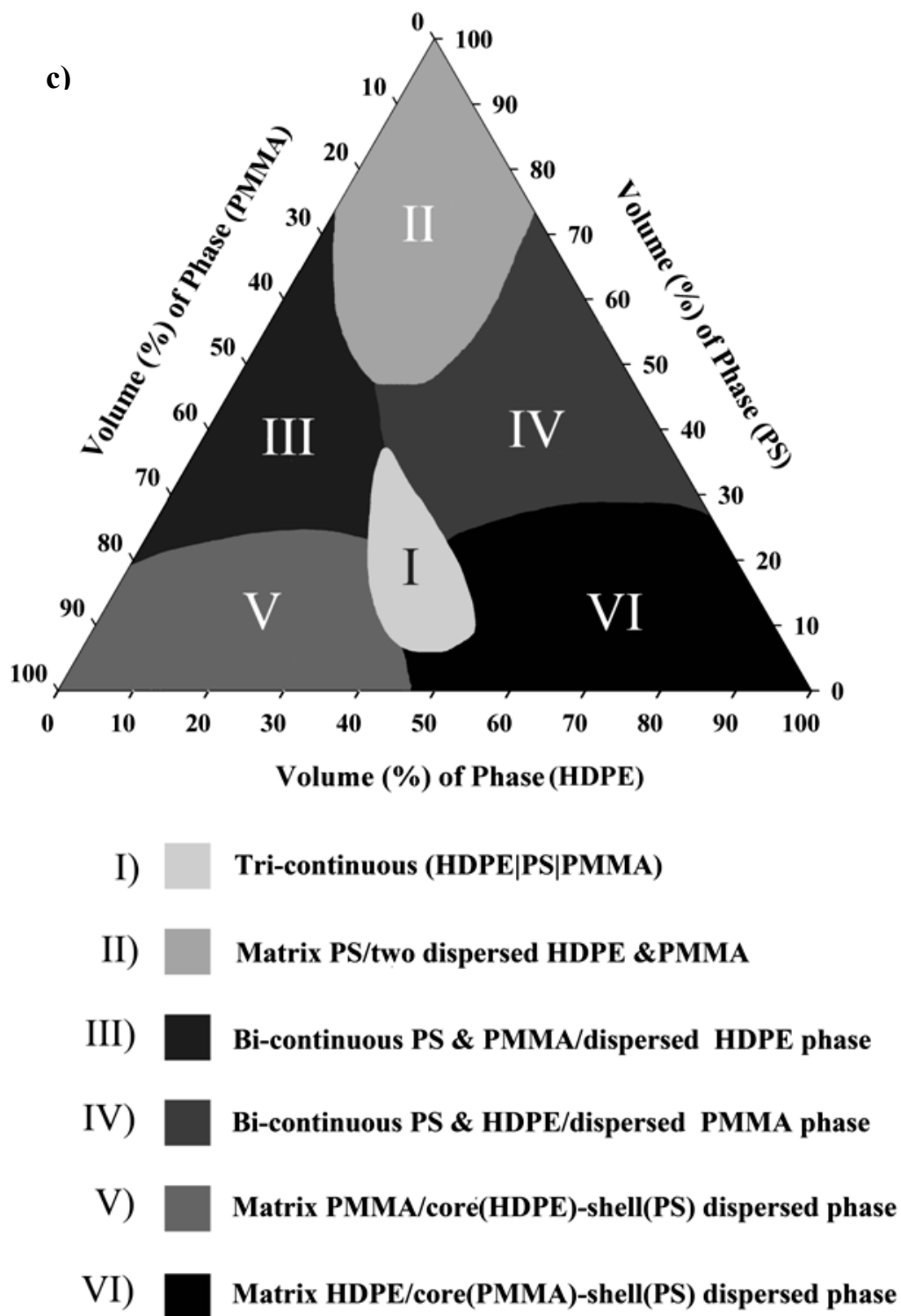


Figure 6-8. a) Triangular concentration diagram showing the composition of the various ternary HDPE/PS/PMMA blends examined in this study, b) various morphological states for ternary HDPE/PS/PMMA, and c) triangular concentration diagram showing the various regions of in the morphological states for ternary HDPE/PS/PMMA

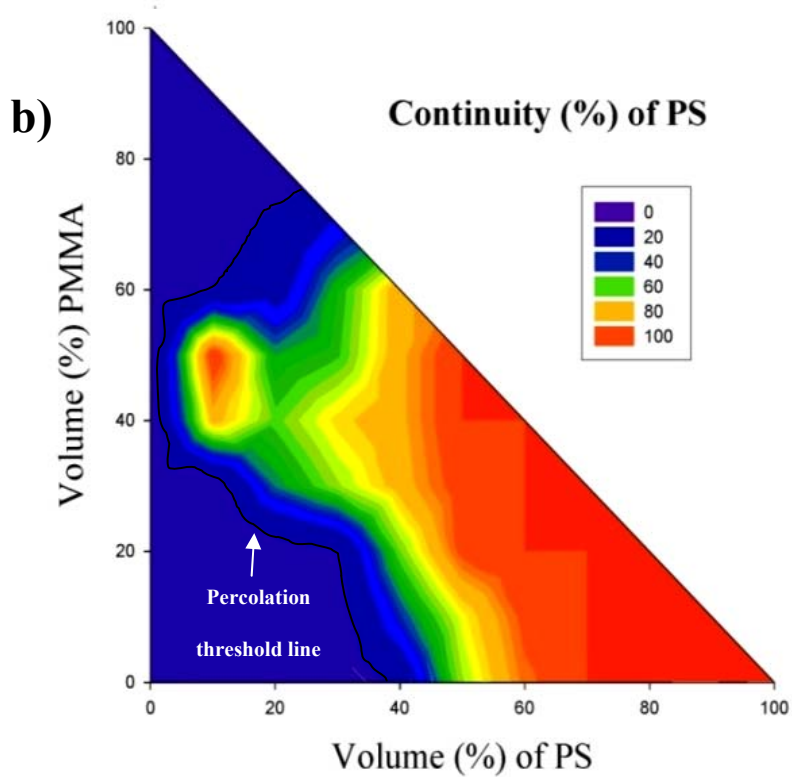
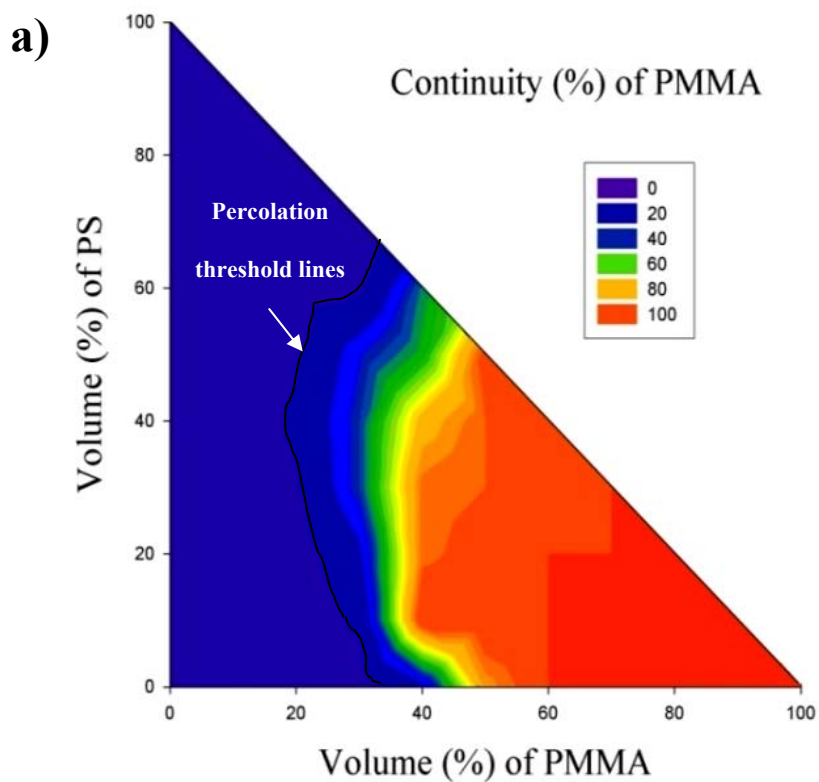
6.4.6 Continuity, Co-continuity, and Tri-continuity of Phases

One very important issue in the selection of a ternary blend for a particular application is the continuity level of each phase. In this part of the work the effect of the composition of phases on continuity levels is examined. The same 30 samples examined in the previous section above for morphology are also examined here for their quantitative PS and PMMA continuity. It was not possible to obtain the continuity of the HDPE phase since HDPE could not be selectively extracted. Triangular continuity plots are introduced (Figures 6-9a and 6-9b) to show the continuity of the PS and PMMA phases respectively. In this HDPE/PS/PMMA system, the continuity levels of PS and PMMA phases are identified through the selective solvent extraction/gravimetry of PMMA by acetic acid (Figure 6-9a) and of PS by cyclohexane (Figure 6-9b). The axes in Figures 6-9a and 6-9b represent the volume fraction of PMMA and PS. Note that the volume fraction of HDPE for these plots can be estimated by subtracting the combined volume fractions of PS and PMMA from 100%. For example, in the sample comprising 40% PS and 40% PMMA the remaining 20% would be HDPE. Figures 6-9a and 6-9b reveal the various continuity levels for both PS and PMMA in the ternary system. These diagrams show that increasing the concentration of phases results in increased continuity levels until that phase becomes the matrix and continuity achieves 100%. In Figure 6-9b there are two regions with a 100% continuity level of the PS phase representing tri-continuous morphologies type I (low PS concentration) and type II (high PS concentration).

In a binary blend the continuity percolation threshold is only one point. In a ternary blend it becomes a line due to the simultaneously changing concentration of two of the phases in the blend. The percolation threshold lines for PS and PMMA are represented in both Figures 6-9a and 6-9b where the colour changes from purple to blue.

The data from the continuity diagrams for PS and PMMA in Figures 6-9a) and 6-9b), can be combined with the morphological study shown in the triangular diagram of Figure 6-8c) in order to produce even more well defined continuity boundaries for the various morphological states. The new 3-axes triangular diagram is shown in Figure 6-9c). Since it is impossible to selectively extract HDPE without also extracting PS and PMMA, the upper border of region

IV cannot be accurately determined by quantitative continuity measurements and remains defined by morphological observation. All the various morphological states are presented.



c)

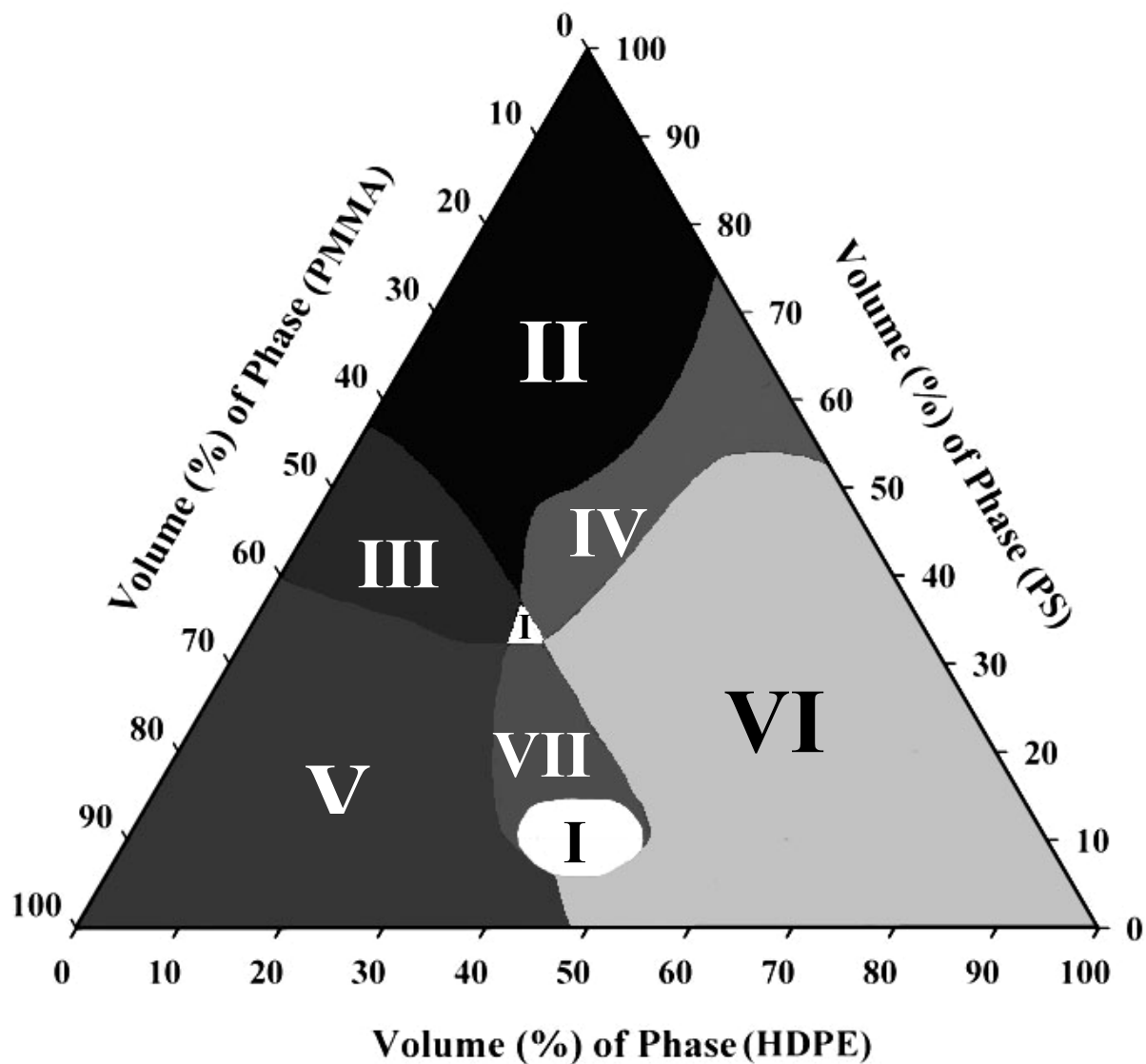


Figure 6-9. Continuity diagrams for ternary HDPE/PS/PMMA blends. a) quantitative continuity level of PMMA (percolation threshold line is shown in black), b) quantitative continuity level of PS (percolation threshold line is shown in black), and c) triangular concentration diagram showing the various regions of in the morphological states for ternary HDPE/PS/PMMA after correction with the PS and PMMA continuity data.

Region I is divided into two regions since in some parts of region I in Figure 6-8c, the continuity of the PS phase is lower than 80%(around 60%). This additional region of lower continuity is shown as region VII in Figure 6-9 and is termed the tricontinuous type I-type II *transition* region. It represents the case where there is a PS layer at the interface of HDPE and PMMA with numerous PS droplets within the PMMA.

6.4.7 Morphology Evolution due to Concentration Ratio of Two Components in Complete Wetting Case

Figure 6-10 indicates two compositional lines, or schemes, across the 3 axes triangular diagram which traverse multiple morphological states as shown in Figure 6-9c).

Scheme (a) in Figure 6-10 is the case where the PMMA concentration is held at 40% while the combined concentration of HDPE and PS is always held at 60%. This scheme allows one to study the morphology development of the PS phase in the ternary HDPE/PS/PMMA blend at different composition ratios of HDPE to PS. In scheme a, the effect of the concentration of the inner(HDPE) and middle(PS) phases on the morphology of the middle phase is examined. The morphology development is quantified and supported by the PS continuity data obtained via selective extraction/gravimetric measurements.

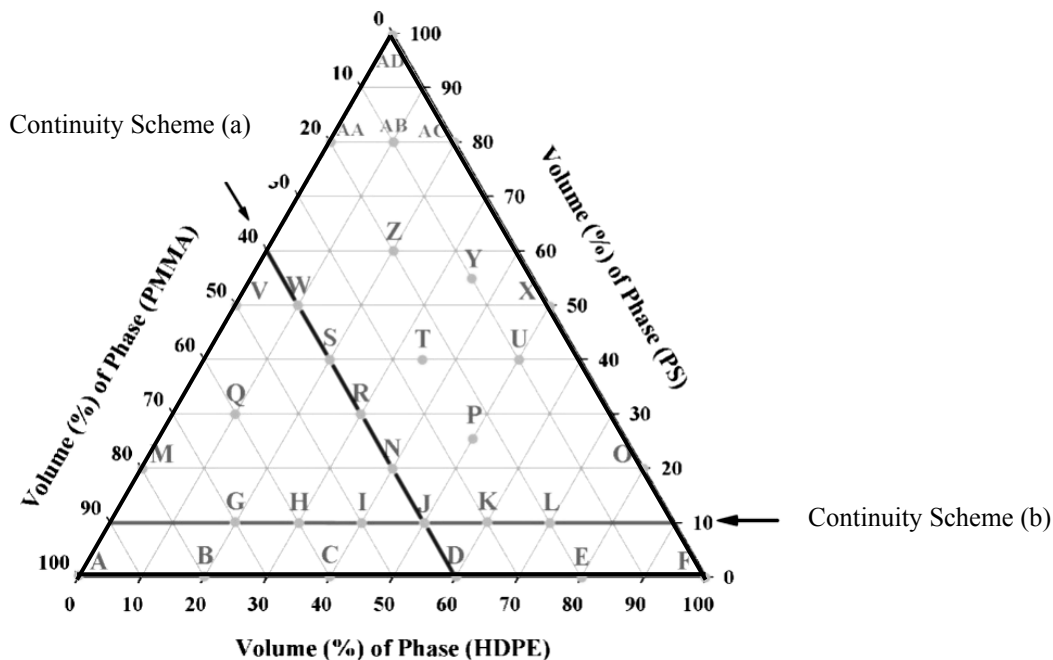


Figure 6-10. Triangular concentration diagram showing two pathways: Continuity Scheme (a), and Continuity Scheme (b). Scheme (a) is shown in Figure 6-11 and represents the case where the concentration of PMMA is kept constant at 40% of total while the concentration ratio of the PS and HDPE phases change. Scheme (b) is shown in Figure 6-12 where the concentration of PS is kept constant at 10% of total while the concentration ratio of PMMA and HDPE phases change. These two pathways were chosen since they pass through a range of different morphological states.

In Figure 6-11, the continuity of the PS phase following Scheme a is examined as a function of the % concentration of HDPE in (HDPE plus PS) where HDPE plus PS always equals 60% in the ternary blend with PMMA. Thus 100% HDPE refers to the 60%HDPE/40%PMMA blend while 50% HDPE in Figure 6-11 refers to the 30%HDPE/30%PS/40%PMMA blend. At 0% of HDPE a co-continuous morphology of 40/60 PMMA/PS is formed (point a in Figure 6-11).

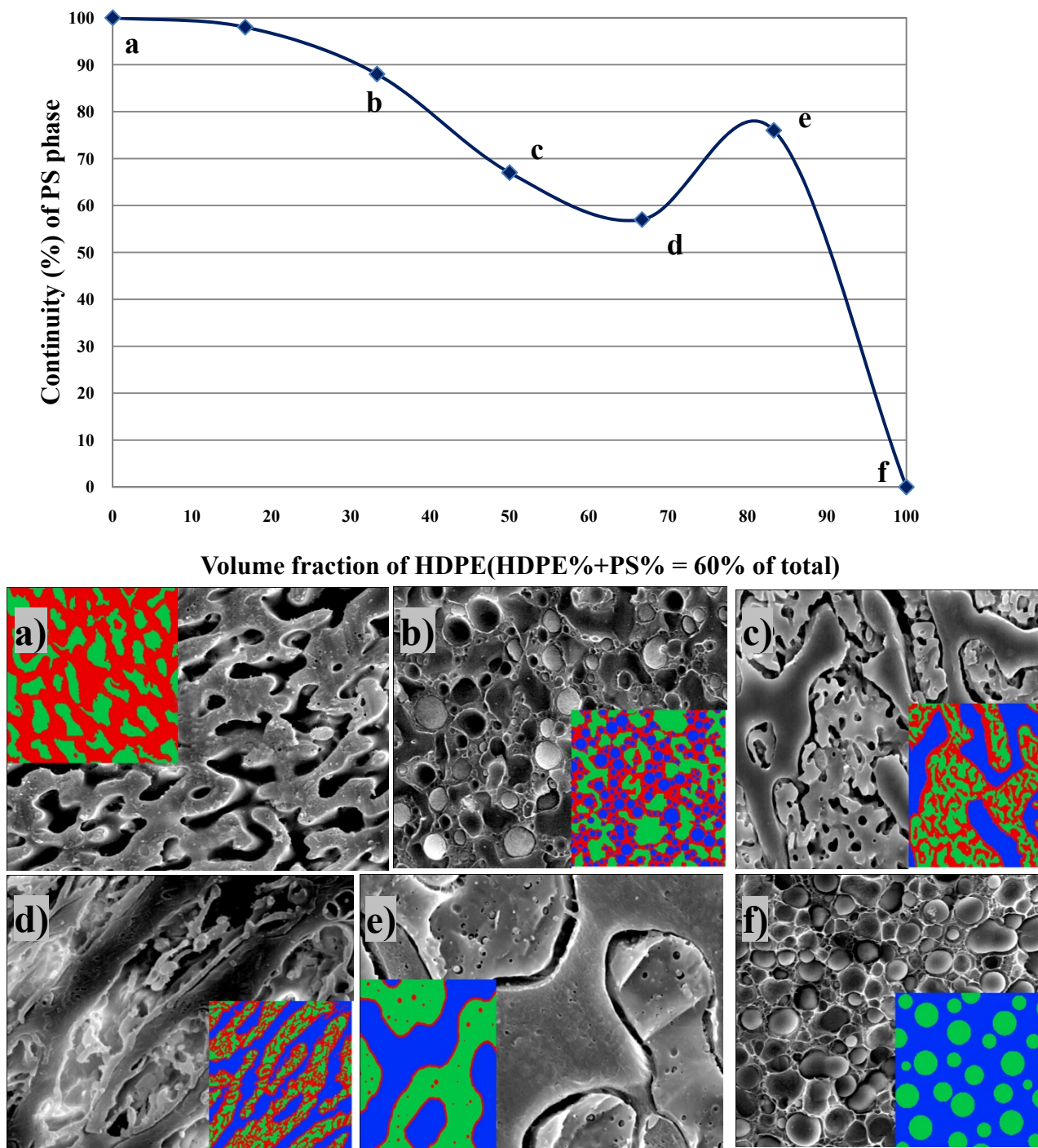


Figure 6-11. PS continuity and the corresponding morphology as a function of HDPE concentration following Scheme (a) from Figure 6-10. The PMMA phase concentration is held constant at 40% volume fraction in all samples. In the schematics, green is the PMMA phase, red is the PS phase and blue is the HDPE phase.

Addition of a low concentration of HDPE to the system leads to the encapsulation of HDPE droplets in a highly continuous PS network resulting in a bi-continuous/dispersed phase morphology and a slight reduction of PS continuity (point b in Figure 6-11). A further increase of HDPE phase generates a tri-continuous morphology (type II) where the coalescence of HDPE droplets forms a continuous phase of HDPE in highly continuous PS (point c in Figure 6-11). Note that at point c for the 30/30/40 HDPE/PS/PMMA blend, the continuity level of PS is lowered to 68%. Such a decrease in the continuity level is attributed to the entrapment of some parts of the PS phase in the PMMA network. Point d indicates the expected drop in continuity after the formation of the type I tri-continuous structure at point e. At point e, the 82% HDPE volume fraction corresponds to the 50/10/40 HDPE/PS/PMMA blend. This type I tri-continuous structure with a PS continuity of 76% represents the case where 50% HDPE and 40% PMMA form a co-continuous structure with a thin PS layer situated at the HDPE/PMMA interface. Finally, replacing all the PS with HDPE results in a (60%HDPE matrix/40%PMMA dispersed phase) blend (point f in Figure 6-11).

Local maximum continuity of 78% is obtained for 48/12/40 HDPE/PS/PMMA blend from Figure 6-11. The most important observation for scheme a, where the PMMA concentration is held at 40%, is that due to the thermodynamic limitations of spreading, the system is never able to form PS droplets even at a very low concentration of PS. PS always spreads between HDPE and PMMA in order to separate those two components. Thus even the smallest amount of PS in scheme a) presents a layer structure as opposed to droplets.

In scheme (b), from Figure 6-10, the concentration of the PS phase is kept constant at 10% volume fraction and the concentration ratio of the two other phases changes. In Figure 6-12, the continuity of the PS phase following Scheme b is examined as a function of the % concentration of HDPE in (HDPE plus PMMA) where HDPE plus PMMA always equals 90% in the ternary blend with PMMA. Thus, 100% HDPE refers to the 90%HDPE/10%PS blend, while 50% HDPE in Figure 6-12 refers to the 45%HDPE/10%PS/45%PMMA blend. This scheme allows for the study of the effect of the composition of the inner phase (HDPE) and the outer phase (PMMA) on the morphology of the middle phase (PS). It is interesting to note that in this case, the PS continuity curve is almost symmetric. At 0% HDPE, the continuity of PS is zero due to the presence of PS droplets within the matrix of PMMA (point a in Figure 6-12).

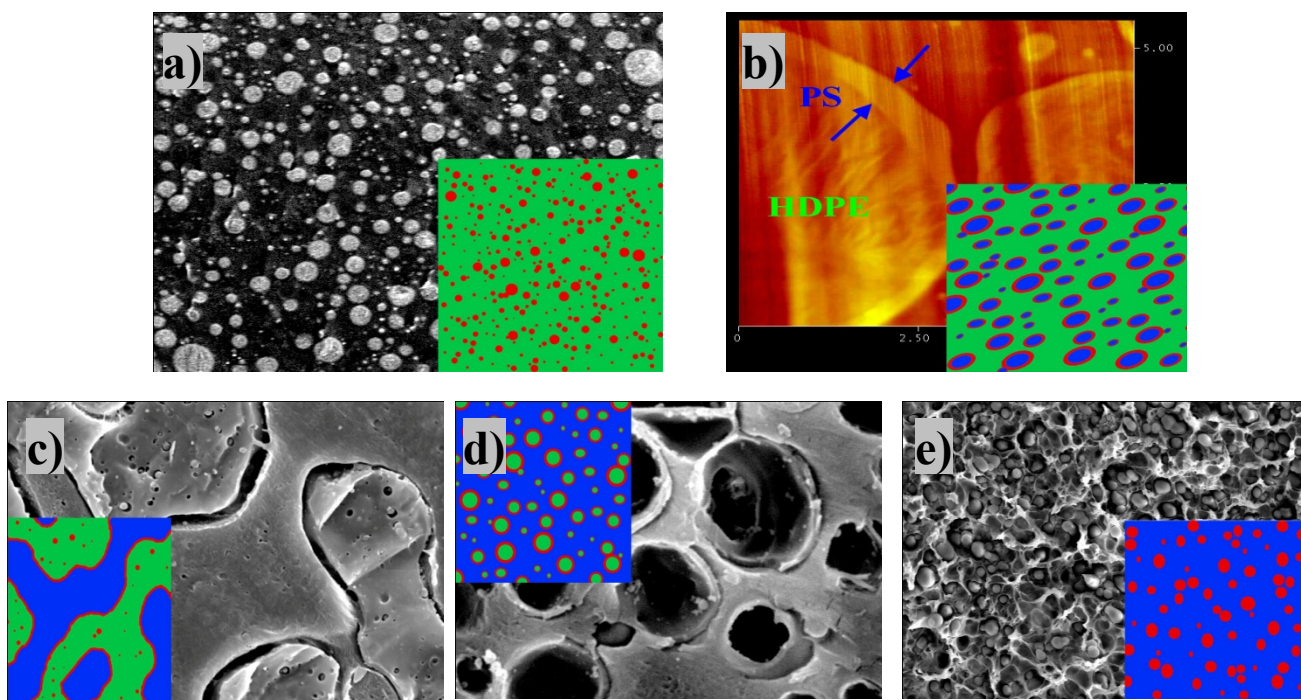
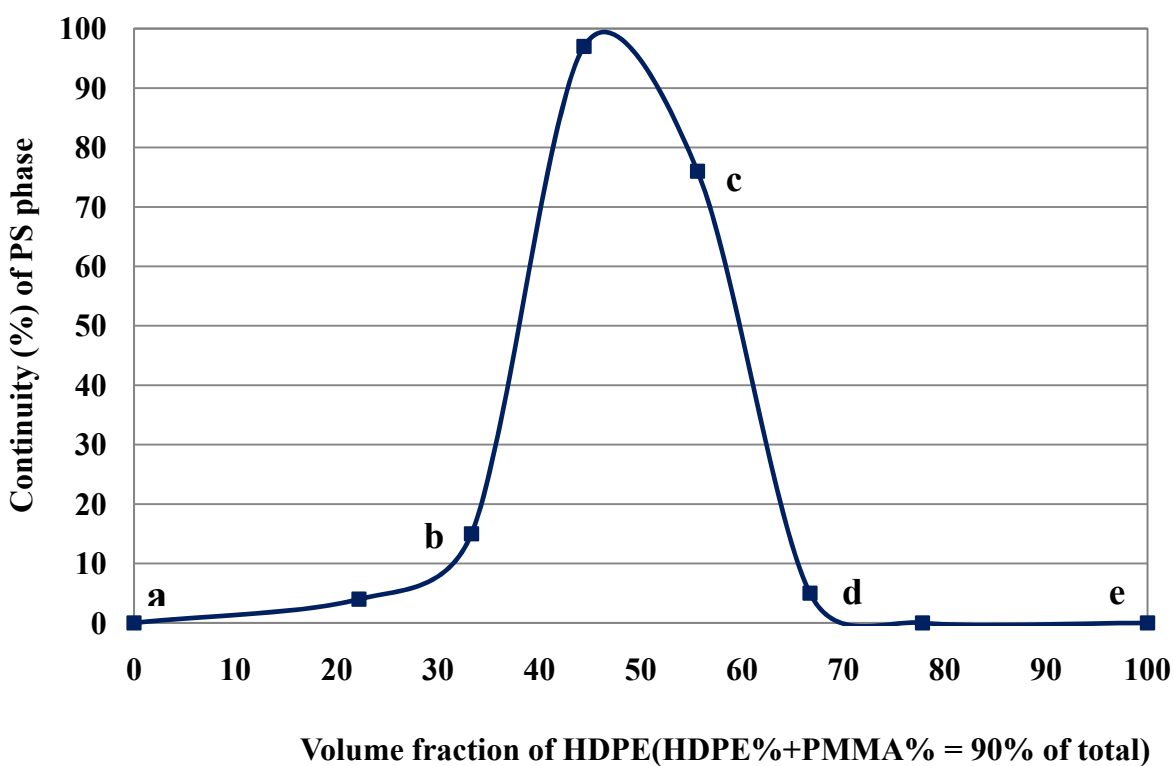


Figure 6-12. PS continuity and the corresponding morphology as a function of HDPE concentration following Scheme (b) from Figure 6-10. The PS phase concentration is held constant at 10% volume fraction in all samples. In the schematics, green is the PMMA phase, red is the PS phase and blue is the HDPE phase.

Addition of small amounts of HDPE to the binary blend of PS/PMMA results in a matrix/core-shell dispersed phase morphology where the PS is the shell and HDPE is the core (point b in Figure 6-12). Further increasing the concentration of HDPE leads to an increase in both the number of core-shell dispersions and the core volume. At 33% HDPE, the continuity data shows that HDPE forms its first connected pathway, the percolation threshold for HDPE. A further increase of HDPE to 44% results in the formation of a tri-continuous (type I) morphology as shown at point c where all phases, HDPE, PS and PMMA, are continuous. Figure 6-12 indicates that, at the peak of the continuity diagram, a perfectly uniform and continuous layer of 10%PS with a continuity of 97% situates at the interface of co-continuous HDPE and PMMA phases. In a previous paper (J. Zhang, et al., 2007) from this laboratory, a PS continuity level of 69% was observed for a 3%PS/50%HDPE/47%PMMA blend. Figure 6-12 suggests that the maximum continuity for PS is obtained at a blend concentration of 10PS/43HDPE/47PMMA. Further increasing the quantity of HDPE at point d, results in droplets of PMMA encapsulated in PS shells. Finally, at 100%HDPE a matrix/droplet morphology of 90/10 HDPE/PS is observed (point e in Figure 6-12).

6.4.8 Observations on the Effect of Viscosity on the Morphological State

It is well known that the viscosity ratio can have a significant effect on both the size and shape of dispersed phases in a polymer blend (B. D. Favis, 2000). In this section it will be shown that extreme changes in the viscosity of the PMMA phase (L-PMMA and H-PMMA) in a HDPE/PS/PMMA blend of constant composition still results in morphological structures where the PS separates HDPE and PMMA. Note that L-PMMA is the same PMMA used in all the rest of this work. The viscosity of high molecular weight PMMA used here is almost 200 times that of the viscosity of low molecular weight PMMA leading to a huge corresponding increase in the PS/PMMA viscosity ratio. Two ternary blends comprised of 35/40/25 HDPE/PS/L-PMMA and 35/40/25 HDPE/PS/H-PMMA are prepared and the resulting morphology is shown in Figure 6-13. Both blends using low molecular weight PMMA and high molecular weight PMMA demonstrate a bi-continuous/PMMA droplet morphology, Figures 6-13a and 6-13b show that the L-PMMA phase is present as numerous small droplets encapsulated in PS. In Figure 6-13a the L-

PMMA is selectively extracted while in Figure 6-13b, only the PS is extracted. The micrographs clearly show a bicontinuous morphology of HDPE and PS with L-PMMA dispersed as droplets in the PS phase. PS separates the HDPE and L-PMMA. In this case, PS interpenetrates into the L-PMMA phase rather than the HDPE phase due to lower interfacial tension of PS/PMMA and the low viscosity of the L-PMMA.

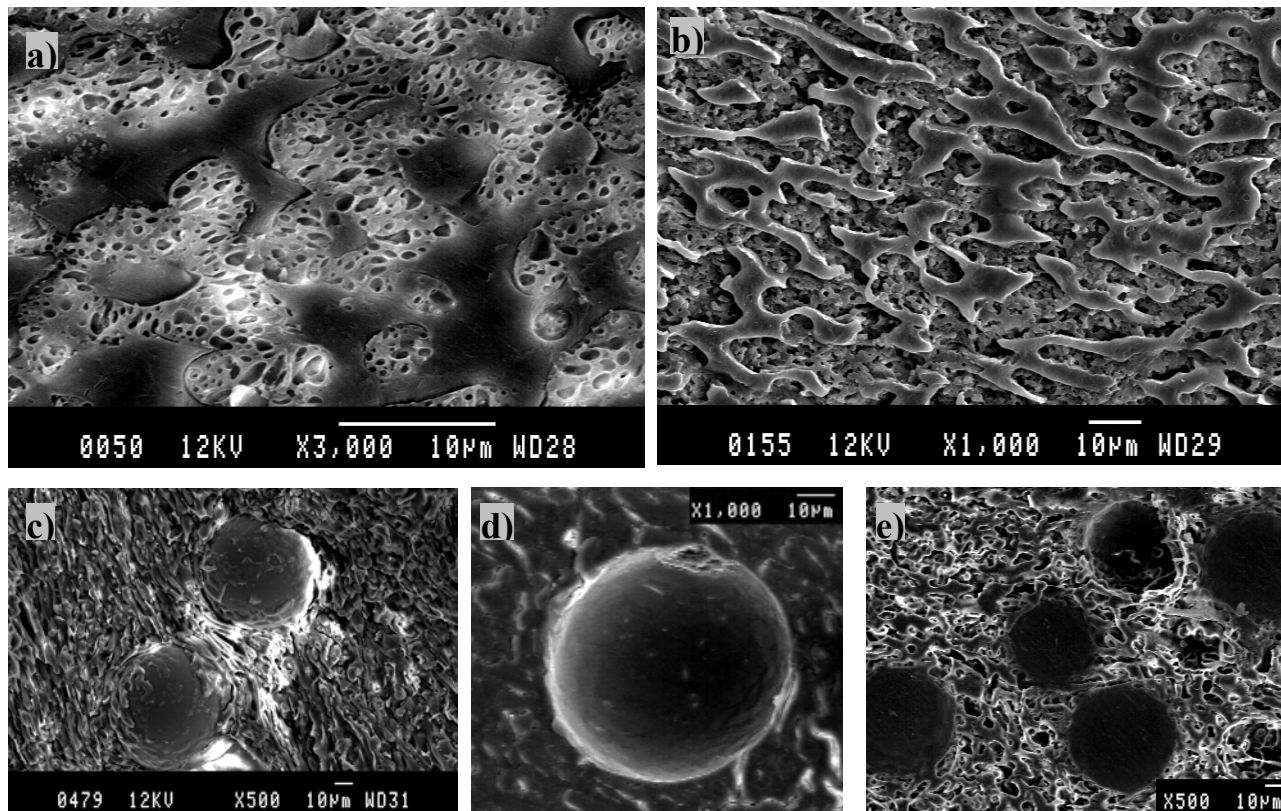


Figure 6-13. SEM micrograph of morphology of (a) 35/40/25 HDPE/PS/L-PMMA after extraction of L-PMMA by acetic acid, (b) 35/40/25 HDPE/PS/L-PMMA after extraction of PS by cyclohexane, (c) 35/40/25 HDPE/PS/H-PMMA(cryofracture), (d) 35/40/25 HDPE/PS/H-PMMA after extraction of PMMA by acetic acid, and (e) 35/40/25 HDPE/PS/H-PMMA after extraction of PS by cyclohexane,

In Figures 6-13c) and d), H-PMMA is used instead of L-PMMA and the PS is selectively extracted to indicate its position. In that case, H-PMMA is present as a few large droplets encapsulated in thin PS shells(see Figure 6-13c). Figure 6-13d) shows that the PS forms a

bicontinuous network with the HDPE. Thus, in both the L-PMMA case and the H-PMMA case, the morphological classification of bicontinuous/dispersed PMMA phase is unchanged. Nevertheless, the scale of the resulting morphological structures has been significantly modified by the viscosity of the PMMA as the system attempts to respond to the dramatically reduced interfacial area of the H-PMMA droplets. In addition, it is more difficult for the PS to penetrate the H-PMMA (as compared to L-PMMA) due to its significantly higher viscosity. Thus, the use of H-PMMA results in a significant increase in the interfacial area between HDPE and PS phases. A comparison of the thickness of the continuous HDPE branches in the L-PMMA blend as compared to that in the H-PMMA blend clearly show that the HDPE branches are significantly thicker in the L-PMMA case. This unambiguously supports the conclusion of an increased HDPE/PS interfacial area for the H-PMMA blend.

The surface free energy for a blend system is given by the following equation:

Equation 6-3
$$G = \sum \gamma_{ij} A_{ij}$$

where G is the Gibbs free energy, γ_{ij} represents the interfacial tension between phases i and j , and A_{ij} is the interfacial area between phases i and j . Since the system is unable to dissipate the applied mechanical energy applied during mixing by generating a high interfacial area between H-PMMA and PS, it must compensate by generating an increased interfacial area between the HDPE and PS phases (Figure 6-13g).

6.4.9 Factors Influencing Phase Sizes

It is well known that the composition, interfacial tension, and viscosity ratio are three of the most important factors influencing the phase size in binary polymer blends (A. K. Gupta, 1993; Guo, Packirisamy, et al., 1997; Hobbs, et al., 1988; Nemirovski, et al., 1995). It will be shown in this section that these factors also play an important role in determining the phase size in ternary polymer blends.

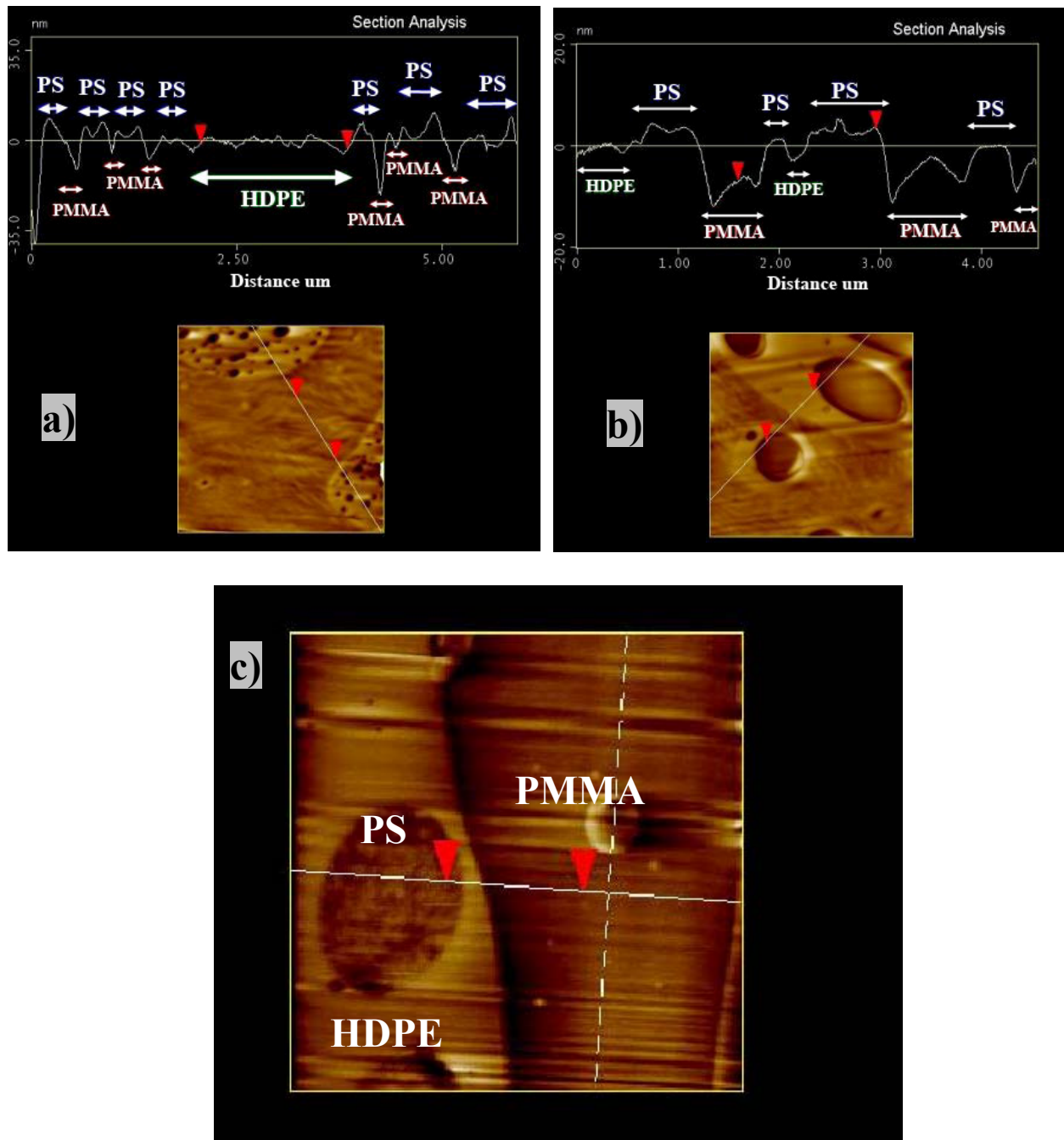


Figure 6-14. FIB-AFM topographic surface image of HDPE/PS/PMMA at various compositions, (a) 50/40/10, (b) 50/25/25, and (c) 10/30/60. The white lines in the images indicate the sections analyzed for each blend.

Three examples are shown in Figure 6-14: 50/40/10 HDPE/PS/PMMA, 10/30/60 HDPE/PS/PMMA, and 50/25/25 HDPE/PS/PMMA. PMMA has a much lower viscosity than PS which has a lower viscosity than HDPE. Also, the PS/PMMA interfacial tension is much lower than the PS/HDPE or PMMA/HDPE one (see Table 6-2). In the case of 50/40/10 HDPE/PS/PMMA(Figure 6-14a), the PMMA phase is at a low concentration (10%), low PMMA/PS viscosity ratio and a low PMMA/PS interfacial tension (see Tables 6-1 and 6-2). It can be seen that the PMMA is distributed in the PS phase as numerous small PMMA droplets leading to high interfacial area between PS/PMMA. In that same sample, PS and HDPE form a co-continuous structure. The FIB/AFM micrographs allow for a clear identification of the small PMMA droplet phases in the PS. The topographical heights following the trace line show the short interval between PS and PMMA phases and the long interval for the HDPE phase. In the ternary 50/25/25 HDPE/PS/PMMA blend, the increased concentration of PMMA results in the coalescence of PMMA droplets resulting in the formation of large PMMA droplets. In the case of the ternary blend comprised of 10/30/60 HDPE/PS/PMMA large droplets of HDPE are observed in the PS phase while PS and PMMA comprise a co-continuous structure(Figure 6-14c). These results are consistent with the low viscosity ratio and interfacial tension of PS/PMMA and high viscosity ratio and interfacial tension of HDPE/PS.

6.5 Conclusions

Complete wetting in a ternary polymer blend is an interfacial tension driven state where one of the components will always tend to completely separate the other two. It occurs when one of the three possible binary spreading coefficients in the system has a positive value, as defined by Harkins spreading theory. This work examines the complete range of morphological states possible for such a system over the entire ternary composition diagram as prepared by melt mixing. High-density polyethylene(HDPE), polystyrene(PS), and poly(methyl methacrylate)(PMMA) are selected as a model system showing a positive spreading coefficient of PS over PMMA, thus in all cases the PS phase separates HDPE and PMMA. Four sub-categories of morphologies can be identified, depending on the composition of phases, including: a) matrix/core-shell dispersed phase; b) tri-continuous; c) bi-continuous/dispersed phase;, and d)

matrix/two separate dispersed phases morphologies. The phases in these sub-morphologies are identified and illustrated qualitatively by electron microscopy as well as a technique based on the combination of focused ion beam irradiation and atomic force microscopy. Both qualitative and quantitative data are shown in triangular compositional diagrams to distinguish these various morphological regions and the results are interpreted in light of the interfacial tension of the various binary combinations and their subsequent spreading coefficients. Solvent extraction/gravimetry is used as quantitative experiment to confirm the morphological observations and to examine the extent of continuity of the systems so as to effectively identify regions of high continuity. It is shown that the viscosity of the phases can have a significant influence on the interfacial area generated between the phases in the blend system, but does not effect the classification or type of morphological state which appears to be governed solely by spreading theory.

6.6 Acknowledgement

The authors express appreciation to the Natural Sciences and Engineering Research Council of Canada for supporting this work.

6.7 References

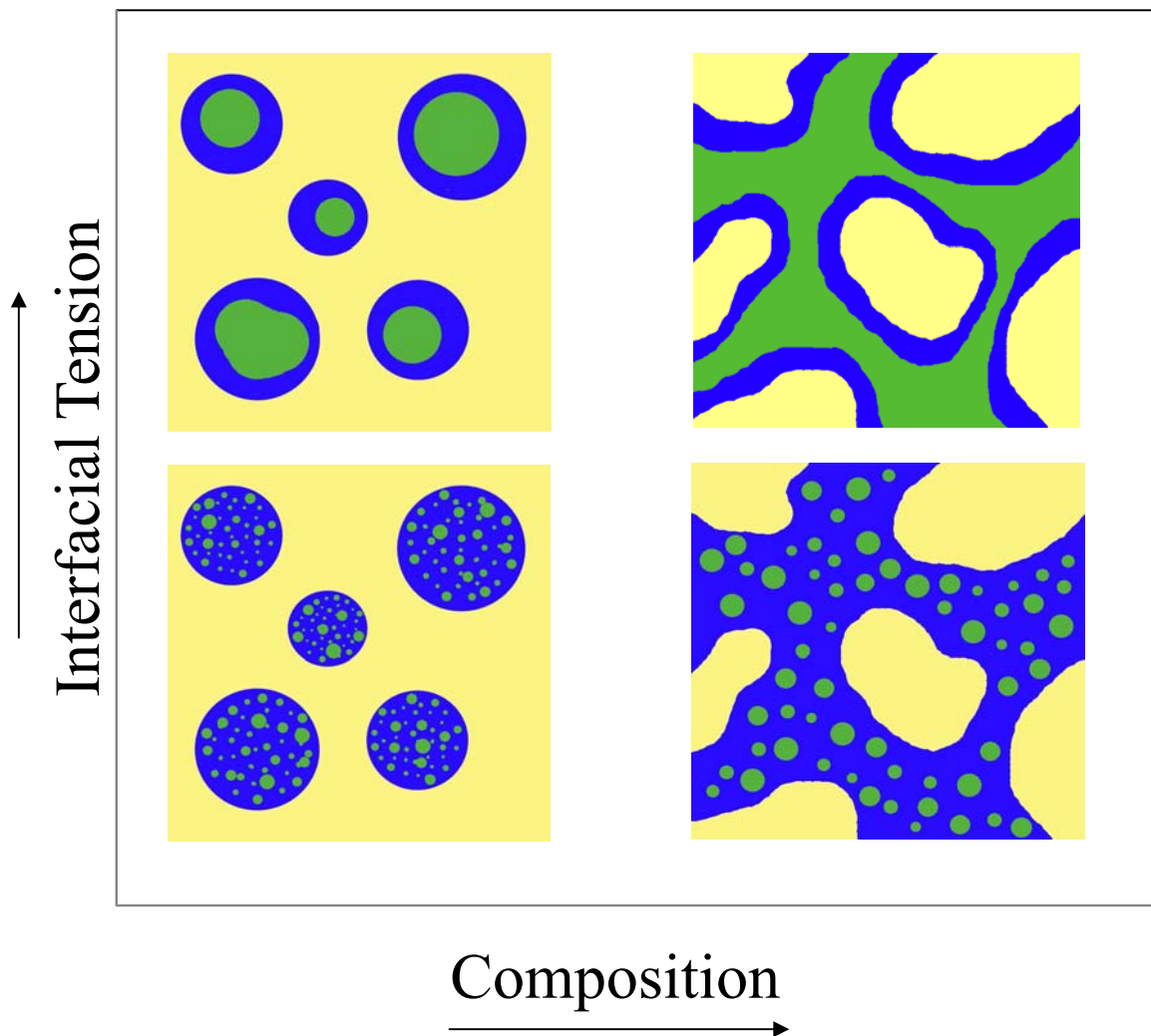
- (1) Paul, D.; Newman, S. *Polymer Blends*; Academic Press: New York, 1978; Vol. 1, 2.
- (2) Utracki, L. A. *Commercial Polymer Blends* Springer - Verlag, 1998.
- (3) Favis, B. D. In *Polymer Blends: Formulation and Performance, Two-Volume Set*; Paul, D. R., Bucknall, C. B., Eds.; John Wiley & Sons, Inc: New York, 2000; Vol. 1, p 239.
- (4) Potschke, P.; Paul, D. R. *Journal of Macromolecular Science - Polymer Reviews* **2003**, *43*, 87.
- (5) Molau, G. E.; Keskkula, H. *Journal of Polymer Science Part A-1: Polymer Chemistry* **1966**, *4*, 1595.
- (6) Reignier, J.; Favis, B. D. *Macromolecules* **2000**, *33*, 6998.
- (7) Scher, H.; Zallen, R. *The Journal of Chemical Physics* **1970**, *53*, 3759.
- (8) Jordhamo, G. M.; Manson, J. A.; Sperling, L. H. *Polymer Engineering and Science* **1986**, *26*, 517.

- (9) Mekhilef, N.; Verhoogt, H. *Polymer* **1996**, *37*, 4069.
- (10) Reignier, J.; Favis, B. D.; Heuzey, M.-C. *Polymer* **2003**, *44*, 49.
- (11) Zhang, J.; Ravati, S.; Virgilio, N.; Favis, B. D. *Macromolecules* **2007**, *40*, 8817.
- (12) Torza, S.; Mason, S. G. *Journal of Colloid and Interface Science* **1970**, *33*, 67.
- (13) Virgilio, N.; Marc-Aurele, C.; Favis, B. D. *Macromolecules* **2009**, *42*, 3405.
- (14) Harkins, W. D.; Feldman, A. *Journal of the American Chemical Society* **1922**, *44*, 2665.
- (15) Torza, S.; Mason, S. G. *J. Coll. Interface Sci.* **1970**, *33*, 67.
- (16) Hobbs, S. Y.; Dekkers, M. E. J.; Watkins, V. H. *Polymer* **1988**, *29*, 1598.
- (17) Guo, H. F.; Gvozdic, N. V.; Meier, D. J. *Polymer* **1997**, *38*, 4915.
- (18) Guo, H. F.; Packirisamy, S.; Gvozdic, N. V.; Meier, D. J. *Polymer* **1997**, *38*, 785.
- (19) A. K. Gupta, K. R. S. *Journal of Applied Polymer Science* **1993**, *47*, 167.
- (20) Nemirovski, N.; Siegmann, A.; Narkis, M. *Journal of Macromolecular Science - Physics* **1995**, *B34*, 459.
- (21) Luzinov, I.; Pagnouille, C.; Jerome, R. *Polymer* **2000**, *41*, 7099.
- (22) Tchomakov, K. P.; Favis, B. D.; Huneault, M. A.; Champagne, M. F.; Tofan, F. *Polymer Engineering and Science* **2004**, *44*, 749.
- (23) Vanoene, H. *Journal of Colloid and Interface Science* **1972**, *40*, 448.
- (24) Legros, A.; Carreau, P. J.; Favis, B. D.; Michel, A. *Polymer* **1997**, *38*, 5085.
- (25) Virgilio, N.; Favis, B. D.; Pepin, M.-F.; Desjardins, P.; L'Esperance, G. *Macromolecules* **2005**, *38*, 2368.
- (26) Reignier, J.; Favis, B. D. *Polymer* **2003**, *44*, 5061.
- (27) Reignier, J.; Favis, B. D. *AIChE Journal* **2003**, *49*, 1014.
- (28) Favis, B. D. In *Polymer Blends: Formulation and Performance*; Paul, D. R., Bucknall, C. B., Eds.; John Wiley & Sons: John Wiley & Sons, 2000; Vol. I, p 239.

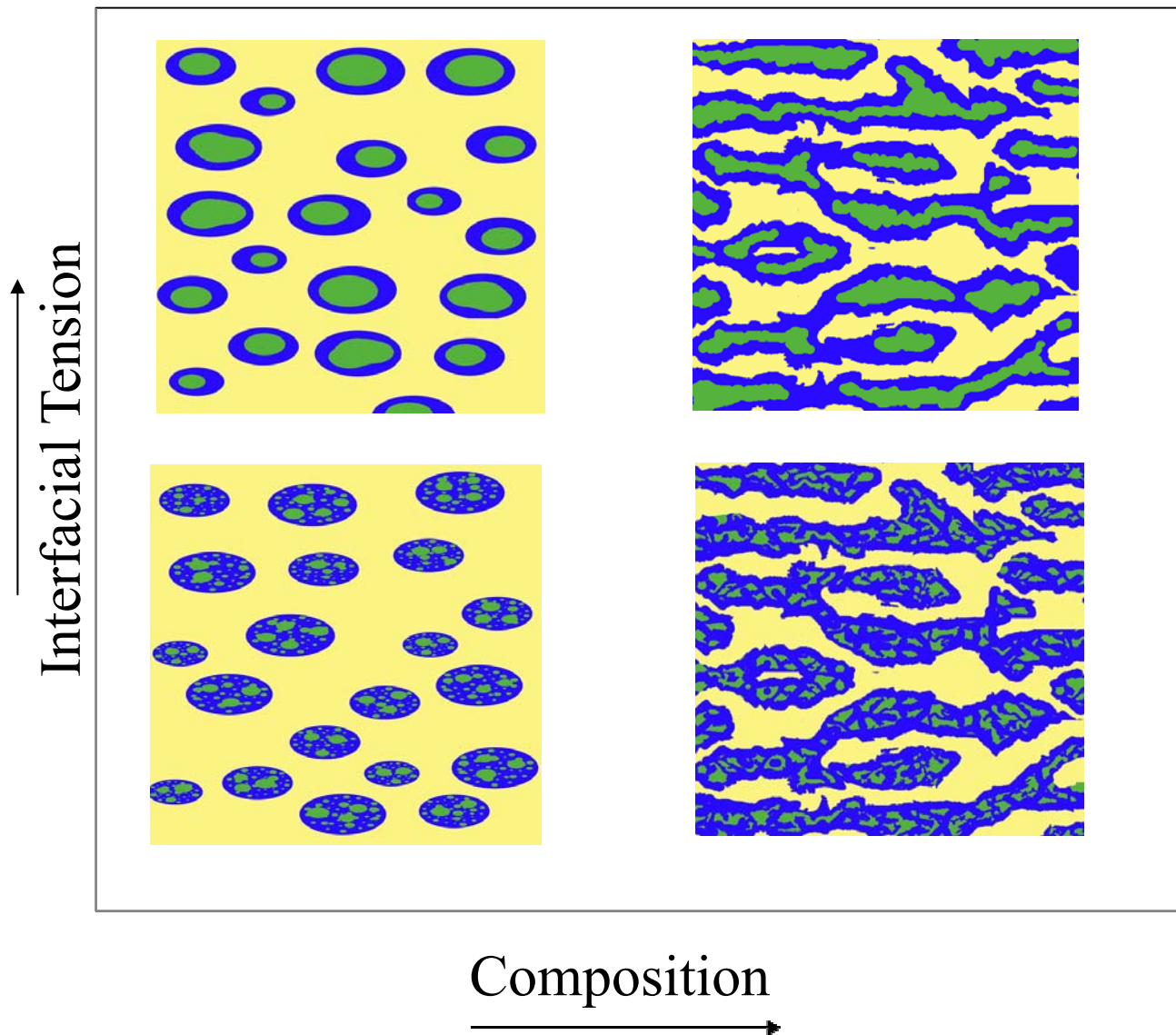
CHAPTER 7 - GENERAL DISCUSSIONS AND PERSPECTIVE

In the previous chapters, it was shown that a hierarchically ordered, interfacial tension driven morphology can be assembled. In this multiple-percolated structure, thermodynamic properties can determine the number of interfaces between phases (the number of contacts between phases). In the next perspective of the work the influence of viscous forces on the morphology by changing the shape and size of the phases can be studied. For example, by increasing the shear stress in a bi-continuous/dispersed phase morphology, the size of the droplets should be decreased due to the increasing breakup rate as compared to coalescence. Moreover, due to the higher shear force, the shape of the droplets may also become more elongated. Therefore, changing the applied shear stress on the system would be expected to result mostly in the variation of the size and shape of the phases. Changing the hierarchical order of phases in the blend, which depends significantly on the thermodynamic properties of the system, is almost impossible. It is well-known that the third factor affecting the morphology of multi-component blends is the composition of phases. This factor affects the morphology by imposing a geometrical restriction between phases and controls the rate of breakup and coalescence. At high concentration of one phase the droplets of that phase coalesce further with each other and therefore the rate of coalescence increases until a continuous structure is constructed. For blends comprised of more than three components, composition can also play a role in the prediction of the phase morphology. Thermodynamics plays another role in the morphology of ternary blends through the governing Harkins equation and the prediction of three-phase contact and two-phase contact morphologies as mentioned in detail in chapter 6. In both cases of complete and partial wetting, a high interfacial tension between phases results in a decrease of the interfacial area between them leading to larger phase sizes. All the effects of these three parameters (composition, interfacial tension, and shear stress) are schematically shown for a complete wetting case of a ternary blend in Figures 7-1 and 7-2. Figures 7-1 and 7-2 illustrate various morphologies of a blend with a matrix of phase (A) depending on the interfacial tension of B/C and the composition of phases B and C at low shear rate and high shear rate, respectively. It is shown that at low concentration of minor phases, a matrix/core-shell morphology is observed. At higher concentration of minor phases, tri-continuous and bi-continuous/dispersed

structures are formed due to the coalescence of droplets. At low interfacial tension of B/C the interfacial area between these phases increases and small droplets of phase (C) are dispersed in phase (B). For the case of a high interfacial tension of B/C, the droplets coalesce with each other and large droplets or a continuous structure of that phase is observed. Finally the effect of shear rate is shown and at low shear rate, the shape of the phases are more regular and the phase sizes are larger due to the higher capillary number. At high shear rate, the structures become more elongated and the number of composite droplets and continuous islands increase due to the smaller size of the phases.



Equation 7-1. Dependence of the morphology of a ternary blend demonstrating complete wetting on the interfacial tension of B and C and as a function of the composition of Phases B and C at low shear rate. Note that in the schematics, yellow represents phase (A) which is the matrix, blue represents phase (B) and green represents phase (C).



Equation 7-2. Dependence of the morphology of a ternary blend demonstrating complete wetting on the interfacial tension of B and C and as a function of the composition of Phases B and C at high shear rate. Note that in the schematics, yellow represents phase (A) which is the matrix, blue represents phase (B) and green represents phase (C).

CONCLUSION AND RECOMMENDATIONS

In this dissertation, we developed the phase morphology of multi-component blends via melt-processing, assisted by solvent etching, in order to generate novel conductive devices with an ultra-low percolation threshold. This thesis evaluates and develops continuity evolution in co-continuous, double-percolated, triple-percolated, and quadruple-percolated morphologies to find a way to considerably reduce the percolation threshold of all phases in the blend.

In order to achieve the aforementioned objective (reducing the percolation threshold of the conductive polymer and other phases), a comprehensive systematic study on binary, ternary, quaternary, and quinary blends with particular complete wetting morphology is investigated for the first time. In this case, reduction of the continuity and/or electrical percolation threshold of phases, particularly of a conductive polymer, is carried out by developing the novel and original structures defined as multi-percolated structures. These special structures are constituted of hierarchically ordered self-assembled continuous phases in polymer blends. Since the first condition for the preparation of hierarchically ordered phase structures in a multi-component blend is satisfying all Harkins equation sets, based on the various interfacial tensions for the polymer pairs in the blend, the components must be precisely selected to meet the condition. For this reason, polyaniline and four other commercial polymers with specific surface tensions, polarities and interfacial tensions are precisely selected. The interfacial tensions between the various components range from 1 mN/m for PVDF/PMMA to 26.9 mN/m for PANI/HDPE. Morphological sample characterization is performed by both SEM and FIB-AFM techniques. The polymer blends are prepared in a melt-blending process in an internal mixer at 50 rpm for 8 min at 200°C. Selective solvent extraction of phases either assists in better detection of phases in order to collect qualitative data, or is employed to produce porous samples. A combination of FIB treatment and AFM technique allows us to clearly distinguish the phases based on the topographical contrast formed by the difference in the FIB etching rate of materials. In order to study the effect of viscosity ratio on the ternary blends, both low molecular weight and high molecular weight poly(methyl methacrylate) are selected.

In this thesis, fundamental studies are developed as models to prepare novel morphologies such as onion morphology and multi-percolated morphologies. By employing a melt-processable

conductive polymer, the applicability of these original morphologies is confirmed mostly by conductivity results. It is shown that the order of phases in a complete wetting case such as a multi-percolated structure is dependent only on the thermodynamic properties; although viscosity and composition of phases play a major role in the determination of the morphology, they do not change the order of phases. In this case, addition of the copolymer of adjacent phases in a multi-percolated structure induces a reduction in the phase size of the other phases, lowering the percolation threshold of phases, which leads to higher conductivity of the samples. Though the order of phases in multi-percolated structures is determined by the interfacial tension between phases, it is shown that the viscosity of phases significantly influences the distribution of interfacial energy between phases, and ultimately, the morphology.

It is shown that fully interconnected porous materials are prepared via the production of a multi-percolated structure followed by selective phase extraction. These porogens are used as substrates for alternate deposition of PSS and PANI. A detailed study on the behaviour of polyelectrolytes in the deposition process is carried out.

This thesis presents a systematic technique for study and prediction the morphology of quaternary and quinary blends. To date, there is no theory for prediction of the morphology and order of the phases in hierarchical self-assembled systems prepared by melt-blending. This is the first study which begins to develop some mechanism and methods to predict the morphology of multi-component blends.

REFERENCES

- A. K. Gupta, K. R. S. (1993). Melt rheology and morphology of PP/SEBS/PC ternary blend. *Journal of Applied Polymer Science*, 47(1), 167-184.
- Adjari, A., Brochard-Wyart, F., de Gennes, P.-G., Leibler, L., Viovy, J.-L., & Rubinstein, M. (1994). Slippage of an entangled polymer melt on a grafted surface. *Physica A: Statistical Mechanics and its Applications*, 204(1-4), 17-39.
- Al-Saleh, M. H., & Sundararaj, U. (2008). An innovative method to reduce percolation threshold of carbon black filled immiscible polymer blends. *Composites Part A: Applied Science and Manufacturing*, 39(Copyright 2008, The Institution of Engineering and Technology), 284-293.
- Alexander, S. (1977). Polymer adsorption on small spheres. A scaling approach *Journal de Physique (Paris)*, 38(8), 977-981.
- Anand, J., Palaniappan, S., & Sathyanarayana, D. N. (1998). Conducting polyaniline blends and composites. *Progress in Polymer Science (Oxford)*, 23(6), 993-1018.
- Andreatta, A., Cao, Y., Chiang, J. C., Heeger, A. J., & Smith, P. (1988). Electrically-conductive fibers of polyaniline spun from solutions in concentrated sulfuric acid. *Synthetic Metals*, 26(4), 383-389.
- Angappane, S., Rajeev Kini, N., Natarajan, T. S., Rangarajan, G., & Wessling, B. (2002). *PAni-PMMA blend/metal Schottky barriers*, Singapore, Singapore.
- Antonoff, G. (1942). On the Validity of Antonoff's Rule. *The Journal of Physical Chemistry*, 46(4), 497-499.
- Antonoff, G. N. (1907). *J Chim Phys* 5, 364-371.
- Avgeropoulos, G. N., Weissert, F. C., Biddison, P. H., & Boehm, G. G. A. (1976). Hetrogeneous Blends of Polymers Rheology and Morphology. *Rubber Chemistry and Technology*, 49(1), 93-104.
- Baba, A., Kaneko, F., & Advincula, R. C. (1999). *Adsorption properties of polyelectrolytes in ultrathin multilayer assemblies: Investigations using the quartz crystal microbalance (QCM) technique*, Anaheim, CA, USA.
- Baradie, B., & Shoichet, M. S. (2003). Insight into the Surface Properties of Fluorocarbon-Vinyl Acetate Copolymer Films and Blends.. *Macromolecules*, 36(7), 2343-2348. doi: 10.1021/ma0216019
- Bashforth, F., & Adams, J. C. (1883). *An Attempt to Test the Theories of Capillary Action*. Cambridge: Cambridge Univ. Press and Deighton Bell & Co.
- Bauhofer, W., & Kovacs, J. Z. (2009). A review and analysis of electrical percolation in carbon nanotube polymer composites. *Composites Science and Technology*, 69(10), 1486-1498.
- Berger, W., Kammer, H. W., & Kummerlowe, C. (1984). *Makromol Chem Suppl B*, 8, 101.

- Bhattacharya, A., & De, A. (1999). Conducting polymers in solution - progress toward processibility. *Journal of Macromolecular Science - Reviews in Macromolecular Chemistry and Physics*, C39(1), 17-56.
- Bhattacharya, S. (1986). *Metal-Filled Polymers*. New York: Marcel Dekker.
- Bliznyuk, V. N., Baig, A., Singamaneni, S., Pud, A. A., Fatyeyeva, K. Y., & Shapoval, G. S. (2005). Effects of surface and volume modification of poly(vinylidene fluoride) by polyaniline on the structure and electrical properties of their composites. *Polymer*, 46(Copyright 2006, IEE), 11728-11736.
- Blodgett, K. B. (1934). Monomolecular films of fatty acids on glass. *J. Am. Chem. Soc.*, 56(2), 495-495.
- Blunt, M., Barford, W., & Ball, R. (1989). Polymer adsorption and electron binding on rough and fractal surfaces. *Macromolecules*, 22(3), 1458-1466.
- Bourry, D., & Favis, B. D. (1998a). Cocontinuity and phase inversion in HDPE/PS blends: Influence of interfacial modification and elasticity. *Journal of Polymer Science, Part B: Polymer Physics*, 36(11), 1889-1899.
- Braga, G. S., Paterno, L. G., Lima, J. P. H., Fonseca, F. J., & de Andrade, A. M. (2008). Influence of the deposition parameters on the morphology and electrical conductivity of PANI/PSS self-assembled films. *Materials Science and Engineering C*, 28(4), 555-562.
- Bridge, B., & Tee, H. (1990). Large-scale simulation of the critical volume fraction for the percolation threshold in metal-fibre-loaded polymer composites. *International Journal of Electronics*, 69(6), 785-792.
- Burroughes, J. H., Bradley, D. D. C., Brown, A. R., Marks, R. N., Mackay, K., Friend, R. H., et al. (1990). Light-emitting diodes based on conjugated polymers. *Nature*, 347(6293), 539-541.
- Burroughes, J. H., Jones, C. A., & Friend, R. H. (1988). New Semiconductor Device Physics in Polymer Diodes and Transistors. *Nature*, 335(6186), 137-141.
- Calberg, C., Blacher, S., Gubbels, F., Brouers, F., Deltour, R., & Jerome, R. (1999). Electrical and dielectric properties of carbon black filled co-continuous two-phase polymer blends. *Journal of Physics D: Applied Physics*, 32(13), 1517-1525.
- Campbell, D. J., Freidinger, E. R., Hastings, J. M., & Querns, M. K. (2002). Spontaneous assembly of soda straws. *Journal of Chemical Education*, 79(2), 201.
- Cao, Y., Smith, P., & Heeger, A. J. (1992). Counter-ion induced processibility of conducting polyaniline and of conducting polyblends of polyaniline in bulk polymers. *Synthetic Metals*, 48(1), 91-97.
- Carmona, F. (1989). Conducting filled polymers. *Physica A: Statistical and Theoretical Physics*, 157(1), 461-469.
- Carmona, F., Prudhon, P., & Barreau, F. (1984). Percolation in short fibres epoxy resin composites: Conductivity behavior and finite size effects near threshold. *Solid State Communications*, 51(4), 255-257.

- Caruso, F. (2003). Hollow Inorganic Capsules via Colloid-Templated Layer-by-Layer Electrostatic Assembly (pp. 145-168).
- Caruso, F., Caruso, R. A., & Mohwald, H. (1998). Nanoengineering of inorganic and hybrid hollow spheres by colloidal templating. *Science*, 282(Copyright 1999, IEE), 1111-1114.
- Caruso, F., Caruso, R. A., & Mohwald, H. (1999). Production of Hollow Microspheres from Nanostructured Composite Particles. *Chemistry of Materials*, 11(11), 3309-3314.
- Caruso, F., Furlong, D. N., Ariga, K., Ichinose, I., & Kunitake, T. (1998). Characterization of polyelectrolyte-protein multilayer films by atomic force microscopy, scanning electron microscopy, and Fourier transform infrared reflection-absorption spectroscopy. *Langmuir*, 14(16), 4559-4565.
- Caruso, F., Lichtenfeld, H., Giersig, M., & Mohwald, H. (1998). Electrostatic Self-Assembly of Silica Nanoparticle-Polyelectrolyte Multilayers on Polystyrene Latex Particles. *J. Am. Chem. Soc.*, 120(33), 8523-8524.
- Caruso, F., & Schuler, C. (2000). Enzyme Multilayers on Colloid Particles: Assembly, Stability, and Enzymatic Activity. *Langmuir*, 16(24), 9595-9603.
- Cheung, J. H., Fou, A. F., Ferreira, M., & Rubner, M. F. (1993). Molecular self-assembly of conducting polymers. A new layer-by-layer thin film deposition process. *Polymer Preprints, Division of Polymer Chemistry, American Chemical Society*, 34(2), 757.
- Cheung, J. H., Fou, A. F., & Rubner, M. F. (1994). Molecular self-assembly of conducting polymers. *Thin Solid Films*, 244(1-2 pt 3), 985-989.
- Cheung, J. H., Stockton, W. B., & Rubner, M. F. (1997). Molecular-level processing of conjugated polymers. 3. Layer-by-layer manipulation of polyaniline via electrostatic interactions. *Macromolecules*, 30(9), 2712-2716.
- Chiang, C. K., Druy, M. A., Gau, S. C., Heeger, A. J., Louis, E. J., MacDiarmid, A. G., et al. (1978). Synthesis of highly conducting films of derivatives of polyacetylene, (CH)_x. *Journal of the American Chemical Society*, 100(3), 1013-1015.
- Chiang, C. K., Fincher, C. R., Park, Y. W., Heeger, A. J., Shirakawa, H., Louis, E. J., et al. (1977). Electrical Conductivity in Doped Polyacetylene. *Physical Review Letters*, 39(17), 1098.
- Chiang, C. K., Park, Y. W., Heeger, A. J., Shirakawa, H., Louis, E. J., & MacDiarmid, A. G. (1978). Conducting polymers: Halogen doped polyacetylene. *The Journal of Chemical Physics*, 69(11), 5098-5104.
- Chipara, M. I., Munteanu, I., Notingher, P., Chipara, M. D., Reyes Romero, J., Negreanu, B., et al. (1998). *On polyaniline-polyvinylchloride blends*, Vasteras, Sweden.
- Chung, K. T., Sabo, A., & Pica, A. P. (1982). Electrical permittivity and conductivity of carbon black-polyvinyl chloride composites. *Journal of Applied Physics*, 53(10), 6867-6879.
- Clark, S. L., Montague, M. F., & Hammond, P. T. (1997). Ionic Effects of Sodium Chloride on the Templated Deposition of Polyelectrolytes Using Layer-by-Layer Ionic Assembly. *Macromolecules*, 30(23), 7237-7244.
- Clausius, R. (1864). *Abhandlungen über die mechanische wärme theorie*, 2, 44.

- Clerc, J. P., Giraud, G., Laugier, J. M., & Luck, J. M. (1990). The electrical conductivity of binary disordered systems, percolation clusters, fractals and related models. *Advances in Physics*, 39(3), 191 - 309.
- Contractor, A. Q., Sureshkumar, T. N., Narayanan, R., Sukeerthi, S., Lal, R., & Srinivasa, R. S. (1994). Conducting polymer-based biosensors. *Electrochimica Acta*, 39(8-9), 1321-1324.
- Cox, W. P., & Merz, E. H. (1958). Correlation of dynamic and steady flow viscosities. *Journal of Polymer Science*, 28(118), 619-622.
- Dan, L., Yadong, J., Zhiming, W., Xiangdong, C., & Yanrong, L. (2000). *Self-assembly of polyaniline ultrathin films based on doping-induced deposition effect and applications for chemical sensors*, Beijing, China.
- Dautzenberg, H., Jaeger, W., Kotz, J., Phillip, B., C., S., & Stscherbina, D. (1994). Polyelectrolytes—Formation, Characterization, Application. *Carl Hanser Verlag: Munich, Germany*.
- Decher, G. (1997). Fuzzy Nanoassemblies: Toward Layered Polymeric Multicomposites. *Science*, 277(5330), 1232-1237.
- Decher, G., & Hong, J. D. (1991a). Buildup of ultrathin multilayer films by a self-assembly process, 1 consecutive adsorption of anionic and cationic bipolar amphiphiles on charged surface. *Chem.M acromol. Symp.*, 46, 321.
- Decher, G., & Hong, J. D. (1991b). Buildup of ultrathin multilayer films by a self-assembly process, 1. Consecutive adsorption of anionic and cationic bipolar amphiphiles on charged surfaces. *European Conference on Organized Organic Thin Films*, 321.
- Decher, G., Hong, J. D., & Schmitt, J. (1992a). Buildup of ultrathin multilayer films by a self-assembly process: III. Consecutively alternating adsorption of anionic and cationic polyelectrolytes on charged surfaces. [doi: DOI: 10.1016/0040-6090(92)90417-A]. *Thin Solid Films*, 210-211(Part 2), 831-835.
- Decher, G., Hong, J. D., & Schmitt, J. (1992b). Buildup of ultrathin multilayer films by a self-assembly process: III. Consecutively alternating adsorption of anionic and cationic polyelectrolytes on charged surfaces. *Thin Solid Films*, 210/211, 831-835.
- Decher, G., Lvov, Y., & Schmitt, J. (1994). Proof of multilayer structural organization in self-assembled polycation-polyanion molecular films. *Thin Solid Films*, 244(1-2 pt 3), 772-777.
- Decher, G., & Schlenoff, J. B. (2003). *Multilayer Thin Films*.
- Decher, G., & Schmitt, J. (1992). Fine-tuning of the film thickness of ultrathin multilayer films composed of consecutively alternating layers of anionic and cationic polyelectrolytes. *Progress in Colloid & Polymer Science*, 89(Trends Colloid Interface Sci. VI), 160-164.
- DeLongchamp, D., & Hammond, P. T. (2001). Layer-by-layer assembly of PEDOT/polyaniline electrochromic devices. *Advanced Materials*, 13(19), 1455-1459.
- Denbigh, K. G. (1971). *The principles of chemical equilibrium, with applications in chemistry and chemical engineering*. Cambridge [Eng.: University Press.

- Domenech, S. C., Bortoluzzi, J. H., Soldi, V., & Franco, C. V. (2002). Electroactive mixtures of polyaniline and EPDM rubber: Chemical, thermal, and morphological characterization. *Journal of Applied Polymer Science*, *87*(3), 535-547.
- Donahue, D. J., & Bartell, F. E. (1952). *J. Phys. Chem.*, *56*, 480.
- Dong-Uk, C., Kitae, S., Young Chul, K., Yun Heum, P., & Jun Young, L. (2001). *Electrically conducting polymer blends with thermally processable polyaniline*, Kyoto, Japan.
- Du, F., Scogna, R. C., Zhou, W., Brand, S., Fischer, J. E., & Winey, K. I. (2004). Nanotube Networks in Polymer Nanocomposites: Rheology and Electrical Conductivity. *Macromolecules*, *37*(24), 9048-9055.
- Dubas, S. T., & Schlenoff, J. B. (1999). Factors Controlling the Growth of Polyelectrolyte Multilayers. *Macromolecules*, *32*(24), 8153-8160.
- Dubas, S. T., & Schlenoff, J. B. (2001b). Polyelectrolyte Multilayers Containing a Weak Polyacid: Construction and Deconstruction. *Macromolecules*, *34*(11), 3736-3740.
- Dubas, S. T., & Schlenoff, J. B. (2001c). Swelling and Smoothing of Polyelectrolyte Multilayers by Salt. *Langmuir*, *17*(25), 7725-7727. doi: doi:10.1021/la0112099
- Epstein, A. J., Ginder, J. M., Zuo, F., Woo, H. S., Tanner, D. B., Richter, A. F., et al. (1986). Insulator-to-metal transition in polyaniline: effect of protonation in emeraldine. *Synthetic Metals*, *21*(1), 63-70.
- Everaert, V., Aerts, L., & Groeninckx, G. (1999). Phase morphology development in immiscible PP/(PS/PPE) blends influence of the melt-viscosity ratio and blend composition. *Polymer*, *40*(24), 6627-6644.
- Farhat, T., Yassin, G., Dubas, S. T., & Schlenoff, J. B. (1999). Water and ion pairing in polyelectrolyte multilayers. *Langmuir*, *15*(20), 6621-6623.
- Farhat, T. R., & Schlenoff, J. B. (2002). Corrosion control using polyelectrolyte multilayers. *Electrochemical and Solid-State Letters*, *5*(4), 13-15.
- Favis, B. D. (2000). Factors Influencing the Morphology in Immiscible Polymer Blends in Melt Processing. In D. R. Paul & C. B. Bucknall (Eds.), *Polymer Blends: Formulation and Performance, Two-Volume Set* (Vol. 1, pp. 239-289). New York: John Wiley & Sons, Inc.
- Favis, B. D., & Chalifoux, J. P. (1988). Influence of composition on the morphology of polypropylene/polycarbonate blends. *Polymer*, *29*(10), 1761-1767.
- Feng, L., & Kamal, M. R. (2005). Crystallization and melting behavior of homogeneous and heterogeneous linear low-density polyethylene resins. *Polymer Engineering and Science*, *45*(Copyright 2006, IEE), 1140-1151.
- Ferreira, M., Cheung, J. H., & Rubner, M. F. (1994). Molecular self-assembly of conjugated polyions: A new process for fabricating multilayer thin film heterostructures. *Thin Solid Films*, *244*(1-2 pt 3), 806-809.
- Ferreira, M., & Rubner, M. F. (1995). Molecular-level processing of conjugated polymers. 1. Layer-by-layer manipulation of conjugated polyions. *Macromolecules*, *28*(21), 7107-7114.

- Flandin, L., Bréchet, Y., & Cavaillé, J. Y. (2001). Electrically conductive polymer nanocomposites as deformation sensors. *Composites Science and Technology*, 61(6), 895-901.
- Flory, P. J. (1942). Thermodynamics of High Polymer Solutions. *The Journal of Chemical Physics*, 10(1), 51-61.
- Flory, P. J. (1944). Thermodynamics of Heterogeneous Polymers and Their Solutions. *The Journal of Chemical Physics*, 12(11), 425-438.
- Flory, P. J. (1953). *Principles of Polymer Chemistry*. New York: Cornell Univ. Press.
- Flory, P. J. (1965). Statistical Thermodynamics of Liquid Mixtures. *Journal of the American Chemical Society*, 87(9), 1833-1838.
- Flory, P. J., Orwoll, R. A., & Vrij, A. (1964). Statistical Thermodynamics of Chain Molecule Liquids. I. An Equation of State for Normal Paraffin Hydrocarbons. *Journal of the American Chemical Society*, 86(17), 3507-3514.
- Fou, A. C., Onitsuka, O., Ferreira, M., & Rubner, M. F. (1996). Fabrication and properties of light-emitting diodes based on self-assembled multilayers of poly(phenylene vinylene). *Journal of Applied Physics*, 79(10), 7501-7509.
- Fou, A. C., & Rubner, M. F. (2002). Molecular-Level Processing of Conjugated Polymers. 2. Layer-by-Layer Manipulation of In-Situ Polymerized p-Type Doped Conducting Polymers. *Macromolecules*, 28(21), 7115-7120.
- Foulger, S. H. (1999). Reduced percolation thresholds of immiscible conductive blends. *Journal of Polymer Science Part B: Polymer Physics*, 37(15), 1899-1910.
- Fraysse, J., Planes, J., & Dufresne, A. (2000). *Transport and mechanical properties of polyaniline - Poly(methyl methacrylate) blends exhibiting low percolation threshold*, Poznan.
- Fricke, H. A. (1924). mathematical treatment of the electrical conductivity and capacity of disperse systems. I. The electrical conductivity of a suspension of homogeneous spheroids. *J. Physical Rev.*, 24, 575-587.
- Galal, A., Atta, N. F., & Mark Jr, H. B. (1998). Sensors Based on Organic Conducting-Polymer Electrodes. *ACS Symposium Series*, 690, 210-230.
- Garnier, F., Hajlaoui, R., Yassar, A., & Srivastava, P. (1994). All-polymer field-effect transistor realized by printing techniques. *Science*, 265(Copyright 1994, IEE), 1684-1686.
- Gaylord, N. G. (1969). USA Patent No.: U. Patent.
- Gaylord, N. G., , Vol.142,P.76,(ACS,Washington,1975). (1975). Copolymers, Polyblends and Composites. *ACS Advances in Chemistry Series*, 142, 76.
- Gelves, G. A., Lin, B., Sundararaj, U., & Haber, J. A. (2006). Low electrical percolation threshold of silver and copper nanowires in polystyrene composites. *Advanced Functional Materials*, 16(Compendex), 2423-2430.
- Gerard, M., Chaubey, A., & Malhotra, B. D. (2002). Application of conducting polymers to biosensors. *Biosensors and Bioelectronics*, 17(5), 345-359.

- Geuskens, G., Gielens, J. L., Geshef, D., & Deltour, R. (1987). The electrical conductivity of polymer blends filled with carbon-black. *European Polymer Journal*, 23(12), 993-995.
- Gibbs, J. W. (1876). *Trans. Conn. Acad. Sci.*, 3228.
- Ginder, J. M., Richter, A. F., MacDiarmid, A. G., & Epstein, A. J. (1987). Insulator-to-metal Transition in Polyaniline. *Solid State Communications*, 63(2), 97-101.
- Girifalco, L. A., & Good, R. J. (1957). A Theory for the Estimation of Surface and Interfacial Energies. I. Derivation and Application to Interfacial Tension. *The Journal of Physical Chemistry*, 61(7), 904-909.
- Goh, S. H., Chan, H. S. O., & Ong, C. H. (1998). Miscible blends of conductive polyaniline with tertiary amide polymers. *Journal of Applied Polymer Science*, 68(11), 1839-1844.
- Golestanian, R., & Sens, P. (1999). Comment on "Adsorption of polyelectrolyte onto a colloid of opposite charge" [and reply]. *Physical Review Letters*, 83(12), 2473-2474.
- Good, R. J., & Girifalco, L. A. (1964). *Adv. Chem.*, 43, 74.
- Graul, T. W., & Schlenoff, J. B. (1999). Capillaries modified by polyelectrolyte multilayers for electrophoretic separations. *Analytical Chemistry*, 71(18), 4007-4013.
- Greene, R. L., Street, G. B., & Suter, L. J. (1975). Superconductivity in Polysulfur Nitride (SN)_X. *Physical Review Letters*, 34(10), 577.
- Grimmett, G. R. (1999). *Percolation*: Springer.
- Gubbels, F., Blacher, S., Vanlathem, E., Jerome, R., Deltour, R., Brouers, F., et al. (1995). Design of electrical conductive composites: key role of the morphology on the electrical properties of carbon black filled polymer blends. *Macromolecules*, 28(5), 1559-1566.
- Gubbels, F., Jerome, R., Teyssie, P., Vanlathem, E., Deltour, R., Calderone, A., et al. (1994). Selective localization of carbon black in immiscible polymer blends: a useful tool to design electrical conductive composites. *Macromolecules*, 27(7), 1972-1974.
- Guo, H. F., Gvozdic, N. V., & Meier, D. J. (1997). Prediction and manipulation of the phase morphologies of multiphase polymer blends: II. Quaternary systems. *Polymer*, 38(19), 4915-4923.
- Guo, H. F., Packirisamy, S., Gvozdic, N. V., & Meier, D. J. (1997). Prediction and manipulation of the phase morphologies of multiphase polymer blends: 1. Ternary systems. *Polymer*, 38(4), 785-794.
- Gurovitch, E., & Sens, P. (1999). Adsorption of Polyelectrolyte onto a Colloid of Opposite Charge. *Physical Review Letters*, 82(2), 339-342.
- Ha, B. Y., & Thirumalai, D. (1995). Electrostatic persistence length of a polyelectrolyte chain. *Macromolecules*, 28(Compendex), 577-581.
- Haba, Y., Segal, E., Narkis, M., Titelman, G. I., & Siegmann, A. (2000). Polyaniline-DBSA/polymer blends prepared via aqueous dispersions. *Synthetic Metals*, 110(3), 189-193.

- Halls, J. J. M., Walsh, C. A., Greenham, N. C., Marseglia, E. A., Friend, R. H., Moratti, S. C., et al. (1995). Efficient photodiodes from interpenetrating polymer networks. *Nature*, 376(6540), 498-500.
- Hammond, P. T. (2004). Form and Function in Multilayer Assembly: New Applications at the Nanoscale. *Advanced Materials*, 16(15), 1271-1293.
- Han, M. G., & Im, S. S. (1999). Electrical and structural analysis of conductive polyaniline/polyimide blends. *Journal of Applied Polymer Science*, 71(13), 2169-2178.
- Hara, M., & Sauer, J. A. (1998). Synergism in mechanical properties of polymer/polymer blends. *Journal of Macromolecular Science - Reviews in Macromolecular Chemistry and Physics*, C38(2), 327-362.
- Harkins, W. D., & Feldman, A. (1922). Films. The Spreading of Liquids and the Spreading Coefficient. *Journal of the American Chemical Society*, 44(12), 2665-2685. doi: 10.1021/ja01433a001
- Harrats, C., Omonov, T. S., & Groeninckx, G. (2005). Co-continuous and encapsulated three phase morphologies in uncompatibilized and reactively compatibilized polyamide 6/polypropylene/polystyrene ternary blends using two reactive precursors. *Polymer*, 46(Copyright 2006, IEE), 12322-12336.
- Harris, J. J., & Bruening, M. L. (2000). Electrochemical and in Situ Ellipsometric Investigation of the Permeability and Stability of Layered Polyelectrolyte Films. *Langmuir*, 16(4), 2006-2013.
- Hartikainen, J., Lahtinen, M., Torkkeli, M., Serimaa, R., Valkonen, J., Rissanen, K., et al. (2001). Comb-Shaped Supramolecules Based on Protonated Polyaniline and Their Self-Organization into Nanoscale Structures: Polyaniline Sulfonates/Zinc Sulfonates. *Macromolecules*, 34(22), 7789-7795.
- He, J., Bu, W., & Zeng, J. (1997). Co-phase continuity in immiscible binary polymer blends. *Polymer*, 38(26), 6347-6353.
- Heywang, G., & Jonas, F. (1992). Poly(alkylenedioxythiophene)s - new, very stable conducting polymers. *Advanced Materials*, 4(2), 116-118.
- Ho, R. M., Wu, C. H., & Su, A. C. (1990). Morphology of plastic/rubber blends. *Polymer Engineering and Science*, 30(9), 511-518.
- Hobbs, S. Y., Dekkers, M. E. J., & Watkins, V. H. (1988). Effect of interfacial forces on polymer blend morphologies. *Polymer*, 29(9), 1598-1602.
- Hoganand, J. P., & Banks, R. L. (1958). US Patent.
- Hone, D., Ji, H., & Pincus, P. A. (1987). Polymer adsorption on rough surfaces. 1. Ideal long chain. *Macromolecules*, 20(10), 2543-2549.
- Horiuchi, S., Matchariyakul, N., Yase, K., & Kitano, T. (1997). Morphology Development through an Interfacial Reaction in Ternary Immiscible Polymer Blends. *Macromolecules*, 30(12), 3664-3670.
- Hosokawa, K., Shimoyama, I., & Miura, H. (1996). Two-dimensional micro-self-assembly using the surface tension of water. *Sensors and Actuators, A: Physical*, 57(2), 117-125.

- Hou, S., Harrell, C. C., Trofin, L., Kohli, P., & Martin, C. R. (2004). Layer-by-Layer Nanotube Template Synthesis. *Journal of the American Chemical Society*, 126(18), 5674-5675.
<http://web.mit.edu/newsoffice/2009/cartilage-0511.html>.
<http://www.chem.fsu.edu/multilayers/>.
http://www.veeco.com/library/resources/Sample_Preparation/index.aspx.
- Huang, W. S., D., H. B., & MacDiarmid, A. G. (1986). *J. Chem. Soc. Faraday Trans.*, 82, 2385.
- Huggins, M. L. (1942). Some Properties of Solutions of Long-chain Compounds. *The Journal of Physical Chemistry*, 46(1), 151-158.
- Ikkala, O. T., Laakso, J., Väkiparta, K., Virtanen, E., Ruohonen, H., Järvinen, H., et al. (1995). Counter-ion induced processibility of polyaniline: Conducting melt processible polymer blends. *Synthetic Metals*, 69(1-3), 97-100.
- Inzelt, G., Pineri, M., Schultze, J. W., & Vorotyntsev, M. A. (2000). Electron and proton conducting polymers: Recent developments and prospects. *Electrochimica Acta*, 45(15-16), 2403-2421.
- Israelachvili, J. (1992). *Intermolecular and Surface Forces, Second Edition: With Applications to Colloidal and Biological Systems (Colloid Science)*: {Academic Press}.
- Ito, T., Shirakawa, H., & Ikeda, S. (1996). Simultaneous polymerization and formation of polyacetylene film on the surface of concentrated soluble Ziegler-type catalyst solution. *Journal of Polymer Science, Part A: Polymer Chemistry*, 34(13), 2533-2542.
- Jaber, J. A., & Schlenoff, J. B. (2007). Counterions and water in polyelectrolyte multilayers: A tale of two polycations. *Langmuir*, 23(2), 896-901.
- Jaffar, S., Nam, K. T., Khademhosseini, A., Xing, J., Langer, R., & Belcher, A. (2004). Layer-by-layer surface modification and patterned electrostatic deposition of quantum dots. *Nano Letters*, 4(8), 1421-1425.
- Jagur-Grodzinski, J. (2002). Electronically conductive polymers. *Polymers for Advanced Technologies*, 13(9), 615-625.
- Jing, X., Yang, Q., Zheng, M., & Lan, L. (1999). Study on the electrically conductive polyamide/polyaniline blends. *Hsi-An Chiao Tung Ta Hsueh/Journal of Xi'an Jiaotong University*, 33(8), 74-77.
- Joanny, J. F. (1999). Polyelectrolyte adsorption and charge inversion. *The European Physical Journal B - Condensed Matter and Complex Systems*, V9(1), 117-122.
- Johnson, K. L., Kendall, K., & Roberts, A. D. (1971). Surface Energy and the Contact of Elastic Solids. *Proceedings of the Royal Society of London. A. Mathematical and Physical Sciences*, 324(1558), 301-313.
- Joly, S., Kane, R., Radzilowski, L., Wang, T., Wu, A., Cohen, R. E., et al. (2000). Multilayer nanoreactors for metallic and semiconducting particles. *Langmuir*, 16(3), 1354-1359.
- Jordhamo, G. M., Manson, J. A., & Sperling, L. H. (1986). Phase Continuity and Inversion in Polymer Blends and Simultaneous Interpenetrating Networks. *Polymer Engineering and Science*, 26(8), 517-524.

- Jousseume, V., Morsli, A., & Bonnet, A. (2002). Thermal behavior of polyaniline films and polyaniline-polystyrene blends. *Journal of Applied Polymer Science*, 84(10), 1848-1855.
- Jousseume, V., Morsli, M., Bonnet, A., Tesson, O., & Lefrant, S. (1998). Electrical properties of polyaniline-polystyrene blends above the percolation threshold. *Journal of Applied Polymer Science*, 67(7), 1205-1208.
- Kababya, S., Appel, M., Haba, Y., Titelman, G. I., & Schmidt, A. (1999). Polyaniline-Dodecylbenzene Sulfonic Acid Polymerized from Aqueous Medium: A Solid State NMR Characterization. *Macromolecules*, 32(16), 5357-5364.
- Kaneto, K., Kaneko, M., Min, Y., & MacDiarmid, A. G. (1995). "Artificial muscle": Electromechanical actuators using polyaniline films. *Synthetic Metals*, 71(1-3), 2211-2212.
- Keller, S. W., Kim, H.-N., & Mallouk, T. E. (1994). Layer-by-Layer Assembly of Intercalation Compounds and Heterostructures on Surfaces: Toward Molecular "Beaker" Epitaxy. *J. Am. Chem. Soc.*, 116(19), 8817-8818.
- Kim, H. S., Sohn, B. H., Lee, W., Lee, J. K., Choi, S. J., & Kwon, S. J. (2002). Multifunctional layer-by-layer self-assembly of conducting polymers and magnetic nanoparticles. *Thin Solid Films*, 419(1-2), 173-177.
- Kirkpatrick, S. (1973). Percolation and Conduction. *Reviews of Modern Physics*, 45(Copyright (C) 2009 The American Physical Society), 574.
- Klason, C., & Kubát, J. (1975). Anomalous behavior of electrical conductivity and thermal noise in carbon black-containing polymers at T_g and T_m . *Journal of Applied Polymer Science*, 19(3), 831-845.
- Klitzing, R., & Moehwald, H. (1995). Proton Concentration Profile in Ultrathin Polyelectrolyte Films. *Langmuir*, 11(9), 3554-3559.
- Klitzing, R. v., Espert, A., Asnacios, A., Hellweg, T., Colin, A., & Langevin, D. (1999). Forces in foam films containing polyelectrolyte and surfactant. *Colloids and Surfaces A: Physicochemical and Engineering Aspects*, 149(1-3), 131-140.
- Koh, J. C. Y., & Fortini, A. (1973). Prediction of thermal conductivity and electrical resistivity of porous metallic materials. *Int. J. Heat Mass Transfer*, 16, 2013-2021.
- Kotov, N. A., Dekany, I., & Fendler, J. H. (1995). Layer-by-Layer Self-Assembly of Polyelectrolyte-Semiconductor Nanoparticle Composite Films. *J. Phys. Chem.*, 99(35), 13065-13069.
- Kotov, N. A., Haraszti, T., Turi, L., Zavala, G., Geer, R. E., Dekany, I., et al. (1997). Mechanism of and defect formation in the self-assembly of polymeric polycation-montmorillonite ultrathin films. *Journal of the American Chemical Society*, 119(29), 6821-6832.
- Kraft, A., Grimsdale, Andrew C., & Holmes, Andrew B. (1998). Elektrolumineszierende konjugierte Polymere - Polymere erstrahlen in neuem Licht. *Angewandte Chemie*, 110(4), 416-443.

- Krass, H., Papastavrou, G., & Kurth, D. G. (2003). Layer-by-layer self-assembly of a polyelectrolyte bearing metal ion coordination and electrostatic functionality. *Chemistry of Materials*, 15(1), 196-203.
- Krieger, I. M., & Dougherty, T. J. (1959). A Mechanism for Non-Newtonian Flow in Suspensions of Rigid Spheres. *Journal of Rheology*, 3(1), 137-152.
- Kumar, D., & Sharma, R. C. (1998). Advances in conductive polymers. *European Polymer Journal*, 34(8), 1053-1060.
- Kumin, Y., & Chang Dae, H. (1996). Effects of shear flow and annealing on the morphology of rapidly precipitated immiscible blends of polystyrene and polyisoprene. *Polymer*, 37(26), 5795-5805.
- Kunze, K. K., & Netz, R. R. (2002). Morphologies of semiflexible polyelectrolyte complexes. *Europhysics Letters*, 58(2), 299-305.
- Ladam, G., Schaad, P., Voegel, J. C., Schaaf, P., Decher, G., & Cuisinier, F. (2000). In situ determination of the structural properties of initially deposited polyelectrolyte multilayers. *Langmuir*, 16(3), 1249-1255.
- Laska, J., Zak, K., & Pron, A. (1997). Conducting blends of polyaniline with conventional polymers. *Synthetic Metals*, 84(1-3 pt 1), 117-118.
- Lavalle, P., Gergely, C., Cuisinier, F. J. G., Decher, G., Schaaf, P., Voegel, J. C., et al. (2002). Comparison of the structure of polyelectrolyte multilayer films exhibiting a linear and an exponential growth regime: An in situ atomic force microscopy study. *Macromolecules*, 35(11), 4458-4465.
- Lavalle, P., Picart, C., Mutterer, J., Gergely, C., Reiss, H., Voegel, J.-C., et al. (2004). Modeling the Buildup of Polyelectrolyte Multilayer Films Having Exponential Growth. *Journal of Physical Chemistry B*, 108(2), 635-648.
- Lefaux, C. J., Zimmerlin, J. A., Dobrynin, A. V., & Mather, P. T. (2004). Polyelectrolyte spin assembly: influence of ionic strength on the growth of multilayered thin films. *Journal of Polymer Science, Part B (Polymer Physics)*, 42(19), 3654-3666.
- Legros, A., Carreau, P. J., Favis, B. D., & Michel, A. (1997). Morphology modification by interfacial chemical reaction in a polyester/ethylene vinyl acetate/polyethylene blend. *Polymer*, 38(20), 5085-5089.
- Levon, K., Margolina, A., & Patashinsky, A. Z. (1993). Multiple percolation in conducting polymer blends. *Macromolecules*, 26(15), 4061-4063.
- Levon, K., Margolina, A., & Patashinsky, A. Z. (2002). Multiple percolation in conducting polymer blends. *Macromolecules*, 26(15), 4061-4063.
- Li, J., & Favis, B. D. (2001a). Characterizing co-continuous high density polyethylene/polystyrene blends. *Polymer*, 42(11), 5047-5053.
- Li, J., Ma, P. L., & Favis, B. D. (2002). The role of the blend interface type on morphology in cocontinuous polymer blends. *Macromolecules*, 35(6), 2005-2016.

- Liang, Z., Cabarcos, O. M., Allara, D. L., & Wang, Q. (2004). Hydrogen-Bonding-Directed Layer-by-Layer Assembly of Conjugated Polymers. *Advanced Materials*, 16(9-10), 823-827.
- Liangcai, L., Ming, W., Huoming, S., Haiying, L., Qingdong, Q., & Yuanlong, D. (2001). Preparation and EIS studies on polyimide/polyaniline blend film for corrosion protection. *Polymers for Advanced Technologies*, 12(11-12), 720-723.
- Lifshitz, E. M., Landau, L. D., & Pitaevskii, L. P. (1984). *Electrodynamics of Continuous Media* (Vol. 8).
- Lin, B., Gelves, G. A., Haber, J. A., Potschke, P., & Sundararaj, U. (2008). Electrical, morphological and rheological study of melt-mixed polystyrene/copper nanowire nanocomposites. *Macromolecular Materials and Engineering*, 293(Compendex), 631-640.
- Love, J. C., Estroff, L. A., Kriebel, J. K., Nuzzo, R. G., & Whitesides, G. M. (2005). Self-Assembled Monolayers of Thiolates on Metals as a Form of Nanotechnology. *Chemical Reviews*, 105(4), 1103-1170.
- Luciani, A., & Jarrin, J. (1996). Morphology development in immiscible polymer blends. *Polymer Engineering & Science*, 36(12), 1619-1626.
- Luckham, P. F., & Klein, J. (1985). Interactions between smooth solid surfaces in solutions of adsorbing and nonadsorbing polymers in good solvent conditions. *Macromolecules*, 18(4), 721-728.
- Lutt, M., Fitzsimmons, M. R., & DeQuan, L. (1998). X-ray reflectivity study of self-assembled thin films of macrocycles and macromolecules. *Journal of Physical Chemistry B*, 102(2), 400-405.
- Luzinov, I., Pagnouille, C., & Jerome, R. (2000). Ternary polymer blend with core-shell dispersed phases: effect of the core-forming polymer on phase morphology and mechanical properties. *Polymer*, 41(19), 7099-7109.
- Lvov, Y., Ariga, K., Ichinose, I., & Kunitake, T. (1995). Assembly of Multicomponent Protein Films by Means of Electrostatic Layer-by-Layer Adsorption. *J. Am. Chem. Soc.*, 117(22), 6117-6123.
- Lvov, Y., Decher, G., & Sukhorukov, G. (1993). Assembly of thin films by means of successive deposition of alternate layers of DNA and poly(allylamine). *Macromolecules*, 26(20), 5396-5399.
- Lvov, Y. M., & Decher, G. (1994). Assembly of multilayer ordered films by alternating adsorption of oppositely charged macromolecules. *Crystallography Reports*, 39(4), 628-647.
- Lyngaae-Jorgensen, J., & Utracki, L. A. (2003). Structuring polymer blends with bicontinuous phase morphology. II. Tailoring blends with ultralow critical volume fraction. *Polymer*, 44(5), 1661-1669.
- M. Dimitrova, Y. A. P. L. F. M. M. W. C. S. Y. H. J. C. V. J. O. (2007). Adenoviral Gene Delivery from Multilayered Polyelectrolyte Architectures. *Advanced Functional Materials*, 17(2), 233-245.

- Macdiarmid, A. G., Jin-Chih, C., Halpern, M., Wu-Song, H., Shao-Lin, M., Somasiri, L. D., et al. (1985). 'Polyaniline': interconversion of metallic and insulating forms. Paper presented at the Proceedings of the International Conference on the Physics and Chemistry of Low-Dimensional Synthetic Metals (ICSM 84), 17-22 June 1984, UK.
- Malek, G., Johnson, L. V., Mace, B. E., Saloupis, P., Schmechel, D. E., Rickman, D. W., et al. (2005). Apolipoprotein E allele-dependent pathogenesis: A model for age-related retinal degeneration. *Proceedings of the National Academy of Sciences of the United States of America*, 102(33), 11900-11905.
- Malmonge, L. F., Lopes, G. d. A., Langiano, S. d. C., Malmonge, J. A., Cordeiro, J. M. M., & Mattoso, L. H. C. (2006). A new route to obtain PVDF/PANI conducting blends. *European Polymer Journal*, 42(11), 3108-3113.
- Man, W., & Shaw, L. (2006). Electrical and mechanical behaviors of carbon nanotube- filled polymer blends. *Journal of Applied Polymer Science*, 99(2), 477-488.
- Maoz, R., Frydman, E., Cohen, S. R., & Sagiv, J. (2000). Constructive nanolithography: Site-defined silver self-assembly on nanoelectrochemically patterned monolayer templates. *Advanced Materials*, 12(6), 424-429.
- Margolis, J. M. (1989). *Conductive Polymers and Plastics*. New York: Chapman and Hall.
- Mateescu, E. M., Jeppesen, C., & Pincus, P. (1999). Overcharging of a spherical macroion by an oppositely charged polyelectrolyte. *Europhysics Letters*, 46(4), 493-498.
- Mathur, P., Misra, S. C. K., Singh, B. P., & Tripathi, P. (2002). *Semiconducting polyaniline nanocrystalline thin films for electronic and sensor applications*, Delhi, India.
- Matos, M., Favis, B. D., & Lomellini, P. (1995). Interfacial modification of polymer blends--the emulsification curve: 1. Influence of molecular weight and chemical composition of the interfacial modifier. *Polymer*, 36(20), 3899-3907.
- Mattoso, L. H. C., Leite, F. L., Paterno, L. G., Borato, C. E., Herrmann, P. S. P., & Oliveira, O. N., Jr. (2005). Study on the adsorption of poly(o-ethoxyaniline) nanostructured films using atomic force microscopy. *Polymer*, 46(26), 12503-12510.
- McMaster, L. P. (2002). Aspects of Polymer-Polymer Thermodynamics. [doi: 10.1021/ma60035a024]. *Macromolecules*, 6(5), 760-773.
- Mekhilef, N., & Verhoogt, H. (1996). Phase inversion and dual-phase continuity in polymer blends: theoretical predictions and experimental results. *Polymer*, 37(18), 4069-4077.
- Meli, M.-V., & Lennox, R. B. (2003). Preparation of Nanoscale Au Islands in Patterned Arrays. *Langmuir*, 19(22), 9097-9100.
- Metelkin, V. I., & Blekht, V. S. (1984). Formation of a Continuous Phase in Heterogeneous Polymer Mixtures. *Colloid Journal of the USSR (English Translation of Kolloidnyi Zhurnal)*, 46(3), 425-429.
- Miles, I. S., & Zurek, A. (1988a). Preparation, structure, and properties of two-phase co-continuous polymer blends. *Polymer Engineering & Science*, 28(12), 796-805.

- Miyasaka, K., Watanabe, K., Jojima, E., Aida, H., Sumita, M., & Ishikawa, K. (1982a). Electrical conductivity of carbon-polymer composites as a function of carbon content. *Journal of Materials Science*, 17(6), 1610-1616.
- Molau, G. E., & Keskkula, H. (1966). Heterogeneous polymer systems. IV. Mechanism of rubber particle formation in rubber-modified vinyl polymers. *Journal of Polymer Science Part A-1: Polymer Chemistry*, 4(6), 1595-1607.
- Montes, J. M., Cuevas, F. G., Rodriguez, J. A., & Herrera, E. J. (2005). Electrical conductivity of sintered powder compacts. *Powder Metallurgy*, 48(4), 343-344.
- Moon Gyu, H., & Seung Soon, I. (2001). Morphological study of conductive polyaniline/polyimide blends. I. Determination of compatibility by small-angle X-ray scattering method. *Polymer*, 42(17), 7449-7454.
- Morgan, H., Foot, P. J. S., & Brooks, N. W. (2001). The effects of composition and processing variables on the properties of thermoplastic polyaniline blends and composites. *Journal of Materials Science*, 36(22), 5369-5377.
- Moussaif, N., & Jérôme, R. (1999). Compatibilization of immiscible polymer blends (PC/PVDF) by the addition of a third polymer (PMMA): analysis of phase morphology and mechanical properties. *Polymer*, 40(14), 3919-3932.
- Munson-McGee, S. H. (1991). Estimation of the critical concentration in an anisotropic percolation network. *Physical Review B (Condensed Matter)*, 43(4), 3331-3336.
- Narkis, M., Haba, Y., Segal, E., Zilberman, M., Titelman, G. I., & Siegmann, A. (2000a). Structured electrically conductive polyaniline/polymer blends. *Polymers for Advanced Technologies*, 11(8-12), 665-673.
- Narkis, M., & Vaxman, A. (1984). Resistivity behavior of filled electrically conductive crosslinked polyethylene. *Journal of Applied Polymer Science*, 29(5), 1639-1652.
- Narkis, M., Zilberman, M., & Siegmann, A. (1997). On the "curiosity" of electrically conductive melt processed doped-polyaniline/polymer blends versus carbon-black/polymer compounds. *Polymers for Advanced Technologies*, 8(8), 525-528.
- Nauman, E. B., & He, D. Q. (2001). Nonlinear diffusion and phase separation. *Chemical Engineering Science*, 56(6), 1999-2018.
- Nemirovski, N., Siegmann, A., & Narkis, M. (1995). Morphology of ternary immiscible polymer blends. *Journal of Macromolecular Science - Physics*, B34(4), 459-475.
- Netz, R. R., & Andelman, D. (2003). Neutral and charged polymers at interfaces. *Physics Reports*, 380(1-2), 1-95.
- Nguyen, T. T., & Shklovskii, B. I. (2001). Overcharging of a macroion by an oppositely charged polyelectrolyte. *Physica A*, 293(3-4), 324-338.
- Nicol, E., Habib-Jiwan, J. L., & Jonas, A. M. (2003). Polyelectrolyte Multilayers as Nanocontainers for Functional Hydrophilic Molecules. *Langmuir*, 19(15), 6178-6186.
- Nicolau, Y. F. (1985). Solution deposition of thin solid compound films by a successive ionic-layer adsorption and reaction process, Sydney, NSW, Australia.

- Niziol, J., & Laska, J. (1999). Conductivity of blends of polyaniline with PMMA and cellulose acetate: aging studies, Montpellier, France.
- Odijk, T. (1980). Binding of Long Flexible Chains to a Rodlike Macromolecule. *Macromolecules*, 13(6), 1542-1546.
- Omonov, T. S., Harrats, C., & Groeninckx, G. (2005). Co-continuous and encapsulated three phase morphologies in uncompatibilized and reactively compatibilized polyamide 6/polypropylene/polystyrene ternary blends using two reactive precursors. *Polymer*, 46(26), 12322-12336.
- Ong, C. H., Goh, S. H., & Chan, H. S. O. (1997). Conductive polyaniline/poly(vinylphosphonic acid) blends. *Polymer Bulletin (Berlin)*, 39(5), 627.
- P. Bertrand, A. J. A. L. R. L. (2000). Ultrathin polymer coatings by complexation of polyelectrolytes at interfaces: suitable materials, structure and properties. *Macromolecular Rapid Communications*, 21(7), 319-348.
- Paloheimo, J., Laakso, K., Isotalo, H., & Stubb, H. (1995). Conductivity, thermoelectric power and field-effect mobility in self-assembled films of polyanilines and oligoanilines. *Synthetic Metals*, 68(3), 249-257.
- Panipol. (2000). Polyaniline - Processing and Applications. <http://www.azom.com/details.asp?ArticleID=1197>.
- Park, M.-K., Deng, S., & Advincula, R. C. (2005). Sustained Release Control via Photo-Cross-Linking of Polyelectrolyte Layer-by-Layer Hollow Capsules. *Langmuir*, 21(12), 5272-5277.
- Paul, D., & Newman, S. (1978). *Polymer Blends* (Vol. 1, 2). New York: Academic Press.
- Paul, D. R., & Barlow, J. W. (1980b). Polymer Blends (or Alloys). *Journal of Macromolecular Science- Reviews in Macromolecular Chemistry*, C18(1), 109-168.
- Paul, R. K., Vijayanathan, V., & Pillai, C. K. S. (1999). Melt/solution processable conducting polyaniline: doping studies with a novel phosphoric acid ester. *Synthetic Metals*, 104(3), 189-195.
- Picart, C., Ladam, G., Senger, B., Voegel, J. C., Schaaf, P., Cuisinier, F. J. G., et al. (2001). Determination of structural parameters characterizing thin films by optical methods: A comparison between scanning angle reflectometry and optical waveguide lightmode spectroscopy. *Journal of Chemical Physics*, 115(2), 1086-1094.
- Picart, C., Lavallo, P., Hubert, P., Cuisinier, F. J. G., Decher, G., Schaaf, P., et al. (2001). Buildup mechanism for poly(L-lysine)/hyaluronic acid films onto a solid surface. *Langmuir*, 17(23), 7414-7424.
- Picart, C., Mutterer, J., Richert, L., Luo, Y., Prestwich, G. D., Schaaf, P., et al. (2002). Molecular basis for the explanation of the exponential growth of polyelectrolyte multilayers. *Proceedings of the National Academy of Sciences of the United States of America*, 99(20), 12531-12535.

- Planes, J., Wolter, A., Cheguettine, Y., Pron, A., Genoud, F., & Nechtschein, M. (1998). Transport properties of polyaniline-cellulose-acetate blends. *Physical Review B (Condensed Matter)*, 58(12), 7774-7785.
- Potschke, P., & Paul, D. R. (2003). Formation of co-continuous structures in melt-mixed immiscible polymer blends. *Journal of Macromolecular Science - Polymer Reviews*, 43(1), 87-141.
- Pramanik, P. K., Khastgir, D., & Saha, T. N. (1992). Conductive nitrile rubber composite containing carbon fillers: Studies on mechanical properties and electrical conductivity. *Composites*, 23(3), 183-191.
- Pratt, C. (2001). Applications of Conducting Polymers
- Privalko, V. P., Ponomarenko, S. M., Privalko, E. G., Lobkov, S. V., Rekheta, N. A., Pud, A. A., et al. (2005). Structure/property relationships for poly(vinylidene fluoride)/doped polyaniline blends. *Journal of Macromolecular Science - Physics*, B44(Copyright 2006, IEE), 749-759.
- Pron, A., & Rannou, P. (2002). Processible conjugated polymers: From organic semiconductors to organic metals and superconductors. *Progress in Polymer Science (Oxford)*, 27(1), 135-190.
- Pron, A., Zagorska, M., Nicolau, Y., Genoud, F., & Nechtschein, M. (1997). *Highly conductive composites of polyaniline with plasticized cellulose acetate*, Snowbird, UT, USA.
- Pud, A., Ogurtsov, N., Korzhenko, A., & Shapoval, G. (2003). Some aspects of preparation methods and properties of polyaniline blends and composites with organic polymers. *Progress in Polymer Science (Oxford)*, 28(12), 1701-1753.
- Qinghua, Z., Xianhong, W., Yanhou, G., Dajun, C., & Xiabin, J. (2002). Morphology and thermal properties of conductive polyaniline/polyamide composite films. *Journal of Polymer Science, Part B (Polymer Physics)*, 40(22), 2531-2538.
- R. Gunawidjaja, C. J. S. P. M. O. S. S. V. V. T. (2006). Flexible and Robust 2D Arrays of Silver Nanowires Encapsulated within Freestanding Layer-by-Layer Films. *Advanced Functional Materials*, 16(15), 2024-2034.
- Rahmy, T. R. (2001). Action of cobra venom on the renal cortical tissues: electron microscopic studies. *Journal of Venomous Animals and Toxins*, 7, 85-112.
- Ram, M. K., Salerno, M., Adami, M., Faraci, P., & Nicolini, C. (1999). Physical properties of polyaniline films: assembled by the layer-by-layer technique. *Langmuir*, 15(4), 1252-1259.
- Raposo, M., & Oliveira Jr, O. N. (2002). Adsorption of poly(o-methoxyaniline) in layer-by-layer films. *Langmuir*, 18(18), 6866-6874.
- Ravati, S. (2010). *Novel Conductive Polymer Blends*. PhD thesis, École Polytechnique de Montréal, Montreal.
- Ravati, S., & Favis, B. D. (2010). *Polymer, Submitted*.

- Reghu, M., Yoon, C. O., Yang, C. Y., Moses, D., Smith, P., Heeger, A. J., et al. (1994). Transport in polyaniline networks near the percolation threshold. *Physical Review B*, 50(Copyright (C) 2009 The American Physical Society), 13931.
- Reif, J. H., Sahu, S., & Yin, P. (2006). *Complexity of graph self-assembly in accretive systems and self-destructible systems*, London, Ont., Canada.
- Reignier, J., & Favis, B. D. (2000). Control of the Subinclusion Microstructure in HDPE/PS/PMMA Ternary Blends. *Macromolecules*, 33(19), 6998-7008.
- Reignier, J., & Favis, B. D. (2003a). Core-shell structure and segregation effects in composite droplet polymer blends. *AIChE Journal*, 49(4), 1014-1023.
- Reignier, J., & Favis, B. D. (2003b). On the presence of a critical shell volume fraction leading to pseudo-pure droplet behavior in composite droplet polymer blends. *Polymer*, 44(18), 5061-5066.
- Reignier, J., Favis, B. D., & Heuzey, M.-C. (2003). Factors influencing encapsulation behavior in composite droplet-type polymer blends. *Polymer*, 44(1), 49-59.
- Rodrigues, P. C., & Akcelrud, L. (2003). Networks and blends of polyaniline and polyurethane: Correlations between composition and thermal, dynamic mechanical and electrical properties. *Polymer*, 44(22), 6891-6899.
- Rodrigues, P. C., Lisboa-Filho, P. N., Mangrich, A. S., & Akcelrud, L. (2005). Polyaniline/polyurethane networks. II. A spectroscopic study. *Polymer*, 46(7), 2285-2296.
- Roman, L. S., Andersson, M. R., Yohannes, T., & Inganás, O. (1997). Photodiode performance and nanostructure of polythiophene/ C₆₀ blends. *Advanced Materials*, 9(15), 1164-1168.
- Rosner, R. B. (2000). *Conductive Materials for ESD Applications: An Overview*
- Roy, X., Sarazin, P., & Favis, B. D. (2006). Ultraporous nanosheath materials by layer-by-layer deposition onto co-continuous polymer-blend templates. *Advanced Materials*, 18(8), 1015-1019.
- Rudra, J. S., Dave, K., & Haynie, D. T. (2006). Antimicrobial polypeptide multilayer nanocoatings. *Journal of Biomaterials Science, Polymer Edition*, 17(11), 1301-1315.
- Ruokolainen, J., Eerikainen, H., Torkkeli, M., Serimaa, R., Jussila, M., & Ikkala, O. (2000). Comb-Shaped Supramolecules of Emeraldine Base Form of Polyaniline Due to Coordination with Zinc Dodecyl Benzenesulfonate and Their Plasticized Self-Organized Structures. *Macromolecules*, 33(25), 9272-9276.
- Sarazin, P., & Favis, B. D. (2003). Morphology control in co-continuous poly(L-lactide)/polystyrene blends: A route towards highly structured and interconnected porosity in poly(L-lactide) materials. *Biomacromolecules*, 4(6), 1669-1679.
- Sarazin, P., Roy, X., & Favis, B. D. (2004). Controlled preparation and properties of porous poly(L-lactide) obtained from a co-continuous blend of two biodegradable polymers. *Biomaterials*, 25(28), 5965-5978.

- Sau, K., Chaki, T., & Khastgir, D. (1997). Conductive rubber composites from different blends of ethylene-propylene-diene rubber and nitrile rubber. *Journal of Materials Science*, 32(21), 5717-5724.
- Sau, K. P., Chaki, T. K., & Khastgir, D. (1998). Carbon fibre filled conductive composites based on nitrile rubber (NBR), ethylene propylene diene rubber (EPDM) and their blend. *Polymer*, 39(25), 6461-6471.
- Scher, H., & Zallen, R. (1970). Critical Density in Percolation Processes. *The Journal of Chemical Physics*, 53(9), 3759-3761.
- Schlenoff, J. B., & Dubas, S. T. (2001). Mechanism of Polyelectrolyte Multilayer Growth: Charge Overcompensation and Distribution. *Macromolecules*, 34(3), 592-598.
- Schlenoff, J. B., Ly, H., & Li, M. (1998). Charge and mass balance in polyelectrolyte multilayers. *Journal of the American Chemical Society*, 120(30), 7626-7634.
- Schmidt, V. M., Tegtmeier, D., & Heitbaum, J. (1995). Transport of protons and water through polyaniline membranes studied with on-line mass spectrometry. *Journal of Electroanalytical Chemistry*, 385(2), 149-155.
- Schmitt, J., Gruenewald, T., Decher, G., Pershan, P. S., Kjaer, K., & Loesche, M. (1993). Internal structure of layer-by-layer adsorbed polyelectrolyte films: A neutron and X-ray reflectivity study. *Macromolecules*, 26(25), 7058-7063.
- Schneider, G., & Decher, G. (2004). From Functional Core/Shell Nanoparticles Prepared via Layer-by-Layer Deposition to Empty Nanospheres. *Nano Letters*, 4(10), 1833-1839.
- Schoeler, B., Kumaraswamy, G., & Caruso, F. (2002). Investigation of the influence of polyelectrolyte charge density on the growth of multilayer thin films prepared by the layer-by-layer technique. *Macromolecules*, 35(3), 889-897.
- Schwarz, S., Eichhorn, K. J., Wischerhoff, E., & Laschewsky, A. (1999). Polyelectrolyte adsorption onto planar surfaces: A study by streaming potential and ellipsometry measurements. *Colloids and Surfaces A: Physicochemical and Engineering Aspects*, 159(2-3), 491-501.
- Scott, R. L. (1949). The Thermodynamics of High Polymer Solutions. IV. Phase Equilibria in the Ternary System: Polymer---Liquid 1---Liquid 2. *The Journal of Chemical Physics*, 17(3), 268-279.
- Segal, E., Haba, Y., Narkis, M., & Siegmund, A. (2001). On the structure and electrical conductivity of polyaniline/polystyrene blends prepared by an aqueous-dispersion blending method. *Journal of Polymer Science, Part B: Polymer Physics*, 39(5), 611-621.
- Shacklette, L. W., Han, C. C., & Luly, M. H. (1993). Polyaniline blends in thermoplastics. *Synthetic Metals*, 57(1), 3532-3537.
- Shimazaki, Y., Mitsuishi, M., Ito, S., & Yamamoto, M. (1997). Preparation of the Layer-by-Layer Deposited Ultrathin Film Based on the Charge-Transfer Interaction. *Langmuir*, 13(6), 1385-1387.

- Shirakawa, H., Louis, E. L., MacDiarmid, A. G., Chiang, C. K., & Heeger, A. J. (1977). Synthesis of electrically conducting organic polymers: halogen derivatives of polyacetylene, $(\text{CH})_x$. *J. Chem. Soc., Chem. Commun.*, 578 - 580.
- Shiratori, S. S., & Rubner, M. F. (2000). pH-Dependent Thickness Behavior of Sequentially Adsorbed Layers of Weak Polyelectrolytes. *Macromolecules*, 33(11), 4213-4219.
- Sichel, E. (1982). *Carbon Black-Polymer Composites*. New York: Marcel Dekker.
- Siggia, E. D. (1979). Late stages of spinodal decomposition in binary mixtures. *Physical Review A (General Physics)*, 20(2), 595-605.
- Skorokhov, V. V. (1972). *The Rheological Principles of Sintering Theory*. Kiev: Nauka.
- Smuckler J, H., & Finnerty P, M. (1974). Performance of Conductive Carbon Blacks in a Typical Plastics System *Fillers and Reinforcements for Plastics* (pp. 171-183). Washington, D. C.: American Chemical Society.
- Soares, B. G., Gubbels, F., Jerome, R., Teyssie, P., Vanlathem, E., & Deltour, R. (1995). Electrical conductivity in carbon black-loaded polystyrene-polyisoprene blends. Selective localization of carbon black at the interface. *Polymer Bulletin (Berlin)*, 35(1-2), 223.
- Solis, F. J., Cruz, d. l., & M., O. (1999). Surface-induced layer formation in polyelectrolytes. *Journal of Chemical Physics*, 110(23), 11517-11522.
- Solonin, S. M., & Chernyshev, L. I. (1975). Effects of sintering conditions on the physicomechanical properties of porous tungsten. *Soviet Powder Metallurgy and Metal Ceramics (English translation of Poroshkovaya Metallurgiya)*, 14(10), 806-808.
- Stauffer, D., & Aharony, A. (1994b). *Introduction to Percolation Theory*. London: Taylor and Francis.
- Steinmann, S., Gronski, W., & Friedrich, C. (2001). Cocontinuous polymer blends: Influence of viscosity and elasticity ratios of the constituent polymers on phase inversion. *Polymer*, 42(15), 6619-6629.
- Steinmann, S., Gronski, W., & Friedrich, C. (2002). Quantitative rheological evaluation of phase inversion in two-phase polymer blends with cocontinuous morphology. *Rheologica Acta*, 41(1-2), 77-86.
- Stockton, W. B., & Rubner, M. F. (1997). Molecular-level processing of conjugated polymers. 4. Layer-by-layer manipulation of polyaniline via hydrogen-bonding interactions. *Macromolecules*, 30(9), 2717-2725.
- Stratouras, G., & Kosmas, M. (1992). Are ring polymers adsorbed on a surface more than linear polymers? *Macromolecules*, 25(12), 3307-3308.
- Su, T. M., Ball, I. J., Conklin, J. A., Huang, S.-C., Larson, R. K., Nguyen, S. L., et al. (1997). Polyaniline/polyimide blends for pervaporation and gas separation studies. *Synthetic Metals*, 84(1-3 pt 1), 801-802.
- Sui, Z., Salloum, D., & Schlenoff, J. B. (2003). Effect of Molecular Weight on the Construction of Polyelectrolyte Multilayers: Stripping versus Sticking. *Langmuir*, 19(6), 2491-2495.

- Sumita, M., Kayaki, H., & Miyasaka, K. (1986). Effect of Melt Viscosity and Surface Tension of Polymers on the Percolation Threshold of Conductive-Particle-Filled Polymeric Composites. *Journal of Macromolecular Science - Physics*, *B25*(1-2), 171-184.
- Sumita, M., Sakata, K., Asai, S., Miyasaka, K., & Nakagawa, H. (1991). Dispersion of fillers and the electrical conductivity of polymer blends filled with carbon black. *Polymer Bulletin (Berlin)*, *25*(2), 265-271.
- Sumita, M., Sakata, K., Hayakawa, Y., Asai, S., Miyasaka, K., & Tanemura, M. (1992). Double percolation effect on the electrical conductivity of conductive particles filled polymer blends. *Colloid & Polymer Science*, *270*(2), 134-139.
- Sundararaj, U., & Macosko, C. W. (1995). Drop breakup and coalescence in polymer blends: the effects of concentration and compatibilization. *Macromolecules*, *28*(Compendex), 2647-2657.
- Tang, Z., Kotov, N. A., & Giersig, M. (2002). Spontaneous Organization of Single CdTe Nanoparticles into Luminescent Nanowires. *Science*, *297*(5579), 237-240.
- Tchomakov, K. P., Favis, B. D., Huneault, M. A., Champagne, M. F., & Tofan, F. (2004). Composite droplets with core/shell morphologies prepared from HDPE/PS/PMMA ternary blends by twin-screw extrusion. *Polymer Engineering and Science*, *44*(4), 749-759.
- Tchoudakov, R., Breuer, O., Narkis, M., & Siegmann, A. (1996). Conductive polymer blends with low carbon black loading: Polypropylene/polyamide. *Polymer Engineering & Science*, *36*(10), 1336-1346.
- Tessler, N., Denton, G. J., & Friend, R. H. (1996). Lasing from conjugated-polymer microcavities. *Nature*, *382*(6593), 695-697.
- Tjahjadi, M., Ottino, J. M., & Stone, H. A. (1994). Estimating interfacial tension via relaxation of drop shapes and filament breakup. *AIChE Journal*, *40*(3), 385-394.
- Tjipto, E., Quinn, J. F., & Caruso, F. (2007). Layer-by-layer assembly of weak-strong copolymer polyelectrolytes: a route to morphological control of thin films. *Journal of Polymer Science, Part A (Polymer Chemistry)*, *45*(Copyright 2008, The Institution of Engineering and Technology), 4341-4351.
- Tomotika, S. (1935a). Instability of a cylindrical thread of a viscous liquid surrounded by another viscous fluid. *Proceedings of the Royal Society of London*, *150A*, 322-337.
- Tomotika, S. (1935b). On the instability of a cylindrical thread of a viscous liquid surrounded by another viscous liquid. *Proc. Roy. Soc.*, *A150*, 322-337.
- Torza, S., & Mason, S. G. (1970). Three-phase interactions in shear and electrical fields. *Journal of Colloid and Interface Science*, *33*(1), 67-83.
- Tse, C. W., Man, K. Y. K., Cheng, K. W., Mak, C. S. K., Chan, W. K., Yip, C. T., et al. (2007). Layer-by-layer deposition of rhenium-containing hyperbranched polymers and fabrication of photovoltaic cells. *Chemistry - A European Journal*, *13*(1), 328-335.
- Urashita, S., Kawakatsu, T., & Doi, M. (2000). *Morphologies of multiphase polymer blend systems*, Kanazawa, Japan.

- Utracki, L. A. (1991). On the viscosity-concentration dependence of immiscible polymer blends. *Journal of Rheology*, 35(8), 1615-1637.
- Utracki, L. A. (1998). *Commercial Polymer Blends* Springer - Verlag.
- Valera, T. S., Morita, A. T., & Demarquette, N. R. (2006). Study of morphologies of PMMA/PP/PS ternary blends. *Macromolecules*, 39(7), 2663-2675.
- Van Lent, B., Scheutjens, J., & Cosgrove, T. (1987). Self-consistent field theory for the adsorption of ring polymers from solution. *Macromolecules*, 20(2), 366-370.
- Van Oene, H. J. (1972). Modes of dispersion of viscoelastic fluids in flow. *Colloid Interface Sci.*, 40, 448-467.
- Vanoene, H. (1972). Modes of dispersion of viscoelastic fluids in flow. *Journal of Colloid and Interface Science*, 40(3), 448-467.
- Veenstra, H., Norder, B., van Dam, J., & Posthuma de Boer, A. (1999). Stability of co-continuous polystyrene/poly(ether-ester) blends in shear flow. *Polymer*, 40(18), 5223-5226.
- Veenstra, H., Van Dam, J., & Posthuma de Boer, A. (2000). On the coarsening of co-continuous morphologies in polymer blends: Effect of interfacial tension, viscosity and physical cross-links. *Polymer*, 41(8), 3037-3045.
- Veenstra, H., Verkooijen, P. C. J., van Lent, B. J. J., van Dam, J., de Boer, A. P., & Nijhof, A. P. H. J. (2000). On the mechanical properties of co-continuous polymer blends: Experimental and modelling. *Polymer*, 41(5), 1817-1826.
- Verhelst, W. F., Wolthuis, K. G., Voet, A., Ehrburger, P., & Donnet, J. B. (1977). The role of morphology and structure of carbon blacks in the electrical conductance of vulcanizates. *Rubber Chem. Technol.*, 50, 735-746.
- Vikki, T., Pietila, L.-O., Osterholm, H., Ahjopalo, L., Takala, A., Toivo, A., et al. (1996). Molecular Recognition Solvents for Electrically Conductive Polyaniline. *Macromolecules*, 29(8), 2945-2953.
- Virgilio, N., Desjardins, P., L'Esperance, G., & Favis, B. D. (2009). In situ measure of interfacial tensions in ternary and quaternary immiscible polymer blends demonstrating partial wetting. *Macromolecules*, 42(19), 7518-7529.
- Virgilio, N., Favis, B. D., Pepin, M.-F., Desjardins, P., & L'Esperance, G. (2005a). High contrast imaging of interphases in ternary polymer blends using focused ion beam preparation and atomic force microscopy. *Macromolecules*, 38(Compendex), 2368-2375.
- Virgilio, N., Marc-Aurele, C., & Favis, B. D. (2009). Novel self-assembling close-packed droplet array at the interface in ternary polymer blends. *Macromolecules*, 42(Compendex), 3405-3416.
- Volodkin, D. V., Petrov, A. I., Prevot, M., & Sukhorukov, G. B. (2004). Matrix Polyelectrolyte Microcapsules: New System for Macromolecule Encapsulation. *Langmuir*, 20(8), 3398-3406.
- Wallin, T., & Linse, P. (1996). Monte Carlo simulations of polyelectrolytes at charged micelles. 1. Effects of chain flexibility. *Langmuir*, 12(2), 305.

- Wang Gusukuma, L., Prates, J. C., & Smith, R. L. (2004). Chorade Tendineae Architecture in the Papillary Muscle Insertion. *International Journal of Morphology*, 22, 267-272.
- Wang, Y., & Rubner, M. F. (2002). Electrically conductive semiinterpenetrating polymer networks of poly(3-octylthiophene). *Macromolecules*, 25(12), 3284-3290.
- Watcharaphalakorn, S., Ruangchuay, L., Chotpattananont, D., Sirivat, A., & Schwank, J. (2005). Polyaniline/polyimide blends as gas sensors and electrical conductivity response to CO-N₂ mixtures. *Polymer International*, 54(8), 1126-1133.
- Wessling, B. (1994). Passivation of metals by coating with polyaniline: Corrosion potential shift and morphological changes. *Advanced Materials*, 6(3), 226-228.
- Willemse, R. C., de Boer, A. P., van Dam, J., & Gotsis, A. D. (1998). Co-continuous morphologies in polymer blends: A new model. *Polymer*, 39(24), 5879-5887.
- Willemse, R. C., Posthuma de Boer, A., van Dam, J., & Gotsis, A. D. (1999). Co-continuous morphologies in polymer blends: the influence of the interfacial tension. *Polymer*, 40(4), 827-834(828).
- Willemse, R. C., Ramaker, E. J. J., van Dam, J., & Posthuma de Boer, A. (1999). Morphology development in immiscible polymer blends: initial blend morphology and phase dimensions. *Polymer*, 40(24), 6651-6659.
- Wise, D. L., Wnek, G. E., Trantolo, D. J., Cooper, T. M., & Gresser, J. D. (1997). *Electrical and optical polymer systems*. New York: Marcel Dekker.
- Wolter, A., Banka, E., Genoud, F., Pron, A., & Nechtschein, M. (1997). Electronic transport in composites based on polyaniline blended with cellulose acetate - a DC-conductivity and ESR analysis. *Synthetic Metals*, 84(1-3 pt 1), 753-754.
- Won-Jung, K., Tae-Young, K., Jung-Woo, K., Yun-Sang, K., Chang-Mo, P., & Suh, K. S. (2004). Charge transport phenomena of polyaniline-DBSA/polystyrene blends. *Transactions of the Korean Institute of Electrical Engineers, C*, 53(6), 305-311.
- Wong, C. P. (2003-2008). *Fundamental Understanding and Performance Enhancement of Conductive Adhesive for Microelectronic Packaging Applications*. Georgia Institute of Technology
- Woo Jin, B., Won Ho, J., & Yun Heum, P. (2003). Preparation of polystyrene/polyaniline blends by in situ polymerization technique and their morphology and electrical property. *Synthetic Metals*, 132(3), 239-244.
- Wu, S. (1971). *J. Polym. Sci.*, C34, 19.
- Wu, S. (1982). *Polymer Interface and Adhesion*. New York: Marcel Dekker Inc.
- Yang, C. Y., Cao, Y., Smith, P., & Heeger, A. J. (1993a). Morphology of conductive, solution-processed blends of polyaniline and poly(methyl methacrylate). *Synthetic Metals*, 53(3), 293-301.
- Yang, C. Y., Cao, Y., Smith, P., & Heeger, A. J. (1993b). Morphology of polyaniline in solution processed blends with poly(methyl methacrylate). *Polymer Preprints, Division of Polymer Chemistry, American Chemical Society*, 34(1), 790.

- Yasuda, K., Armstrong, R., & Cohen, R. (1981). Shear flow properties of concentrated solutions of linear and star branched polystyrenes. *Rheologica Acta*, 20(2), 163-178.
- Yipeng Sun, X. Z. C. S. B. W. J. S. (1996). Fabrication of ultrathin film containing bienzyme of glucose oxidase and glucoamylase based on electrostatic interaction and its potential application as a maltose sensor. *Macromolecular Chemistry and Physics*, 197(1), 147-153.
- Yoshikawa, H., Hino, T., & Kuramoto, N. (2006). Effect of temperature and moisture on electrical conductivity in polyaniline/polyurethane (PANI/PU) blends. *Synthetic Metals*, 156(18-20), 1187-1193.
- Yuan, Z., & Favis, B. D. (2004). Macroporous poly(L-lactide) of controlled pore size derived from the annealing of co-continuous polystyrene/poly(L-lactide) blends. *Biomaterials*, 25(11), 2161-2170.
- Yuan, Z., & Favis, B. D. (2006). Influence of the efficacy of interfacial modification on the coarsening of cocontinuous PS/HDPE blends during quiescent annealing. *Journal of Polymer Science, Part B: Polymer Physics*, 44(4), 711-721.
- Zasadzinski, J. A., Viswanathan, R., Madsen, L., Garnæs, J., & Schwartz, D. K. (1994). Langmuir-Blodgett films. *Science*, 263(5154), 1726-1733.
- Zhang, J., Ravati, S., Virgilio, N., & Favis, B. D. (2007). Ultralow percolation thresholds in ternary cocontinuous polymer blends. *Macromolecules*, 40(25), 8817-8820.
- Zhang, Q., Jin, H., Wang, X., & Jing, X. (2001). Morphology of conductive blend fibers of polyaniline and polyamide-11. *Synthetic Metals*, 123(3), 481-485.
- Zhenhua Yuan, B. D. F. (2005). Coarsening of immiscible co-continuous blends during quiescent annealing. *AIChE Journal*, 51(1), 271-280.
- Zilberman, M., Siegmann, A., & Narkis, M. (1998). *Polyaniline containing ternary immiscible polymer blends: A melt processable conductive system*, Anaheim, CA, USA.
- Zilberman, M., Siegmann, A., & Narkis, M. (2000a). Electrically conductive extruded filaments of polyaniline/polymer blends. *Journal of Polymer Engineering*, 20(2), 97-110.
- Zilberman, M., Siegmann, A., & Narkis, M. (2000c). Melt-processed, electrically conductive ternary polymer blends containing polyaniline. *Journal of Macromolecular Science - Physics*, B39(3), 333-347.
- Zilberman, M., Titelman, G. I., Siegmann, A., Haba, Y., Narkis, M., & Alperstein, D. (1997). Conductive blends of thermally dodecylbenzene sulfonic acid-doped polyaniline with thermoplastic polymers. *Journal of Applied Polymer Science*, 66(2), 243-253.

APPENDIX I

A- 1 Ultra-Low Percolation Thresholds in Ternary Co-Continuous Polymer Blends

*Jianhong Zhang, Sepehr Ravati, Nick Virgilio, and Basil D. Favis**

CREPEC, Department of Chemical Engineering, École Polytechnique de Montréal, Montréal,
Québec, H3C 3A7 Canada

Published in Macromolecules in December 2007

A-1.1. Introduction. In binary immiscible polymer blends, as the concentration of the minor component increases, the structure percolates and its continuity also increases (Potschke & Paul, 2003; Reignier & Favis, 2000). At higher concentrations, closely associated with the region of phase inversion, a co-continuous morphology is obtained and is characterized by two fully continuous phases. By selectively controlling the interface, composition, processing temperature, shear rate and annealing time of the blends, it is possible to control the pore size of the co-continuous network over 2-3 orders of magnitude (Yuan & Favis, 2004, 2006). Co-continuous polymer blends have the potential of opening particular application fields where the presence of interconnected structures are a necessary feature (as in separation phenomena, electrical conductivity, tissue engineering scaffolds and drug delivery devices). A significant body of

* Corresponding author. E-mail: basil.favis@polymtl.ca Tel: +1-(514)3404711 ext.4527. Fax: +1-(514)3404159

literature has examined factors influencing the percolation threshold in binary co-continuous polymer blends and also the width and concentration range of the region of dual-phase continuity (Yuan & Favis, 2004, 2006). Most studies on binary systems report percolation thresholds in a range of about 15-20% concentration of minor component. This significant amount of the second phase, necessary to obtain a co-continuous structure, considerably limits the range of possible applications. However, very few studies have examined the continuity phenomena in multiphase (more than two phases) systems. The possibility of dramatically decreasing the percolation threshold of one component in order to achieve co-continuity at concentration levels of a few percent would be an important achievement. A few studies have contributed towards attaining such a result. Jérôme and co-workers reported on the preparation of a co-continuous polymer blend with the addition of a solid filler showing a very low percolation threshold for the filler at about 0.2 volume percent. Interestingly, this filler was located at the interface in a chain-like structure shape (Gubbels, et al., 1994; Soares, et al., 1995). However, the limitation in that case is that the particle is not thermodynamically stable at the interface. It has a particular affinity for one of the phases and is simply transiting from one phase to the other. Jorgensen and Utracki report very low percolation thresholds for polyethylene in polystyrene binary blends of very high molecular weight (Lyngaae-Jorgensen & Utracki, 2003). In other studies, Narkis, Zilberman and coworkers (Narkis, et al., 2000a; Zilberman, Siegmann, & Narkis, 2000c) achieved multiple percolation by dispersing a third phase into one of the phases in a co-continuous binary blend. This ultimately creates a third percolated system, but the percolation thresholds are relatively high at 8-12% composition of this third phase.

A potentially interesting way to achieve low percolation threshold materials is to combine a co-continuous structure with a composite droplet type of morphology. The composite droplet morphology is a matrix/dispersed phase system in which the dispersed phase has a droplet-in-droplet structure. Although little work has been published on polymeric versions of such systems, a number of key papers have appeared (Berger, Kammer, & Kummerlowe, 1984; Omonov, Harrats, & Groeninckx, 2005; Reignier & Favis, 2003a; Reignier, et al., 2003; Van Oene, 1972). The spreading coefficients (Torza & G. Mason, 1970) (Equation A-1.1) and variations on that concept have been successfully used (Hobbs, et al., 1988; Reignier & Favis, 2000; Valera, et al., 2006) to predict the thermodynamically stable preferential encapsulation of one polymeric phase by another. Encapsulation is governed by the various interfacial tension

pairs within a ternary polymer blend and is related to the minimization of the interfacial free energy. In Equation A-1.1,

Equation A-1.1

$$\lambda_{ij} = \gamma_{jk} - \gamma_{ik} - \gamma_{ij}$$

λ_{ij} is defined as the spreading coefficient describing the tendency of component i to encapsulate or spread around component j in a matrix of component k . γ_{jk} , γ_{ik} and γ_{ij} are the interfacial tensions of the different polymer pairs. In blends of one major constituent (polymer A) and two minor ones (polymers B and C , the dispersed phases), four different morphologies are possible (Figure A-1.1) : a) separate dispersions; b) partial encapsulation and c), d) two possibilities of complete wetting (composite droplets). Each morphology has a distinct set of spreading coefficients.

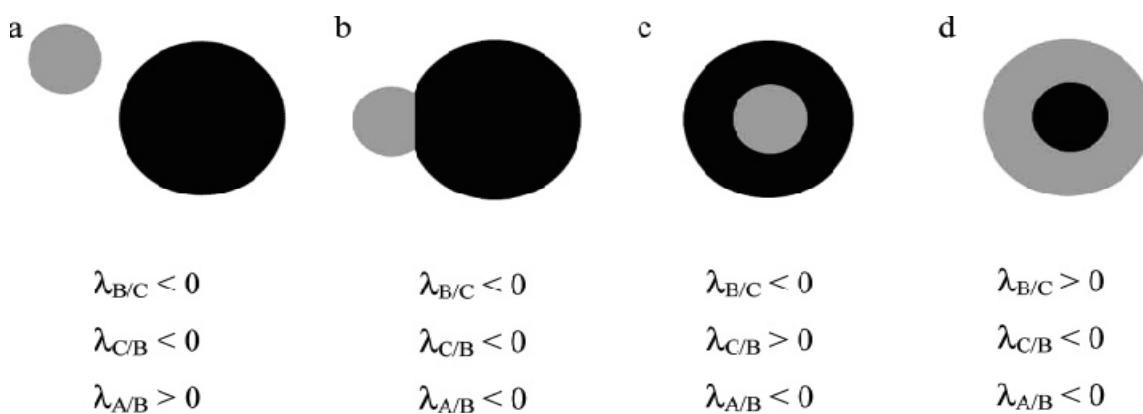


Figure A-1.1. Morphologies of ternary polymer blends containing one major phase (polymer A (white)) and two minor ones (polymers B (gray) and C (black)): (a) separate dispersions; (b) partial encapsulation; (c and d) composite droplets (complete wetting)

Recently, in our group, studies have been conducted on ternary immiscible polymer blends of high-density polyethylene (HDPE), polystyrene (PS) and poly(methyl methacrylate) (PMMA)

(Reignier & Favis, 2000, 2003a; Reignier, et al., 2003). When PS and PMMA are dispersed in a HDPE matrix, composite droplets constituted of a well-segregated PMMA core and PS shell are formed. By controlling the relative amounts of PS and PMMA, it is possible to control the thickness of the PS shell down to 30-40 nm, near the range of a molecular layer of PS. Furthermore, virtually all of the PMMA is present as sub-inclusions within the PS dispersed phase after approximately 2 minutes of mixing.

This paper reports on the development of ternary percolated co-continuous systems in HDPE/PS/PMMA blends in which HDPE and PMMA form two continuous networks, while the PS forms a continuous sheath structure at the HDPE/PMMA interface (Figure A-1.2). By controlling the relative amounts of HDPE, PS and PMMA, it will be shown that it is possible to decrease the percolation threshold of the PS layer down to less than 3%, resulting in a PS continuous network of ultra low composition.

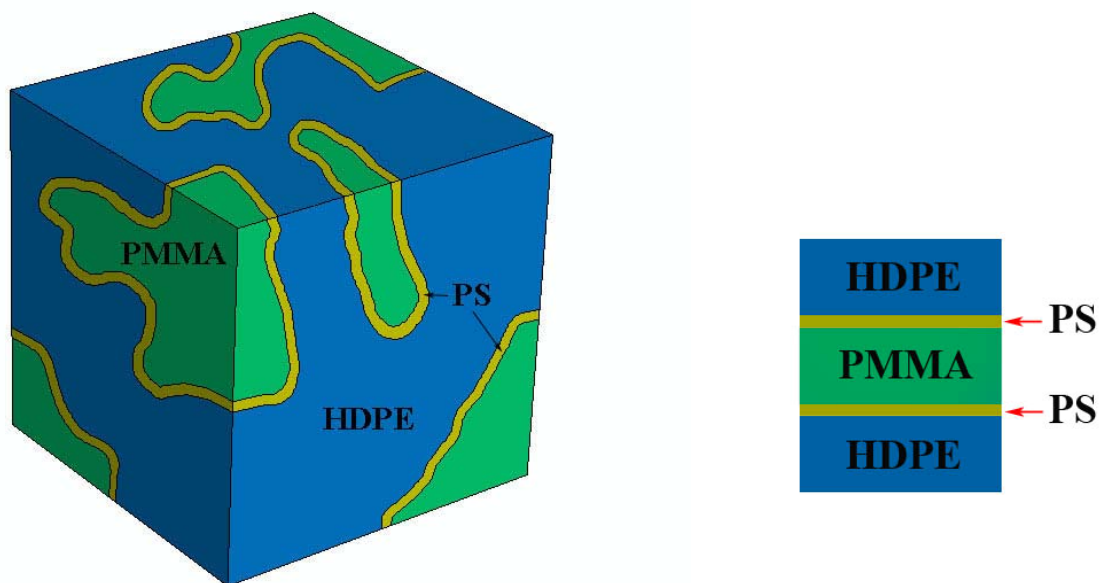


Figure A-1.2. Schematic of the HDPE/PS/PMMA multiple percolated structure. a) Three-dimensional view of the blend structure, showing the thin PS layer at the HDPE/PMMA interface. b) Section showing the relative position of the different phases.

A-1.2. Experimental Section

A-1.2.1. Materials: HDPE 04352N and PS 615APR were both obtained from the Dow Chemical Company. PMMA 200336 was purchased from Sigma-Aldrich. An antioxidant, Irganox B225 from Ciba-Geigy, was added to the mixture to reduce thermal oxidation of polyethylene (0.2 weight percent). Physical properties of the materials were measured previously (Reignier & Favis, 2003a) and are given in Table A-1.1.

Table A-1.1. Homopolymer properties

Polymers	$M_w^a \times 10^{-3}$ g/mol	$M_n^a \times 10^{-3}$ g/mol	Melt Index ^b ASTM g/10min	Density ^b g/cm ³ at		$\eta_1^* \times 10^{-3}$ ^c Pa.s at 200°C		$N_1 \times 10^{-4}$ ^d Pa at 200°C	
				20°C	200°C	$\dot{\gamma}$	τ^e	$\dot{\gamma}$	τ^f
HDPE	79	24	4	0.96	0.75	1.2	1.2	2.2	2.2
PS	290	141	15	1.04	0.97	1.7	2.6	11	5.1
PMMA	11.9	7.8	-	-	1	0.04	0.04	0.02	0.6

^a Measured by GPC, ^b Obtained from supplier, ^c η_1^* is the complex viscosity, ^d N_1 is the first normal stress difference, ^e At average shear rate during blending: $\dot{\gamma} = 25s^{-1}$, ^f At average shear stress during blending: $\tau = 2.7 \times 10^4 Pa$

A-1.2.1. Measurement of the interfacial tensions and calculation of the spreading coefficients:

The interfacial tensions were measured using the breaking thread method, as described in an earlier publication (Reignier & Favis, 2000). The different interfacial tensions and spreading coefficients for the HDPE/PS/PMMA ternary blends are given in Table A-1.2.

Table A-1.2. Interfacial tensions and spreading coefficients for HDPE/PS/PMMA blends at 200°C.

Polymer pairs	Interfacial tension γ (mN/m)	Polymer pairs Spreading of i on j (i/j)	Spreading coefficients λ (mN/m)
HDPE/PS	5.1	PS/PMMA	1.1
PS/PMMA	2.4	PMMA/PS	-5.9
HDPE/PMMA	8.6	HDPE/PS	-11.3

A-1.2.3. Blend preparation: Prior to melt mixing, all polymers were pre-dried for 24h at 80°C in a vacuum oven to remove any moisture from the pellets or powders. Ternary blends were prepared by melt-mixing in a 50 ml Haake internal mixer with twin cam rotors, with the temperature of the mixing chamber initially set at 200°C and rotor speed set at 50 rpm. After mixing for 7 minutes under a constant flow of dry nitrogen, samples were immediately quenched in a bath of liquid nitrogen to freeze-in the morphology.

A-1.2.4. Continuity measurement: Solvent extraction has been used to determine the composition region of co-continuity of the blends. As a primary advantage, solvent extraction is an absolute measurement (Steinmann, et al., 2001) and is capable of detecting the existence of co-continuous microstructures when the components are soluble in specific solvents (Potschke & Paul, 2003). The level of continuity of a phase in a sample is given by Equation A-1.2:

$$\text{Equation A-1.2} \quad \% \text{ Continuity} = \frac{m_{\text{initial}} - m_{\text{final}}}{m_{\text{initial}}(i)} \times 100$$

In this equation, m_{initial} is the initial mass of the sample, m_{final} is the final mass of the sample and $m_{\text{initial}}(i)$ is the mass of polymer i contained in the sample before selective extraction, calculated by considering the blend as homogeneous. Selective solvent extraction of the PMMA and PS phases were performed respectively in acetic acid and cyclohexane in a soxhlet extraction apparatus. Mass loss measurements were carried out for one week and were used to calculate the extent of continuity of the PMMA and PS phases using Equation A-1.2.

A-1.2.5. Focused Ion Beam (FIB) preparation and Atomic Force Microscopy (AFM) morphology analysis: The specimens were initially cryomicrotomed to create a plane face using

a Leica RM2165 microtome equipped with a cooling chamber. FIB surface etching was performed using a Hitachi 2000A Ga⁺ focused ion beam operated at 30 keV and 0.8 nA, with a dwelling time of 3 μ sec. The etched surface was then analyzed by tapping mode atomic force microscopy (AFM) using a scanning probe microscope Dimension 3100 from Veeco Instruments equipped with a Nanoscope IVa controller. Silicon tips, model PPP-NCH-W from Nanosensors, with a force constant of 10-130 N/m (nominal value of 42 N/m) and resonance frequency of 204-497 kHz (nominal value of 330 kHz), were used. The cantilever was oscillated at approximately 98% of the resonance frequency and topographic (height) images were taken at approximately 95% of the free oscillating amplitude. The samples were fixed on a metallic support using graphite tape. This procedure is thoroughly described in a previous paper (Virgilio, Favis, Pepin, Desjardins, & L'Esperance, 2005b).

A-1.3. Results and Discussion

Initially, the continuity development of the PMMA phase in binary HDPE/PMMA blends was examined in order to determine the boundaries required to achieve co-continuity in HDPE/PMMA. After preparation by melt-mixing, the blends were immediately quenched in liquid nitrogen to freeze-in the morphology. To measure the continuity of the PMMA phase in each blend, a selective solvent extraction of the PMMA phase, using acetic acid, was performed. As the PMMA volume fraction increases from 30% to 40%, the continuity increases very rapidly from 17% to 95%. A further increase of the PMMA volume fraction to 45% yields a 98% continuous PMMA phase and results in a binary co-continuous polymer blend.

Subsequently, ternary HDPE/PS/PMMA blends were prepared at different compositions (given in Table A-1.3) based on the co-continuity region found for HDPE/PMMA binary blends. The qualitative microstructural features of the blends were analyzed using a Focused Ion Beam (FIB)-Atomic Force Microscopy (AFM) method described in a previous article (Virgilio, et al., 2005b). FIB etching involves the interaction of a gallium ion beam with the blend surface and is a surface preparation step prior to the AFM surface analysis. Since the gallium ion beam has significantly different etching rates for each of the individual components, this etching process induces a topological contrast between the different phases, each surface level corresponding to a specific phase. Observation of these surfaces by AFM in the topological mode allows for the

acquisition of images with a very high contrast. Since all the three polymers are immiscible, the three different levels observed on the AFM images each correspond to a given polymer. In HDPE/PS/PMMA ternary blends, PS is the less etched material, and thus corresponds to the high-level domains, while HDPE corresponds to the mid-level domains and PMMA to the low-level ones. This method of analysis is particularly useful for multicomponent blends and for fine structure analysis since the etching process is sensitive to the nature of the materials and eliminates some artifacts related to classical microtomy and staining preparation methods.

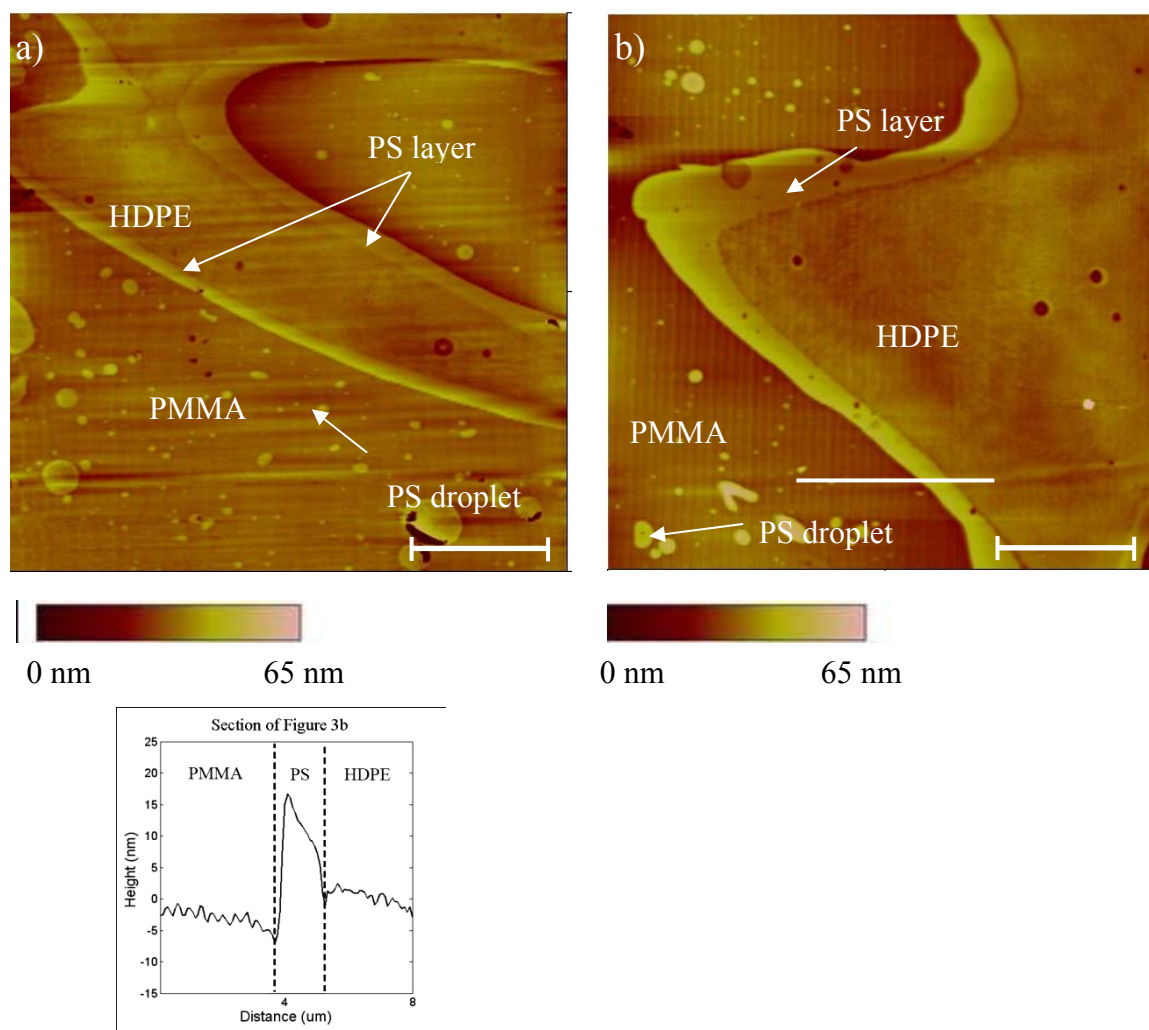


Figure A-1.3. FIB-AFM images of HDPE/PS/PMMA ternary blends: a) 50/10/40(% vol.) and b) 50/12.5/37.5. Images were taken at 95% of the free oscillation amplitude. Scan sizes are $20\ \mu\text{m} \times 20\ \mu\text{m}$. The white line in Figure A-1.3b indicates the section analyzed below.

Figure A-1.3 shows AFM images after FIB treatment of the microstructure of ternary blends No.5 and No.6, as described in Table A-1.3. The HDPE (mid-level domains, notice the fine texture corresponding to the crystalline structure) and PMMA phases (low-level domains, in dark orange) appear as the main components and are separated by a thin PS layer (high-level domains, in yellow). PS/PMMA and PS/HDPE composite droplets can also be seen in the HDPE and PMMA phases respectively, while some pure dispersed PS is observed in the PMMA. Finally, small quantities of PMMA and HDPE are visible in the PS layer. Even though the segregation is not perfect, it is clear that most of the PS is located at the interface between the PMMA and the HDPE phases. The white bar in Figure A-1.3b) corresponds to the section analyzed below the AFM image, quantitatively showing the relative topographical levels of each phase.

The presence of a PS layer at the interface of the co-continuous HDPE/PMMA blends significantly reduces the PS volume fraction required for its percolation and continuity development as compared to classical binary HDPE/PS and PMMA/PS blends. Continuity data based on gravimetric solvent extraction clearly demonstrate this effect and are shown in Table A-1.3 and Figure A-1.4. Cyclohexane and acetic acid were used to extract PS and PMMA respectively. It can be seen that in this triple percolated system, a PS volume composition as low as 3% results in a PS phase continuity of about 70%, a very high level of continuity for such a small volume fraction of PS. Moreover, the PS layer continuity increases with increasing PS volume content, reaching an apparent maximum value of approximately 80%. Interestingly, it seems impossible to further increase the PS continuity by increasing its relative composition. This upper limit in the apparent continuity of the PS is most probably due to the PS trapped as droplets and composite droplets in the PMMA and HDPE phases as shown in Figure A-1.3. Nevertheless, most of the PS has clearly and spontaneously structured itself at the HDPE/PMMA interface.

Table A-1.3. Continuity of the PMMA and PS phases as a function of composition using the selective solvent dissolution technique

Blend No.	Volume fractions (%)			Extracting PMMA	Extracting PS
	HDPE	PMMA	PS	PMMA continuity (%)	PS continuity (%)
1	50	50	0	103	0
2	50	47	3	103	69
3	50	45	5	102	73
4	50	42.5	7.5	103	74
5	50	40	10	102	76
6	50	37.5	12.5	104	77

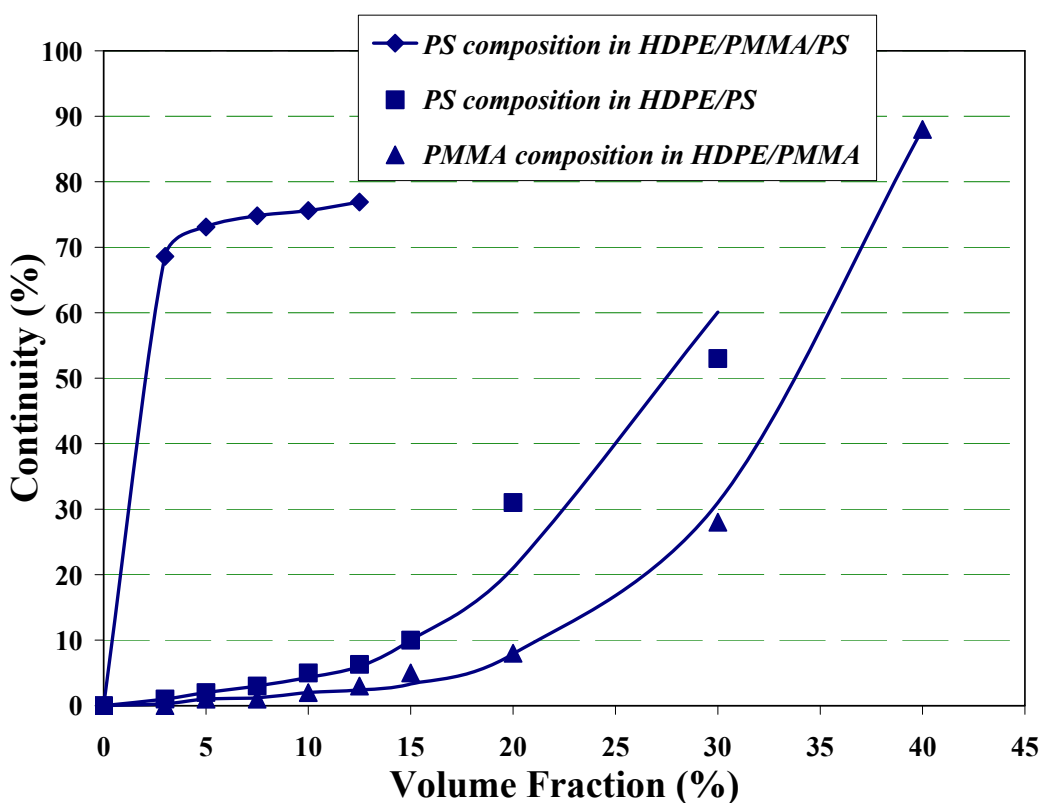


Figure A-1.4. Continuity of PS or PMMA as a function of the composition using the solvent dissolution technique

A-1.4. Conclusions

Through a combination of composite droplet and co-continuous blend morphology preparation methodologies, a continuous shell structure of polystyrene has been situated at the interface of a co-continuous polyethylene/poly(methyl methacrylate) blend. This multiple percolated, interfacial tension driven structure results in a dramatic decrease in the percolation threshold volume fraction of the encapsulating PS component. As little as 3% polystyrene is shown to generate a continuous PS network. The encapsulation effect follows the prediction based on the spreading coefficient theory. This approach could be used as a route to generate novel co-continuous structures and also as a technique to significantly reduce percolation thresholds in multiphase blends.

A-1.5. References

- (1) Favis, B. D., In *Polymer Blends: Formulation and Performance*, Paul, D. R.; Bucknall, C. B., Eds. John Wiley & Sons, Inc: New York, 2000; Vol. 1, pp 239-289.
- (2) Potschke, P.; Paul, D. R., *Journal of Macromolecular Science - Polymer Reviews* **2003**, 43, (1), 87-141.
- (3) Yuan, Z.; Favis, B. D., *Journal of Polymer Science, Part B: Polymer Physics* **2006**, 44, (4), 711-721.
- (4) Yuan, Z.; Favis, B. D., *Biomaterials* **2004**, 25, (11), 2161-2170.
- (5) Soares, B. G.; Gubbels, F.; Jerome, R.; Teyssie, P.; Vanlathem, E.; Deltour, R., *Polymer Bulletin (Berlin)* **1995**, 35, (1-2), 223.
- (6) Gubbels, F.; Jerome, R.; Teyssie, P.; Vanlathem, E.; Deltour, R.; Calderone, A.; Parente, V.; Bredas, J. L., *Macromolecules* **1994**, 27, (7), 1972-1974.
- (7) Lyngaae-Jorgensen, J.; Utracki, L. A., *Polymer* **2003**, 44, (5), 1661-9.
- (8) Zilberman, M.; Siegmann, A.; Narkis, M., *Journal of Macromolecular Science - Physics* **2000**, B39, (3), 333-47.
- (9) Narkis, M.; Haba, Y.; Segal, E.; Zilberman, M.; Titelman, G. I.; Siegmann, A., *Polymers for Advanced Technologies* **2000**, 11, (8-12), 665-673.
- (10) Omonov, T. S.; Harrats, C.; Groeninckx, G., *Polymer* **2005**, 46, (26), 12322-12336.
- (11) Reignier, J.; Favis, B. D., *AIChE Journal* **2003**, 49, (4), 1014-1023.
- (12) Reignier, J.; Favis, B. D.; Heuzey, M.-C., *Polymer* **2003**, 44, (1), 49-59.
- (13) Berger, W.; Kammer, H. W.; Kummerlowe, C., *Makromol Chem Suppl B* **1984**, 8, 101.
- (14) Van Oene, H. J., *Colloid Interface Sci.* **1972**, 40, 448-467.
- (15) Torza, S.; Mason, G., *J. Coll. Interface Sci.* **1970**, 33, (1), 67-83.
- (16) Hobbs, S. Y.; Dekkers, M. E. J.; Watkins, V. H., *Polymer* **1988**, 29, (9), 1598-1602.

- (17) Reignier, J.; Favis, B. D., *Macromolecules* **2000**, 33, (19), 6998-7008.
- (18) Valera, T. S.; Morita, A. T.; Demarquette, N. R., *Macromolecules* **2006**, 39, (7), 2663-2675.
- (19) Steinmann, S.; Gronski, W.; Friedrich, C., *Polymer* **2001**, 42, (15), 6619-6629.
- (20) Virgilio, N.; Favis, B. D.; Pepin, M.-F.; Desjardins, P.; L'Esperance, G., *Macromolecules* **2005**, 38, (6), 2368-2375.

APPENDIX II

A- 2 Estimation of Conductivity of Porous Conductive Devices by Semi-Empirical Models

Assembly of dimensional structures through the templating of multilayers onto 3D nanometer to micrometer scale objects was one of the most outstanding strategy modifications for LbL preparation. A few works have been devoted to developing 3D structures as the substrate in other areas of science such as drug delivery, but to date 3D templates have not been used for fabrication of LbL conductive multilayers. The pioneering works in which the LbL films were assembled on a 3D colloidal core(Caruso, Caruso, et al., 1998; Caruso, Caruso, & Mohwald, 1999) and 3D nano-sized porous templates(Hou, Harrell, Trofin, Kohli, & Martin, 2004) were carried out for controlled release, encapsulation of guest substances, and other purposes(Caruso & Schuler, 2000; Hou, et al., 2004; Park, Deng, & Advincula, 2005; Schneider & Decher, 2004; Volodkin, Petrov, Prevot, & Sukhorukov, 2004). Fabrication of a highly-controlled porous 3D substrate on which the LbL multilayer can be deposited is of great importance, whereas controlling the surface area can influence on the absorbed multilayer(Caruso, 2003). Applying a 3D structure enables us to not only manipulate the function of singular LbL multilayer films, but to create highly-controlled complex structures with a hierarchy of order and function that can be used to create devices and microsystems with special properties. The effect of porosity on mechanical, physical, and electrical properties of porous materials has been studied. For sintered metals, the presence of pores causes a decrease in strength and ductility and a detrimental effect on conductivity and magnetic properties. Hence, the study of the relationship between microstructure, and particularly porosity, of conductive porous samples and conductivity is of great importance.

In this part of the work, a semi-empirical model is obtained to calculate the conductivity of porous samples represented in Chapter 5 as a function of porosity and conductivity of the pure

PANI. Theoretically, the extent of the PANI phase in sample B is calculated from the mass increase of sample B from gravimetric data represented in Figure A-2.1.

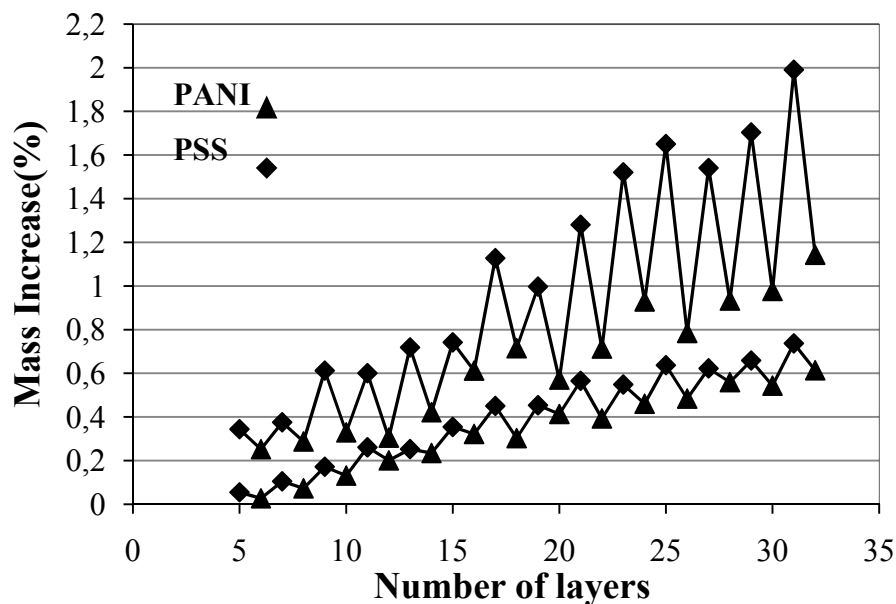


Figure A-2.1. Mass increase (%) indicating cumulative deposited mass for both cases of solutions containing salt and without salt as a function of number of layers for sample(B)

The oscillated behavior in Figure A-2.2 is neglected and the linear increase of PANI layers is taken into account. In 32 deposited PSS/PANI multilayers, the value of the average increase in thickness is 0.04% for PANI. Hence, for the 19 PANI layers, the mass increase becomes 0.76%. This means that for a 1g porous sample (HDPE+PANI+PSS), 0.0076g of PANI is available. By supposing that the density of PANI is equal to 1, the total volume of the blend equivalent to 1g of HDPE is calculated as:

$$\text{Equation A-2.1} \quad V_{HDPE} = \frac{m_{HDPE}}{\rho_{HDPE}} = \frac{(1-0.0076)}{0.85} = 1.167 \text{ cm}^3$$

$$\text{Equation A-2.2} \quad \frac{V_{HDPE}}{V_{Total}} = \frac{0.333}{1} \Rightarrow V_{Total} = 3.5 \text{ cm}^3$$

Now, as the conductivity of HDPE, air, and PSS polyelectrolytes are very low, it is assumed that the entire sample, except the PANI network, is void. This implies that the HDPE substrate and PSS network are considered as porous parts in order to propose a model to predict the conductivity of the PANI network. Thus, porosity of the sample, including HDPE, voids, and the PSS network can be calculated as follows:

$$\text{Equation A-2.3} \quad \Theta = \frac{V_{\text{void}}}{V_{\text{total}}} = \frac{(3.5 - 0.0076)}{3.5} = 0.9978$$

Therefore, a total porosity of 99.78% for this sample is observed.

The oldest and most well-known theory of low porosity levels was devised by Maxwell and predicts the conductivity of CPPD as follows:

$$\text{Equation A-2.4} \quad \sigma = \sigma_0 \left(\frac{2 - 2\Theta}{2 + \Theta} \right) = 0.00147 \sigma_0$$

where σ is the conductivity of the porous material, σ_0 is the conductivity of the pure material, and Θ is value of porosity. The porosity of a porous system ranges from 0 to 1. Fricke (Fricke, 1924) in 1924 added a shape factor due to the geometry of pores in the expression:

$$\text{Equation A-2.5} \quad \sigma = \sigma_0 \left(\frac{1 - \Theta}{1 - (1 - f)\Theta} \right) = \left(\frac{0.0022}{0.0022 + 0.9978f} \right) \sigma_0$$

f varies from 1.5 for spherical pores to infinity for thin, disc-shaped pores. Koh (Koh & Fortini, 1973) developed the following equation for highly porous materials with porosity ranging from 0.38 to 0.9:

$$\text{Equation A-2.6} \quad \sigma = \sigma_0 \left(\frac{1 - \Theta}{1 + 10\Theta^2} \right) = 0.0002 \sigma_0$$

Skorokhod (Skorokhov, 1972) found that for porous bodies with wide porosity, the equation would become:

Equation A-2.7
$$\sigma = \sigma_0(1 - \Theta)^{1.5} = 0.0001\sigma_0$$

Hence, these semi-empirical relations predict the conductivity of porous sample A as low as 0.00147 to 0.0001 times that of pure PANI. Since in our case there is a PANI network with ultra-high porosity (> 99%), an equation based on measured conductivity data should be developed.

Knowing that the conductivity of pure PANI is around 10 S.cm, and assuming that samples A and B have similar mass deposition behaviours, from the measured conductivity data the following equation for the deposition of 38 layers of PSS/PANI (after reaching the stable plateau) can be given:

Equation A-2.8
$$\sigma = 0.000002 \sigma_0$$

The coefficient obtained from the plot is 50 times less than that of the equation suggested by Skorokhod (Skorokhov, 1972), due to the disconnection of some clusters in the PANI network.

Skorokhod (Skorokhov, 1972) corrected equation A-2.9 by introducing a relative linear dimension of contact (ξ) to account for the effect of the imperfection of particle contacts:

Equation A-2.9
$$\sigma = \sigma_0(1 - \Theta)^{1.5\xi}$$

A value of 1.43 was calculated for ξ of sample B through the comparison of equations A-2.8 and A-2.9. Consequently, the specific relation for the calculation of the conductivity of 3D CPPD on substrate B can be presented as:

Equation A-2.10
$$\sigma = \sigma_0(1 - \Theta)^{2.14}$$

APPENDIX III

A- 3 Mechanism of Aggregation of Weak Polyelectrolytes

Weak polyelectrolytes have some advantages compared to strong ones, such as the possibility of tuning their properties by simple pH adjustment. In strong polyelectrolytes, the charges remain over the entire pH range. On the contrary, for weak polyelectrolytes, the degree of ionization depends on the pH of the solution. In this thesis, the pH of polyaniline solution is set constant at 2.5 for all samples in order to have the equal fraction of charges for layers. Moreover, the weak PANI shows a “poor” nature in aqueous solutions(Cheung, et al., 1997). Such poor solvent quality indicates that the polyaniline solution can only be used for about 1-2 weeks before important aggregation of the polyaniline chains happens(Cheung, et al., 1997). In this case, a large amount of polymer chains is adsorbed per layer and multilayer deposition cannot be controlled. The aggregation of polyelectrolytes in a solution throughout layer-by-layer experiments was studied over time for sample B in Chapter 5 in two steps (Figure A-3.1). In the first continuous process, 22 layers were deposited onto the 3D substrate. After the deposition of the 22nd layer, all the solutions were left for three weeks to allow the chains to make aggregates. The second LbL process was continued by the same solutions and substrates, whereas layers 23 to 37 were deposited on the previously prepared multilayer. In this protocol, two different growth rates of deposition of NaPSS for either step were obtained. The deposition process with fresh solutions exhibited a growth rate of 3.04, while a higher growth rate value of 6.27 was obtained for the remaining sample. Such a high growth rate demonstrates the aggregation deposition of chains in the second step instead of the deposition of a few chains in the first step. Correspondingly, a solution containing fresh PANI shows a rate of desorption of 2.28, compared to the solution used in the second step with a rate of 5.22. The aggregation of PANI resulting from the poor nature of the PANI solution is proposed as the main reason for the increase of the growth and desorption rates. Therefore, in the second step, a large number of aggregated PANI chains was deposited, yielding a significant increase in electrostatic force. In the subsequent

dipping PSS process, a proportional extent of PSS was deposited to compensate for this electrostatic force.

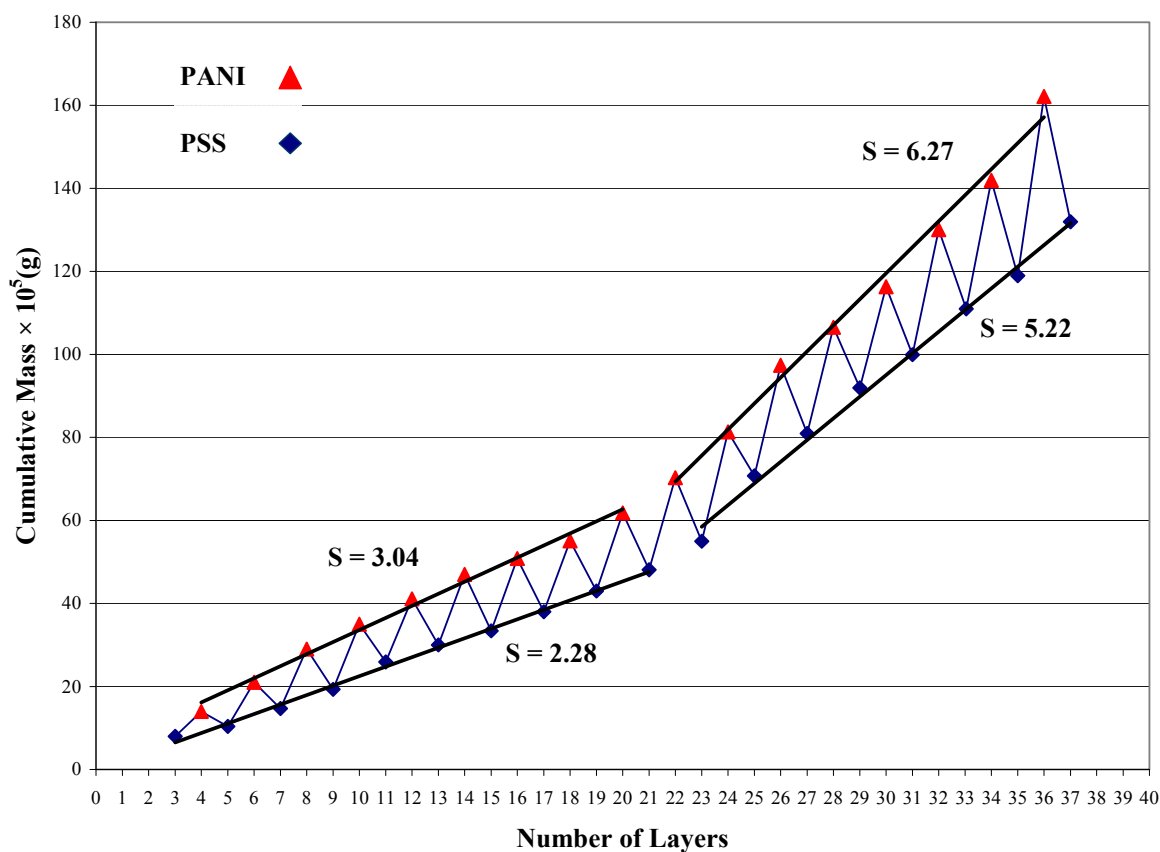


Figure A-3.1. Cumulative deposited mass in LbL process on sample(B) for both PANI and NaPSS polyelectrolytes as a function of number of layers.

APPENDIX IV

A- 4 Relationship between Conductivity and Morphology of Ternary Polymer Blends

This annex is a comprehensive study of a ternary blend for the case of complete wetting in which conductivity data are used to justify the behavior of a ternary blend, which is attributed to its morphology and is based on the composition of its components. It was observed that the lowest percolation threshold (as low as 3%) for a ternary blend has been found in a double percolated structure for the complete wetting case. Due to high interfacial tension between PANI and common polymers, it is almost impossible to situate PANI at the interface.

According to the positive spreading coefficient of PVDF over PANI ($\lambda_{\text{PVDF/PANI}} = 7.3 \text{ mN/m}$ in HDPE/PVDF/PANI) (Figure A-4.1), PVDF is forced to the interface. In this case, PANI and HDPE situate in the inside and outside, and PVDF locates at the interface. The lower interfacial tension between PVDF and PANI results in the interpenetration of the entire PANI and PVDF in each other, and the formation of small phase sizes. Some big parts of PVDF polymer have been clearly removed after extraction of PVDF by DMF in such a morphology (Figure A-4.1a). Solvent extraction/gravimetric measurement reveals that some part of the PANI entrapped in the PVDF phase is removed with PVDF. By decreasing the amount of PVDF to as little as 20%, as shown in Figure A-4.1b, the number of large PVDF islands reduces. These disappearances of large PVDF parts continue with the reduction of the amount of PVDF until no large PVDF parts are observed in the 45/10/45 HDPE/PVDF/PANI blend (Figure A-4.1c). However, the large parts of PVDF play an important role in reducing the percolation threshold of PANI, as they occupy some spaces in the blend and limit the presence of PANI in those areas. It can be concluded that one of the best ways of reducing the percolation threshold, despite the double-percolated structure, is occupying places with other components. In a 33/33/33 HDPE/PVDF/PANI blend, the area occupied by PANI has been limited because of continuous phases of PVDF and HDPE, and large PVDF areas. This results in a lower percolation threshold

of PANI, and an increase in the conductivity of the sample, as for this blend conductivity reaches a relatively high value of 0.017 S/cm.

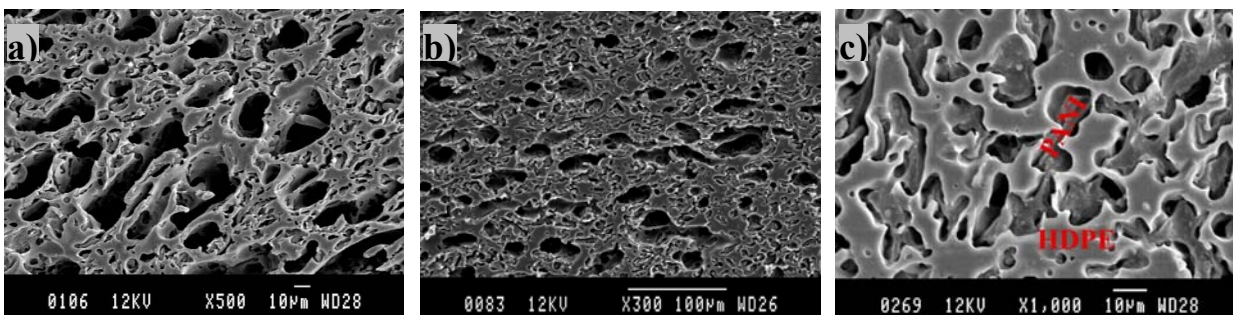


Figure A-4.1. Scanning electron micrographs of HDPE/PVDF/PANI after extraction of PVDF by DMF (a) 33/33/33, (b) 40/20/40, and (c) 45/10/45

The approach obtained for HDPE/PVDF/PANI can be used to decrease the percolation threshold of PANI in a HDPE/PEMA/PANI blend. In such a conversion, HDPE plays a major role as it forms a continuous structure containing large rods and branches, and consequently limiting the space, whereas PANI can generate clusters only in limited routes. In this part, two ternary blends of HDPE/PEMA/PANI and PS/PEMA/PANI are studied from electrical and morphological points of view. It is shown that the high surface tension of HDPE and PANI results in a positive spreading coefficient: $\lambda_{\text{PEMA/PANI}} = 8 \text{ mN/m}$ in HDPE/PEMA/PANI, according to the Harkins equation (interfacial tensions are listed in Table A-4.1). Therefore, PEMA locates at the interface of HDPE and PANI, separating them. In such a morphology, due to high interfacial tension between HDPE and PEMA, large continuous parts of HDPE exist in the blend, which restricts the area for diffusion of PANI. Therefore, connected pathways of PANI are achieved at a lower amount of PANI, leading to a decrease in the percolation threshold of PANI, and subsequently increasing the value of conductivity. In the ternary PS/PEMA/PANI, due to a positive spreading coefficient of $\lambda_{\text{PEMA/PANI}} = 3.2 \text{ mN/m}$, the PEMA phase is located at the interface of the PS and PANI phases (Table A-4.1). Contrary to the previous case, with a low amount of PANI, the percolation threshold is not reached due to the low interfacial tension of PS and PEMA, resulting in PANI droplets remaining in the blend.

Table A-4.1. Interfacial Tensions for Polymer Pairs

Theoretical data(Harmonic mean equation) γ (mN/m)			
HDPE/PEMA	8.3	PEMA/PANI	10.6
HDPE/PANI	26.9	PS/PANI	15.1
PEMA/PANI	10.6	PS/PEMA	1.3

Ternary polymer blends comprised of HDPE/PEMA/PANI with various compositions of PANI are prepared. In such samples, the ratios of HDPE and PEMA concentrations are changed while constant volume fractions of PANI (10%, 20%, and 30%) were selected. Figure A-4.2 shows the results of resistance for various compositions of HDPE/PEMA/PANI. It is observed that the binary blend of HDPE and PANI has the highest value of resistance, which is attributed to droplet-matrix morphology, because of the high interfacial tension between HDPE and PANI. A percolation threshold of 25% PANI can be detected for this binary blend, as at 25% of PANI, the value of resistance starts to decrease. It is found that addition of PEMA to the HDPE/PANI binary blend decreases the resistance of the blend. It is proposed that the interfacial tension between PEMA and PANI is low, leading to a reduction in the size of the PANI phases in the blend. Connection of such small phases of PANI and the presence of large branches of continuous HDPE in the blend result in the formation of small connected pathways, and subsequently helps to reduce the total percolation threshold. Consequently, addition of PEMA to the binary blend reduces both the percolation threshold of PANI and the resistance of the blend for samples with PANI compositions more than 20%. For concentrations of less than 10% PANI, due to lack of sufficient PANI to form clusters, other components and morphology play a major role in determining the value of resistance.

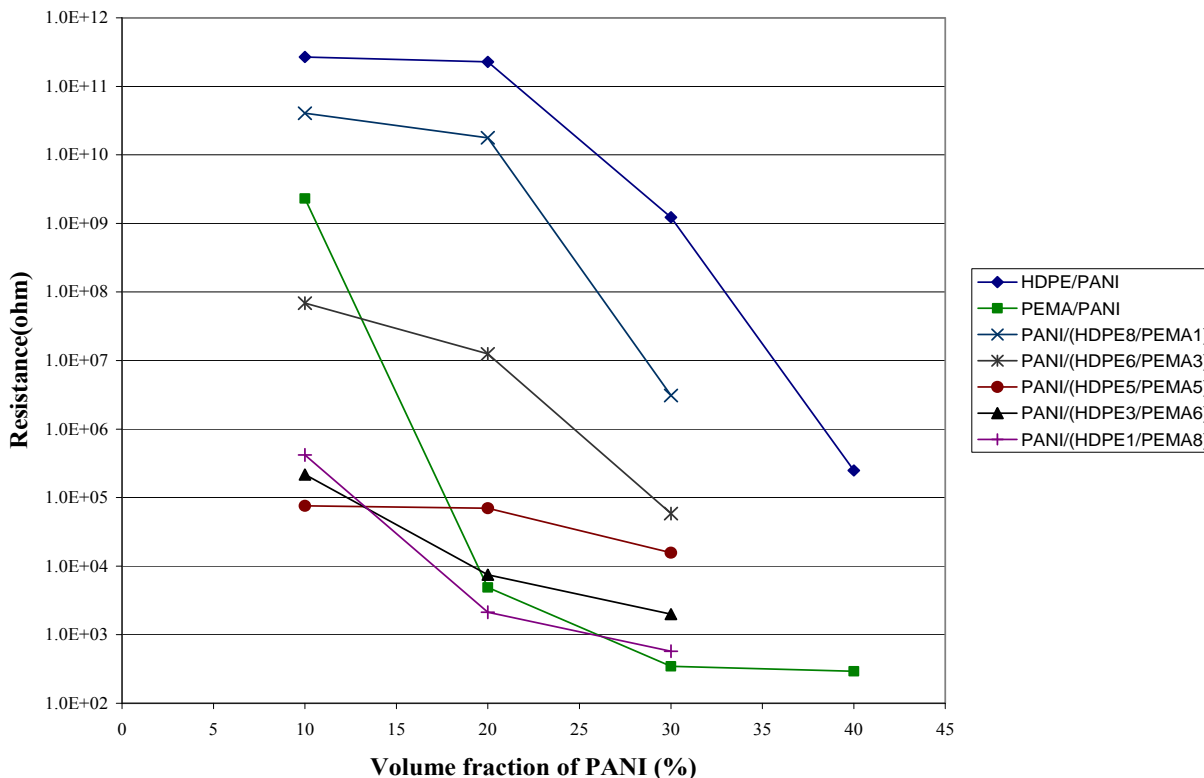


Figure A-4.2. Resistance values for ternary blends of HDPE/PEMA/PANI with various compositions as a function of volume fraction of PANI

Figure A-4.3 represents the same results as Figure A-4.2 from another point of view, since the resistance has been plotted against volume fraction of one of the components (PEMA). As expected, Figure A-4.3 shows higher values of resistance for samples comprising 10% of PANI compared with samples containing 20% or 30% of PANI. Resistance values of samples containing 10% PANI are represented in the first curve in Figure A-4.3, revealing that increasing the concentration of PEMA decreases the resistance value of the blend, up to 45% of PEMA. Further increase of PEMA leads to an increase in the resistance value. This experiment clearly illustrates the dependence of the conductivity percolation threshold to sample morphology. The conductivity value decreases when morphology of matrix-droplet for 90/10 HDPE/PANI changes to matrix/core-shell morphology for the 80/10/10 HDPE/PEMA/PANI ternary blend. At a composition of 60/30/10 HDPE/PEMA/PANI, shells of PEMA coalesce with each other and make several connected pathways. The relatively high interfacial tension between HDPE and PEMA ($\gamma_{\text{PEMA/HDPE}} = 8.3 \text{ mN/m}$) results in a lower interfacial area value, demonstrating the

continuous structure of PEMA and HDPE with larger phase sizes. Therefore, a large part of the blend is occupied by thick rods of HDPE. Since the PEMA phase, located at the interface, makes some connected pathways, and PANI is distributed in the PEMA, in this case geometrical restriction results in producing a few connected pathways of PANI in 30% PEMA. Because of the constitution of small clusters of PANI in the PEMA intermediate phase, the resistance slightly decreases. Increasing further the amount of PEMA results in a tri-continuous morphology for 45/45/10 HDPE/PEMA/PANI, since with a sufficient content of PEMA, a continuous phase of PEMA forms and consequently the small amount of PANI phase inside it becomes continuous. As the continuous HDPE phase still occupies 45% of the blend, and due to the formation of larger connected pathways of PANI, resistance reduces by almost three orders of magnitude. Addition of further PEMA to the blend results in a preparation of 30/60/10 in which the continuous structure of HDPE starts to convert to droplets. Due to the lower occupation of space with HDPE, and the dispersion of PANI in a higher amount of PEMA, 10% PANI distributes as droplets and connected pathways are hardly constructed. Increasing the concentration of PEMA to 10/80/10 HDPE/PEMA/PANI results in the formation of bicontinuous/droplet morphology, whereas a small content of HDPE causes a vast occupation area of PEMA. Therefore, 10% PANI particles disperse in PEMA, showing a higher value of resistance. Finally, for a binary blend of 90/10 PEMA/PANI, matrix/droplet morphology is predicted, although still one or two connected pathway of PANI in PEMA can be found. As it is observed, concentration and morphology of HDPE and PEMA affect the conductivity and continuity of PANI, where the percolation threshold of samples with a constant 10% of PANI is obtained at 35% of PEMA and 90% of PEMA in a HDPE/PEMA/PANI ternary blend.

In samples containing 20% of PANI, a similar behavior for small contents of PEMA with a slight difference in the value of resistance is observed. At 40/40/20 HDPE/PEMA/PANI, tri-continuous morphology is generated, demonstrating a sharp decrease of the resistance. The important points are samples containing 20% PANI and 66.6/33.3 PEMA/HDPE and 90/10 PEMA/HDPE in which, in contrast to samples containing 10% of PANI at these points, resistance has a low value. As mentioned above, higher value of resistance at these points for samples containing 10% of PANI is related to droplets of PANI distributed in PEMA, due to lack an insufficient amount of PANI. On the contrary, for samples containing 20% of PANI, the concentration of PANI is high enough to form a number of connected pathways of PANI inside PEMA, yielding the decrease of

resistance value. Samples containing 30% of PANI, because of the high amount of PANI in the sample, reveal high values of conductivity for a wide range of concentrations. Only in the first region of the curve (high concentration of HDPE), due to the presence of a large volume fraction of HDPE, is the value of conductivity low. The percolation threshold occurs at 10% of PEMA, as a double-percolated morphology is predicted for this ternary blend containing of 60/10/30 HDPE/PEMA/PANI. By increasing the amount of PEMA, the morphology tends to become tri-continuous, since the network of PANI contributes throughout the entire sample. The second ternary blend, comprised of PS/PEMA/PANI, was chosen with the same compositions of components. Since the interfacial tension between PS and PEMA ($\gamma_{\text{PEMA/PS}} = 1.3 \text{ mN/m}$) is much lower than that for HDPE and PEMA ($\gamma_{\text{PEMA/HDPE}} = 8.3 \text{ mN/m}$), it is predicted that PS and PEMA will make smaller phase sizes than HDPE and PEMA. Although it is difficult to show the morphological features of a ternary PS/PEMA/PANI blend, the decrease of the phase sizes between PS and PEMA are shown in the HDPE/PS/PANI blend. Figure A-4.4 shows the morphology of an interdiffusion of PEMA and PS in the HDPE/PS/PANI blend, representing very small rods and branches of PEMA after extraction of PS, while the rods of the continuous phase of HDPE are so large. Such differences in the sizes of trunks of continuous HDPE and PEMA indicate how much the interfacial tension differs between PEMA and either of these two phases.

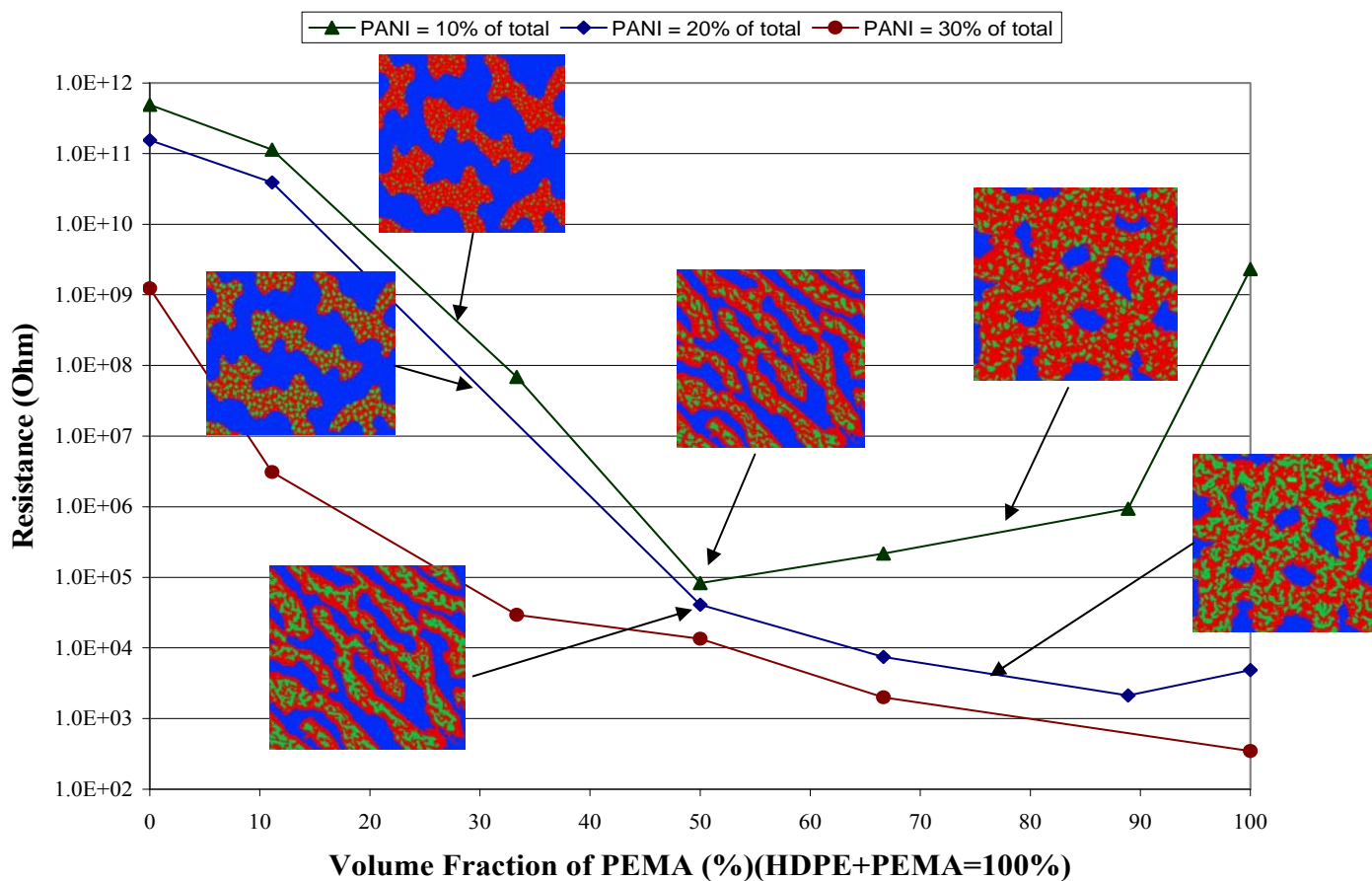


Figure A-4.3. Resistance values for ternary blends of HDPE/PEMA/PANI comprising of 10%, 20%, and 30% of PANI with various compositions ratio of PEMA and HDPE as a function of volume fraction of PEMA

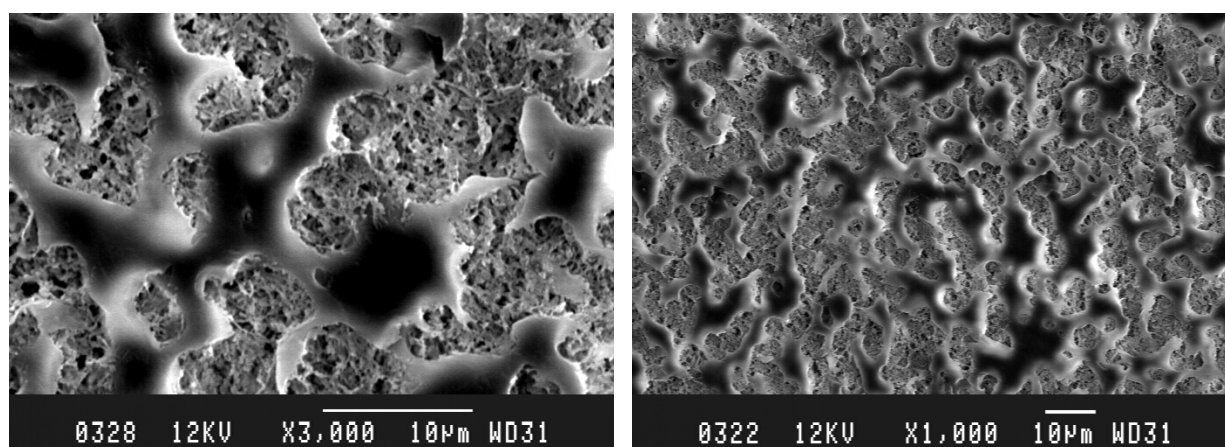


Figure A-4.4. Scanning electron micrographs of 40/10/50 HDPE/PS/PEMA compounded by melt-blending after extraction of PS by cyclohexane

The results of resistance for PS/PEMA/PANI are plotted as a function of volume fraction of PEMA in Figure A-4.5. The plot of resistance values for PS/PEMA/PANI samples containing 10% of PANI is completely different from what was observed for HDPE/PEMA/PANI, represented in Figure A-4.3. Figure A-4.5 reveals that for blends containing 10% of PANI at all concentrations of PEMA, the resistance value is significantly high, since for all concentrations of PEMA the resistance is approximately constant and the percolation threshold is not reached. The reason for not achieving the formation of PANI connected pathways in blends with a low amount of PANI (10%) is proposed to be attributed to the low value of interfacial tension between PEMA and PS. Such a low interfacial tension results in the constitution of a co-continuous network of PEMA and PS, leading to dispersion of droplets of PANI in a large volume. In the previous case (HDPE/PEMA/PANI), because of many parts of blend being occupied by HDPE, PANI was forced in geometrically restricted paths, and a few connected pathways of PANI, even at low concentration, are formed. In the PS/PEMA/PANI case, there is no force to get the PANI droplets coalesced because of the interdiffused network of PEMA and PS resulting in the distribution and dispersion of PANI in the droplet shape throughout the sample. Such morphology represents unconnected droplets of PANI, and subsequently, due to the absence of formation of a PANI connected network, a high value of resistance for all compositions of PEMA is revealed. However, for samples containing 20% PANI, due to the sufficient amount of PANI at a high content of PEMA, networks of PANI are formed, and for this plot a percolation threshold of 20% of PEMA can be considered. High concentrations of PS reveal a matrix-droplet morphology, as the value of resistance is high.

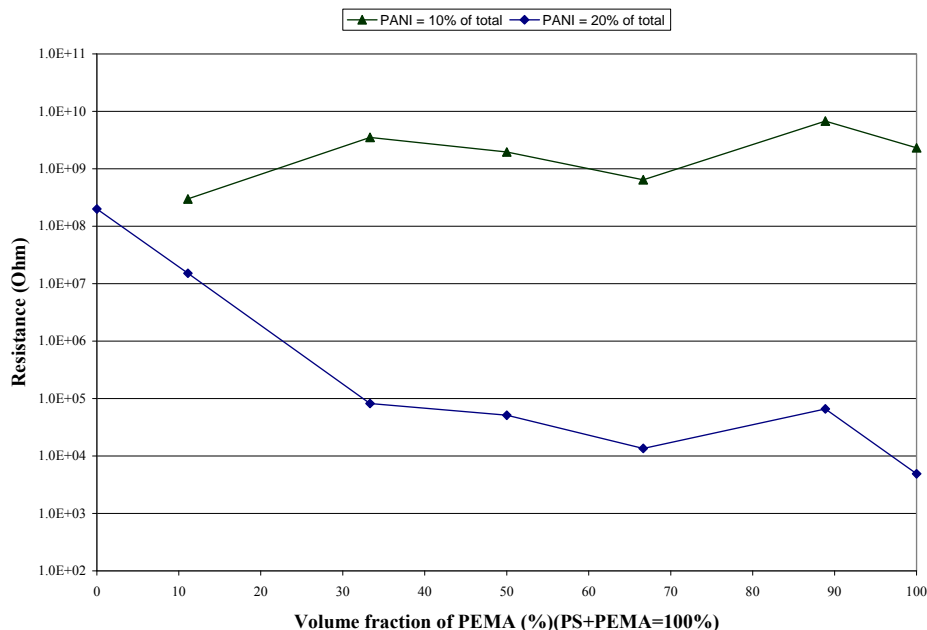


Figure A-4.5. Resistance values for ternary blends of PS/PEMA/PANI comprising of 10% and 20% of PANI with various compositions ratio of PEMA and PS as a function of volume fraction of PEMA

It is concluded that the composition of the inner and outer phases in a double percolated structure can either be effective or ineffective, depending on the interfacial tension of the phases.

References of Annexes

- Berger, W., Kammer, H. W., & Kummerlowe, C. (1984). *Makromol Chem Suppl B*, 8, 101.
- Caruso, F. (2003). Hollow Inorganic Capsules via Colloid-Templated Layer-by-Layer Electrostatic Assembly (pp. 145-168).
- Caruso, F., Caruso, R. A., & Mohwald, H. (1998). Nanoengineering of inorganic and hybrid hollow spheres by colloidal templating. *Science*, 282(Copyright 1999, IEE), 1111-1114.
- Caruso, F., Caruso, R. A., & Mohwald, H. (1999). Production of Hollow Microspheres from Nanostructured Composite Particles. *Chemistry of Materials*, 11(11), 3309-3314.

- Caruso, F., & Schuler, C. (2000). Enzyme Multilayers on Colloid Particles: Assembly, Stability, and Enzymatic Activity.. *Langmuir*, 16(24), 9595-9603.
- Cheung, J. H., Stockton, W. B., & Rubner, M. F. (1997). Molecular-level processing of conjugated polymers. 3. Layer-by-layer manipulation of polyaniline via electrostatic interactions. *Macromolecules*, 30(9), 2712-2716.
- Fricke, H. A. (1924). mathematical treatment of the electrical conductivity and capacity of disperse systems. I. The electrical conductivity of a suspension of homogeneous spheroids. *J. Physical Rev.*, 24, 575-587.
- Gubbels, F., Jerome, R., Teyssie, P., Vanlathem, E., Deltour, R., Calderone, A., et al. (1994). Selective localization of carbon black in immiscible polymer blends: a useful tool to design electrical conductive composites. *Macromolecules*, 27(7), 1972-1974.
- Hobbs, S. Y., Dekkers, M. E. J., & Watkins, V. H. (1988). Effect of interfacial forces on polymer blend morphologies. *Polymer*, 29(9), 1598-1602.
- Hou, S., Harrell, C. C., Trofin, L., Kohli, P., & Martin, C. R. (2004). Layer-by-Layer Nanotube Template Synthesis. *Journal of the American Chemical Society*, 126(18), 5674-5675.
- Koh, J. C. Y., & Fortini, A. (1973). Prediction of thermal conductivity and electrical resistivity of porous metallic materials. *Int. J. Heat Mass Transfer*, 16, 2013-2021.
- Lyngaae-Jorgensen, J., & Utracki, L. A. (2003). Structuring polymer blends with bicontinuous phase morphology. II. Tailoring blends with ultralow critical volume fraction. *Polymer*, 44(5), 1661-1669.
- Narkis, M., Haba, Y., Segal, E., Zilberman, M., Titelman, G. I., & Siegmann, A. (2000). Structured electrically conductive polyaniline/polymer blends. *Polymers for Advanced Technologies*, 11(8-12), 665-673.
- Omonov, T. S., Harrats, C., & Groeninckx, G. (2005). Co-continuous and encapsulated three phase morphologies in uncompatibilized and reactively compatibilized polyamide 6/polypropylene/polystyrene ternary blends using two reactive precursors. *Polymer*, 46(26), 12322-12336.
- Park, M.-K., Deng, S., & Advincula, R. C. (2005). Sustained Release Control via Photo-Cross-Linking of Polyelectrolyte Layer-by-Layer Hollow Capsules. *Langmuir*, 21(12), 5272-5277.
- Potschke, P., & Paul, D. R. (2003). Formation of co-continuous structures in melt-mixed immiscible polymer blends. *Journal of Macromolecular Science - Polymer Reviews*, 43(1), 87-141.
- Reignier, J., & Favis, B. D. (2000). Control of the subinclusion microstructure in HDPE/PS/PMMA ternary blends. *Macromolecules*, 33(19), 6998-7008.

- Reignier, J., & Favis, B. D. (2003). Core-shell structure and segregation effects in composite droplet polymer blends. *AIChE Journal*, 49(4), 1014-1023.
- Reignier, J., Favis, B. D., & Heuzey, M.-C. (2003). Factors influencing encapsulation behavior in composite droplet-type polymer blends. *Polymer*, 44(1), 49-59.
- Schneider, G., & Decher, G. (2004). From Functional Core/Shell Nanoparticles Prepared via Layer-by-Layer Deposition to Empty Nanospheres. *Nano Letters*, 4(10), 1833-1839.
- Skorokhov, V. V. (1972). *The Rheological Principles of Sintering Theory*. Kiev: Nauka.
- Soares, B. G., Gubbels, F., Jerome, R., Teyssie, P., Vanlathem, E., & Deltour, R. (1995). Electrical conductivity in carbon black-loaded polystyrene-polyisoprene blends. Selective localization of carbon black at the interface. *Polymer Bulletin (Berlin)*, 35(1-2), 223.
- Steinmann, S., Gronski, W., & Friedrich, C. (2001). Cocontinuous polymer blends: Influence of viscosity and elasticity ratios of the constituent polymers on phase inversion. *Polymer*, 42(15), 6619-6629.
- Torza, S., & Mason, G. (1970). Three- phase interactions in shear and electrical fields. 33(1), 67-83.
- Valera, T. S., Morita, A. T., & Demarquette, N. R. (2006). Study of morphologies of PMMA/PP/PS ternary blends. *Macromolecules*, 39(7), 2663-2675.
- Van Oene, H. J. (1972). Modes of dispersion of viscoelastic fluids in flow. *Colloid Interface Sci.*, 40, 448-467.
- Virgilio, N., Favis, B. D., Pepin, M.-F., Desjardins, P., & L'Esperance, G. (2005). High contrast imaging of interphases in ternary polymer blends using focused ion beam preparation and atomic force microscopy. *Macromolecules*, 38(6), 2368-2375.
- Volodkin, D. V., Petrov, A. I., Prevot, M., & Sukhorukov, G. B. (2004). Matrix Polyelectrolyte Microcapsules: New System for Macromolecule Encapsulation. *Langmuir*, 20(8), 3398-3406.
- Yuan, Z., & Favis, B. D. (2004). Macroporous poly(L-lactide) of controlled pore size derived from the annealing of co-continuous polystyrene/poly(L-lactide) blends. *Biomaterials*, 25(11), 2161-2170.
- Yuan, Z., & Favis, B. D. (2006). Influence of the efficacy of interfacial modification on the coarsening of cocontinuous PS/HDPE blends during quiescent annealing. *Journal of Polymer Science, Part B: Polymer Physics*, 44(4), 711-721.
- Zilberman, M., Siegmann, A., & Narkis, M. (2000). Melt-processed, electrically conductive ternary polymer blends containing polyaniline. *Journal of Macromolecular Science - Physics*, B39(3), 333-347.